

Investigating the Effects of Venom Peptides on Canine Mammary

Cancer



By

Alice Emily Upton

Canterbury Christ Church University

**Thesis submitted
for the Degree of MSc by Research**

2020

Table of Contents

<i>List of Figures</i>	VI
<i>List of Tables</i>	VIII
<i>List of Abbreviations</i>	IX
<i>Acknowledgements</i>	1
<i>Abstract</i>	2
CHAPTER 1: Introduction	3
1.1 Cancer	3
1.1.1 Cancer Biology	3
1.1.2 Canine Mammary Cancer	7
1.1.2 Causes and Risk Factors	8
1.1.2.1 Breed.....	8
1.1.3.2 Oestrus cycle and Hormones	9
1.1.3.3 Diet and Obesity	10
1.1.3.4 Environmental.....	10
1.2 Treatment	11
1.2.1 Diagnosis and Surgery	11
1.2.2 Adjuvant therapies.....	13
1.2.2.1 Radiotherapy.....	13
1.2.2.2 Chemotherapy	14
1.3 Biomarkers in Canine Mammary Cancer	15
1.3.1 Molecular markers	15
1.3.2 HER2.....	16
1.3.2.1 HER2 Expression in Canine Mammary Cancer	16
1.3.2.2 HER2 Structure, Activation and Cell Signalling.....	17
1.4 Dogs as a model for Human Breast Cancer	19
1.5 Animal Venom	21
1.5.1 Venom components	21
1.5.2 Toxins in Medicine	21
1.5.3 Venoms in Modern medicine	22
1.5.4 Anticancer activity	23
1.6 Statement of Purpose and Experimental Aims	24
CHAPTER 2 – Materials and Methods	26
2.1 Introduction.....	26
2.2 Cell Culture	26
2.2.1 Cell lines	26
2.2.2 Maintenance and Culturing of Cell lines	27
2.2.3 Freezing and Thawing of Cell Line Stocks.....	27
2.3 Venom Resazurin Assay.....	28
2.3.1 Cell Counting and Cell Plating	28
2.3.2 Venom Treatment for Resazurin Assay.....	29

2.4 Statistical Analysis and Graphical representation	30
CHAPTER 3 – Venom Assay Optimisation and Screening of Whole Venoms.....	31
3.1 Introduction.....	31
3.2 Aims	32
3.3 Materials and Methods	32
3.3.1 Optimisation of the Resazurin Assay to Determine Cellular Cytotoxicity of Snake Venom.....	32
3.4 Results and Discussion	35
3.4.1 Selection of the Optimal Cell Number for an Effective Plate-Based Resazurin Assay	35
3.4.2 Z' Analysis of Selected Cell Number.....	38
3.4.3 Initial screening of <i>Naja nigricollis</i> Venom Using the Optimised Resazurin Assay	39
3.4.4 Cytotoxic Screening of Snake Venom from the <i>Naja</i> genus Using the Optimised Resazurin Assay	41
3.5 Conclusion	42
CHAPTER 4: High-throughput screening of Venom Fractions using T-VDA^{ctx} assay and Identification of fraction using Mass Spectrometry	45
4.1 Introduction.....	45
4.2 Aims	46
4.3 Materials and Methods	47
4.3.1 Optimisation of the Resazurin Assay for the T-VD ^{ctx} assay	47
4.4 Results and Discussion	51
4.4.1 Selection of the Optimal Cell Number for an Effective Plate-Based Resazurin Assay in 384 well plates	51
4.4.2 Z' Analysis of Selected Cell Number.....	52
4.4.3 Determining the Appropriate Concentration to Screen the Venom Fractions of the T-VDA ^{ctx} Assay	55
4.4.4 Screening the T-VDA ^{ctx} assay to Identify Cytotoxic Fractions on CMM26 cells.....	56
4.4.5 Hit Fraction screening from T-VDA assay CMM26, CMT28 and MDCK.....	59
4.4.6 Identifying Cytotoxic Doses of Hit Fractions on CMT28, CMM26 and MDCK cells	64
4.4.7 Conclusion.....	68
Chapter 5: HER2 Receptor Expression and Molecular Docking of Venom Peptides on the Canine HER2 Receptor	69
5.1 Introduction.....	69
5.2 Aims	70
5.3 Materials and Methods	71
5.3.1 HER2 Receptor Expression in CMT28, CMM26 and MDCK using Fluorescence Microscopy ...	71
5.3.2 Cell lysis for Dot Blot Analysis	72
5.3.3 Determining Protein Concentration of Cell lysates via DS-11 Analysis.....	72
5.3.4 Dot Blot Preparation for Assessing HER2 Binding ability to Whole Snake Venoms.....	72
5.3.5 Generating Homology models for the Extracellular domain of the Canine HER2 receptor using I-TASSER	73
5.3.6 Minimisation of the Canine HER2 receptor system	74
5.3.7 Heating of the Canine HER2 receptor system.....	74
5.3.8 Equilibration of the Canine HER2 receptor system.....	75
5.3.9 Generating a Model of the Cytotoxin Naniproin using Quark	75
5.3.10 Structure-Activity-Relationship Analysis of Cytotoxin	76
5.3.11 Molecular Docking of Cytotoxins to the Canine HER2 receptor	76
5.4 Results and Discussion	76

5.4.1 Expression levels of the HER2 Receptor in CMT28, CMM26, MDCK	76
5.4.2 Binding Affinity of HER2 in Response to Whole Snake Venom	79
5.4.3 Optimisation of the I-TASSER Homology model of the Canine HER2 receptor.....	80
5.4.4 Electrostatic analyse on the Canine HER2 receptor.....	86
5.4.5 Generating and Analysing the Structures of Identified Cytotoxins from Mass Spectrometry Data.....	88
5.4.6 Molecular docking of Venom Peptides on the Canine HER2 Receptor.....	91
5.5 Conclusion	93
CHAPTER 6: Discussion.....	100
6.1 Discussion.....	100
6.2 Conclusion and Future Work	104
Reference	105
Appendix.....	I
APPENDIX I: CHAPTER 3: Plate Layout for determining the Optimal Cell Number for CMT28, CMM26 and MDCK in 96 well plates	I
CMT28 and CMM26 Pate layout.....	I
MDCK plate layout	II
APPENDIX II: CHAPTER 3: Plate Layout for Z' Analysis of CMT28, CMM26, MDCK in 96 well plates	III
APPENDIX III: CHAPTER 3: Plate layout Initial Screen of <i>N.nigricollis</i> Venom on CMT28, CMM26 and MDCK in 96 well plate	IV
APPENDIX IV: CHAPTER 3: Dose Response of venom for <i>Naja</i> genus for CMT28, CMM26 and MDCK	V
APPENDIX V: CHAPTER 3: Selection of Optimal Cell Number for an Effective Plate-Based Resazurin Assay at Different Concentrations	VI
CMT28.....	VI
CMM26	VII
MDCK	VIII
APPENDIX VI: CHAPTER 3: Statistical Analysis of Initial Screen of <i>N.nigricollis</i> Venom on CMT28, CMM26 and MDCK.....	IX
CMT28.....	IX
CMM26	X
MDCK	XI
APPENDIX VII: CHAPTER 3: Statistical Analysis of Screening Venom from the <i>Naja</i> genus on CMT28, CMM26 and MDCK.....	XIV
APPENDIX VIII: CHAPTER 4: Plate Layout for determining the Optimal Cell Number for CMT28, CMM26 and MDCK in 384 well plates	XX
CMT28 and CMM28 Plate Layout	XX
MDCK Plate Layout	XXI
APPENDIX VIII: CHAPTER 4: Plate Layout for Z' Analysis of CMT28, CMM26, MDCK in 384 well plates.....	XXII
CMT28, CMM28, MDCK Plate Layout	XXII
APPENDIX IX: CHAPTER 4: Plate Layout for CMT28 and CMM26 Whole venom screen for determining appropriate Cell line and Concentration to T-VDA^{cyx}.....	XXIII
APPENDIX X: CHAPTER 4: Plate Layout for T-VDA^{cyx} Assay	XXIV
APPENDIX XI: Plate Layout for Hit fractions screened CMM26, CMT28 and MDCK from T- VDA assay	XXV

APPENDIX XII: CHAPTER 4: Statistical Analysis of CMT28 and CMM26 Whole venom screen for determining appropriate Cell line and Concentration to T-VDA^{cyx} Assay	XXVI
APPENDIX XIII: CHAPTER 4: Statistical Analysis of Hit Fractions Screened on CMM26 Cells from T-VDA^{cyx} Assay	XXX
APPENDIX XIV: HPLC Chromatogram traces from Fractionated Venoms	XXXII
APPENDIX XV: Statistical Analysis of Hit fractions screened CMM26, CMT28 and MDCK from T-VDA assay	XXXV
APPENDIX XVI: Chapter 4: Mass Spectrometry Data produced from Peak Proteins	XLI
APPENDIX XVII: CHAPTER 5: Dot Blot layout for Determining the Binding of HER2 to Whole Venoms for SKBR3, CMT28 and CMM26	XLVII
APPENDIX XVIII: CHAPTER 5: Dot Blot Analysis Pixel Intensity Data Generated in Biorad ImageLab	XLVIII
Appendix XIX: Chapter 5: Amino Acid sequence of Canine HER2 receptor.....	XLIX
APPENDIX XX: CHAPTER 5: Binary Files produced from HER2 Minimisation	L
APPENDIX XXI: CHAPTER 5: Binary Files produced from HER2 Heating.....	LIII
APPENDIX XXII: CHAPTER 5: Binary Files produced from HER2 Equilibration	LVI

List of Figures

Figure 1.1 Hallmarks of Cancer

Figure 1.2: Emerging Hallmarks of Cancer

Figure 1.3: Four receptors of the Epidermal Growth Factor Receptor Family

Figure 1.4: Activation of EGFR receptor

Figure 3.1: CMT28 Cell Number Resazurin Assay

Figure 3.2: CMM26 Cell Number Resazurin Assay

Figure 3.3: MDCK Cell Number Resazurin Assay

Figure 3.4: Dose Response of *Naja nigricollis* Venom on CMT28, CMM26 and MDCK Cell Lines

Figure 3.5: Dose Response of *Naja nigricollis* Venom on MDCK cells at Higher Doses

Figure 3.6A: African Cobras Dose Response on CMT28, CMM26 and MDCK

Figure 3.6B: Asian Cobras Dose Response on CMT28, CMM26 and MDCK

Figure 4.1: Resazurin Cell Concentration Analysis of CMT28, CMM26 and MDCK

Figure 4.2: Dose Response curves of Whole Venom from *Naja atra*, *Naja kaouthia*, *Naja siamensis* and *Naja nigricollis* on CMT28 and CMM26 cell lines

Figure 4.3: 535 fractions from 13 species of Snake and Invertebrates from the T-VDActx assay

Figure 4.4A: Dose response of Hit Venom Fractions from the T-VDActx Assay

Figure 4.4B: Dose response of Hit Venom Fractions from the T-VDActx Assay

Figure 4.4C: Dose response of Hit Venom Fractions from the T-VDActx Assay

Figure 4.5: Sequence Alignment of Cytotoxins from the *Naja* genus

Figure 4.6: Sequence Alignment of N.kao_i9_r2 and Cytotoxin 3

Figure 4.7: Sequence alignment of N.nig_i11r3 and Naniproin

Figure 5.1: Detection of HER2 expression levels in CMT28, CMM26 and MDCK cell lines using Fluorescent Microscopy

Figure 5.2: Binding of HER2 to Whole Venoms on SKBR3, CMT28 and CMM26 cells

Figure 5.3: Factors Associated with Minimisation of HER2

Figure 5.4: Factors Associated with Heating of HER2

Figure 5.5: Factors Associated with Equilibration of HER2

Figure 5.6: Timeline of Frames of RMSD during Equilibration of the Canine HER2 receptor

Figure 5.7: Electrostatic Mapping of the Canine HER2 Receptor

Figure 5.8: Structural Alignments of Model 3 and known Cytotoxins

Figure 5.9: Structure-Activity-Relationship Analysis of Cytotoxins

Figure:5.10: Electrostatic mapping of Cytotoxin 3 and Naniproin

Figure 5.11: MODEL 1 - Binding between Cytotoxin 3 and the HER2 receptor

Figure 5.12: MODEL 2 - Binding between Cytotoxin 3 and the HER2 receptor

Figure 5.13: MODEL 3 - Binding between Cytotoxin 3 and the HER2 receptor

Figure 5.14: MODEL 1 - Binding between Naniproin and the HER2 receptor

Figure 5.15: MODEL 2- Binding between Cytotoxin 3 and the HER2 receptor

Figure 5.16: MODEL 3 - Binding between Naniproin and the HER2 receptor

List of Tables

Table 1.1: Staging Classification of Canine Mammary Tumours

Table 3.1: Species of Snake from the *Naja* genus used in the Venom Panel Screen

Table 3.2: Z' Values for the Resazurin assay for CMT28, CMM26 and MDCK

Table 4.1: Fractionated whole venom from 13 species found in the T-VDA^{ctx} assay

Table 4.2: Z' Analysis of CMT28, CMM26 and MDCK cells

Table 4.3: LD₅₀ Value for CMT28 and CMM26 exposed to Whole Venoms

Table 4.4: Hit venom fractions to induce >70% inhibition

Table 4.5: LD₅₀ for Venom Fractions causing >70% inhibition

Table 4.6: Venom fractions sent for Mass Spectrometry Analysis

Table 5.1: ECL reagent solution makeup

Table 5.2: Hydrogen bonds between Cytotoxin 3 and HER2

Table 5.3: Hydrogen bonds between Naniproin and HER2

List of Abbreviations

- ANOVA:** Analysis of Variance
- BSA:** Bovine Serum Albumin
- CMM26:** Canine mammary cancer cell line – 26
- CMT28:** Canine mammary cancer cell line - 28
- COS7:** African Green Monkey kidney cell line
- COX-2:** CytooxygenaseCyclooxygenase 2
- DAPI:** 4',6-diamidino-2-phenylindole
- DMEM:** Dulbecco's modified eagles medium
- DMSO:** Dimethyl sulfoxide
- DNA:** Deoxyribonucleic acid
- EDTA:** Ethylenediaminetetraacetic acid
- EGF:** Epidermal Growth factor
- EGFR:** Epidermal Growth factor receptor
- FFT:** Fast fourier transform algorithm
- GFP:** Green fluorescent protein
- HER2:** Human epidermal growth factor receptor 2
- HER3:** Human epidermal growth factor receptor 3
- HER4:** Human epidermal growth factor receptor 4
- HIF:** hypoxia-inducible transcription factor
- HPLC:** High performance liquid chromatography
- HTS:** High-throughput screening
- I-TASSER:** Iterative threating assembly refinement
- MDCK:** Madin-Darby canine kidney cell line
- NAMD:** Nanoscale Molecular Dynamics
- PBS:** Phosphate-buffered saline
- PDB:** Program database file
- PLA2s:** Phospholipases A

RIPA: Radioimmunoprecipitation lysis buffer

RMSD: Root-mean-square deviation of atomic positions

RNA: Ribonucleic acid

RT: Room temperature

SACC/SADC: Sequence-activity correlation/ determination coefficient

SAR: Structure-activity relationship

SKBR3: Human breast cancer cell line

T-VDA^{cvx}: Targeted Venom Discovery Array

TGF α : Transforming growth factor alpha

VEGF: VacularVascular endothelial growth factor receptor

VMD: Visual Molecular Dynamics

Z': Z-factor measure of statistical effect size

Acknowledgements

I would like to express my deepest appreciation to my supervisor Carol Trim for the guidance and support that she has given throughout the journey of becoming the person I am today. I would also like to thank my second supervisor Kris Leslie for the collaboration of this project, bringing a new perspective into this Masters. I am thankful for his patience and dedication in teaching me a new discipline of science. I have thoroughly enjoyed learning the 'dark side' of science. I would also like to thank Daniel Carey for his continuous support through this journey and his contribution towards this project.

I would like to thank my industrial collaborator Venomtech Ltd for the generous supply of venoms and use of your facilities in this project. I would like to thank Steve Trim for his expertise in providing continuous support and guidance to help pave the way of this research.

I would like to acknowledge and thank Dr Bill Gullick of the University of Kent for his kind gifts of both the cancer cell lines and antibodies. I would also like to thank Edith Blackburn from the University of Kent for also providing continuous stocks of cell lines.

I want to personally acknowledge Danielle McCullough for her dedication and patience with assisting me in times of need throughout my masters. Not only have you been an amazing mentor, supporting and encouraging me to delve into science, but you are the inspiration that pushed me to succeed in perusing research. I am very grateful that I was given the opportunity to work alongside you. I would also like acknowledge Alice Tirnovceanu for her expertise in new techniques and providing me with assistance in achieving my goals.

Furthermore, a huge thank you to the team at the CCCU Industry Liaison Lab for keep spirits up when times were low, and for being a supportive team. Finally, I would like to thank my family, in particular my Mum for always believing in me and encouraging me to peruse my passion, and also to my partner Dennis for being by my side when I needed him the most, Thank you!

Abstract

Mammary Cancer is the most prevalent form of malignancy to occur in female dogs. With metastasised malignancies representing 50% of diagnosis, current treatments produce little efficacy towards survival and induce harsh adverse side effects, thus there is need for novel therapeutics. Venoms have been shown to exploit anti-cancer properties with specific selective effects towards many forms of human cancers, thus, the prospect of anti-cancer inhibition towards Canine Mammary Cancer is a feasible hypothesis. Utilising *in-vitro* cell viability assays, panels of venoms from snake, scorpions and spiders were profiled against canine mammary cancer cells lines, CMT28 and CMM26, and an immortalised normal canine kidney cell line, MDCK. Screening of these venom fractions identified selectivity towards the cancerous cells utilising venoms from the *Naja* genus by >70% inhibition. Mass spectrometry data of 5 fractions identified them as 3-finger toxins with 3 of the fractions identifying as novel cytotoxins and 2 matched to sequence in the database of the same species.

Epidermal Growth factor receptor- 2 (HER2) is a key antigenic target in Human breast cancer and has been shown to be as a potential therapeutic target for Canine Mammary Cancer. Utilising computational modelling and molecular docking simulations, the identified cytotoxins obtained from mass spectrometry have been predicted to bind to the dimerisation loop of the extracellular domain of HER2, that is hypothesised to inhibit dimer formation. In practice Canine HER2 demonstrated to have a high binding affinity for proteins in whole snake venoms, signifying the potential of HER2 being a therapeutic target for the treatment of Canine Mammary Cancer.

CHAPTER 1: Introduction

1.1 Cancer

1.1.1 Cancer Biology

Common across multiple species, Cancer is a communal name for a group of diseases that share common features of unregulated and uncontrollable growth of cells. The transformation of a normal cell to a malignancy acquires the progression of hallmark capabilities (Hanahan and Weinberg, 2000; Hanahan and Weinberg., 2011). The hallmarks of cancer show that cancer is a multistep process, with normal cells acquiring the subsequent characteristic traits to enable them to become malignant: 1) the capability to sustained proliferative signalling; 2) by-passing inhibiting growth signals with the ability to avoid growth suppression; 3) enabling replicative immortality; 4) resistance to apoptotic death; 5) activation of angiogenesis; 6) the ability of tissue invasion and metastasis (Figure 1.1) (Hanahan and Weinberg, 2000; Hanahan and Weinberg., 2011; Pavlova and Thompson., 2016; Tassy and Assi *et al.*, 2020). In addition, Hanahan and Weinberg (2011) proposed further emerging hallmarks of cancer: 7) tumour promoting inflammation; 8) avoiding destruction from the immune system; 9) genomic instability and mutations; and 10) dysregulation of cellular energetics (Figure 1.2).

Normal cells depend on a carefully regulated cell-cycle to control proliferation and maintenance of tissues (Malumbres and Barbacid., 2009; Fouad and Aanei.,2017). Controlling the production and release of growth promoting signals allows a stable transition through cell growth and division, thus ensuring homeostatic balance of cells to sustain the normal tissue architecture and function. (Hanahan and Weinberg., 2011). Cancers ability to sustain persistent proliferation is the most predominant trait of the disease. Proliferative efforts are thought to be dependent upon the over production of growth factor stimulation, whether its self-production or influences by reciprocate cancer cells (Horne and Pollick *et al.*, 2015). Dependence of growth factors resulting the excess proliferation may originate from the disruption of downstream signalling of receptors. A key regulator in the cell cycle process that is disrupted through tumour transformation is Retinoblastoma (RB) which plays a role in suppressing tumour progression.

This deregulation of RB renders the tumour cells to be insensitive to tumour antigrowth signalling, as well as other key hallmarks such as genomic stability, regulation of apoptosis, cell metabolism, senescence, angiogenesis, and suppression of invasion and metastasis (Dick, *et al.*, 2013; Fouad and Aanei., 2017). Dysregulation of receptor signalling may be altered through various alterations: receptor overexpression through gene amplification; 2) permanent receptor activation; 3) chromosomal translocation leading to protein fusion and aberrant signalling and 4) impaired receptor recycling and degradation (Lemmon and Schlessinger., 2010; Fouad and Aanei.,2017).

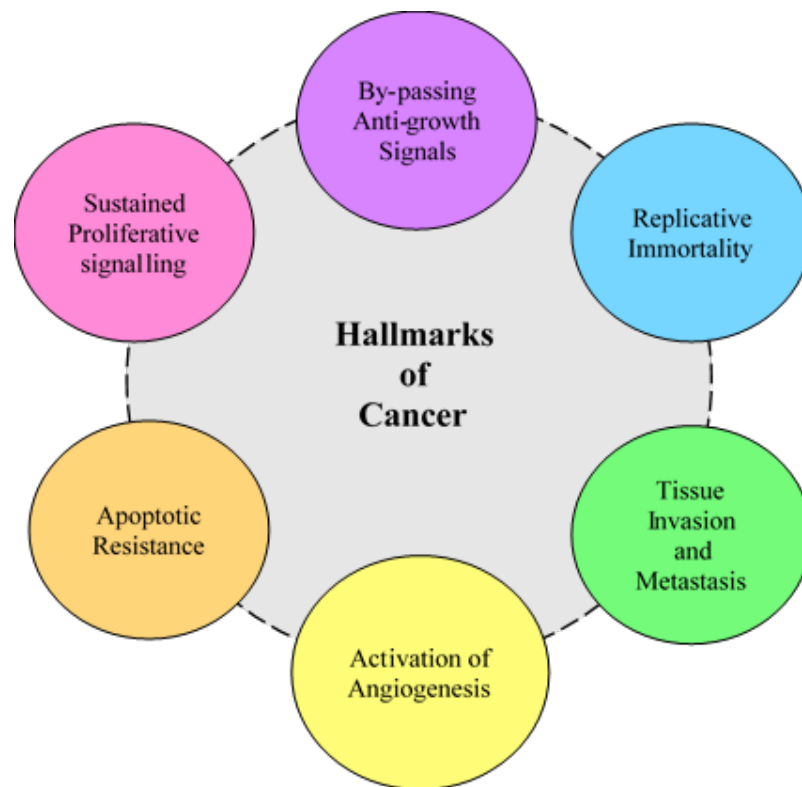


Figure 1.1 Hallmarks of Cancer

Visual display of the six hallmarks of cancer that are essential for developing cells to progress to cancerous cells. Adopted from Hanahan and Weinberg, 2000.

In response to full transformation to malignant cells, physiologically cellular stress is abundant due to excessive signalling, DNA (Deoxyribonucleic acid) damage, hypoxia and nutrient insufficiency (Hanahan and Weinberg., 2011). Dysregulation of DNA repair mechanisms pave the way for further mutations to occur. In healthy cells, there is a finite number of replications a cell can undergo before reaching programmed apoptotic death, yet in malignant cells, replication is an ongoing process, marking these cells as immortalised (De Vitis, *et al.*, 2018). Suggested as

a contributing factor, telomeres found at the 3' and 5' ends of chromosomes, naturally shorten in proliferation of healthy cells, losing about 200 nucleotides in telomere length (De Vitis, *et al.*, 2018). The length of the telomere dictates the number of successive generations a cell can undertake before telomeres are degraded and lose their protective function (Haycock, *et al.*, 2017). Nevertheless, in cancerous cells, continuous degradation of telomeres leads to karyotypic instability, yet in some cancers upregulation of the telomerase enzyme extends the telomeric DNA, replacing the lost sequences during extreme replication (Haycock, *et al.*, 2017; Hannen and Bartsch, 2018).

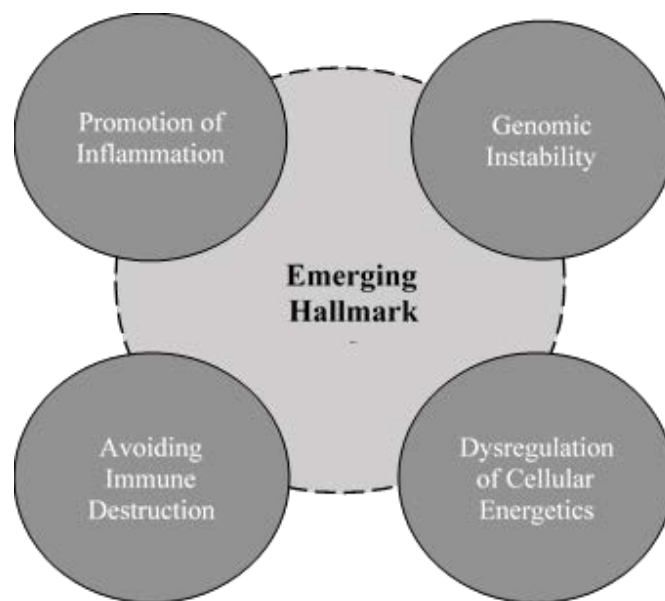


Figure 1.2 Emerging Hallmarks of Cancer

Visual display of the four emerging hallmarks of cancer. Adopted from Hanahan and Weinberg, 2000.

The inability of cancer cells to carry out cellular apoptotic death is due to cells being able to suppress apoptotic mechanisms (Koff, *et al.*, 2015). Cancer cells acquire the ability to resist apoptotic regulators such as the p53 transcription factor that is normally induced through stress in a normal cell (Labi and Erlacher, 2015). However, cancers ability to bypass such mechanisms assist in cancers infinite ability to proliferate (Mello and Attardi, 2018). The instability of cancers genomics is also influenced through tumour-associated inflammation (Hanahan and Weinberg., 2011). This extrinsic pathway of inflammation facilitates cancer development through influences of biological active molecules, such as growth factors, angiogenic stimulating factors, promotion

of sustaining proliferative capability and apoptotic resistance (Colotta, *et al.*, 2009; Hanahan and Weinberg., 2011).

The ability of cancer cells to continuously proliferate and actively avoid suppression from many contributing factors, requires excessive access to energy producing fuel. For healthy cells to undertake cellular maintenance and proliferative mechanisms requires the metabolic activity of glucose through glycolysis. Glucose is transformed in pyruvate and under normal cell conditions, pyruvate would enter the mitochondria where it would be oxidised by the Krebs cycle to generate adenosine triphosphate (ATP). However, the transformation of energy in cancer cells due to their proliferate activities, pyruvate is directed away from the mitochondria to generate lactate through the action of lactate dehydrogenase (Heiden, *et al.*, 2009; Ferreirs, 2010; Hanahan and Weinberg., 2011). This transforms the metabolic activity of cancer cells from aerobic to anaerobic mechanisms that is suggested to contribute to prolonged proliferation, angiogenesis, metastasis and out-competition of surrounding healthy cells; this is referred to as the Warburg effect (Hanahan and Weinberg., 2011; Liberti and Locasale, 2016).

In an attempt to avoid insufficient levels of nutrients and oxygen cells require good blood supply to facilitate growth, and tumour growth is stunted beyond 2.3mm³ without vascularisation (Prager and Zielinski, 2013). Stimulation of forming new blood vessel, known as angiogenesis, is predominantly triggered through hypoxic stress, this is then known to induce stabilised hypoxia-inducible transcription factor (HIF) that initiates an adaptive transcriptional response, triggering angiogenic formation from pre-existing vasculature (Kieran, *et al.*, 2012). Expression of the vascular endothelial growth factor (VEGF) is tightly regulated by HIF, however in many malignancies, VEGF is overexpressed due to the dysregulation of HIF causing excessive proliferative effects in vessel formation influencing migration and differentiation and mediation in vascular permeability (Hicklin, *et al.*, 2015; Fouad and Aanei.,2017).

Cancers ability to invade surrounding tissues and form secondary growths in distinct sites is contributed through mutagenic alterations within cancer cells that disrupt cell adhesion, promote metastasis progression and epithelial-mesenchymal transition (Ye and Weinberg, 2015). Vascular permeabilisation contributes to metastasis invasion, circulating cancer cells to new locations. Circulating new regions of the body assist in additional mutagenic changes to the cells, due to

exposure to harsh conditions, forcing adaptation (Alix- Panabières and Pantel, 2016; Fouad and Aanei.,2017). Additional mutagenic changes and influences through the selective pressures of the immune system influencing the final outcome of the cancerous cells. The immune system has the ability to detect and kill, however as they cancerous cell continuously proliferative this causes them to mutate and adapt a functionality to avoid suppression from the immune system (El-Kenawi, *et al.*, 2020). Three mechanisms have been described for which cancer cells avoid detection from the immune system (Malmberg, 2004): 1) lack of tumour antigen recognition; 2) resistance to cell death and 3) tolerance to the immune system through immunosuppressive factors secreted by cancer cells.

1.1.2 Canine Mammary Cancer

Mammary tumours are the most common form of neoplasm diagnosed in female dogs, with annual incidence rates in dogs being 198 dogs per 100,000, which is three times higher than that in women (Sorenmo, 2003; Kumaraguruparan *et al*, 2006; Bohrer, *et al*, 2017; Nieves, *et al.*, 2018; Benavente *et al*, 2019). Several epidemiological studies across Europe and the USA state increases in occurrence of this disease is associated with the improved advancement of animal health and welfare, resulting in life expectancy of dogs to steadily increase, permitting late-in-life disease such as mammary cancer to represent between 25 to 30 % of all tumours diagnosed in both male and female dogs (Dobson *et al*, 2002; Egenvall *et al*, 2005; Grupa, 2012; Davis, *et al.*, 2014; Baioni *et al*, 2017; Nieves, *et al.*, 2018). Mammary cancers largely affect un-spayed bitches or bitches spayed later in life, with this disease representing approximately 50 % of all neoplasms, irrespective of breed (Sleeckx *et al*, 2011; Varallo *et al*, 2019). Benign tumours represent 60% of mammary tumours diagnosed, whilst 40% of tumours would have metastasised consequently with a high rate of relapsing with 50 to 70 % of dogs having tumours in multiple mammary gland tumours (Sorenmo, 2003; Grupa, 2012; Nieves, *et al.*, 2018; Stephens, 2019). Malignant mammary tumours have a low survival outcome reported to be 25 to 40 % with a median survival time of 4-17 months (Sorenmo, 2003; Sleeckx *et al.*, 2011; Nguyen, *et al*, 2018). This disease represents a significant clinical problem, thus studying canine mammary cancer is of great

importance as of the high mortality and morbidity that affects this species (Lori, *et al*, 2010; Sleenckx *et al*, 2011).

1.1.2 Causes and Risk Factors

1.1.2.1 Breed

The identification of dog breeds was not formally established until the 19th century when dog showing and breeding during the Victorian Era become a popular interest (Frank, 2005; Dobson, 2013; Davis, *et al.*, 2014). With the desirability of owning a purebred dog increasing, stud books were introduced to monitor breeding tendencies by Kennel Clubs with little regard to health impacts (Sampson, 2011; Lewis, *et al.*, 2018). Although breed documentation is strictly maintained in purebred dogs' genetic diversity has been implicated though reproductive isolation of breeds. (Farrell *et al*, 2015; Lewis, *et al.*, 2018). The formation of breed barriers has been paved by artificial selection with sort-after traits being retained, subsequently undesirable disease-causing gene variants have increased in frequency or even fixed within a breed gene pools (Karlsson and Lindblad-Toh, 2008; Doherty, *et al.*, 2020). Phenotypic homogeneity and the limitations of genetic diversity in dog breeds have caused populations to bottleneck with up to 90% of purebreds losing genetic variation through inbreeding (Farrell *et al*, 2015; Jansson and Laikre, 2018) Consequently, these actions are known to be a significant causative factor in the number of inherited disorders in specific breeds (Lewis, *et al.*, 2018; O'Neill, *et al.*, 2020; Doherty, *et al.*, 2020). Aesthetic features of particular breeds for example flat-faced dogs is an increasing trend that has conflicting health effects. Breeds such as the Pug, Bulldog, and Boston Terrier have acquired this favoured featured that has now been correlated with respiratory conditions, predominantly brachycephalic airway syndrome (Riecks, *et al.*, 2007; Dupré and Oechtering, 2013). This disorder results in the pinching of the nares and extension of the soft palate into the nasopharynx stemming breathing difficulty with a reduction in oxygen intake (Dupré and Oechtering, 2013). Selection towards these life-threatening traits is not helped by human intervention, for instance, traits that are distinctive to the English Bulldog of their large-flat-faced heads and barrel shaped bodies present issues at birth (Wydoodhe, *et al*, 2013).

Genetic disposition and the association with cancer development has been significantly correlated with the reduction in genetic variability found in purebreds compared to mixed breed dogs (Nunes, *et al*, 2019). Many studies have recognised the incidence rates of cancer development and the connection with breeds, however the consistency of breeds observed to show high susceptibility vary (Dobson, 2012; Davis and Ostrander, 2014). Breeds that are described to have high occurrences with cancer may vary due to the geographical location of the study suggesting environmental factors and the breed prevalence within the population influence the outcome of the study (Dobson, 2012). Several studies have identified pure breeds to be more prone to cancer development such as the Irish Water Spaniel, Wirehaired Vizsla, Labrador retriever, Bernese mountain dog, Rottweiler, Staffordshire bull Terrier, and the Giant Schnauzer to have an increased risk of developing cancer (Proschowskt, *et al.*, 2003; Bonnett, *et al.*, 2005; Adams, *et al.*, 2010; Dobson, 2012; Lewis, *et al.*, 2018). Incidences of mammary cancer development have been associated with pure breed dogs such as particularly in smaller breeds such as Poodles, Chihuahuas, Dachshunds, Yorkshire Terriers, Maltese, and Cocker Spaniels are frequently; and larger breeds that are also at higher risk, includes the English Springer Spaniel, English Setters, Brittany Spaniels, German Shepherds, Pointers, Doberman Pinschers, and Boxers (Sorenom, *et al.*, 2013; Sleenckx, *et al.*, 2011; Sales, *et al.*, 2015).

1.1.3.2 Oestrus cycle and Hormones

Functional development and differentiation of the mammary gland occurs postnatally under hormone control and is further development with reproductive growth during pregnancy and with every productive cycle (Timmermans-Sprang *et al.*, 2017). Oestrogen, progesterone, prolactin and growth hormone are the essential hormones for mammary gland development. Oestrogen, progesterone and prolactin initiate puberty with the elongation and branching of the ductal system and stimulation of lobulo-alveolar development (Queiroga, *et al.*, 2005; Spoerri, *et al.*, 2015). Throughout pregnancy prolactin promotes the alveolar buds to differentiate into lactating alveoli (Queiroga, *et al.*, 2005; Spoerri, *et al.*, 2015). The effects of these hormones are dependent on the expression levels of their respective receptors within the mammary gland and changes to their

expression have been described in normal canine mammary tissue during different phases of the oestrus cycle (Van Garderen et al., 1999; Rehm *et al.*, 2007; Spoerri *et al.*, 2015; Burrai, *et al.*, 2020). Associations between hormone exposure through reproductive growth or pregnancy and the risk of mammary tumours has been suggested by several epidemiological studies, reporting significantly decreased incidences of mammary tumours in dogs that have undergone ovariectomy or ovariohysterectomy (Schneider et al., 1969; Beauvais, *et al.*, 2012; Kristiansen *et al.*, 2016). Dogs that were spayed prepubertal, with both the removal of the ovaries and cervix, before their first heat cycle, have a 0.5% risk of developing mammary tumours, compared to those that were not spayed; the risk increases to 8% and 26% if the dog has not been spayed until after their first or second heat cycle (Schneider et al., 1969; Salas et al, 2015; Burrai, *et al.*, 2020).

1.1.3.3 Diet and Obesity

Obesity is known to have a negative impact on the health of dogs, yet many studies have associated the development of cancer with the development of unnecessary adipose tissue. Excessive development of adipose tissues is a known factor that contributes to the progression of mammary cancer (Weeth, 2016; Magalhães, *et al.*, 2020). At a molecular level adipocyte have been studied and observed to influence normal and malignant epithelial cells in the mammary glands through the secretion of cytokines and hormones, including leptin, adiponectin, insulin-like growth factor 1, tumor necrosis factor- α , interleukin-6, resistin, and aromatase (laflamme, 2006; Lim, *et al.*, 2015; German, 2016). Leptin is a representative hormone that is released from adipose cells. Although the function of leptin is stimulating mammary gland development in puberty, leptin also stimulates the growth of mammary cancer cells (Ressel, *et al.*, 2012). Leptin has been associated with the poor prognosis of mammary cancer after studies founded a positive correlation with the abundance with leptin and the accumulation of adipose tissues (Miyoshi, *et al.*, 2006; Magalhães, *et al.*, 2020).

1.1.3.4 Environmental

Many epidemiological studies have established the conventional risk factors associated with mammary cancer in humans such as reproductive cycle (early age at menarche, nulliparity, late

age at first full-term pregnancy, late age at lactation and short duration, and late menopause), and inheritance (Coyle, 2004; Strumylaitė, 2010). With incidences increasing in varying geographical locations, it is suggested that environmental factors may play a role in the etiology of mammary cancer. Dogs live in the same environment as humans, both urban and rural, and are exposure to the same carcinogens as humans are; thus, the potential of environmental factors influencing tumour development is inevitable. There are a number of environmental carcinogens that are linked to the development of many cancers in dogs (Andrade *et al*, 2010), however there is little knowledge around the carcinogens causing mammary cancer. Pesticides are among the environmental contaminants that are used at an increasing rate (Andrade *et al*, 2010), in particular pyrethroids have shown to stimulate the growth of mammary tumours (Sévère *et al*, 2015). Pyrethroids, a group of synthetically made pesticides, induce a breakdown in the homeostatic balance of hormones, in particular oestrogen, indirectly influencing cell proliferation or apoptosis and initiating neoplasm growth (Garey *et al*, 1998; In, et al, 2005; Montes-Grajales, D., and Olivero-Verbel, J. 2020). Pyrethroids have been shown to be present in abundance in canine mammary carcinomas, for which 33.3 % of pyrethroids were found in the adipose tissue of the mammary gland (Andrade et al, 2010; Sévère *et al*, 2015).

1.2 Treatment

1.2.1 Diagnosis and Surgery

Dogs that are diagnosed with cancer of the mammary glands are presented to veterinarians with the occurrence of lumps or malformations of the mammary gland. Dogs may also be presented to veterinarians due to the sudden appearance of symptoms such as fatigue, lethargy, and weight loss and lymphoedema (Sorenmo, 2003; Sleenckx, *et al.*, 2011). Early assessments are made upon the patients' profile which include age; age at which ovariectomy or ovariohysterectomy, clinical history including any reproductive cycles, pregnancy and lactation, general condition and physical examination (Cassali, *et al.*, 2017). The severeness of the symptoms presented are dependent on the progression and location of the tumour.

Veterinarians analyse the severity of the tumours through a process of staging the progress of tumour development, this allows accurate and conclusive information to be gathered that will ultimately influence the outcome of treatment options. Tumour staging is correlated with the size of the tumour and the presence of local and distant metastases found within lymph nodes and surrounding tissues (Table 1.1). Dogs diagnosed at Stage 1 are reported to have the longest survival time with 97.6% of dogs remaining in remission for more than 2 years (Augusto, 2014; Gundim, *et al.*, 2016). Survival is then greatly reduced to 13.6% of dogs that are diagnosed with Stage 3 and further (Augusto, 2014). Haematological and biochemistry profiles may be performed to the presence in abnormalities such as thrombocytosis, hyperproteinaemia and leukopenia to determine the staging of cancer, alongside a three-view thoracic radiograph to evaluate the presence of metastasis in the lungs (Sleeckx *et al.*, 2011; Lallo, *et al.*, 2016). X-rays are typically taken before surgical intervention of the primary tumour due to the high risk of pulmonary metastasis, shown as rounded radiodensities (Novosad, 2003) this procedure influences the decision to perform surgery or not.

Table 1.1: Staging Classification of Canine Mammary Tumours

Adapted from Anderson, 2014 and Gundim, *et al.*, 2016.

Stage classification	Primary Tumour	Regional Lymph nodes	Distant Metastasis
Stage 1	<3cm	No presence of regional lymph node involvement	No presence of distant metastasis
Stage 2	3-5cm	No presence of regional lymph node involvement	No presence of distant metastasis
Stage 3	>5cm	No presence of regional lymph node involvement	No presence of distant metastasis
Stage 4	Any size	Metastasis in ipsilateral lymph nodes	No presence of distant metastasis
Stage 5	Any size	Metastasised to numerous lymph nodes	Distinct metastasis detected

Surgical biopsy of the tumour is recommended as the initial diagnostic approach to perform cytological analysis to identify the cellular composition of the tumour structure, size and shape of the cell, nuclear size and establish the extent of the cancer progress (Simon, *et al.*, 2009; Dolka, *et al.*, 2018).

Prior to diagnosis and establishing whether the mammary cancer is benign or has metastasised, surgical intervention is the initial source of treatment. The approach of surgery is also determined

by the location, size and current health status of the dog, yet if surgery is approved various surgical techniques are implemented dependent on those factors (Tran, *et al.*, 2016). Localised tumorous lumps can be removed via a lumpectomy which simply remove the cancerous tissue with little removal of surrounding healthy tissue. Regional mastectomies are performed with tumours that have been associated with metastasising to localised glands and lymph nodes. In more extreme cases when several mammary glands are diagnosed as malignant, a unilateral or bilateral mastectomy may be performed to remove complete or half of the mammary glands to prevent further spread of cancer to lymph nodes (Tran, *et al.*, 2016; Litterine-Kaufman, *et al.*, 2019). In addition to surgery, benign mammary cancers are treated with surgery, but mammary cancers that have metastasised may benefit with the addition of adjuvant therapies such as radiotherapy and chemotherapy (Arenas, *et al.*, 2016).

1.2.2 Adjuvant therapies

1.2.2.1 Radiotherapy

Radiotherapy is an additional effective source of treatment utilised to treat solid tumours or to treat surrounding tissues after surgical excision. The aim of radiation is to damage cancerous cells both directly and indirectly through the formation of free radicals that ultimately target the DNA and other organelle structures inducing apoptosis in the cells (Ward, 1988; Kumar, *et al.*, 2010). Therapeutic use of radiotherapy is determined through type, size and location of the tumour and thus influencing the form of radiation used (LaRue and Gordon, 2012). Electromagnetic, such as x-rays or gamma rays and Particle radiation such as proton, electron or neutron-based therapy are commonly used forms of radiotherapy mainly due to the cost and availability (Del Portillo, *et al.*, 2020). Electron therapy is predominantly used for superficial lesions, due to the penetration of the electron being limited and thus less effective in deep tissues, whilst photon therapy is used for deep tissue cancer (Del Portillo, *et al.*, 2020). Radiotherapy is used to numerous cancer tumours in dogs such as nasal carcinomas, sarcomas, brain tumours, oral tumours, thyroid and mediastinal neoplasia, spinal cord and many others (Farrelly, and McEntee, 2014; Serras, *et al.*, 2019). The use of external beam radiotherapy isn't a favoured approach when treating mammary cancer,

predominately due to the reported damages and side effects associated with tissue damage to localised organs (Murphy, 2008; Serras, *et al.*, 2019; Del Portillo, *et al.*, 2020).

1.2.2.2 Chemotherapy

Surgery alone is not effective on mammary cancers diagnosed as metastasised malignancies (Moe, 2001; Dolka, *et al.*, 2018). Malignancy of mammary cancer is problematic, as systemic treatment is not readily available with the addition of no established guidelines for treatment beyond surgery (Sleeckx, *et al.*, 2011). Chemotherapy is an option with regards to systemic treatment of metastases, however reports have stated the several chemotherapy drugs either produce no significant improvement to the patient, or induce high toxicity causing severe side effects which led to death (Sleeckx *et al.*, 2011; Chaisakul *et al.*, 2016).

Commonly used Cyclophosphamide is an alkylating agent that induces a cytotoxic effect by replacing hydrogen atoms on biologically active molecules with an alkyl radical, disrupting DNA replication and RNA transcription (Karayannopoulou, and Lafioniatis, 2016). Although effective on treating mammary cancer it has been reported that after 1 and 2 weeks of treatment leukopenia is observed with the addition of anaemia and thrombocytopenia (Todorova, *et al.*, 2005). Chemotherapy drug combinations have been reported to increase efficacy on cancer treatment compared to individually. 5-fluorouracil a pyrimidine analogue interfering with DNA and RNA synthesis and cyclophosphamide has been shown to increase the overall survival time of dogs by 24 months with reduced side effects, yet mild neutropenia was observed within the normal limits (Karayannopoulou, *et al.*, 2001). Doxorubicin, another cytotoxic drug that binds to the nucleic acids between DNA strands inhibiting DNA and RNA synthesis, is another chemotherapeutic drug that can be used in combination with other drugs such as 5-fluorouracil and cyclophosphamide, but yet again severe side effects are observed such as haematological and gastrointestinal toxicity (Todorova, *et al.*, 2005; Finotello, *et al.*, 2017). Anti-cancer drugs are excreted from the body through the kidneys and liver, yet if these organs are damaged through treatment and their function is not restored, then rapid accumulation of these drugs can result in severe and non-controllable intoxication, leading to death; with Doxorubicin is an example of

an anti-cancer drug that is observed to cause liver damage. (Todorova, *et al.*, 2005; Simon, *et al.*, 2006).

The efficacy of chemotherapy treatment for any cancer in dogs and the toxic side effects have a very small boundary. The common side effects produced through various chemotherapy drugs are not life threatening, such as lethargy, anorexia, vomiting, diarrhoea, fever; however, more adverse side effects produced such as gastrointestinal signs, bone marrow suppression and immunosuppression have a negative impact upon the survival of dogs, which is reported in many studies (Karayannopoulou, *et al.*, 2001; Novosad, 2003; Augusto, 2014; Chaisakul *et al.*, 2016).

1.3 Biomarkers in Canine Mammary Cancer

1.3.1 Molecular markers

Heterogeneity of mammary cancers is clearly observed within the clinical environment, with cancers consisting of complex phenotypes (Nunes, *et al.*, 2019). Limited literature has attempted to examine the histopathological classifications and associate to the type of mammary tumours and prognostic features (Varallo., *et al.*, 2019), with few studies investigating the classification of immunohistochemical markers on canine mammary cancers. Furthermore, classification of mammary cancer in dogs has adapted the classification of Human breast cancer (Goldschmidt, *et al.*, 2011). Utilising this classification has proved to be effective as current phenotypic profiles of canine mammary cancer have showed accurate association with prognosis (Im, *et al.*, 2014; Nunes, *et al.*, 2019).

The most studied biomarker in canine mammary cancer is Ki-67. Used as a prognostic biomarker, Ki-67 is a nuclear non-histone protein that is only detectable during interphase in mitosis (Giziński, *et al.*, 2003). Ki-67 has been reported to be undetectable in normal canine tissues, whilst high levels are observed in aggressive metastasised mammary tumours (Nowak, *et al.*, 2016; Neumann, *et al.*, 2017). Another important biomarker in canine mammary cancer associated with cell proliferation is P53. Commonly found within human breast cancer, P53 is responsible for controlling the cell cycle process, and suppresses tumour development. However, during cancerous

development a genetic mutation alters the P53 gene and as a result its role has transforms to an oncogene (Sorenmo, 2003).

Represented in inflammatory canine mammary cancer, the cyclooxygenase enzyme, primarily cyclooxygenase 2 (Cox-2) responsible for prostanoid biosynthesis, plays an important role in tumour development (Queiroga, *et al.*, 2011; Caralho, *et al.*, 2016)). Cox-2 is not detectable in normal tissue, but is present in high levels in tumours due to inflammatory reactions, growth factors and tumour promoters (Queiroga, *et al.*, 2010). Identified as a good prognostic factor, Cox-2 inhibitors such as meloxicam or piroxicam that inhibit cell proliferation and angiogenesis, produce an increase survival rate in dogs compared to traditional chemotherapies (Knottenbelt, *et al.*, 2006; Carlos, *et al.*, 2009).

Exposure to sex hormones, predominantly oestrogen and progesterone have been associated with tumour growth. Overexpression of oestrogen and progesterone receptors in association with prolactin receptors have been shown in metastasised tumours, with low levels in benign tumours. Expression of these receptors have been deemed a good prognostic factor in terms of treatment outcomes (Mainenti, *et al.*, 2014), however tumours that do not express these receptors have a poor prognostic outcome with regard to the efficacy of chemotherapy (Kim, *et al.*, 2014). In terms of targeting these receptors in treatment, it has been observed to be a success in humans such as Tamoxifen, however a study revealed a negative impact of hormone-based therapies due to the development of estrogenic side effects, such as vulva edema, purulent vaginal discharge and pyometra (Morris, *et al.*, 1993; Tavares, *et al.*, 2010). Alongside the expression of oestrogen and progesterone receptors, the human Epidermal Growth Factor Receptor 2 (HER2) receptor is known to be overexpressed in cancer. Expression of the HER2 receptor is an indicative marker of a poor prognosis in both benign and metastasised malignancies.

1.3.2 HER2

1.3.2.1 HER2 Expression in Canine Mammary Cancer

HER2 has been reported to be overexpressed in canine mammary cancer by 30%, which is equivalent to the overexpression observed in human breast cancer (Singer, *et al.*, 2012; Campos. *et al.*, 2015; Kaszak, *et al.*, 2018). HER2 overexpression has only been identified in metastasises

and not in benign tumours, thus it is implied that HER2 plays a role in malignant progression (Peña, *et al.*, 2013). In relation to human breast cancer, HER2 has been associated with shorter time of relapsing, and a low survival rate in women (Seung, *et al.*, 2020). The relevance of overexpressed HER2 and the association with tumour progression and a poor prognostic indicator is not clearly outlined within literature, predominantly due to the lack of structured evaluation of significant biomarkers and their implications towards canine mammary cancer (Peña, *et al.*, 2013; Uزابaci, *et al.*, 2020; Seung, *et al.*, 2020)

HER2 is an established therapeutic target in human breast cancer with the development of several anti-HER2 drugs trastuzumab, pertuzumab, lapatinib, neratinib and trastuzumab emtansine (Lopez-Albaitero, *et al.*, 2017; Oh and Bang, 2020). In addition, with many sources of literature accumulating evidence in the abundance of HER2 expression in canine mammary cancer, HER2 is becoming a dominant reoccurring biomarker present in canine cancers, with the potential of developing an anti-HER2 therapeutic to combat canine mammary cancer (Peruzzi, *et al.*, 2010; Mason, *et al.*, 2016).

1.3.2.2 HER2 Structure, Activation and Cell Signalling

HER2 is a member of the Epidermal Growth Factor Receptor (EGFR) from the tyrosine kinase family consisting of four homologous members; EGFR, also known as ERBB1 or HER1, HER2, also known as ERBB2, HER3 or ERBB3 and HER4 or ERBB4 (Mitchell *et al.*, 2018). Receptor tyrosine kinases are a subclass of the tyrosine kinases, which are essential components in the signal transduction pathways that effect cell proliferation, differentiation, migration and metabolism (Hubbard, 1999; Hubbard and Miller, 2007; Du and Loyly, 2018). Genomic alternations of the receptor tyrosine kinases have been associated with the development of many cancers and are a predominant area of studying human cancer development and treatment innovation (Du and Loyly, 2018; Fedorova, *et al.*, 2020).

The four receptors in the epidermal growth factor receptor family collectively share homologous structures (Figure 1.3) with each EGFR receptor, comprised of a large extracellular region, a single spanning transmembrane domain, an intracellular juxtamembrane region, a tyrosine kinase domain and a C-terminal regulatory region.

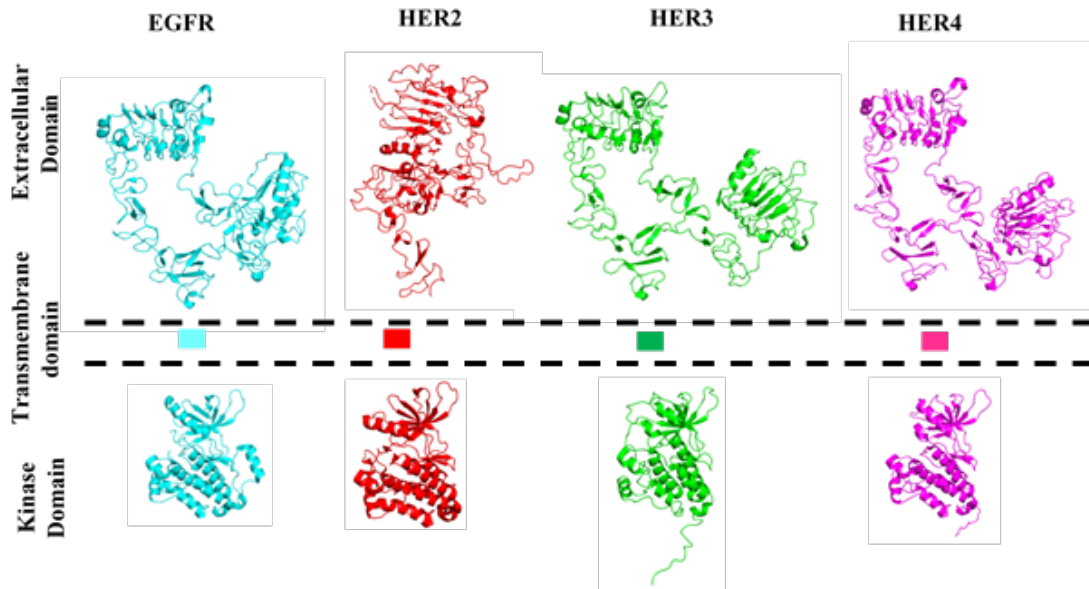


Figure 1.3: Four receptors of the Human Epidermal Growth Factor Receptor Family

Displays the four members of the Human EGFR family: EGFR (Blue) (PDB: 4UV7 and 5D41), HER2 (Red) (PDB: 1N82 and 3PP0), HER3 (Green) (PDB: 4LEO and 5KEX) and HER4 (Pink) (PDB: 2AHX and 3BBW).

Activation of the receptors rely on the binding of ligands such as Epidermal growth factor (EGF), Transforming growth factor alpha (TGF α), or the Neuregulins (N-1), to the extracellular domains, where the EGFR receptors undergo homo/hetero-dimerisation and transphosphorylation of the intracellular domains (Figure 1.4) (Garrett, *et al.*, 2003). The phosphorylation of tyrosine kinase residues initiates an abundance of intracellular signalling molecules, leading to the activation of a plethora of downstream signalling pathways responsible for a diverse range of biological effects. Across EGFR, HER3 and HER4 the receptor proteins initially express the extracellular domain in a closed inhibited conformation, with the need of ligand binding to induce conformational change and promotes dimerisation activation and transphosphorylation (Burgess, *et al.*, 2003; Moasser, 2017). The formation of dimers appears to occur in a hierarchical order, favouring heterodimers or homodimers. The functionality of HER2 shows a dominance of favouring heterodimers over homodimers, due to HER2 having the strongest kinase activity and the formation of heterodimers producing the strongest signalling function (Moasser, 2007). HER2 does not possess the pivoting action between active and inactive conformation unlike the other members of the EGFR family. HER2 remains within an activated form due to domains I and III interacting with each other

(Garret, *et al.*, 2003). As a result of HER2 remaining in the conformational active state, HER2 lacks the ligand binding activity and thus relies on its signalling function induced by ligand activation from heterodimer formation (Wang, *et al.*, 2006). HER3 also lacks structural integrity with the lack of ATP binding located in the catalytic domain on the tyrosine domain, resulting in HER3 being catalytically inactive (Wallasch, *et al.*, 1995; Amin, *et al.*, 2010). Alike HER2, HER3 relies on the formation of heterodimers to seek kinase activity, with observation highly suggesting HER2 and HER3 complex forms the most active signalling heterodimer and is essential for biological processes (Amin, *et al.*, 2010; Timmermans-Sprang, *et al.*, 2017).

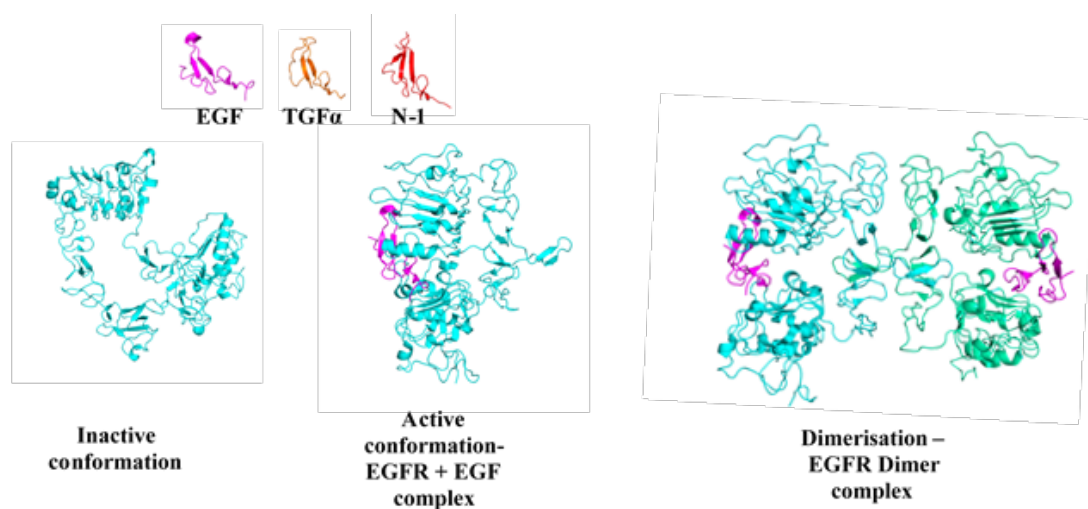


Figure 1.4: Activation of EGFR receptor

Displays the conformational change from inactive EGFR (PDB:4UV7) to the active conformation in protein-ligand complex with Epidermal growth factor (EGF) (PDB: 1IVO) or other ligands Transforming growth factor alpha (TGF α) (PDB: 1MOX), or the Neuregulins (N-1) (PDB: 3U7U). Formation of a homodimer after activation of EGFR.

1.4 Dogs as a model for Human Breast Cancer

Comparative oncology represents an important field in biology that integrates the study of naturally occurring cancers in animals into the study of human cancers and therapies (Paoloni and Khanna.,2008). Naturally occurring cancers in humans and dogs share a number of similarities, including histological appearance, tumour genetics, molecular biomarkers and biological behaviour (Paoloni and Khanna.,2008). Studying dogs with cancer provides a valuable insight

into disease development, as with humans they share a common environment, and therefore exposed to the same carcinogenic risks.

Dogs develop spontaneous tumours and share a common environment with people and, therefore, may be exposed to the same carcinogens. In addition, as in humans, advancing age, progesterone treatment, obesity in early life and diet increases the risk of mammary tumours in dogs. Therefore, dogs are considered a natural animal model of human breast cancer for testing new drugs and preventive modalities, prior to human clinical trials (Rezia et al 2009, Rivera and von Euler, 2011; Gray, *et al.*, 2020). Similarities between humans and dogs at molecular level are highly observed, with overexpression of steroid hormone receptors which include oestrogen, progesterone and androgens; proliferation marker such as EGFRs, metalloproteinase and cyclooxygenase overexpression, and p53 mutation (Queiroga, *et al.*, 2011; Abdelmegeed and Mohammah, 2018). Furthermore, comparative oncology is a not a new concept, with many studies utilising dogs to study naturally occurring cancer, however the implementation of using dogs for drug development is not a coming used practice (Paoloni and Khannah, 2008; Gray, *et al.*, 2020).

Utilising the dogs as a comparative model allows researchers to study cancer in a few years instead of decades, due to the shorter lifespan of the dog. In relation to the use of dogs rather than rodents, dogs are more comparable to humans in terms of size, anatomy, physiology, metabolism, immunology and genetics ((Gordon and Khanna, 2010; Gray, *et al.*, 2020). Greater similarities are observed between dog and human with regards to genomic comparisons, compared to human and rodents (Hoffman and Birney, 2007). Rodent models have provided to be a useful model of human cancer research, particularly in research areas of biology pathway, initiation promotion and progression, but rodent models do not accurately represent definitive features found in humans such as genomic instability, heterogeneity in tumour cells and the surrounding microenvironment (Gordon, *et al.*, 2009). The clinical environment for which both human and dogs occupy such as surgery and imaging and treatment are more reproduceable and alike and are harder to apply to the conventionally used model of the rodent (Gray, *et al.*, 2020). This accumulation of similarities and translational results make dogs an excellent model for translational cancer research (Gordon and Khanna, 2010).

1.5 Animal Venom

1.5.1 Venom components

Animal venom consists of a complex mixture of bioactive molecules secreted by specialised glands with a purpose to kill prey through the infliction of a wound delivering venom, which disrupts normal physiological or biochemical processes to facilitate feeding or defence by the producing animals (Utkin, 2015). Molecules within the venom being proteins and peptides, are potent to selective physiological processes dependent on its target (Casewell, et al, 2013). Venoms are comprised of a mixture of protein, peptides, salts and organic components, furthermore the composition of venom varies based on differing species within a family, the geographical location and the ecological niche that the species inhabit (Kuhn-Nentwig, *et al.*, 2011; Tasoulis and Isbister, 2017). The peptide component of the venom is typically responsible for the main pharmacological characteristics of whole venom which can be broadly categorised as neurotoxic, haemolytic, cardiotoxic, digestive, haemorrhagic (Takacs and Nathan, 2014).

1.5.2 Toxins in Medicine

Natural products such as toxic secretions from plants and animals have played a vital role in influencing novel drug design and development (Newman, *et al.*, 2016), from traditional remedies to modern medicines over hundreds of years. They were used to treat a number of health conditions such as arthritis, smallpox, leprosy, fever and wound healing (Pennington *et al.*, 2018). The first recorded medical use of venom dates back to 37 B.C, when Mithridates suffered a sword wound to the thigh, his doctor applied a small amount of viper venom (*Viper ursinii*) to stop the bleeding which saved his life (Bhattacharjee and Bhattacharyya, 2014). While venoms were seen in traditional healing, the use of toxins in medicine began in the 1940s (Harvey, 2014); however, the toxins were from plants not animals. A key ingredient tubocurarine from the toxin curare, was traditionally used to create poison arrows in South America, was then used in the practice of anaesthesia (Wang, *et al.*, 2018). Tubocurarine's toxic effect causes muscle paralysis which was used alongside general anaesthetics to allow patients undergoing major surgery to be paralysed without using dangerously high doses of general anaesthetics (Wang, *et al.*, 2018).

Toxins from animal venoms were not introduced into human medicine until the late 20th century. Studying snake venom originated back to the late 19th century after theories of venom from a South American snake (*Bothrops jararaca*) inhibited the actions of bradykinin (Ferreira, 1965; Opie and Kowolik, 1995); a protein mediator responsible for vessel dilation. After identification of the inhibitor as an angiotensin converting enzyme (ACE) and demonstrated in humans in 1971 to reduce hypertension, it led to the creation of an ACE inhibitor drug called Captopril in 1981 (Cushman, *et al.*, 1977; Harvey, 2014). Manufacturing of Captopril has been recognised as triggering further studies of venom as a source of new medicines (Harvey, 1992; Takacs, and Nathan, 2014).

1.5.3 Venoms in Modern medicine

With the advancement of venom components undergoing purification and the understating of venom structures at a molecular level, proteins and peptides are understood to be the bioactive component within venom. In terms of drug discovery and design, venom proteins and peptides serve as templates and scaffolds to increase the specificity and increase potency of drug development (Bhattacharjee and Bhattacharyy, 2014). Pharmaceutical industries have recognised the therapeutic potential venom beholds, thus exploited the selective and sensitive characteristics to develop drugs used in todays medicine. The first venom derived drug Captopril was derived from bradykinin-potentiating peptides isolated from *Bothrops jararaca* (Brazilian arrowhead viper) venom to inhibit Angiotensin Converting Enzyme for hypertension (Cushman, D.W. *et al.*, 1977; Harvey, A., 2014).

Tirofiban and Eptifibatide are anti-platelet drugs approved from the treatment of patients suffering with angina and heart failure (King, 2011). Tirofiban, also known as Aggrasts, is a small molecule based on the structure of Echistatin, and a protein found in the venom of the saw-scaled viper (*Echis carinatus*) (Lazarovici, *et al.*, 2019).. Eptifibatide, also known as Integrilin, is a heptapeptide derived from Barbourin, a protein found in the venom of the American Southeastern pygmy rattlesnake (*Sistrurus miliarius barbourin*) (Lazarovici, *et al.*, 2019). Exenatide, also known as Byetta, is a synthetically exendin-4 peptide used for the treatment of type 2 diabetes. Derived from the Glucagon-Like Peptide-1 (GLP-1), it stimulates insulin secretion and modulate

gastric emptying to slow the entry of sugars into the bloodstream. GLP-1 peptides were originally derived from the saliva of Gila monster (*Heloderma suspectum*) venomous lizard, and the drug was approved for use in 2005 (Furman, 2012; Calderon *et al.*, 2014). Approved in 2004, Ziconotide, also known as Prialt, was licenced as a non-opioid pain therapeutic. Derived from the Magical cone snail (*Conus magus*) (Safavi-Hemami, *et al.*, 2019). Ziconotide blocks the N-type calcium channels within the spinal cord and inhibits the release of pain related neurotransmitters (Schmidtko, *et al.*, 2010).

1.5.4 Anticancer activity

Cancerous cells have the ability to avoid cell-cycle check points responsible for maintaining intracellular homeostasis making them immortal. This ability to continuously grow and survive have been identified as the Hallmarks of Cancer include sustaining proliferative signalling, evading growth suppressors, activating invasion and metastasis, enabling replication immortality, inducing angiogenesis, and resisting cell death

(Hanahan and Weinberg., 2011) as previously mentioned. Anti-cancer mechanisms have been shown to exploit the hallmarks of cancer across literature, with recent studies revealing the interactions of venom peptides with membrane receptor molecules and non-receptor components, affecting cell signalling pathways and cell organelles initiating cell death (Ma and Kwok, 2017).

Peptides from the venom of a Bee (*Anis mellifera*), Melittin, has been shown to have anti-tumour effects inducing mitochondria-mediate apoptosis; with anti-tumour effects observed across a number of human cancers, such as renal cancer, lung cancer, liver cancer, prostate cancer, bladder cancer, mammary cancer, and leukemia (Dempsey, 1990; Kong, *et al.*, 2016).

Phospholipases A (2) (PLA2s) are enzymes that catalyse the hydrolysis of ester binds in phospholipids to produce free fatty acids and lysophospholipids. A novel PLA2s, Hemilipin purified from *Hemiscorpius lepturus* scorpion venom has been observed to inhibit angiogenesis without inflicting cytotoxic effects on human lung cancer (Jridi, *et al.*, 2015).

Cardiotoxin III from the Chinese Cobra snake (*Naja atra*) has been observed to induce anti-cancer effects towards several forms of human cancers. Cardiotoxin III induces cell death by producing endoplasmic reticulum and mitochondrial stress, that has been observed in Human colorectal

cancer, leukaemia and breast cancer (Yang, *et al.*, 2005; Tsai, *et al.*, 2006; Chien, *et al.*, 2008; Chiu, *et al.*, 2009).

To date there is no literature investigating the anti-cancer effects of venom on canine cancer. However, across a board range of literature, studies are evidently observing promising inhibiting effects of venom peptides towards many human cancer types. Thus, utilising translational and comparative oncology, animal venoms may induce anti-cancer effects on Canine Mammary Cancer.

1.6 Statement of Purpose and Experimental Aims

Treatment for Canine Mammary Cancer has shown to have devastating side effects to dogs, and research into this area is limited and an ongoing issue. Thus, the need for a novel solution in treating the disease is evident. Venoms are composed of a complex mixture of biological proteins and peptides that have shown to suppress cancer viability through a variety of mechanisms inducing apoptotic death in human cancer cells.

Therefore, there is a biological importance to the study of efficacy of venoms in the application of cancer treatment in dogs as a potential novel therapeutic. Utilising two canine mammary cancer cell lines CMT28 and CMM26 to represent the heterogeneity of cancers found in the clinical environment, and an immortalised normal canine kidney cell line MDCK, these cell lines will be screened against a panel of venoms to observe if there are the cytotoxic effects towards the viability of each cell line. Aims within this thesis incorporate assessing the binding affinities of the HER2 receptor, as potential target, to proteins and peptides found within venoms, and use computational modelling to predict possible inhibiting binding regions between identified proteins and HER2.

Overall, the aims of this project are to:

- To optimise an *in-vitro* cell viability assay to screen a panel of whole snake venoms against the CMT28, CMM26 and MDCK cell lines to observe cytotoxic effects
- To screen a compound library assay of snake and invertebrate fractionated venoms for cytotoxicity against the CMT28, CMM26 and MDCK cell lines

- To assess whether selective susceptibility of 'hit' venom fractions can be observed between the cancerous cell lines, CMT28 and CMM26, and a non-cancerous cell line, MDCK
- To identify active venom components using Intact mass and Peptide digest mass spectrometry that show significant reductions in cell viability of the cancerous cell lines compared to the non-cancerous cell line
- To compare and analyse mass spectrometry data to existing sequences found within databases
- To construct the Canine HER2 receptor using protein structure prediction server
- To construct the structures of identified proteins from mass spectrometry using protein structure prediction server
- To simulate and predict the binding between the Canine HER2 receptor and identified proteins using a protein-protein docking prediction server

CHAPTER 2 – Materials and Methods

2.1 Introduction

This chapter includes general methodology that was used across the integrity of the project. Other methodology that are specific to area of the project can be found in the relevant chapters.

Methodology related to the optimisation and validation of the initial cytotoxic screening of venoms using the resazurin assay can be found in **section 3.3**. Optimisation and screening of T-VDA^{ctx} assay is located in **section 4.3**. Methodology in relation to HER2 receptor expression and activity influenced by venom using fluorescent microscopy and molecular dot plots can be found in **section 5.3.1** and **section 5.3.2-5.3.4**. Generation and optimisation of the canine HER2 receptor, as well as molecular docking of the receptors and proteins using computational modelling can be found in **section 5.3.5-5.3.11**

2.2 Cell Culture

2.2.1 Cell lines

This study used two canine mammary cancer cell lines CMT28, derived from a mammary carcinoma (Wolfe, *et al.*, 1986), and CMM26 also derived from a mammary cancer carcinoma (Cassali, *et al.*, 2012) and an immortalised normal canine kidney cell Madin-Darby Canine Kidney (MDCK) derived from a kidney of a normal adult female cocker spaniel, September 1958, by S.H. Madin and N.B. Darby according to the American Type Culture Collection (ATCC). Additional cell lines utilised in this study consisted of a Human breast cancer cell line SKBR3 derived from a metastasis site (pleural effusion) (Trempe, 1976) and the COS 7 cell line derived from the kidney of the African Green Monkey. The cell lines were kindly gifted by Professor Bill Gullick from the University of Kent (Kent, UK).

2.2.2 Maintenance and Culturing of Cell lines

All cell lines were cultured as adherent monolayer cells. CMT28 and MDCK cell lines were cultured in Dulbecco's Modified Eagle Medium (DMEM) (Gibco, UK), supplemented with (10%) Foetal calf Serum (FCS) (Gibco, UK), (1%) L-Glutamine (Gibco, UK) and (1%) penicillin-streptomycin (Gibco, UK). CMM26 cell line were cultured in RPMI-1640 medium supplemented with (10%) Foetal calf Serum (FCS), (1%) L-Glutamine and (1%) penicillin-streptomycin. All cell lines were cultured in 75cm³ culture flasks and were incubated at 37 °C in a humidified atmosphere containing 5% CO₂ and 95% air.

Cell lines were passaged when the cells reached >80% cell confluency. All culture media was removed from the flasks and washed with 10ml of warmed sterile Phosphate buffered saline (PBS) (Gibco, UK) solution. For CMT28 and MDCK cell lines, 1ml of Ethylenediaminetetraacetic acid (EDTA)-trypsin (Gibco, UK) (0.05%) and for the CMM26 cell line 1ml of EDTA-trypsin (0.25%) was added to the flasks and incubated until the cells rounded and detached from the flasks. Flasks were gently tapped on the side to assist in detaching the cells. 5ml of fresh DMEM culture media for CMT28 and MDCK cell lines and 5ml of RPMI culture media for CMM26 cells was added to the trypsinised cells and were gently pipetted up and down to separate any clumps of cells. 1ml of cells were pipetted into a 75cm³ flasks and re-suspended in 15ml of culture media. All reagents used in the passaging of cells were prewarmed to 37 °C.

2.2.3 Freezing and Thawing of Cell Line Stocks

CMT28, CMM26 and MDCK cells were frozen to ensure a sufficient supply of cells were readily available. The same procedure was addressed to all cell lines.

Cells were trypsinised from the culture flasks, following section 2.2.2, until the cells were resuspended in fresh culture media. The resuspended cells were aliquoted into 15ml

falcon tubes and centrifuged (ThermoScientific Heraeus Megafuge 8) for 1 minute at 1000rpm. The culture media was removed from the tube and the cells resuspended in 10% dimethylsulfoxide (DMSO) (Fisher Scientific, UK) in (90%) FCS. The cells are transferred into sterile cryotubes (Fisher, UK) where it was stored at -20°C for 2 hours and then transferred to a -80°C freezer for storage and liquid nitrogen for long term storage.

Cells were revived from the -80°C freezer by thawing the cryotubes at room temperature (~25°C). For CMT28 and MDCK cell lines they were resuspended in 2ml of culture media in a 15ml valcom tube and centrifuged at 1000RPM for 1 minute. After centrifugation the supernatant was removed, leaving a white pellet of cells at the bottom of the tube. The pelleted cells were resuspended in 15 ml of fresh supplemented DMEM media and transferred into a 75cm³ flask. CMM26 cells were sensitive to centrifugation, so were transferred into a 75cm³ flask in 15ml of RPMI-1640 culture media. For all cell lines, cells were left to adhere to the bottom of the flask and after 24 hours the culture media containing DMSO was replaced with fresh supplemented DMEM/ RPMI media.

2.3 Venom Resazurin Assay

2.3.1 Cell Counting and Cell Plating

CMT28, CMM26 and MDCK cells were trypsinised as stated in the protocol for maintenance of cell lines, in **2.1.2**. Trypsinised cells were resuspended in a desired volume of media and 20µl of the resuspended cells were mixed with 20µl of Trypan Blue (Gibco, UK). Cell counting was undertaken using a Haemocytometer (Fisher, UK) at a magnification of x10 on a Leica DMI 3000 B inverted microscope. 20µl of the mixture pipetted into both sides, and the four corners of the Haemocytometer were counted, and an average cell number calculated. The total number of cells in the trypsinised flasks was calculated using the following equations:

$$\text{Cells per ml} = \text{Average cell number} \times 2 \times 10^4$$

$$\text{Total cell number} = \text{cells per ml} \times \text{resuspended volume}$$

To plate the cells at the desired cell number and in the desired number of wells, the value calculated from the Cells per ml was applied to the following equation:

$$\text{Volume per well } (\mu\text{l}) = \frac{\text{Desired number of cells}}{\text{Cells per ml}} \times 1000$$

The value calculated is the volume that was pipetted into wells of the plate either 96 or 384 well plates. Dependent on the volume pipetted into the wells, additional culture media was added to each well to avoid cell death. Plated cells were left to adhere to the bottom of the wells overnight, ready for the Resazurin assay.

2.3.2 Venom Treatment for Resazurin Assay

Cell lines were plated at the desired cell number and using the desired plate of either 96 wells or 384 wells, using the protocol from **2.1.2**. Venoms obtained from Venomtech Ltd. were diluted down to a protein stock concentration of ~100mg/ml. Culture media was used to dilute the venoms from stock to working concentrations; supplemented DMEM was used for CMT28 and MDCK cells and supplemented RPMI media used for CMM26 cells. Working concentrations of venoms were made fresh prior to treating the cells and were calculated using the following equation:

$$\text{Working concentration } \left(\frac{\mu\text{l}}{\text{ml}}\right) = \frac{\text{Desired concentration } \left(\frac{\text{mg}}{\text{ml}}\right)}{\text{Stock concentration } \left(\frac{\text{mg}}{\text{ml}}\right)} \times \text{Desired volume (ml)}$$

Culture media removed from each well and 50 μ l of venom from the desired working concentrations added to each well and left to incubated for 2 hours at 37 °C in a humidified atmosphere containing 5% CO₂ and 95% air. After 2 hours the venom was removed and replaced with 50ul of 160 μ M Resazurin media solution.

Fluorescent readings were taken using the BMG FLOUstar plate reader (excitation 544nm, emission 590nm) every 15 minutes for 1 hour and every 30 minutes there after until 5 hours or until the desired time.

2.4 Statistical Analysis and Graphical representation

Graphs generated throughout this thesis were produced using Microsoft Excel, 2019. Statistical Analysis was conducted using Minitab 2020. Parametric statistical analysis was performed after the appropriate test assumption were met; the Normality test (Anderson-Darling) and the test of equal variance (Levenes test). Significance of the data was determined using the biological probability threshold of 0.05 with a 95% confidence prediction. Calculating the LD₅₀ was generated using Graphpad Prism 9.

CHAPTER 3 – Venom Assay Optimisation and Screening of

Whole Venoms

3.1 Introduction

Screening cancerous cells requires the use of an *in-vitro* assay which assesses the viability of cells and reflects the cytotoxic inhibitory effects of venom; with cytotoxicity referred to as an interference with cellular attachments, alteration in morphology, adverse effects on cell proliferation or apoptotic death (Mosmann, 1983; Horváth, 1980; Niles, et al., 2008). 3-(4,5-Dimethylthiazol-2-yl)-2,5-diphenyltetrazolium bromide, also known as the MTT cellular metabolic assay, is a common assay utilised to detect the viability of cells. This colorimetric assay utilises tetrazolium dye which is metabolised into insoluble formazan in proportion to viable cells; formazan is then solubilised in dimethyl sulfoxide (DMSO) and quantified spectrophotometrically using absorbance (Kumar, et al., 2016; Stockert, et al., 2018). Issues arise with the use of absorbance for cell viability detection due to the detectable scale of cell viability and death ranges being small (Van tonder, et al., 2015; Stockert, et al., 2018). This difficulty can be sidestepped with the use of a cell viability assay that utilises fluorescence to detect viable cells, such as the Resazurin assay. Resazurin, also commercially known as Alamar blue, also detects viability of cells which incorporates a redox reaction converting Resazurin (blue) into a fluorescent compound of resorufin (pink). Fluorescence provides a wider range of detectability of viable cells (Riss, et al., 2004); although absorbance can also be used for the Resazurin assay, fluorescence is more favourable as absorbance is less sensitive. Compared to the MTT assay, Resazurin is a non-toxic compound allowing follow up experiments to be performed, unlike MTT which utilises DMSO for detection which in turn lyses cells (Bonnier, et al., 2015; Präbst, et al., 2017).

Utilising the Resazurin assay to detect cytotoxic effects of cells has been demonstrated in literature to accurately distinguish cell death and cell viability with increased sensitivity, thus the decision was made to utilise this assay for the detection of cytotoxic effects of snake venoms on Canine Mammary Cancers cells (CMT28 and CMM26) and a normal immortalised Canine Kidney cell line (MDCK).

3.2 Aims

- To develop and optimise a statistically robust Resazurin cell viability assay to determine if there is cellular cytotoxicity against Canine Cancer cell lines CMT28 and CMM26, and a normal Canine cell line MDCK.
- To screen a panel of snake venoms from the *Naja* genus for cytotoxicity using the optimised Resazurin assay against Canine Cancer cell lines CMT28 and CMM26, and a normal Canine cell line MDCK.

3.3 Materials and Methods

3.3.1 Optimisation of the Resazurin Assay to Determine Cellular Cytotoxicity of Snake Venom

3.3.1.1 Optimal cell number selection for CMT28, CMM26 and MDCK for Resazurin Cell Viability Assay

To optimise the resazurin assay, a suitable number of cells was determined for each cell line to use in the final screening of venoms. CMT28, CMM26 and MDCK cells were trypsinised and plated in a 96 wells plate as described in section 2.3.1. Each cell line was seeded in 96 well plates with 4 different cell numbers 2×10^5 , 1×10^5 , 5×10^4 , 2.5×10^4 . As the lethal doses of the venom was unknown, for each cell number 4 doses of venom were used for CMT28 and CMM26 and these were 100µg/ml, 10µg/ml, 1µg/ml and 0.1µg/ml of *Naja nigricollis* venom. In contrast the MDCK cell numbers were exposed to 100µg/ml, 200µg/ml, 400µg/ml, 800µg/ml and 1mg/ml of *Naja nigricollis* venom. Each cell number was plated in 2 rows for a positive control (venom) and negative control (culture media), in replicas of 3 (Appendix I). The plate was returned to a humidified incubator at 37 °C, 5% CO₂ overnight for the cells to adhere and settle.

The working venom concentrations were made as described in section 2.3.3, and the cells were treated with the venom doses and incubated for 2 hours and the fluorescence was detected as described in the standard protocol in section 2.3.2.

3.3.1.2 Z' Analysis of Cell Number

Using the optimal cell numbers for the 3 cell lines from previous optimisation experiments described in **3.3.1**; CMT28, CMM26 and MDCK cell lines were trypsinised and counted via the standard protocol stated in **2.3.1**. CMT28 and CMM26 were plated out in 96 well plates at a concentration of 1×10^5 and MDCK cells at 2×10^5 . The plates were returned to a humidified incubator at 37 °C, 5% CO₂ overnight for the cells to adhere and settle.

Once adhered to the plate it was divided into positive and negative control replicates as shown in Appendix II. The positive control wells were treated with 50ul *Naja nigricollis* venom at the concentration of 100ug/ml; working venom concentration was made as stated in section **2.3.3**. The negative controls were treated with 50ul of culture media. The cells were treated with the venom doses and incubated for 2 hours and the fluorescence was detected as described in the standard protocol in section **2.3.2**.

A Z' value was calculated, using the following equation for each cell line at each time point:

$$Z' factor = 1 \frac{3(\sigma_p + \sigma_n)}{[\mu_p - \mu_n]}$$

Z' values of above 0.5 considered the assay to be robust, whilst Z' values above 0.7 consider the assay to be excellent. Z' values below 0.5 suggest the assay is not statistically robust and would require further optimisation to produce values above the threshold.

3.3.1.3 Preparation of Working Concentrations of Snake Venom

A panel of venoms from the *Naja* genus (Table 3.1) were provided by Venomtech Ltd (UK) at a protein stock concentration of ~100mg/ml. The stock concentrations of ~100mg/ml of each snake venom was diluted in the appropriate supplemented media to the working concentrations of 100µg/ml, 10µg/ml, 1µg/ml, via the standard protocol in section **2.3.2**. Supplemented DMEM was used to dilute venoms for CMT28 and MDCK cell lines, while supplemented RPMI media was used to dilute venoms of CMM26 cell line.

Table 3.1: Species of Snakes from the *Naja* genus used in the Venom Panel Screen

Code	Name	Common Name	Origin	Spitting/Non-spitting
N.nig	<i>Naja nigricollis</i>	Black-Necked Spitting Cobra	African	Spitting
N.nub	<i>Naja Nubiae</i>	Nubian spitting cobra	African	Spitting
N.mel	<i>Naja melanoleuca</i>	Black forest cobra	African	Non-Spitting
N.pal	<i>Naja pallida</i>	Red spitting cobra	African	Spitting
N.naj	<i>Naja naja</i>	Indian Cobra	Asian	Non-Spitting
N.ka	<i>Naja Kaouthia</i>	Monocled Cobra	Asian	Spitting
N.atr	<i>Naja atra</i>	Chinese Cobra	Asian	Non-Spitting
N.sia	<i>Naja Siamensis</i>	Indochinese Spitting Cobra	Asian	Spitting
N.nct	<i>Naja nigricincta</i>	Zebra spitting cobra	African	Spitting
N.niv	<i>Naja Nivea</i>	Yellow Cape Cobra	African	Non-spitting

3.3.1.4 Initial screening of whole *Naja nigricollis* venom at three selected concentrations

CMT28, CMM26 and MDCK cells were plated into 96 well plates via the protocol described in section 2.3.1, using the optimal cell number chosen in the previous experiment in section 3.3.1.1. Once the cells were plated, they were returned to the incubator overnight to adhere to the bottom of the wells. Once the cells adhered to the bottom of the wells, the media was removed from the cells and replaced with 3 concentrations of whole *Naja nigricollis* venom at 100µg/ml, 10µg/ml and 1µg/ml in triplicates. CMT28, CMM26 and MDCK were treated with venoms as laid out in the plate layout in Appendix III.

The venom treated plates were returned to the incubator at 37 °C, 5% CO₂ for 2 hours. After incubation all of the venom and media was removed from the wells and the fluorescence was detected as described in the standard protocol in section 2.3.2. Fluorescent readings were taken using the protocol described in section 2.3.2. Plate readings were taken of each cell line till the optimal time point chosen in the previous experiment in section 3.3.1.2.

3.3.1.5 Screening Whole Venoms from the *Naja* genus at three selected concentrations

CMT28, CMM26 and MDCK cells were plated into 96 well plates as described in section 2.3.1, using the optimal cell number selected in section 3.3.1.1. Cells were left to settle and adhere to

the bottom of the wells overnight in an incubator at 37°C. Once the cells had adhered to the wells, the media was removed from the cells and replaced with 3 concentrations of whole venom from the *Naja* genus (Table 3.1) at 100µg/ml, 10µg/ml and 1µg/ml in triplicates. The plated cells of CMT28, CMM26 and MDCK were treated with venoms as laid out in the plate layout in Appendix IV.

The venom treated plates were returned to the incubator at 37 °C, 5% CO₂ for 2 hours. After incubation all of the venom and media was removed from the wells and the fluorescence was detected as described in the standard protocol in section 2.3.2. Fluorescent readings were taken using the protocol described in section 2.3.2. Plate readings were taken of each cell line till the optimal time point chosen in the previous experiment in section 3.3.1.2.

3.4 Results and Discussion

3.4.1 Selection of the Optimal Cell Number for an Effective Plate-Based Resazurin Assay

The selection of an optimal cell number for the cell lines CMT28, CMM26 and MDCK was crucial to ensure that the resazurin assay was a robust plate-based assay. All three cells lines were plated with 4 different cell quantities each with different concentrations of *Naja nigricollis* venom. Each cell number was treated with and without the various concentrations of whole venom due to the lethal dose of venom being unknown. The cells were monitored over a time period of 5 hours to establish which cell quantity produced the greatest fold-change in fluorescence.

The fold-change of the cells was quantified into fluorescent readings and was determined by how much the quantity changes between the cells that were treated with venom and those that were not. Thus, the cell number that would produce the greatest fold-change between the treated and untreated cells would be chosen to take forward for venom screening.

For each cell line the fold-changes in fluorescence were calculated for each concentration and for each cell number at selected timepoints throughout the 5 hour reading. Exposure to the various concentrations of whole *Naja nigricollis* venom showed that the lethal dose was 100µg/ml for CMT28 and CMM26 cells, as it was observed that at 10µg/ml and 1µg/ml had no significant fold-change was produced (Appendix V). Using the lethal dose of 100µg/ml for CMT28, the maximum

fluorescent fold-change produced was 23.4-fold at the cell number 1×10^5 , at the time-point of 120 minutes (Figure 3.1). After this time-point the fold-change began to decrease as the newly

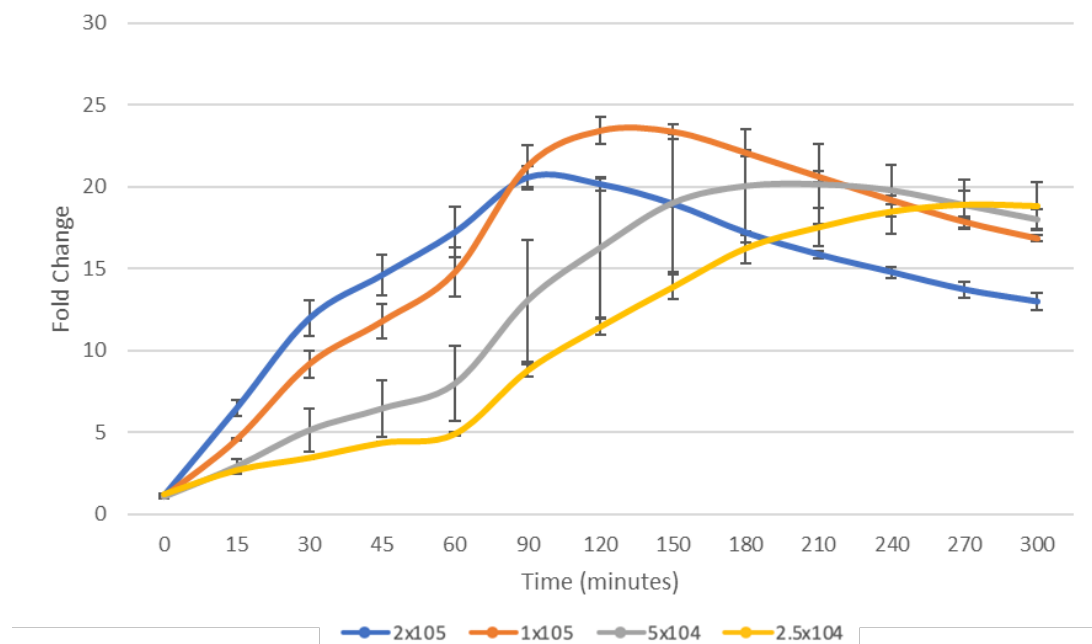


Figure 3.1: CMT28 Cell Number Resazurin Assay

Displays the fluorescent fold-change between the positive ($100 \mu\text{g/ml}$ whole *Naja nigricollis* venom) and negative (No venom, DMEM media only) controls in 4 different cell numbers (2×10^5 , 1×10^5 , 5×10^4 , 2.5×10^4) CMT28 cells. Measured over a time period of 5 hours. (Error bars= STD)

converted resorufin from resazurin was converted to dihydro resorufin, which does not produce fluorescence. None of the other cells numbers were capable to produce such a high fold-change over the 5 hour period, this is was considered to take forward the cell number of 1×10^5 for the Z' analysis.

Observations of the CMM26 cells showed that *Naja nigricollis* whole venom concentrations of $10 \mu\text{g/ml}$ and $1 \mu\text{g/ml}$ showed no lethal inhibitory effects on any of the cell numbers, as the fold-change did not reach higher than a 2 fold-change (Appendix V). Evident fold-changes were shown on all cell numbers (2×10^5 , 1×10^5 , 5×10^4 , 2.5×10^4) that were exposed to the whole venom concentration of $100 \mu\text{g/ml}$ (Figure 3.2). The maximum observed fold-change in fluorescence produced by Resazurin peaked at approximately 30-fold at the cell number of 1×10^5 at 120 minutes thus making this the optimal cell number to take forward for Z' analysis

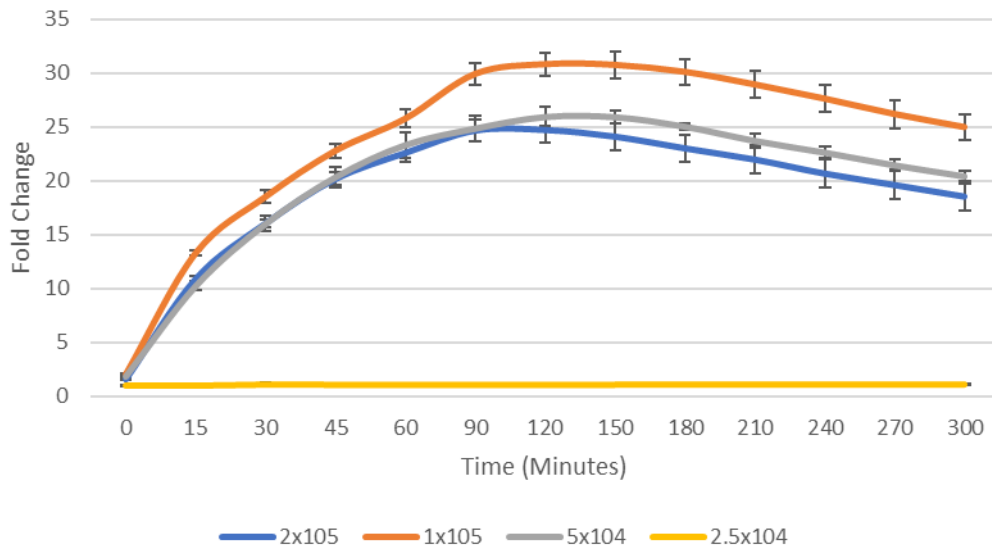


Figure 3.2: CMM26 Cell Number Resazurin assay

Displays the fluorescent fold-change between the positive (100µg/ml whole *Naja nigricollis* venom) and negative (No venom, DMEM media only) controls in 4 different cell numbers (2x10⁵, 1x10⁵, 5x10⁴, 2.5x10⁴) CMM26 cells. Measured over a time period of 5 hours. (Error bars= STD)

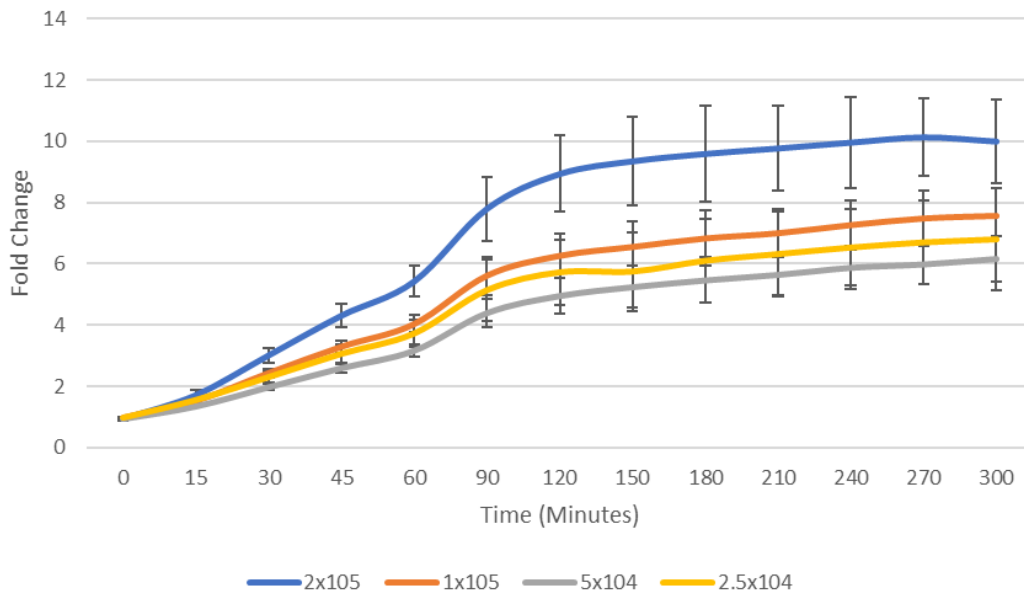


Figure 3.3: MDCK Cell Number Resazurin assay

Displays the fluorescent fold-change between the positive (1mg/ml whole *Naja nigricollis* venom) and negative (No venom, DMEM media only) controls in 4 different cell numbers (2x10⁵, 1x10⁵, 5x10⁴, 2.5x10⁴) MDCK cells. Measured over a time period of 5 hours. (Error bars= STD)

Exposure of 100µg/ml of whole *Naja nigricollis* venom to the MDCK cells did not show any lethal inhibitory effects on the cells, thus it was decided to expose this cell line to higher concentrations. MDCK cells were then exposed to 200µg/ml, 400µg/ml, 800µg/ml and 1mg/ml of whole *Naja nigricollis* venom, where it was found that the lethal dose was 1mg/ml.

Initial comparisons of fold change in the MDCK cells compared to the two cancer cell lines, show that the MDCK cells do not produce as higher fold-change. The maximum fold-change observed was 10.13-fold in 2×10^5 cell number (Figure 3.3). The other cell numbers (1×10^5 , 5×10^4 , 2.5×10^4) did not produce a significantly high fold-change, thus are suitable to take forward.

3.4.2 Z' Analysis of Selected Cell Number

Cell concentrations of 1×10^5 cells were selected for CMT28 and CMM26 cell lines, and 2×10^5 were selected for MDCK cells. The selected cell numbers for each of the cell lines were used to perform the Z' assay to establish if the cell concentrations are appropriate to produce a statistically robust assay. The Z' assay analysis was carried out over a time-period of 5 hours to identify the most robust time point that would be selected to determine the viability of the cells for the following Resazurin assays to determine the inhibitory effects of venom.

Table 3.2: Z' Values for the Resazurin assay for CMT28, CMM26 and MDCK

Displays the Z' values produced for each cell line CMT28, CMM26 and MDCK over a 5 hour time period. Highlighted values (Yellow) indicate the optimal time point chosen.

Time (Minutes)	CMT28Z' value	CMM26 Z' value	MDCK Z' Value
0	-2.07191	0.357309	-3.68981
15	0.473577	0.752566	0.460397
30	0.672429	0.762738	0.533034
45	0.710912	0.781195	0.611446
60	0.811785	0.805692	0.629461
90	0.823946	0.833222	0.62648
120	0.917513	0.847589	0.642681
150	0.915338	0.857336	0.6548
180	0.907563	0.860207	0.643638
210	0.885639	0.863107	0.664549
240	0.853967	0.86394	0.678771
270	0.834572	0.867625	0.713059
300	0.801463	0.872297	0.87354

The CMT28 cell line was considered be a robust assay from 30 minutes, but the assay was verified to be an excellent assay by producing Z' values above 0.7 from the timepoint of 60 minutes (Table

3.2). The greatest Z' value and the most optimal timepoint produced was at 120 minutes producing a value of 0.917. CMM26 cells produced a Z' value which continued to increase at each time point reaching its maximum Z' value of 0.87 at 300 minutes. However, the Z' value began to plateau at 180 minutes producing a value of 0.86, thus this timepoint was chosen at the optimal timepoint to take forward. MDCK cells produced Z' values increased slowly over time until it peaked at 270 minutes producing the optimal timepoint value of 0.713, suggesting that the assay is extremely robust.

Using the Z' assay to determine the robustness of the Resazurin assay on each cell line, it was concluded that each cell line produced an extremely robust assay. This allows each cell line to be taken forward to screen a panel of cobra venoms using the Resazurin assay to determine the inhibitory effects.

3.4.3 Initial screening of *Naja nigricollis* Venom Using the Optimised Resazurin Assay

Initial investigation was conducted using whole venom from the *Naja nigricollis* snake to assess its inhibitory effects on the three cell lines. This was used as a guideline for determining screening concentrations for other venoms. To assess the cytotoxic effects of this venom, the venom was diluted into 3 concentrations of 100 μ g/ml, 10 μ g/ml, 1 μ g/ml.

Both of the Canine Cancer cell lines CMT28 and CMM26 showed significant susceptibility to the whole *Naja nigricollis* venom at 100 μ g/ml (One-way ANOVA with Tukey test $P > 0.05$) (Appendix VI). Cell viability was drastically decreased with 95.84% of CMM26 cells inhibited at 100 μ g/ml and 99.24% of CMT28 cells inhibited by the venom (Figure 3.4). No significant inhibitory effects were observed at 10 μ g/ml and 1 μ g/ml in either of the cancer cell lines.

The Canine Kidney cell line MDCK showed significantly different observations. No inhibitory effects were observed at the concentrations of 100 μ g/ml, 10 μ g/ml and 1 μ g/ml (One-way ANOVA with post-hoc Tukey test $P > 0.05$); suggesting that there is selective cytotoxicity between cancerous and normal cells. Statistical analysis displayed that there is a significant difference between the cancerous cell lines (CMT28 and CMM26) and the normal cell line (MDCK) (Multi-factor ANOVA with post-hoc Tukey test $P > 0.05$) (Appendix VI).

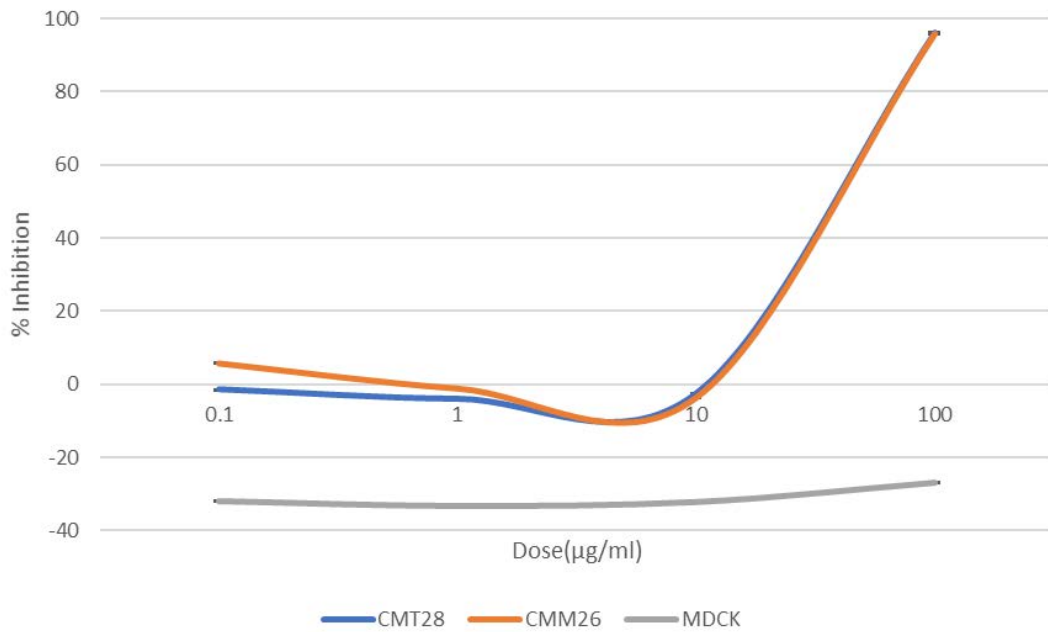


Figure 3.4: Dose Response of *Naja nigricollis* Venom on CMT28, CMM26 and MDCK Cell Lines

Shows the inhibitory effects of whole *Naja nigricollis* venom on CMT28, CMM26, and MDCK cell lines. Inhibitory effects were taken from the optimal time point: CMT28 of 120 minutes, CMM26 of 180 minutes, and MDCK at 270 minutes. (Error bars = STD).

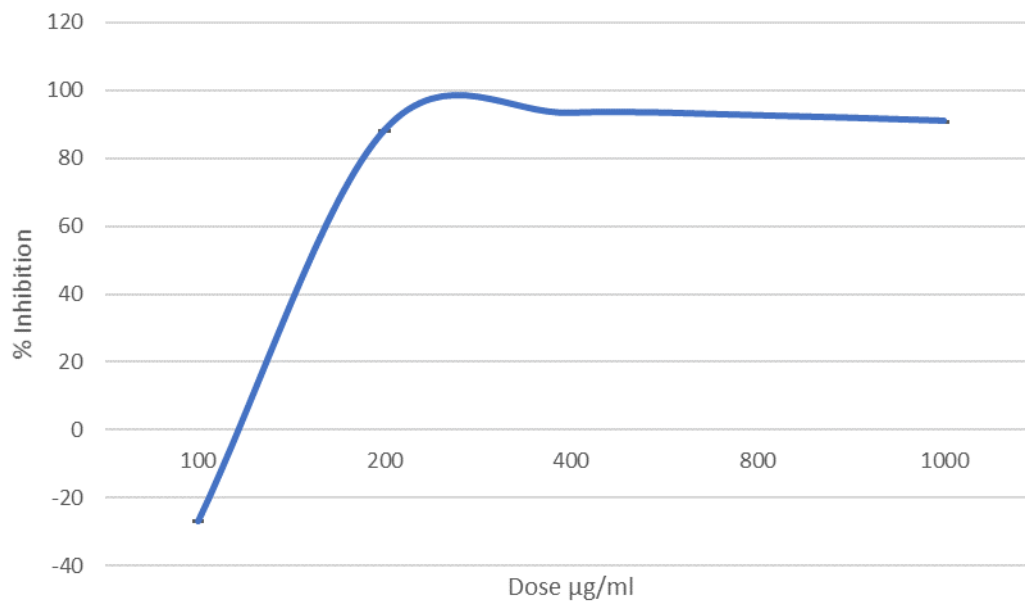


Figure 3.5: Dose Response of *Naja nigricollis* Venom on MDCK cells at Higher Doses

Shows inhibitory effects of whole *Naja nigricollis* venom on MDCK at concentrations of 100µg/ml, 200µg/ml, 400µg/ml, 800µg/ml and 1000µg/ml(1mg/ml). Inhibitory effects taken from the optimal time point of 240 minutes. (Error bars=STD).

Further investigation of the MDCK and identification of the cytotoxic doses of the venom revealed that lethal dose of whole *Naja nigricollis* venom was observed at 200µg/ml (Figure 3.5) (One-way ANOVA with Post-hoc Tukey test $P>0.05$). This confirms that there is selectivity of the venom on cancerous cells, suggesting the target is a molecular mechanism in which the MDCK cells do not share.

3.4.4 Cytotoxic Screening of Snake Venom from the *Naja* genus Using the Optimised Resazurin Assay

Cytotoxic effects were analysed on 9 additional whole Cobra venoms to determine the inhibitory effects these venoms would have on the 3 cell lines. Each cell line (CMT28, CMM26 and MDCK) was exposed to 4 concentrations of each cobra venom to compare the inhibitory effects between cancerous and non-cancerous cells, also to observe the effects between spitting and non-spitting cobras and their geographical locations.

Comparing the cytotoxic effects of the cobras based on geographical location is it observed that cobras from Asia showed a significant increase in toxicity towards both the cancerous and non-cancerous cell line. Whereas cobras from Africa showed a variation in cytotoxicity which is clearly defined between the cobras that spit their venom and those that are non-spitters. CMT28 cells were observed to have an increased sensitivity towards non-spitting African cobra venoms of *Naja nivea* and *Naja melanoleuca*, displaying an inhibition of close to 100% (Figure 3.6 A), whereas marginal inhibitory effects were observed in CMM26 and MDCK in the same venoms, but they were not significant enough to clarify toxicity at the exposed doses. Selective cytotoxicity between the cancerous cell lines may be the result of the expression levels of the target of which the venom influences.

Higher toxic-potency in Asian cobras against human cancer cells has been described in literature (Panagides, *et al.*, 2017), and this was evident towards the 3 cell lines used in this study (Figure 3.6 B). Significantly high cytotoxicity of the Asian cobras (*Naja naja*, *Naja kaouthia*, *N. atra* and *N. siamensis*) was observed across all cell lines (Multi-factor ANOVA with post-hoc Tukey test $P>0.05$) (Appendix VII) with high inhibitory incidence occurring between 10-100µg/ml; no indication of selectivity is present in the dose responses of the venoms towards cancerous and non-cancerous cells.

Spitting cobras have been shown in the literature to have an increased cytotoxic ability towards cells compared to non-spitting cobras, however this has only been evident in cobras from Africa (Kalam, *et al.*, 2011). Relationships have been associated between with toxicity of venom and the physical traits of the cobra, such as hooding, aposematic marking and camouflage. This association is driven by ecological factors, such as prey physiology and defence against predation, which has coevolutionary shifted the composition of venom (Barlow, *et al.*, 2009; Casewell, *et al.*, 2020). Several studies show spitting cobras consistently display cytotoxic traits of inducing local tissue necrosis, whilst non-spitting cobra venom display neurotoxicity inducing muscular paralysis, without necrosis (Kalam, *et al.*, 2011; Kerkkamp, *et al.*, 2018; Abdel-Ghani, *et al.*, 2019; Shahbazi, *et al.*, 2019).

3.5 Conclusion

Optimisation and validation of the Resazurin assay has proven that this is a robust assay to determine the cell-viability of canine cells screened against whole snake venoms. Consistently observed across the *Naja* genus, each species has displayed cytotoxic activity towards the 3 cell lines. Increased potency towards the cancerous cell lines compared to the non-cancerous cell line was expected, predominantly due to the instability of cancer cells having increases sensitivity towards induced apoptotic death. This is because it is hypothesised that the cocktail of components in whole venom induce necrotic activity. It was not conclusive that the data obtained showed that spitting cobras possess increased cytotoxicity compared to non-spitting cobras. Further investigation into doses of the whole venom would draw a clearer conclusion to cytotoxic activity of the cobra venoms.

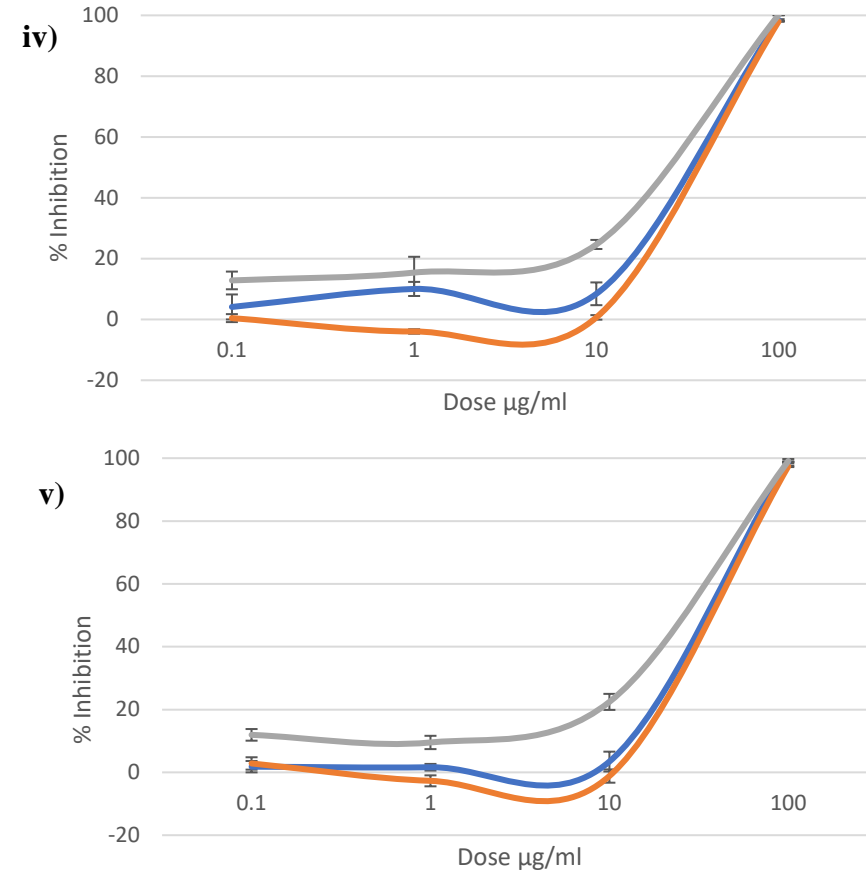
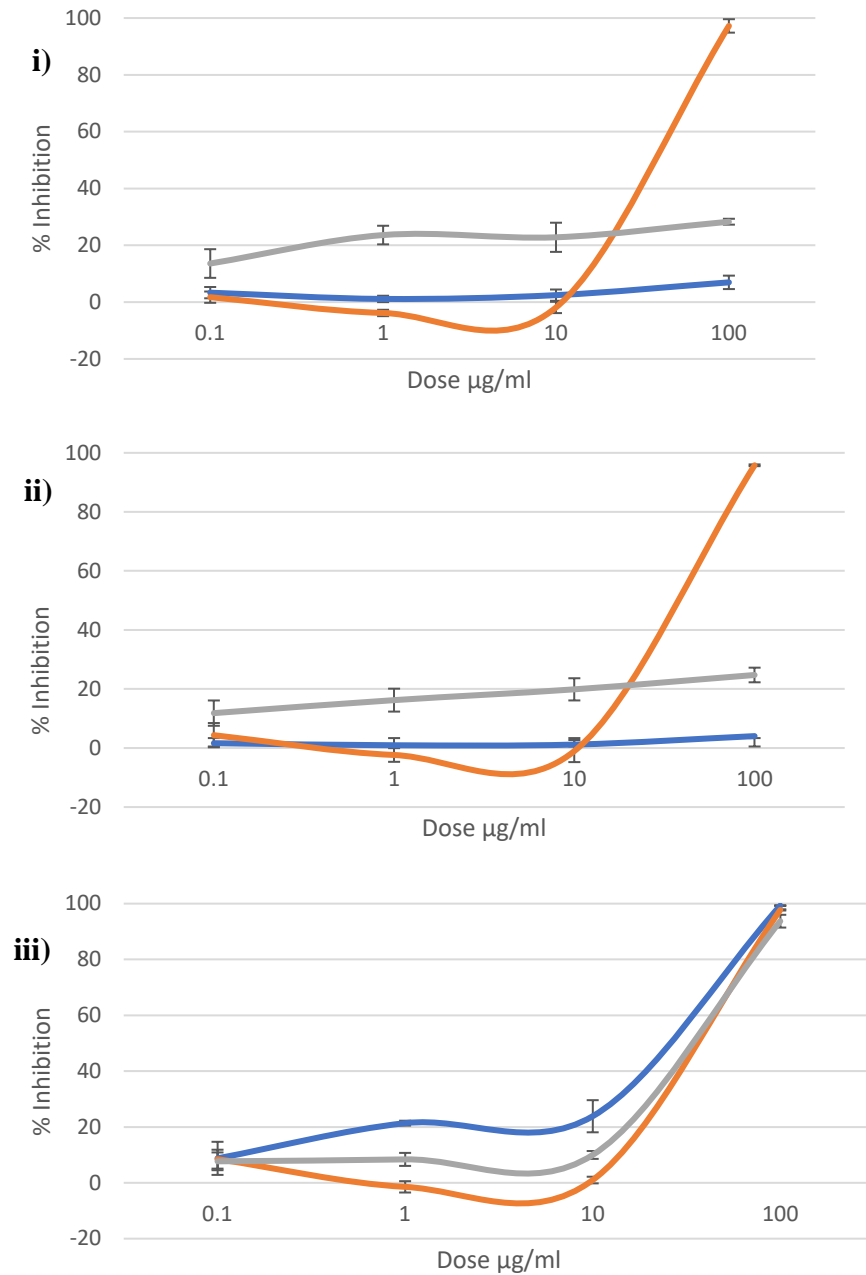


Figure 3.6 A: African Cobras Dose Response on CMT28, CMM26 and MDCK

Displays the dose response of African cobras on CMT28 (Orange), CMM26 (Blue) and MDCK (Grey): i) *N.niv* ii) *N.mel* iii) *N.nct* iv) *N.nub* v) *N.pal*. (Error Bars- STD).

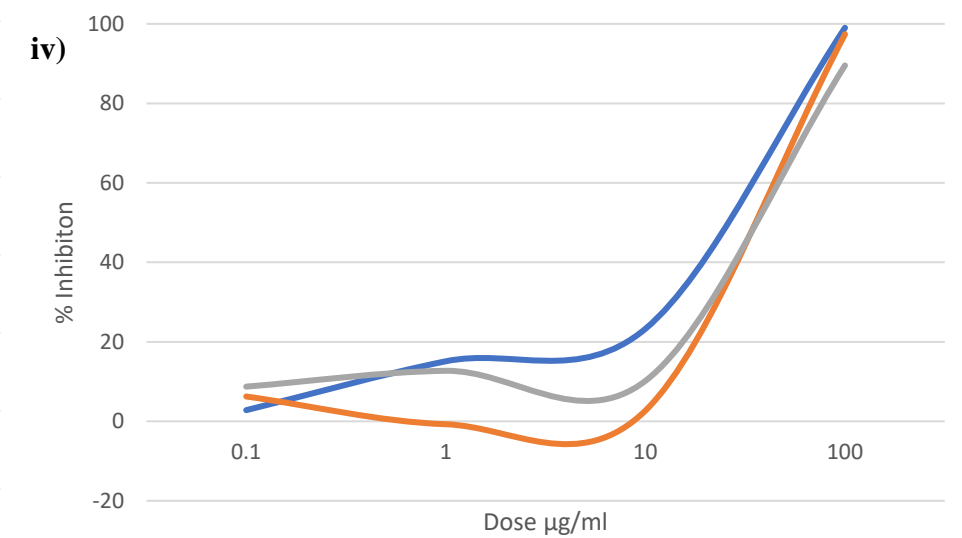
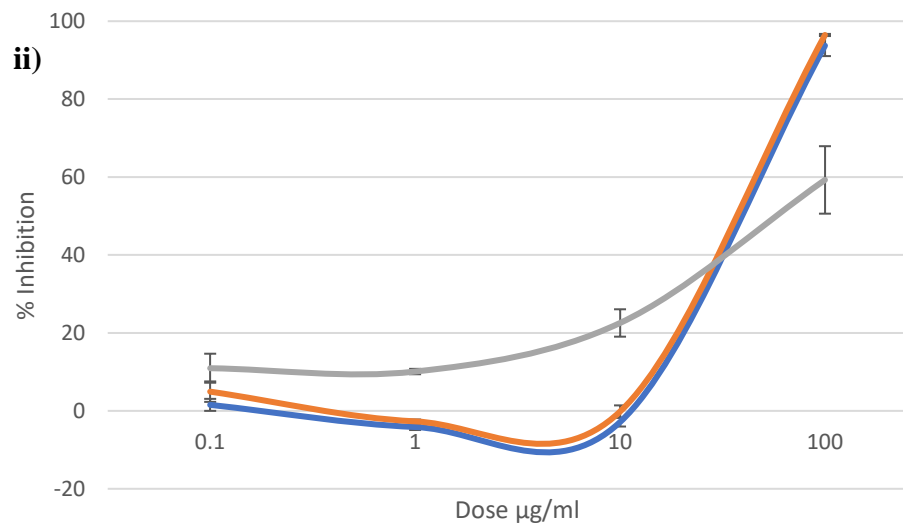
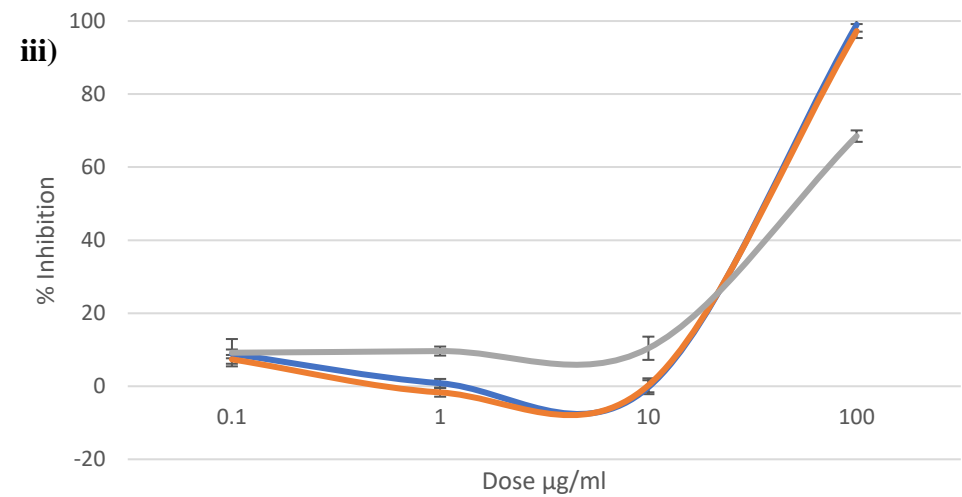
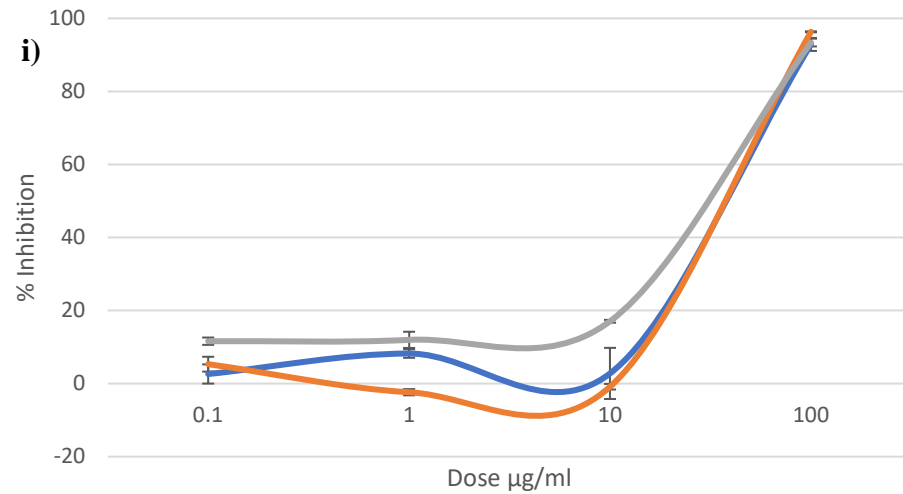


Figure 3.6 B: Asian Cobras Dose Response on CMT28, CMM26 and MDCK

Displays the dose response of Asia cobras on CMT28 (Orange), CMM26 (Blue) and MDCK (Grey): i) *N.naj* ii) *N.kao* iii) *N.atr* iv) *N.sia* (Error Bars-STD).

CHAPTER 4: High-throughput screening of Venom Fractions using T-VDA^{ctx} assay and Identification of fraction using Mass Spectrometry

4.1 Introduction

Venomous snakes of medial importance are found within the families that share the common characteristic of being front-fanged (Tasoulis and Isbister., 2017; Sanhajariya, Suchaya *et al.*, 2018); this includes the Elapidae family of which the *Naja* genus belongs too. Snake Venoms of *Naja* spp are composed of a mixture of low molecular mass proteins and peptides, ranging from 6-15kDa and high molecular masses of ~180KDa (Petras *et al.*, 2011; Tasoulis and Isbister., 2017). The protein and peptide content of snake venom is predominantly composed of phospholipase A2 and three-finger toxins but may also contain other molecules such as L-amino acid oxidases, metalloproteases, serine proteases, 5'-nucleotidases, acetylcholinesterases and hyaluronidases, disintegrins, and cysteine-rich secretory proteins (Ferraz *et al.*, 2019). Toxicity caused by these proteins and peptides within snake venom have been associated with high specificity and affinity for molecular markers on cells (Calderon., *et al* 2014), with the toxicological effects implemented in pharmaceutical agents (Lewis *et al.*, 2003). Likewise, in snake venoms, scorpion venoms contain bioactive molecules that have shown great anti-tumour activity, by reducing cancer growth, induce apoptotic death, and inhibit metastasis progression (Díaz-García, *et al.*,2013; Ding, *et al.*, 2014; Al-Asmari, *et al.*,2016; Tobassum, *et al.*,2020). Scorpion venom contain proteins and peptides with low level enzyme activity, such as polysaccharides, phospholipases, low molecular weight molecules such as serotonin, histamine, histamine releasing peptides, inorganic salts, and many basic small proteins such as neurotoxins (Pal, *et al.*, 2015; Ga, *et al.*, 2017). The low molecular weight compounds have been shown to interact with ion channel using dysregulation in nerve cells and muscle tissues (Tobassum, *et al.*,2020).

The process of developing a novel drug can be a tedious and complex procedure, but with the use of High-Throughput Screening (HTS), this strategy reduces time consumption in identifying hit

compounds on a particular target. Utilising HTS allows large numbers of compounds to be screened at once, to identify molecules that interact with a drug target. Whether the compound is protein or peptide, the goal of compound screening is to accelerate drug discovery screening. The choice of technique is based upon the disease being investigated and target of interest; however, to create such a method, validation of the assay must be performed to establish a robust assay.

The Resazurin assay optimised and utilised in chapter 3 has proved to be a successfully robust and reliable cell-based assay. The Targeted Venom Discovery Array (T-VDA^{cyx}) (Venomtech Ltd, UK) can be utilised to screen a library of venoms using a HTS assay using Resazurin. The T-VDA^{cyx} is designed to screen animal venoms that are specifically chosen to induce cytotoxicity. Venoms included in this array contains snake venoms, along with scorpions and spiders.

In chapter 3, the Resazurin assay utilised 96-well plates, however, to cater this array, the assay will need to be optimised and validated to a 384-well plate format. Establishing cell-based assays for HTS requires the assays to consider factors that allow the assays to be biologically relevant, be sensitive enough for detection, and be statistically robust (Janzen., 2014).

4.2 Aims

- To optimise the Resazurin assay for 384 well format using CMT28, CMM26 and MDCK cell lines.
- To screen a panel of fractionated venoms contained within T-VDA^{cyx} library against the Canine Cancer cell lines CMT28 and CMM26 and Normal Canine Cell line MDCK.
- To select any hit fractions to take forward for Mass Spectrometry analysis (Intact mass and peptide mapping)
- To assess and analysis the data obtained from Mass Spectrometry of fractions using databases and literature to suggest possible component identification of each fraction.

4.3 Materials and Methods

4.3.1 Optimisation of the Resazurin Assay for the T-VD^{ctx} assay

4.3.1.1 Optimal cell number selection for CMT28, CMM26 and MDCK for Resazurin Assay in 384 well plates

To optimise the Resazurin assay in 384 well plates, each cell line was plated at different cell numbers to determine the most suitable seeding density for the T-VDA^{ctx} assay. CMM26 cells were plated at 5 different cell quantities of 2.5×10^4 , 2×10^4 , 1.5×10^4 , 1×10^4 and 0.5×10^4 . CMT28 cell were plated at 4 different cell quantities of 5×10^4 , 2.5×10^4 and 2×10^4 , 1.5×10^4 , 1×10^4 . MDCK cells were plated at 3 different 3 quantities of 7.5×10^4 , 5×10^4 and 2.5×10^4 . Each cell number for each cell line was plated in 2 rows in replicas of 24, shown in Appenix VIII. The plate was returned to a humidified incubator at 37 °C, 5% CO₂ overnight for the cells to adhere and settle.

CMT28 and CMM26 cells were exposed to 100µg/ml of *Naja nigricollis* venom, while the MDCK cells were exposed to 1mg/ml. The working venom concentrations were made as described in section **2.3.2**. The cells were treated with 20µl of venom and incubated for 2h. After incubation the venom was removed and replaced with 25µl of 160µM Resazurin media solution and the fluorescence was read as described in the standard protocol in section **2.3.2**.

4.3.1.2 Z' Analysis of Cell number

Using the optimal cell numbers for the 3 cell lines from previous optimisation experiments described in **4.3.1.1**. CMT28, CMM26 and MDCK cell lines were trypsinised and counted via the standard protocol stated in **2.3.1**. CMT28 were plated out in 384 well plates at a concentration of 2×10^4 , CMM26 cells at a concentration of 2×10^4 and MDCK cells at 7.5×10^4 (Appendix VIII).

Each cell line was treated following the same procedure stated in **3.3.1.2**. Both CMT28 and CMM26 cells were treated with 100µg/ml of *Naja nigricollis* venom, while the MDCK cells were exposed to 1mg/ml. The working venom concentrations were made as described in section **2.3.2**.

The cells were treated with 20µl of venom and incubated for 2h. After incubation the venom was removed and replaced with 25µl of 160µM Resazurin media solution and the fluorescence was detected as described in the standard protocol in section **2.3.2**.

4.3.1.3 Initial Screening of Cobra venoms found in the T-VDA^{ctx} assay

Due to limited resources of venom available in the T-VDA^{ctx} assay, a dose response was performed on the cobra venoms on the plate, to determine the appropriate concentration to screen the venom fractions at. The cobra venoms used were *Naja atra*, *Naja siamensis*, *Naja kaouthia*, *Naja nigricollis* at concentrations of 10µg/ml, 20µg/ml, 30µg/ml, 40µg/ml, 50µg/ml, 60µg/ml, 70µg/ml, 80µg/ml, 90µg/ml and 100µg/ml. CMT28 and CMM26 cells were used in this assay. They were plated in triplicate for each concentration for each venom (Appendix IX). CMT28 and CMM26 cells were plated at 2.5×10^4 and 2×10^4 in 384 well plates and returned to a humidified incubator at 37 °C, 5% CO₂ overnight for the cells to adhere and settle.

Both cell lines were exposed to the chosen concentrations of venom. The working venom concentrations were made as described in section 2.3.2. The cells were treated with 20µl of venom and incubated for 2h. After incubation the venom was removed and replaced with 25µl of 160µM Resazurin media solution and the fluorescence was detected as described in the standard protocol in section 2.3.2.

4.3.1.4 Screening the T-VDA^{ctx} assay on CMM26 cells

The T-VDA^{ctx} assay was supplied by Venomtech Ltd as two compound plates with each venom fraction freeze dried. The T-VDA^{ctx} assay consisted of venoms from 13 species listed in Table 4.1. Each venom fraction was diluted to 35µg/ml using RPMI media. The CMM26 cell line was used to screen the T-VDA^{ctx} assay and was plated at a concentration of 2.5×10^4 per well in 384 well plates and returned to a humidified incubator at 37 °C, 5% CO₂ overnight for the cells to adhere and settle. The T-VDA^{ctx} assay was screened in triplicate; three 384 well plates were used each with replicas of the venom fractions on (Appendix X). The cells were treated with 20µl of venom and incubated for 2h. After incubation the venom was removed and replace with 25µl of 160µM Resazurin media solution and the fluorescence was read as described in the standard protocol in section 2.3.2.

Table 4.1: Fractionated whole venom from 13 species found in the T-VDA^{ctx} assay

Species	Common Name
<i>Agkistrodon contortrix</i>	Copperhead Viper
<i>Bitis arietans</i>	Puff Adder Viper
<i>Crotalus ruber</i>	Red Diamon Rattlesnake
<i>Crotalus viridis</i>	Prairie Rattlesnake
<i>Naja Atra</i>	Chinese Cobra Snake
<i>Naja siamensis</i>	Indochinese Cobra
<i>Naja kaouthia</i>	Monocled Cobra
<i>Naja nigricollis</i>	Black-Necked Cobra
<i>Heterometrus swammerdami</i>	Giant Forest Scorpion
<i>Androctonus australis</i>	Fat Tailed Scorpion
<i>Heteropoda venatoria</i>	Huntsman Spider
<i>Parabuthus liosoma</i>	African Black Tail Scorpion
<i>Centruroides sculpturatus</i>	Arizona Bark Scorpion

4.3.1.5 Dose response screening of cytotoxic fractions on CMM26, CMT28 and MDCK cells

In 384 well plates and using the hit fractions selected from section 4.3.1.4, each cell line was treated with eight different concentrations of venom; 100µg/ml, 33µg/ml 10µg/ml, 3µg/ml 1µg/ml, 0.3µg/ml 0.1µg/ml and 0.03µg/ml. CMM26 cells was seeded in the 384 well plates at a concentration of 2×10^4 , CMT28 at 2×10^4 and MDCK at 7.5×10^4 per well. Each concentration was screened in triplicate (Appendix XI). The cells were treated with 20µl of venom and incubated for 2h. After incubation the venom was removed and replaced with 25µl of 160µM Resazurin media solution and the fluorescence was detected as described in the standard protocol in section 2.2.3.

4.3.1.6 Mass Spectrometry Analysis of Fractions Shown to Display Lethal Inhibitory effects on the Cell Viability of CMT28, CMM26 and MDCK cell lines

10µg of five fractions shown to cause greater than 70% inhibition in cellular viability in both CMT28 and CMM26 cell line were sent to Peak Proteins Ltd (Alderley Park, Macclesfield) for Intact Mass and Peptide Mapping mass spectrometry analysis. Samples were analysed by Peak Proteins and the collected data returned for analysis (Appendix XVI).

The methodology used for intact mass spectrometry by Peak Proteins was performed as follows. 5µg of each lyophilised fraction sample was reconstituted in 40µl of 0.1% formic acid/5% acetonitrile. 10µl of the sample was loaded onto a Sciex Exion liquid chromatography and a 5 min reverse phase gradient run, using a 0.1% formic acid Buffer A and a 0.1% formic acid/100% acetonitrile Buffer B. RP HPLC was performed with a flow of 500ul over a gradient, starting with 5% Buffer B increasing to 45% B over 3min, followed by a 95% B wash and an equilibration of 5% B. The column used was a Phenomenex Jupiter 5um, C4, 300A 50x2.1mm. Flow from the column was passed into the Sciex X500B mass spectrometer, set to collect data in positive ion mode. To enable ionisation of the eluate the source was set to 400°C, 5500V with gas at 50psi. A TOF mass window of 500-3000Da was collected, scanning at 0.5s. The X500B mass spectrometer was calibrated with a positive calibration mix and the error for the experiment was estimated to 0.5Da. The resultant total ion chromatogram (TIC) was deconvoluted using BioToolKit software (Sciex).

Peptide Mapping mass spectrometry was performed using 5µg of each lyophilised sample and was reconstituted in 50µl of 100 mM ammonium bicarbonate. 5µl of 100 mM DTT in 100 mM ammonium bicarbonate was added to each sample and the sample heated at 65°C for 30 min. 5µl of 500 mM iodoacetamide in 100 mM ammonium bicarbonate was added to all samples and the samples re-incubated in the dark at room temperature for 30 min. 10µl of 25 ng/µl trypsin in 50 mM ammonium bicarbonate was added to each sample and they were incubated overnight at 37°C. 10µl of the complete digest was taken and mixed with 10µl of 0.1% trifluoroacetic acid (TFA). 10µl of mixed sample was loaded onto the Sciex Exion liquid chromatography and a 10 min reverse phase gradient run. A Phenomenex Lunar 1.6 µm, PS C18, 100A 150x2.1mm column was used. Buffer compositions were as intact mass MS (0.1% formic acid Buffer A and a 0.1% formic acid/100% acetonitrile Buffer B). Flow was set to 300µl and a gradient performed, starting with 5% buffer B, increasing to 45% B over a 15 min duration, before a 95% buffer B wash and an equilibration at 5% B. Flow from the column was passed into the Sciex X500B mass spectrometer set to collect data in positive ion mode. To enable ionisation of the eluate the source was set to 400oC, 5500V with gas at 30psi. A TOF mass window of 300-1800Da was collected, scanning at 1.2s. Mass spec mass spec (MSMS) data was collected using an information Dependent Acquisition method, where up to 10 MSMS were collected per scan. The

X500B was calibrated with positive calibration mix, the error for the experiment was estimated at 1ppm. The resultant data from the MSMS was analysed using Mascot (Matrix Science) using the Swissprot database.

4.3.1.7 Analysis of sequence fragments data obtained from intact and peptide digest mass spectrometry.

Using the amino acid sequence fragments obtained by peptide digest mass spectrometry from Peak Proteins, they were entered into a BLAST search via Uniprot to identify similar regions within the sequence. Highly similar and comparable sequences were aligned using Uniprot Align to identify missing sequence data and conserved regions.

Data obtained from Intact Mass Spectrometry of each fraction was used to identify the overall molecular mass of the venom component. The overall mass was also used to propose the most likely amino acid in the regions that were missing.

4.4 Results and Discussion

4.4.1 Selection of the Optimal Cell Number for an Effective Plate-Based Resazurin Assay in 384 well plates

Alike section **3.4.1**, the selection of an optimal cell number for the cell lines CMT28, CMM26 and MDCK was to ensure that the resazurin assay was a robust assay in 384 well plates. Each cell line was plated in its chosen cell quantities at one lethal concentration of whole *Naja nigricollis* venom, of 100µg/ml for CMT28 and CMM26 and 1mg/ml for MDCK cells as identified in section **3.4.1**. The cells were monitored over a 5 hour period to establish which cell quantity produced the greatest fold-change in fluorescence between the negative (culture media) and positive (venom) control.

Observations of the CMT28 cell line displayed that all cell numbers excluding 0.5×10^5 showed a significant increase in fold change between the positive and negative control (Figure 4.1 i). In comparison to the other cell numbers, cell numbers of 5×10^5 and 2.5×10^4 produced similar fold-changes reaching the highest fold change of 24 at time point 240 minutes; while the other cell numbers produced fold-changes of 16 and below. As there is no significant difference between the cell numbers of 2×10^5 and 2.5×10^4 , it was concluded that the cell number of 2.5×10^4 would be used for z' analysis.

The CMM26 cell line produced similar fold-changes on cell numbers 2.5×10^4 , 2×10^4 , 1.5×10^4 , and 1×10^4 ; however, no fold-change was produced at 0.5×10^4 (Figure 4.1 ii). The cell number of 2×10^4 produced the maximum fold change which peaked at 23.5 at time point 150 minutes, with the fold-change slowly decreasing overtime until the end time point of 300 minutes. Although initial observation shows that four of the cell numbers produce similar fold-changes over time, a guideline was used from using 1×10^5 cells per well in 96 wells plates. 384 well plates are four times smaller, thus a guided value of approximately 2.5×10^4 was used to screen the correct cell number. Therefore, as the cell number of 2×10^4 produced the highest fold-change, it was determined to be the optimal number of CMM26 to take forward for z' analysis.

Determining the optimal cell number for MDCK cells was established through screening a cell number that was a quarter of the number used in 96 well plates. 2×10^5 cells are used in 96 well plates, thus choosing 5×10^4 to screen. However, as these cells are normal cells compared to the cancer cell lines, the MDCK cells metabolic activity is observed to be considerably reduced, thus cell numbers above and below 5×10^4 were screened. Analysis of the cell concentrations of 5×10^5 and 2.5×10^5 for MDCK cells displayed minimal fold-change production, reaching fold-changes of 5 and 3 (Figure 4.1 iii). However, the cell concentration of 7.5×10^5 produced a significant peak in fold-change reaching 16 fold-changes at time point 300 minutes. With these observations, it was concluded to take forward the cell concentrations of 7.5×10^5 for further analysis in the Z' analysis assay.

4.4.2 Z' Analysis of Selected Cell Number

Using the selected optimal cell numbers of 2.5×10^4 for CMT28, 2×10^4 for CMM26 and 7.5×10^4 for MDCK cells. These cell numbers were chosen to perform a Z' assay to establish if these cell numbers are suitable to produce a statistically robust assay in a 384 well plate format. The Z' assay compares the mean and standard deviations of both the positive and negative control over a time period of 5 hours to identify the most robust time point to be selected to conclude the inhibitory effects of venom on the three cell lines (Table 4.2).

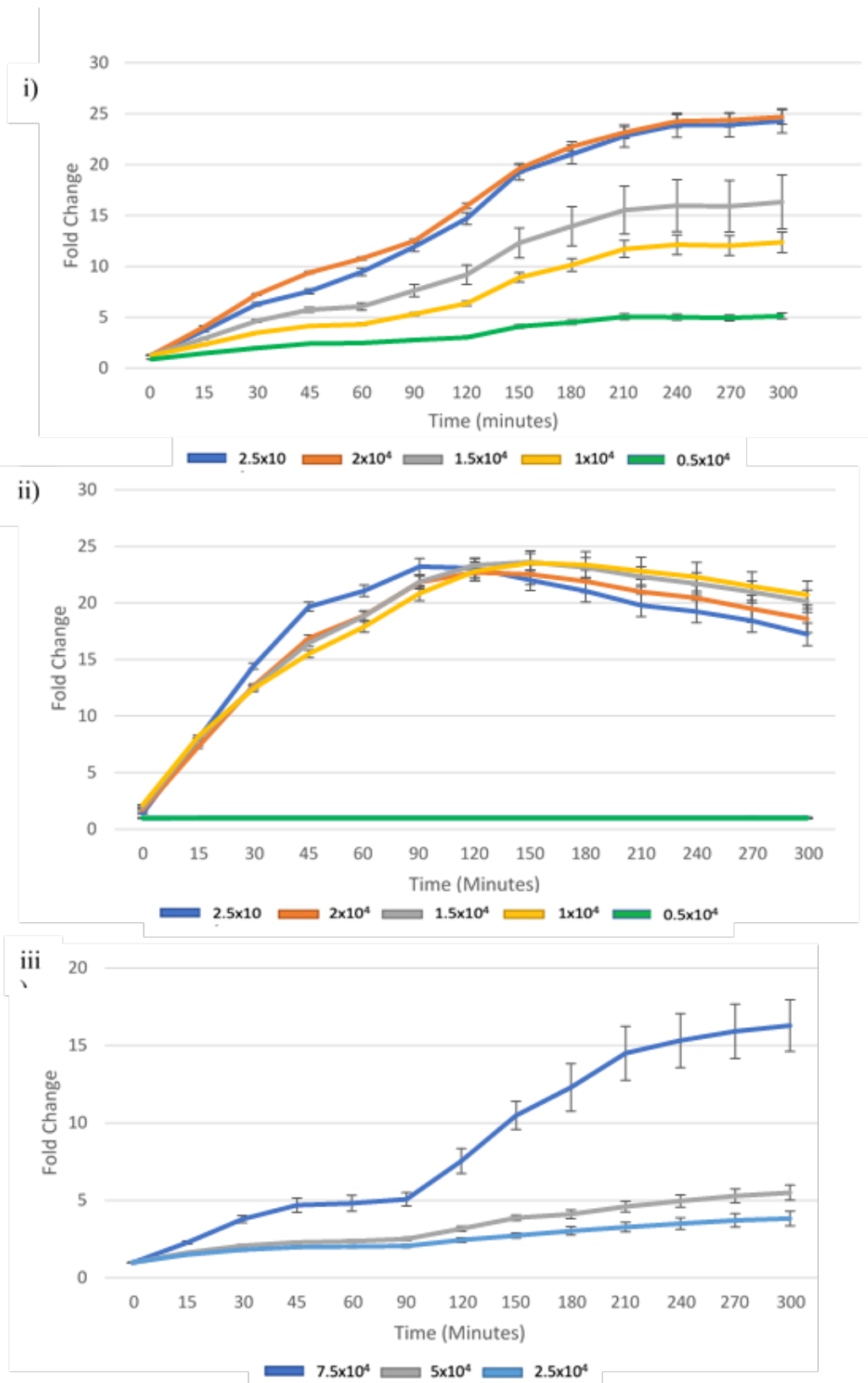


Figure 4.1: Resazurin Cell Concentration Analysis of CMT28, CMM26 and MDCK
 i) CMT28 and ii) CMM26, Shows the fluorescent fold-change between the positive control (100µg/ml lethal dose of whole *Naja nigricollis* venom) and negative control (RPMI/ DMEM media). iii) MDCK Shows the fluorescent fold-change between the positive control (1mg/ml lethal dose of whole *Naja nigricollis* venom) and negative control (DMEM media). Different concentrations of cells observed over 5hour time period

Analysis of the Z' assay for the CMT28 cell line displayed that the assay was not considered a robust assay until 120 minutes into readings, reaching a Z' value of 0.59. The Z' values continued to slowly increase until the end point of 5 hours, reaching a maximum read of 0.73. Using the Z' values and using the fold-change data from section 4.4.1, it is concluded that the time point of 240 minutes was the optimal time for taking assay reading for the CMT28 cell line.

Observations of the CMM26 cell line show that from the time point of 30 minutes the assay was a robust assay with a Z' value of 0.52. From the time point of 120 minutes the assay was considered to be a robust assay providing a Z' value of 0.59. As the Z' value continues to increase over the 5hour time period, and using fold-change data from section 4.4.1, the optimal time point for taking assay readings was 150 minutes.

MDCK Z' was not observed to be a robust assay until the time point of 180 minutes, producing values under the threshold of 0.5. The Z' value increased slowly from 0.5 at the time point of 180 minutes to 0.52 at the time point of 300 minutes. Although this assay is classed as a robust assay an additional time point of 24 hours was taken, as the fluorescence readings hadn't reached the maximum value. The Z' value produced at 24 hours was 0.66 which is not a drastic increase in value, but it confirms that the assay is robust.

Table 4.2: Z' Analysis of CMT28, CMM26 and MDCK cells

Displays the Z' values produced for each cell line CMT28, CMM26 and MDCK over a 5 hour time period. Highlighted values (Yellow) indicate the optimal time point chosen.

Time (Minutes)	Z' Value CMT28	Z' Value CMM26	Z' Value MDCK
0	-1.94482	-1.94482	-3.4684
15	0.076145	0.076145	-1.5632
30	0.240429	0.240429	0.149568
45	0.374534	0.374534	0.135142
60	0.480529	0.480529	0.215872
90	0.498636	0.498636	0.408202
120	0.59149	0.59149	0.44247
150	0.603672	0.603672	0.467891
180	0.595248	0.595248	0.503946
210	0.642167	0.642167	0.513328
240	0.670005	0.670005	0.517822
270	0.709357	0.709357	0.516403
300	0.739289	0.739289	0.520355

4.4.3 Determining the Appropriate Concentration to Screen the Venom Fractions of the T-VDA^{ctx} Assay

Limitations on venom fraction availability in the T-VDA^{ctx} assay meant that only one canine cancer cell line could be screened. Thus, using the *Naja* spp venoms found on the T-VDA^{ctx} assay as determinants to verify which cell line is appropriate to screen; as well as performing a dose response screening of the venoms to determine the concentration at which the chosen cell line will be screened. Both CMT28 and CMM26 cell lines were screened using whole venoms of *Naja atra*, *Naja siamensis*, *Naja kaouthia*, *Naja nigricollis* at concentrations between of 10µg/ml and 100µg/ml (Figure 4.2). Although both of these cell lines have been screened against these whole venoms in chapter 3, this screen was performed again at more precise concentrations, as well as to perform an experimental repeat to confirm the inhibitory effects. Utilising whole venom to determine the appropriate cell line for the T-VDA^{cyx} assay, this screen provided a guideline to understand susceptibility, thus when screening the fractions, the results produced will be more definitive towards cancerous cells.

Statistical analysis of both cell lines across the 4 whole venoms show that the CMM26 cell line is more susceptible to lower concentrations of the whole venoms than the CMT28 cell line (multi-factor ANOVA, $P < 0.05$). Normality and equal variance tests on all treatment groups confirmed that data sets were normally distributed and displayed equal variance (Appendix XII). High levels of cytotoxic inhibition were shown in the venoms of *N.sia* and *N.nig* on the CMM26 cell line, producing an LD₅₀ of 19.40µg/ml and 21.68µg/ml compared to CMT28 which produced a significantly higher LD₅₀ (Table 4.3).

Similarities in lethal doses were observed in CMT28 exposed to *Naja atra*, *Naja kaouthia* and *Naja nigricollis* (Table 4.3), with *Naja siamensis* displaying a lower lethal dose of 35.97µg/ml.

Variations of toxicity observed between the cells lines may a result of protein expression between the cell types. Though they are both canine mammary cancers, at a molecular level, they may express more or less of the target inhibited by the venom. Overall, the CMM26 cell line was observed to be more susceptible to the whole venoms compared to the CMT28 cell line; thus, the CMM26 cell line was chosen to perform the T-VDA^{cyx} assay

Table 4.3: LD₅₀ Value for CMT28 and CMM26 exposed to Whole Venoms

Whole Venoms	LD ₅₀ (µg/ml)	
	CMT28	CMM26
<i>N. atra</i>	59.56	39.63
<i>N. siamensis</i>	35.97	19.40
<i>N. kaouthia</i>	60.39	47.31
<i>N. nigricollis</i>	59.70	21.68

4.4.4 Screening the T-VDA^{ctx} assay to Identify Cytotoxic Fractions on CMM26 cells

Using the data obtained from section 4.4.3 it was observed that CMM26 cell line was more sensitive to the whole venoms, thus it was chosen to perform the T-VDA^{ctx} assay on. Each fraction of the T-VDA^{ctx} assay was plated in replicates over three 384 well plates at the concentration of 35µg/ml. The T-VDA^{ctx} assay consisted of 535 fractionated components of venom from 13 different species of invertebrates and snakes. Each venom was fractionated (by Venomtech Ltd) using Two-dimensional High-Performance Liquid Chromatography (HPLC). The first dimension was performed using an ion exchange column separating the whole venom components based on the ionic charge, and the second dimension was a reverse phase column to further separate the components based on hydrophobicity. During ion-exchange and reverse-phase HPLC fractions were eluted and detected at a wavelength of 280nm which resulted in the collection of venom fractions.

Analysis of the fractionated venoms showed 12 significant fractions induced more than 50% cytotoxic inhibition (One-way ANOVA with Tukey's post-test, P<0.05). Normality and equal variance tests on hit fractions confirmed that data sets were normally distributed and displayed equal variance (Appendix XIII). Inhibitory effects were only observed in venom fractions within the *Naja* spp and not in any of the other snake and invertebrate fractions. Venom fractions were observed to cause >50% inhibition, however they produced high standard deviations; thus, a threshold of 70% was put in place as a minimal inhibitory effect, to be classed as a hit fraction.

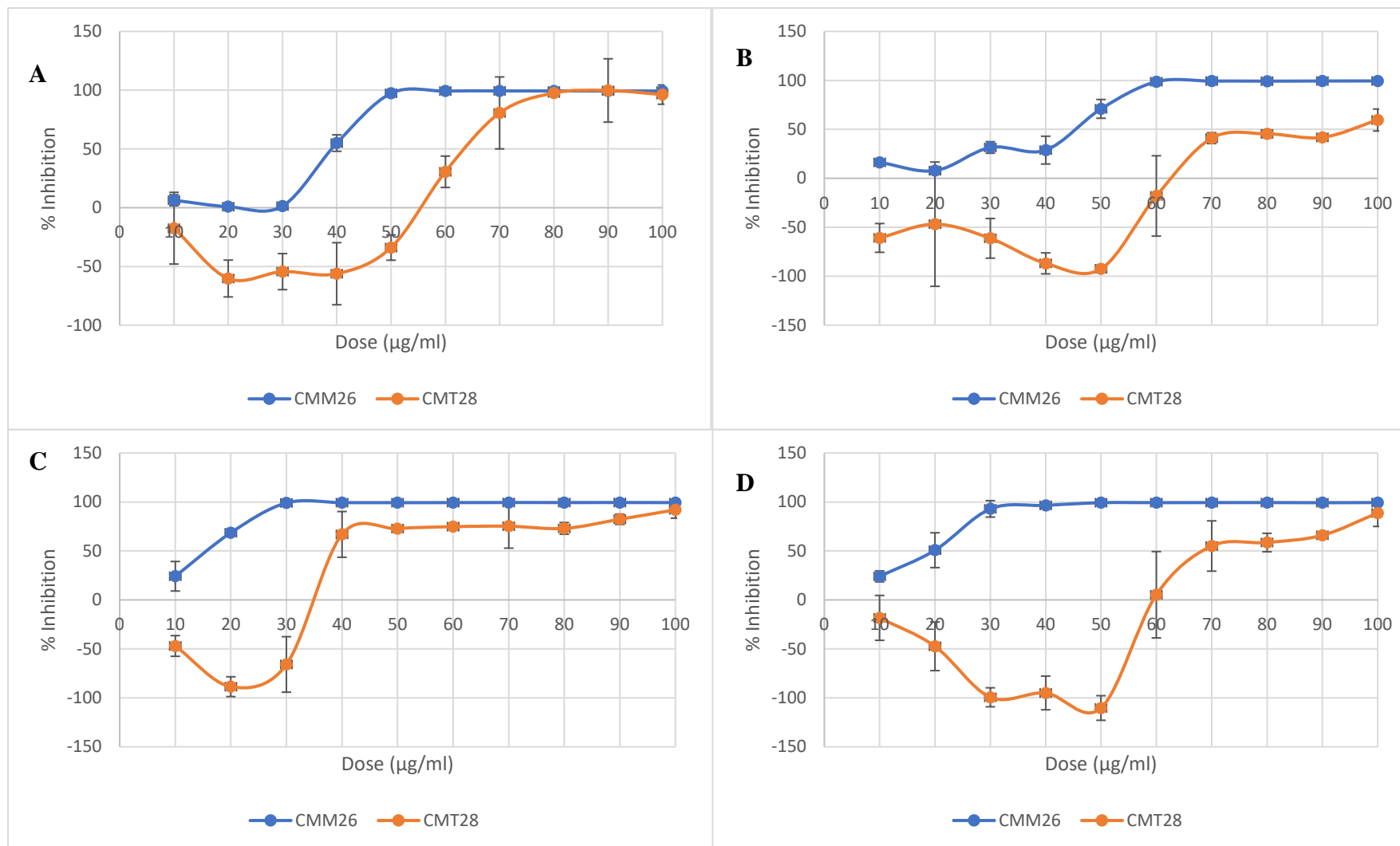


Figure 4.2: Dose Response curves of Whole Venom from *Naja atra*, *Naja kaouthia*, *Naja siamensis* and *Naja nigricollis* on CMT28 and CMM26 cell lines

Figure A shows % inhibition of whole *Naja atra* venom on CMT28 and CMM26 cell lines. Figure B shows % inhibition of whole *Naja kaouthia* venom on CMT28 and MM26 cell lines. Figure C shows % inhibition of whole *Naja siamensis* Venom on CMT28 and CMM26 cell lines. Figure D shows % inhibition of whole *Najanigricollis* venom on CMT28 and CMM26 cell lines. (Error bars = SD)

Analysis of the *Naja atra* venom fractions observed 3 hits overall, showing significant inhibition of >70% (Figure 4.3) (Table 4.4). It was observed that fractions N.atr_i9_r1 and N.atr_i9_r2 are consecutive fraction collected and from viewing the HPLC chromatogram it revealed that both fractions are from the same peak (Appendix XIV). Investigation of the HPLC chromatograms of the other hit fractions showed that they produced peaks that were strong and independent from one another. 2 hit fractions from the *N.sia* snake was observed to cause >70% inhibition, with fractions N.sia_i9_r4 and N.sia_i10_r3 causing inhibitory effects of 89.88% and 70.22%. Venom fractions from *N.kao* displayed 2 hit fractions N.kao_i9_r2 and N.kao_i10_r3 causing inhibitory effects of 74.67% and 97.3%. 7 fractions from *Naja nigricollis* were shown to cause inhibitory effects of the CMM26 cells, with 5 causing >70% inhibition.

Similarities are observed between the fractions that induce >70% inhibition at the times of which the fractions were eluted from the HPLC columns. Elution time of the fractions from the ion-exchange column, indicated similarities between the fractions, due the fraction number of which they were collected in (Table 4.4); this is also observed in the reverse-phase fraction number. As some fractions are observed to be eluted at similar times, between 10-16 minutes, this indicates the fractions maybe contain a structure with a similar electrostatic charge and hydrophilic properties (Zhou and Pang., 2018). Similarities in these properties could indicate the possibility of the structures being alike. This would not be a surprising finding as it has been documented that the venom composition of species across the *Naja* genus are composed of similar structured proteins and peptides (Tasoulis and Isbister., 2017).

Venom fractions that are observed to cause >70% inhibition was taken forward to screen on the CMT28 and MDCK cell line (Table). Due to N.atr_i9_r1 and N.atr_i9_r2 fractions being from the same peak, only N.atr_i9_r1 was not taken forward to screen on the other cell lines.

Table 4.4: Hit venom fractions to induce >70% inhibition

Species	Fraction ID	Ion Exchange Fraction	Reverse phase Fraction	% Inhibition
<i>N. atra</i>	i9_r1	9	1	89.82%
<i>N. siamensis</i>	i9_r4	9	4	89.88%
	i10_r2	10	3	70.22%
<i>N. kaouthia</i>	i9_r2	9	2	74.67%
	i10_r2	10	3	97.30%
<i>N. nigricollis</i>	i8_r6	8	6	90.71%
	i8_r7	8	7	92.99%
	i9_r3	9	3	73.61%
	i9_r4	9	4	87.64%
	i11_r3	11	3	98.61%

4.4.5 Hit Fraction screening from T-VDA assay CMM26, CMT28 and MDCK

CMM26 cells

Using the venom fractions that were shown to induce >70% inhibition in the CMM26 cells in **Section 4.4.4**, these fractions were taken forward to perform a dose response on all 3 cell lines. This in turn will determine the toxicity and inhibitory effects between cancer cells and a non-cancerous cell. Each cell line was dosed with eight concentrations of each venom fraction in half log dilutions (100, 33, 10, 3, 1, 0.3, 0.1, 0.03 μ g/ml). Higher susceptibility is expected to be observed when screening the fractions from the T-VDA^{cyx} compared to screening whole venom. This is a result of the venom fractions being enriched compared to the concentrations at which they are found in the whole venom. Initial observations of the inhibitory effects of the venom fractions suggest that there is specificity towards inhibiting the canine cancer cells lines (CMT28 and CMM26) compared to the normal cell line (MDCK) (Figure 4.4 A, B, C) (Multi-factor ANOVA with Tukey test $P > 0.05$) (Appendix XV). Normality and equal variance tests on all treatment groups confirmed that data sets were normally distributed and displayed equal variance (Appendix XIV).

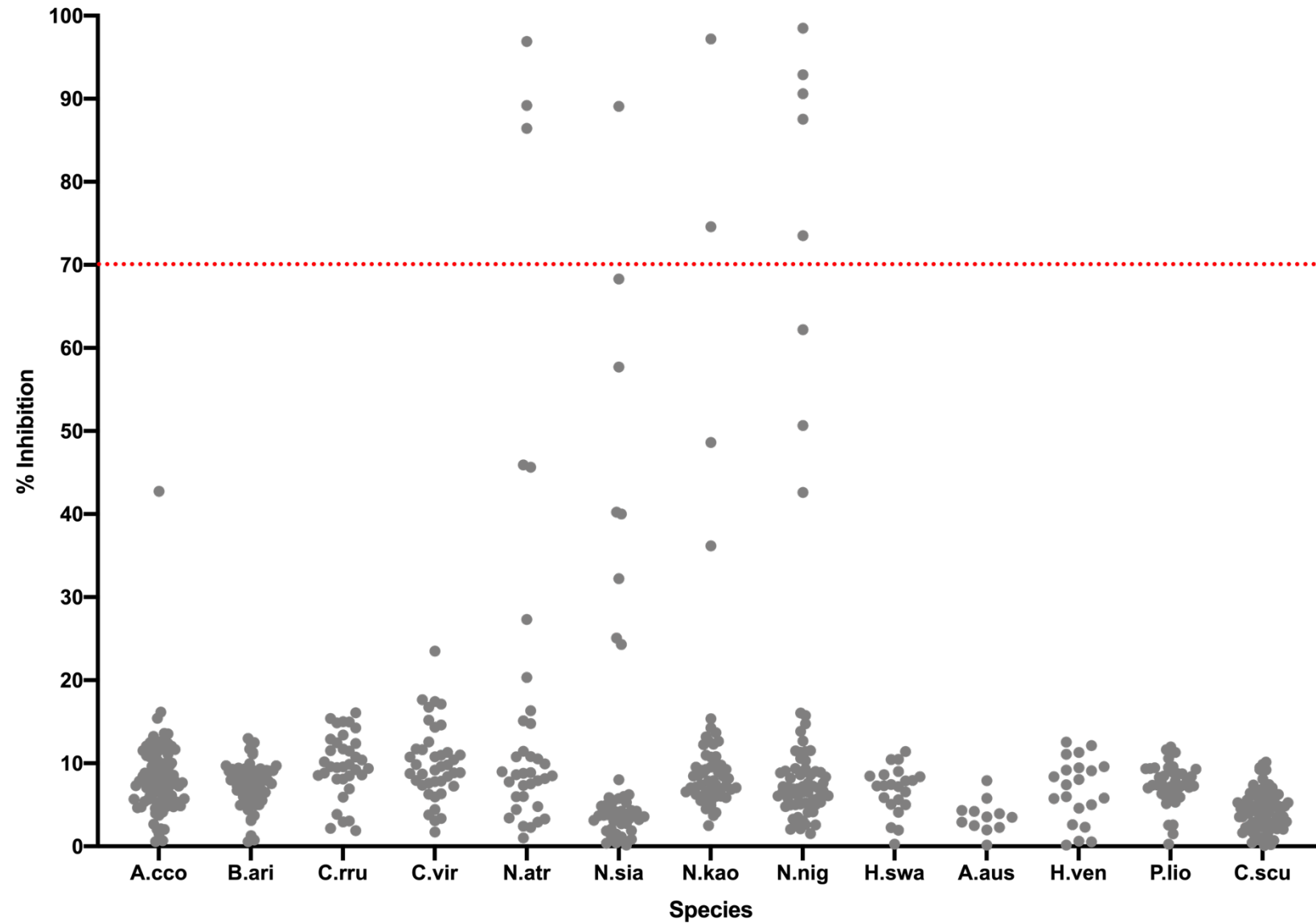


Figure 4.3: 535 fractions from 13 species of Snakes and Invertebrates from the T-VDA^{ctx} assay
 Displays the inhibitory effects of each venom fraction from the 13 species. Using a threshold of 70% (- - -) to determine significance in inhibition.

Comparing the toxicity of the venom fractions on each of the cells lines the Lethal Dose of 50% (LD₅₀) was calculated using GraphPad Prism (Table 4.5). The LD₅₀ determines the specific dose that will lead to deaths of 50% of the cell population (Gad.,2014). It is observed that the LD₅₀ of the CMM26 cell line is considerably lower than the CMT28; with lethal doses of venom inducing 50% cell death in CMT28 was 4.5 times higher than CMM26. Selectivity of the venom fractions between the cancer cells may differ due to the expression levels of the target that the venom fraction inhibits.

Toxicity observed in fractions N.atr_i9_r1, N.kao_i9_r2, N.sia_i9_r4, N.kao_i10_R2, N.nig_i8_r7, N.nig_i9_r4 and N.ni_i11_r3 showed significant inhibitory effects on both the CMT28 and CMM26 cell line; yet 3 of those fractions displayed inhibitory effects on the MDCK cells. 2 of the fractions N.nig_i8_r6 and N.nig_i9_r3 only induced inhibitory effects on the CMM26, while the other cell lines were not affected.

Table 4.5: LD₅₀ for Venom Fractions causing >70% inhibition

LD₅₀ was calculated using the Log inhibitor vs response function (nonlinear regression) in GraphPad Prism. The output produced an LOGLD₅₀ that was transformed into the inverse logarithmic value; this converted the value from LOG to µg/ml. LD₅₀ values for MDCK cells could not be produced due to the lack of dose response curve; some venom fractions did not cause an inhibitory effect on these cells. This was indicated with the symbol (-).

Species	Fraction ID	LD ₅₀ (µg/ml)		
		CMT28	CMM26	MDCK
<i>N.atra</i>	i9_r1	22.54	5.057	79.43
<i>N.siamensis</i>	i9_r4	35.97	5.65	103.03
<i>N.kaouthia</i>	i9_r2	38.81	5.36	-
	i10_r3	40.36	7.07	-
<i>N.nigricollis</i>	i8_r6	35.97	17.02	-
	i8_r7	57.94	10.49	-
	i9_r3	2.23	43.05	-
	i9_r4	48.64	30.34	-
	i11_r3	15.27	3.37	34.04

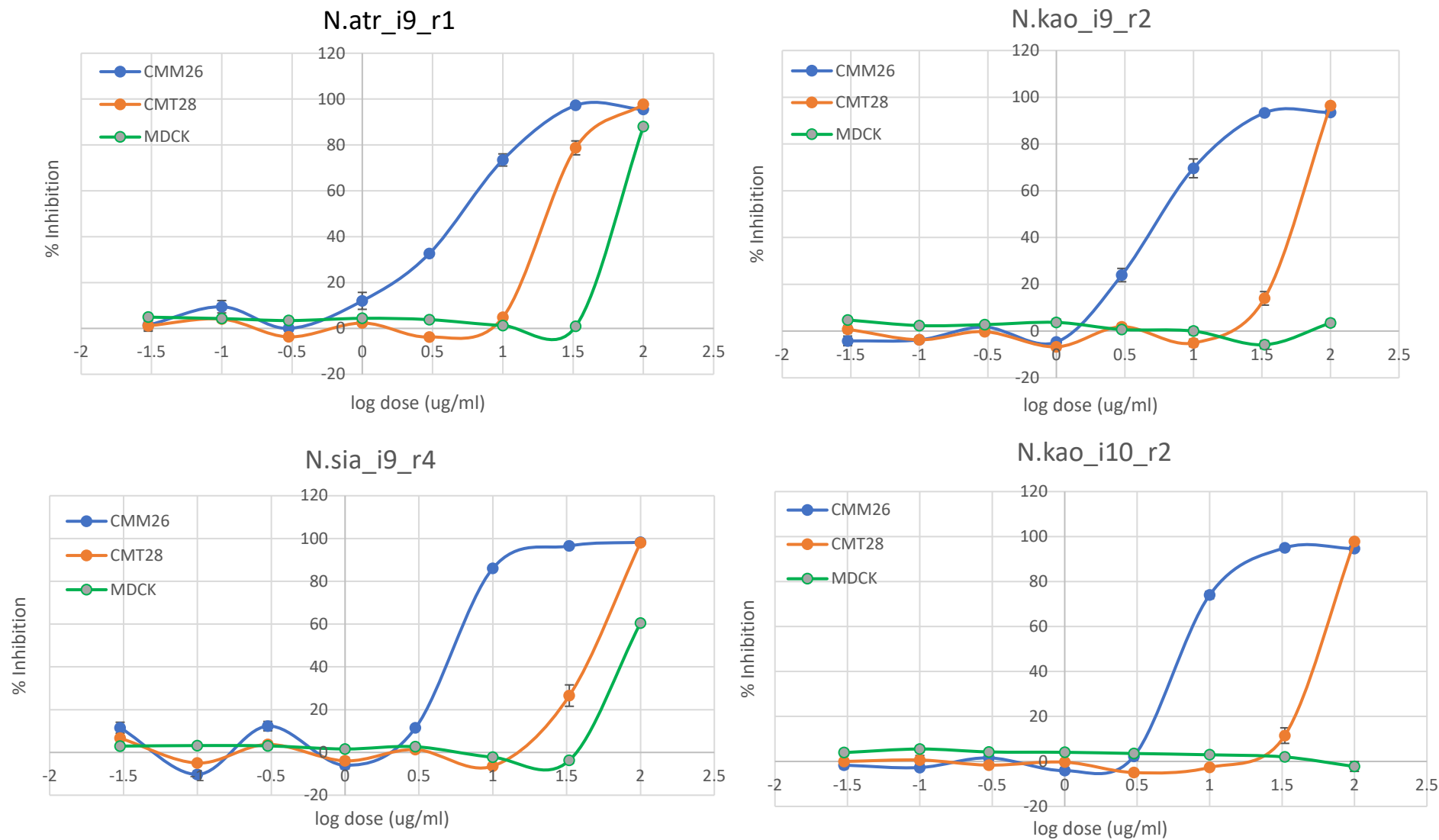


Figure 4.4A: Dose response of Hit Venom Fractions from the T-VDA^{ctx} Assay

Displays % inhibition of CMT28 (Orange), CMM26 (Blue) and MDCK (Green) cell lines exposed to 4 hit venom fractions from the T-VDA assay. (Error bars – Standard deviations)

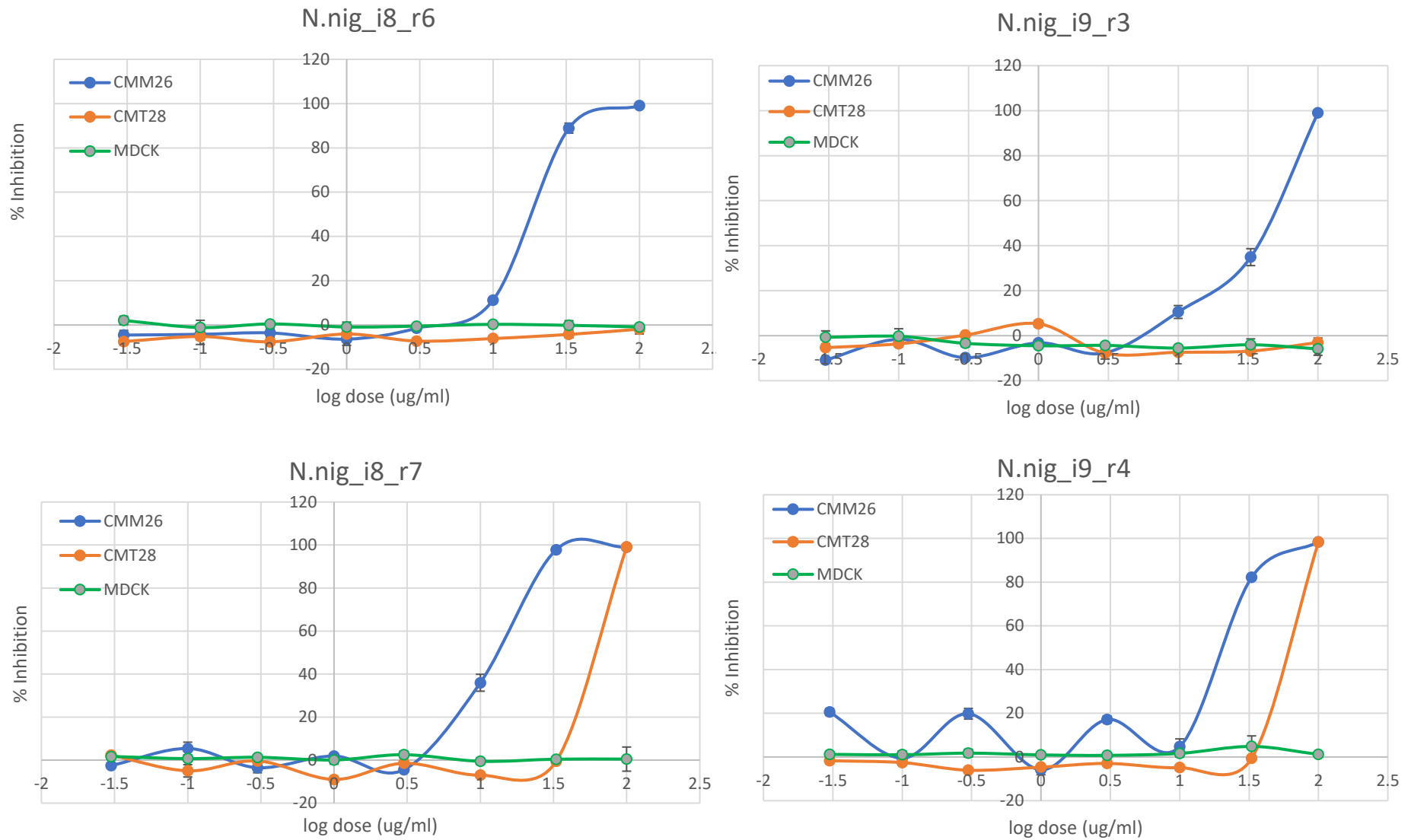


Figure 4.4B: Dose response of Hit Venom Fractions from the T-VDA^{ctx} Assay

Displays % inhibition of CMT28 (Orange), CMM26 (Blue) and MDCK (Green) cell lines exposed to 4 hit venom fractions from the T-VDA assay. (Error bars – Standard deviations)

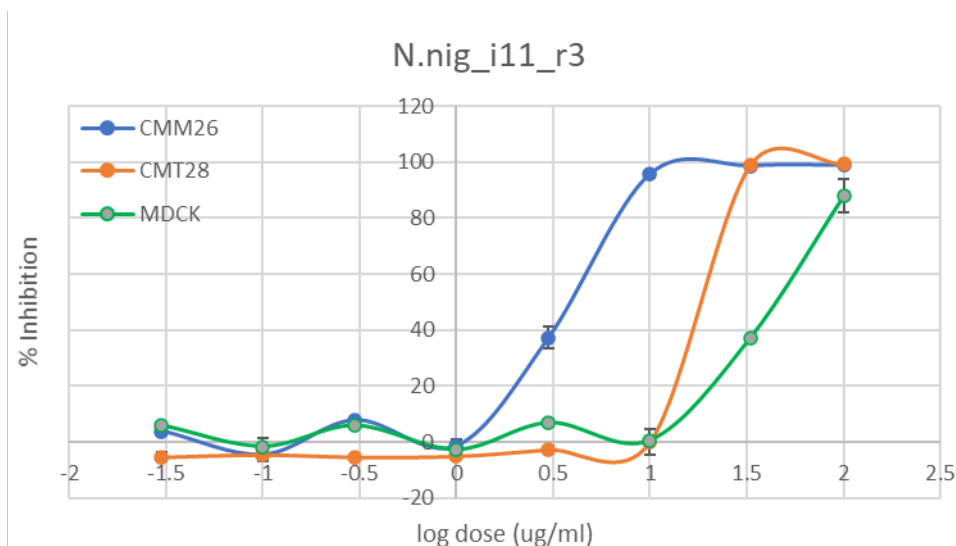


Figure 4.4C: Dose response of Hit Venom Fractions from the T-VDA^{ctx} Assay

Displays % inhibition of CMT28 (Orange), CMM26 (Blue) and MDCK (Green) cell lines exposed to 4 hit venom fractions from the T-VDA assay. (Error bars – Standard deviations)

4.4.6 Identifying Cytotoxic Doses of Hit Fractions on CMT28, CMM26 and MDCK cells

5 Fractions from 4 species within the *Naja* genus were chosen to take forward for Intact Mass Spectrometry and Peptide Digest Mass spectrometry at Peak Proteins (Table 4.6) (Appendix XVI). Data produced from Intact Mass Spectrometry revealed the overall molecular mass of the protein, while Peptide Digest Mass Spectrometry identifies the amino acid sequence of the peptides from the digest.

Table 4.6: Venom fractions sent for Mass Spectrometry Analysis

Species	Fraction ID
<i>N.atra</i>	i9_r1
<i>N.siamensis</i>	i9_r4
<i>N.kaouthia</i>	i9_r2
	i10_r2
<i>N.nigricollis</i>	i11_r3

Mass spectrometry identified all venom fractions as three-finger toxins. This is not an unexpected result as it has been documented that the most abundant protein within the venom of the *Naja* spp is the three-finger-toxin (Tasoulis and Isbister., 2017). The molecular weights produced from each fraction varied

between 6.70-6.88kDa which equates to the low molecular weights of the three-finger toxins (Tasoulis and Isbister., 2017).

BLAST searches on the amino acid sequence fragments of all 5 of the venom fractions identified matches in sequences of cytotoxins within the same species and other toxins such as cardiotoxins within the *Naja* genus. Sequences of high similarity displayed sequence similarities with a sequence length of between 60-80 amino acids in length. This variation in sequence length is due to an evolutionary conserved region made up of 33 amino acids which is only found within the a select few species of the *Naja* genus, such as *Naja atra*, *Naja kaouthia*, and *Naja sputatrix*. Looking into the partial sequences obtained within the Mass Spectrometry data of the five venom fractions, the sequences have not identified this conserved region of 33 amino acids; thus, suggesting that these sequences are likely to have a similar composition to those of a smaller size, of 60 amino acids.

Using the Uniprot database, the cytotoxins with similar sequence lengths of approximately 60 amino acids in length were aligned to identify similarities in sequences (Figure 4.5). Alignment of these sequences revealed areas of evolutionary conserved residues across the different cytotoxins; predominately at the beginning and the end of the sequence, with a region of variability located in the centre of the sequence which is observed to show a combination of residues unique to each cytotoxin. With these identified regions in mind, the sequence fragments obtained from Mass Spectrometry were aligned with the cytotoxin sequence of 60 amino acids in length to identify the conserved and variable regions (Figure 4.5). It is observed that each of the fragmented sequences of the fractions cover the variable region across the cytotoxins, however there are not any matches to the aligned sequences; this indicates that these sequences are novel sequences.

Analysis of N.atr_i9_r1 fraction revealed identification of 2 main peaks with a mass of 6.7387kDa and 6.784kDa, while peptide mapping sequence revealed sections of continuous amino acid sequence. BLAST searches revealed that the fragmented sequences have high identity

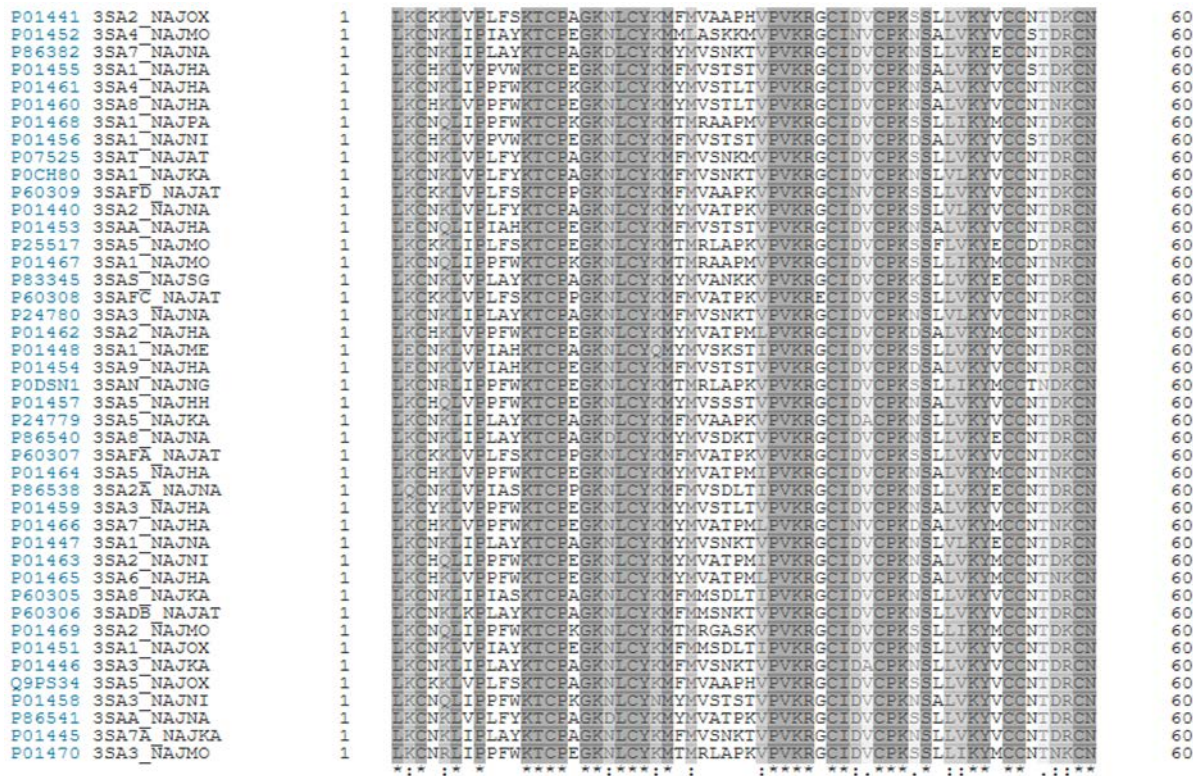


Figure 4.5: Sequence Alignment of Cytotoxins from the *Naja* genus

Shows the alignment of amino acids sequences of cytotoxins from several species of the *Naja* genus with a sequence length of 60 amino acids. An asterisk (*) indicates amino acid positions which have a fully conserved residue. A colon (:) indicates conservation between sequences are strongly similar. A period (.) indicates conservations between sequences are weakly similar..

matches with cardiotoxins within the same species of *Naja atra* with 83% identities. Observing the regions that differ from those that are in the database, it shows consistency that 2 regions between residues 17-21 and 43-47 vary across the aligned sequence. Yet, the sequences which show high identities have much higher molecular weights, potentially suggesting that this is a novel sequence for a cytotoxin from *Naja atra*.

The venom fraction from *Naja siamensis*, N.sia_i9_r4 generated a single main peak with a molecular mass of 6.7385kDa. Using the identified sequence fragments, a BLAST search was carried out which displayed sequences of high identity of 88-87%. These high identity sequences are cardiotoxins from the same species (PDB: Q9W6W9, P01443, P01442, P01443). However, when adding additional amino acids to the fragmented sequence to match any high identity sequences, the molecular weight is calculated to be too low between 7.5-7.7kDa, thus, it cannot be identified as a protein within the database as the molecular weights of the cytotoxins range between 9-9.7kDa.

Query	TCPAGKNLCYKMFVSNKTVPVKGRCIDACPKNSLLVKYVCCNTDR
Subject	TCPAGKNLCYKMFVSNKTVPVKGRCIDACPKNSLLVKYVCCNTDR

Figure 4.6: Sequence Alignment of N.kao_i9_r2 and Cytotoxin 3

Sequence alignment of amino acid sequence fragments from N.kao_i9_r2 and BLAST search match of Cytotoxin 3 (Uniprot: P01446). Shows 100% similarity. The Query sequence displays the N.kao_i9_r2 fragments sequence available and the Subject sequence is Cytotoxin 3.

The data from Mass Spectrometry for the fraction N.kao_i9_r2 produced 2 main peaks with molecular weights of 6.7084kDa and 6.7365kDa. Identification of one of the peaks displayed was Bovine Serum Albumin (BSA) which is a substance that has contaminated the venom fraction sample; however, the molecular weight is unknown between the two which is BSA. A BLAST search identified the protein as Cytotoxin 3 from the *Naja kaouthia* species (Osipo, Astapova et al., 2004) with a 100% match (Figure 4.6). Other high identity sequence matches are various cytotoxins from the *Naja* genus, with residue variations of 1. The molecular masses of both the venom fraction and Cytotoxin 3 vary by 8.6Da, that is using the molecular weight of 6.7084kDa from the Intact Mass Spectrometry data. This variation may be due to not taking into consideration the 4 disulphide bonds that are found in the structure (Osipo, Astapova et al., 2004).

Analysis of the Mass Spectrometry data of the N.kao_i10_r2 venom fraction produced a predominant main peak of a molecular weight of 6.7384kDa. A BLAST search of the fraction displayed high identities at 78.26% across 8 aligned sequence, which identify as cytotoxins from species within the *Naja* genus. The similarities in sequences were mainly located in the regions that are conserved, as previously displayed in Figure 4.5. Yet, the regions within the sequence in which they differ is the variability region that is unique to each cytotoxin.

A BLAST search of the venom fraction N.nig_i11_r3 revealed a sequence match of a cytotoxin in the same species (*Naja nigricollis*) with an identity match of 92% (Figure 4.7). The highly matched sequence is identified as Naniproin, which is a three-finger cardiotoxin (Girish, and Kini., 2016). Two sequence fragments of the venom fraction were obtained through Peptide Digest mass spec. that appear to completely match the sequence of the Naniproin toxin, apart from a region of 4 residues. Comparing

molecular weights with the Naniproin toxin there is 8.86Da difference between the proteins, with N.nig_i11_r3 measuring at 6.8866kDa, and Naniproin at 6.89546kDa. The minimal variations within the molecular weight may be due to the intact mass spectrometry not taking into consideration the 4 disulphide bonds found in the structure (Girish, and Kini., 2016).

Query	TCPAGKNLCYKMFVSNKTVPVKGRCIDACPKNSLLVKYVCCNTDR
Subject	TCPAGKNLCYKMFVSNKTVPVKGRCIDACPKNSLLVKYVCCNTDR

Figure 4.7: Sequence alignment of N.nig_i11r3 and Naniproin

Sequence alignment of amino acid sequence fragments from N.nig_i11r3 and BLAST search match of Naniproin (Uniprot: P0DSN1). Shows 92 % similarity. The Query sequence displays the N.nig_i11r3 fragments sequence available and the Subject sequence is the Naniproin.

4.4.7 Conclusion

9 venom fractions for the T-VDA^{cyx} assay were proven to selectively reduce cell viability across CMT28, CMM26 and MDCK cells respectively. These fractions were from the *Naja* genus, which is not surprising as the Resazurin assay was optimised utilising venoms from this genus.

Fractionation and Mass spectrometry data produced from these fractions prove that they are individual proteins with possible identifications. Although incomplete sequence data was produced for each of the fractions, BLAST searches identified regions of comparability and confirmed evolutionary conserved regions within three-finger toxins found on the Uniprot database. The presence of the preserved regions within the fragmented sequences confirmed the identity of the fractions being three-finger toxins; however, identification of a variable region that is consistent with many toxins found on the database, prove that 3 of the fractions are novel proteins. High sequence compatibility with the calculations of molecular weight confirm the identification of 2 sequences: Cytotoxin 3 from *Naja kaouthia* and Naniproin from *Naja nigricollis*.

Selectivity of inhibition between cancerous and non-cancerous cells suggest that the cancerous cells express a target that the non-cancerous cells do not. In terms of understanding the effects of these fractions at a molecular level, follow up work of performing additional experiments including fluorescence labelling of the protein fractions, would explore the regions on the cells that the fractions target.

Chapter 5: HER2 Receptor Expression and Molecular Docking of Venom Peptides on the Canine HER2 Receptor

5.1 Introduction

Traditional drug discovery process initiates with the identification of a target of interest, as well as a possible drug like molecule. Processing any significance between the target and the drug requires hours of optimisation whether its *in-vitro*, *in-vivo* or in pre-clinical studies, to determine whether the drug is effective and has the potential to be developed into a clinical drug. Conventional methods in understanding the mechanisms between the target and drug would require structural analysis through the use of x-ray crystallography and nuclear magnetic resonance (NMR). With these techniques used, come the efforts in solving the protein structure which can be difficult and often time-consuming (Zheng and Zhang *et al.*, 2018). There is now an ever-increasing rate of experimental structure determination, yet the number of newly discovered sequences grows much faster than the number of structures solved (Dutta and Berman., 2005; Xiang., 2006). The process from drug discovery, drug development and communalisation are complex, thus, to overcome these issues alternative structure predictors such as computational modelling, would allow structures to be easily utilised which would be cost effective and less time-consuming.

Using computational modelling to generate structures has become a powerful tool for the prediction of protein structure when only the sequence data is available (Service, 2020). Homology modelling is an accurate computational method to create reliable structural models. Homology models are created using sequences that share high similarities and identity, with the structures available being retrospectively similar (Gromiha and Nagarajan *et al.*, 2018). I-TASSER (Iterative Threading ASSEMBLY Refinement) is an online-server algorithm which produces automated protein structure prediction (Zhang.,2008; Roy and Zhang.,2010; Yang and Zhang., 2015; Zhang *et al.*, 2018). I-TASSER structure prediction detects structure templates from the Protein Data Bank (PDB) through threading-based fold recognition. Full-length models are structurally constructed though resembling structural fragments and refinement simulations (Zhang *et al.*, 2018).

Generating homology models then allows for the exploration of molecular docking predictions. Investigating the possibilities of protein and drug interactions in *silico* is becoming an increasingly used tool in drug discovery. Yet again this tool is low-cost and allows for hundreds and thousands of compounds, whether its drugs or proteins, to be screened on a single target, which dramatically reduces the time in the laboratory (Malathi and Ramaish., 2018). The approach of molecular docking allows simulated models to be created through the interaction between a small molecule (protein, drug or other compound) at an atomic level; thus, characterising the behaviour of the small molecule and the potential binding sites of the target (Meng, Zhang *et al.*, 2012). Z-DOCK (Pierce *et al.*, 2014) is a rigid-body protein-protein docking programme that produces docking models through combination factors; shape complementarity, electrostatics and statistical potential.

Utilising these programmes, models and simulations of the identified venom peptides from Mass Spectrometry, Cytotoxin 3 from *Naja kaouthia* and Naniproin from *Naja Nigricollis*, can be generated to display the docking abilities on a target receptor of interest. The HER-2 receptor is seen as a potential therapeutic target for breast cancers in woman; as it is noted that approximately 15-30% of breast cancers overexpress this receptor (Burstein., 2005; Iqbal and Iqbal., 2014) and overexpressed in 29.7-38% of mammary cancer cases in dogs (Clavijo-Maldonado *et al.*, 2020). Thus, with the specificity of venoms observed to inhibit canine mammary cancer cell lines in **Chapter 4**, the HER-2 receptor is a justifiable target to cause cell death.

5.2 Aims

- Use Fluorescent microscopy to visualise HER2 receptor expression on CMT28, CMM26 and MDCK cells
- To screen the effects of whole venom and hit venom fractions on the HER2 receptor using Dot Blots against Canine Cancer cell lines CMT28 and CMM26
- Generate a 3D Structural Model for the Canine HER2 receptor
- Perform protein-protein docking with Venom peptides on the Canine HER2 receptor

5.3 Materials and Methods

5.3.1 HER2 Receptor Expression in CMT28, CMM26 and MDCK using Fluorescence Microscopy

Fluorescence microscopy was performed on CMT28, CMM26 and MDCK cell lines to study the expression levels of the HER2 receptor. SKBR3 cells were used as a positive control, as this cell line over-expresses the receptor, while COS7 cells were used as a negative control, as they do not express any receptors. Both SKBR3 and COS7 cells were cultured as stated in the standard protocol in **section 2.2.2**. Cells were seeded in 12 wells plates as stated in the protocol of **section 2.3.1** with a cover slip at the bottom of the wells. After plating the cells, they were left to settle and adhere to the bottom of the wells overnight. The following day, the media was removed from each well and washed three times with 1ml of PBS. The cells were then fixed using 4% Paraformaldehyde and incubated at room temperature (RT) for 10 minutes. After fixation the cells were then washed three times with 1ml of PBS. To permeabilise the cells 1ml of 0.1% triton was added to each well and incubated at RT for 20 minutes. Next, to prevent non-specific binding of the antibodies the cells were blocked using 2.5% BSA for 1.5 hours at RT. After blocking the cells, 250ul of CB11 primary antibody (Gifted by Professor Bill Gullick, University of Kent, UK) was added to each well and incubated overnight at 4°C in the fridge. The next day the primary antibody was taken off and the cells washed three times with 1ml of 0.1% triton. The cells were then incubated in the secondary antibody of ab175470 for 1 hour at RT in the dark. After incubation the cells were then washed in 0.1% triton six times and then washed with PBS three times. The cells were then counterstained with 4',6-diamidino-2-phenylindole (DAPI) stain for 5 minutes at RT in the dark. Once stained, the cells were then washed with PBS twice and then washed with PBS three times. To prepare the slides, 3ul of mounting media (mowiol) was added to each microscope slide. The cover slip with the probed and stained cells were removed from the plate and placed face down onto the mounting media. The mounted slides were then left to dry overnight at RT, and then stored at 4°C until visualised using an Olympus bx63 fluorescence microscope.

5.3.2 Cell lysis for Dot Blot Analysis

CMT28 and CMM26 cells were grown in T25 flasks to a confluency of 90% in supplemented culture media. An additional cell line SKBR3 was also grown in T25 flask to a confluency of 90% in supplemented DMEM culture media.

To begin lysis, the culture media was removed from each flask of cells and washed with 5ml of PBS solution twice. Radioimmunoprecipitation assay (RIPA) lysis buffer (Fisher, UK) was supplemented with 10 μ l of Halt Protease inhibitor cocktail (100x) (Fisher, UK) and 10 μ l Ethylene diamine tetra-acetic acid (EDTA) (100x) (Fisher, UK) for every ml of lysis buffer. 1ml of supplemented RIPA buffer cocktail was added to each flask of cells and incubated on ice for 10 minutes. Complete cell lysis was confirmed by inspecting the flasks using an inverted microscope.

The cell lysates were then transferred from the flask into 1ml Eppendorf tubes (Fisher, UK) and centrifuged for 10 minutes at 4°C and 13,300 rpm (17,000 x g) in a benchtop microcentrifuge. Once centrifuged to pellet cell debris and DNA, 900 μ l of supernatant was transferred from each tube to a new 1ml Eppendorf tube and stored at -80 °C until blot blots were carried out.

5.3.3 Determining Protein Concentration of Cell lysates via DS-11 Analysis

Using the lysed cells of CMT28, CMM26 and SKBR3 prepared in **section 5.3.2**, the protein concentration of each cell line was determined using a DeNovix DS11 spectrophotometer (DeNovix, UK). The DS-11 was blanked using HPLC grade H₂O before being used to read the absorbance at 280nm of 1 μ l of each cell lysate sample. The reading was taken in triplicates and the average protein concentration was then determined from these readings.

5.3.4 Dot Blot Preparation for Assessing HER2 Binding ability to Whole Snake Venoms

Using a nitrocellulose membrane, a total of 10 μ g of protein from the whole venoms of *Naja atra*, *Naja Kaouthia*, *Naia Siamensis* and *Naja nigricollis* was dotted on the membrane (Appendix XVII) and left to dry for 15 minutes at RT. Once dried, the membrane was blocked by adding 20ml of 5% Bovine Serum Albumin in PBS-Tween-20 solution to each blot and left on a rocker for 2hours at RT.

Once blocked the cells were then washed with PBS-Tween-20 solution for 10 minutes, three times.

Using the cell lysates prepared in **section 5.3.2**, 500ug of total protein from each cell lysate was prepared in 20ml of PBS-Tween-20 and added to each membrane and incubated overnight at 4 °C. After overnight incubation the cell lysate solution was removed and the membranes were washed with PBS-Tween-20 solution for 10 minutes, three times. A primary antibody solution (CB11 at a dilution factor of 1:100) of 10ml was added to each membrane and incubated on a rocker for 1hr at RT. After incubated the membranes were then washed with PBS-Tween-20 solution for 10 minutes, three times. A secondary antibody solution (anti-mouse HRP at a dilution factor of 1:20,000) of 10ml was added to each membrane and incubated on a rocker for 1hr at RT. The membrane was then washed with PBS-Tween-20 solution for 10 minutes, three times.

ECL reagents 1 and 2 were prepared as shown in table 5.1. The membranes of each cell line were developed using a Biorad ChemiDoc and the ECL reagents prepared to a 1:1 dilution with 2ml of ECL used for each membrane. The membranes were imaged simultaneously at different exposure times to obtain the optimal exposure timepoint.

Table 5.1: ECL reagent solution makeup

ECL reagent 1	ECL reagent 2
Luminol (250mM/DMSO) - 500µl	30% H ₂ O ₂ - 32µl
Coumaric acid (90mM/DMSO - 220µl	Tris/HCL (pH8.5) (1M) – 5ml
Tris/HCL (pH8.5) (1M) – 5m	dH ₂ O – 44.68ml
dH ₂ O – 44.28ml	

5.3.5 Generating Homology models for the Extracellular domain of the Canine HER2 receptor using I-TASSER

Structural data was not available for the extracellular domain of the HER2 receptor in the Canine, therefore the amino acid sequence of canine HER2 (Appendix XIX) was acquired from Uniprot accession number O18735 and downloaded as a FASTA file (Bateman, A., 2019; The UniProt

Consortium., 2019). The amino acid sequences for the Canine HER2 receptor was submitted onto an online server to generate a 3-dimensional structure.

I-TASSER (Iterative Threading Assembly Refinement) is an online server designed for automated protein structure and function prediction (Zhang, Y., 2008; Yang, J., & Zhang, Y., 2015), (Available at <http://zhanglab.ccmb.med.umich.edu/I-TASSER/>). I-TASSER uses the submitted amino acid sequence which is threaded through the PDB structure library using a pair-wise sequence identity (similarity of 70% or above) to search for feasible folds using alignment algorithms to generate full length models; Markov model (Karplus, K., Barrett, C., & Hughey, R., 1998), PSI-BLAST (Altschul, S. F., et al, 1997), the Needleman-Wunsch (Needleman, S. B., & Wunsch, C. D., 1970) and Smith-Waterman (Smith, T. F., & Waterman, M. S., 1981) alignment algorithms. The full-length model is assembled by reconstructing aligned fragments, whereas unaligned fragments, predominately loops, are assembled by *ab initio* modelling. Using the SPICKER algorithm, structure trajectories are grouped to recognise structures of similar family proteins to improve the model, where low energy conformations are favoured.

5.3.6 Minimisation of the Canine HER2 receptor system

Gradient minimisation was performed on the structure of the HER2 protein. This optimises the geometry of all atoms within the system and finding conformation at the lowest energy point. Minimisation was performed in NAMD utilising the CHARMM36 forcefield. Harmonic constraints were on set to on. The harmonic constraints on the carbon α 's on the backbone of the protein were set to 2. *Langevin* variables were on with *langevinDamping* set to 5. *langevinTemp* was set to 310K. Minimisation was performed for 2500steps (Appendix XX) .

5.3.7 Heating of the Canine HER2 receptor system

Once the HER2 protein was minimised, the system was then subject to being heated to 310K. in addition to the minimization prior within the solvation box. Utilising the binary coordinate, velocity and extended system files generated from minimisation. The protein was subject to the same harmonic constraints as previously mentioned in **section 5.3.6** The initial temperature of the system was set to 0K

and set to increase by 0.001K per timestep using the *reassignTemp* algorithm producing a total amount of timesteps of 310,000 (Appendix XXI).

5.3.8 Equilibration of the Canine HER2 receptor system

Output files from heating the HER2 protein, binary coordinates, velocity and extended system files was utilised to initiate the equilibration process. The system temperature remained set to 310K. Output parameters were on, with *outputenergies* set to 50, *outputtuning* set to 500, *outputpressure* set to 500. *Dcdfreq* and *XSTFreq* was set to every 2000 steps *langevinDampening* was set to 1. Harmonic constraints applied remained the same as previously set in the heating process. Forcefield parameters remained the same using CHARMM36, which was run for 2fs producing 2,000,000 timesteps (Appendix XXII)

5.3.9 Generating a Model of the Cytotoxin Naniproin using Quark

No structural data was available for the Naniproin cytotoxin, therefore the amino acid sequence was acquired from Uniprot accession number P0DSN1 and downloaded as a FASTA file (Xu and Zhang, 2012; The UniProt Consortium., 2019). The amino acid sequence was submitted onto the online server to generate a 3-dimensional structure.

QUARK utilises the query sequence by generating structural fragments from each residue position based on gapless threading through PDB structures. With the gapless threading constraints, torsion angle distribution is collected from each residue position, with a residue-residue connect map that is derived from the distance profiles between fragments. Next replica-exchange Monte Carlo (REMC) stimulations are carried out to assemble the fragments into full-length models under a composite physics- and knowledge-based potential, containing hydrogen bonding, van der Waals, solvation, Coulomb, backbone-torsion, bond-length and bond-angle, atomic distance, and strand pairing interactions (Yang, *et al.*, 2003; Xu and Zhang, 2013; Zhang, *et al.*, 2016). The final models are selected by SPICKER (Zhang and Skolnick, 2004), which clusters all the decoys generated in the REMC simulations and ranks models by the size of the clusters.

5.3.10 Structure-Activity-Relationship Analysis of Cytotoxin

Alignment of sequences was performed with the Mass Spectrometry data obtained in **section 4.4.6**. BLAST searches were performed on all 5 cytotoxins. Sequences that showed high similarity in identify were chosen and an alignment was performed on all sequences through Uniprot alignment tool (The UniProt Consortium., 2019) and downloaded as a FASTA file. The FASTA file was then input into the Open WebProAnalyst server (Ivanisenko, et al., 2005) (available at <http://wwwmgs.bionet.nsc.ru/mgs/programs/panalyst/>) and submitted alongside the LD50 values. The Open WebProAnalyst uses a sequence–activity correlation/determination coefficient (SACC/SADC) that searches for the functionally important positions in a multiple alignment of homologous proteins. The SACC is calculated as the square root of the SADC and expresses the strongest multiple correlation between the physicochemical characteristics of a site in a multiple alignment and the protein activities.

5.3.11 Molecular Docking of Cytotoxins to the Canine HER2 receptor

To predict structures of protein-protein complexes between the Canine HER2 receptor and the cytotoxins of Naniproin and Cytotoxin-3, the HER2 structure generated in section **5.3.5** and the structure of the two cytotoxins were submitted independently to ZDOCK (Pierce, *et al.*, 2014). PDB files of the structures were submitted to the ZDCOK server with the option of no restrictions on amino acid interaction.

ZDOCK is a rigid-docking server that utilises the Fast Fourier Transform (FFT) algorithm which initiates the protein-protein docking server by searching entire rotational and translational space of the ligand with respect to the receptor (Katchalski-Katzir *et al.*, 1992). The Receptor remains fixed to an origin to establish shape complementarity using grid-based shape complementarity and Poisson–Boltzmann electrostatics (Pierce, *et al.*, 2014).

5.4 Results and Discussion

5.4.1 Expression levels of the HER2 Receptor in CMT28, CMM26, MDCK

To identify the abundance of the HER2 receptor on CMT28, CMM26 and MDCK, green fluorescent protein (GFP) alongside antibody exposure allowed the expressions levels to be visualised. Control cell lines were used to determine the expression state; SKBR3 cells which overexpresses the HER2 receptor

was used as a positive control for overexpression. For the negative control to visualise the absence of the HER-2 receptor, COS-7 cells were used.

Visual representation of SKBR3 indicate that the antibody-probe application was successful, as GFP is present in abundance. GFP was not present on the negative control cell line, COS-7 cells, which visually demonstrates a cell with no expression of the HER2 receptor. Fluorescence of GFP was observed on the CMT28 and CMM26 cell line. Both cell lines produced a small observational presence of the HER2 receptor, indicating that the receptor is present in a low abundance, in comparison to the SKBR3 cells (Figure). Small regions on the CMM26 cells displayed dense areas of GFP, signifying that there are compacted areas of the receptor. The MDCK cells did not show green fluorescence indicating that the cell line does not express the HER2.

It is not conclusive where the receptor is located from the images obtained, due to utilising permeabilising agents. GFP is observed to be present in other regions other than the cell membrane. The HER2 receptor is found predominantly on the cell membrane as it is a cell-surface receptor, though HER2 is also known to translocate to the nucleus to carry out transcriptional activity. Nuclear HER2 is recognised to stimulate transcription, as it forms complexes at specific nucleotide sequence for the COX-2 promoter (Wang, S. C., et al, 2004; Hsu, J. L., & Hung, M. C., 2016). HER2 can also be found with the cytoplasm through receptor re-cycling and lysosomal degradation (Yarden, Y., 2001). Thus, to confirm the of the HER2 receptor, using fluorescent microscopy with cells embedded into paraffin wax with the addition of markers to label specific structure within the cell, this would allow cells to be sectioned enabling a clearer identification of the receptor's location.

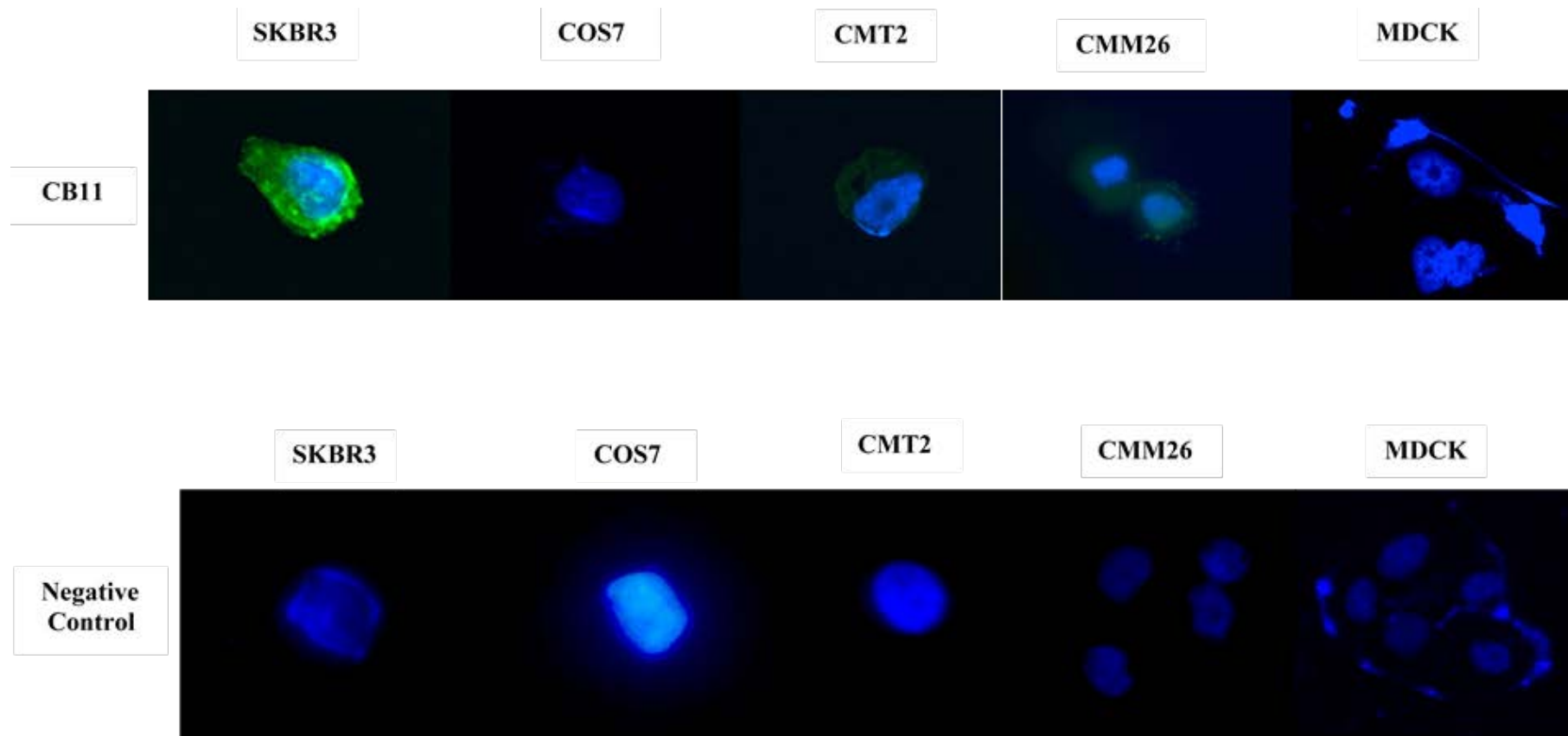


Figure 5.1: Detection of HER2 expression levels in CMT28, CMM26 and MDCK cell lines using Fluorescent Microscopy
 Using CB11 antibody to identify the presence of the HER2 receptor, probed with Green Fluorescent protein (green). DAPI stain used to visualise the nucleus (blue). The Negative controls of each cell line is to visualise any background readings of the secondary antibody with GFP (Magnification x60).

5.4.2 Binding Affinity of HER2 in Response to Whole Snake Venom

Utilising the whole snake venoms of species in **section 4.4.5** which showed the greatest difference in potency between the canine mammary cancer cell lines (CMT28 and CMM26) and the immortalised normal canine kidney cell line (MDCK). These venoms were taken forward to determine the interaction of the venom on the HER2 found on the cell lines. An additional cell line of SKBR3 (Human Mammary Cancer cell line) was used as a control to observe the binding of the whole venom peptides to the receptor, as this cell line over-expresses the HER2 receptor. It was also used to observe the comparison of binding affinities of the venom peptides between species, Human and Canine. Each Dot Blot membrane was analysed using Biorad's Imagelab software. To determine the binding of the HER2 receptor of each cell line to the whole venom peptides, the pixel intensity was calculated of each dot and an average taken of each venom (Appendix XVIII).

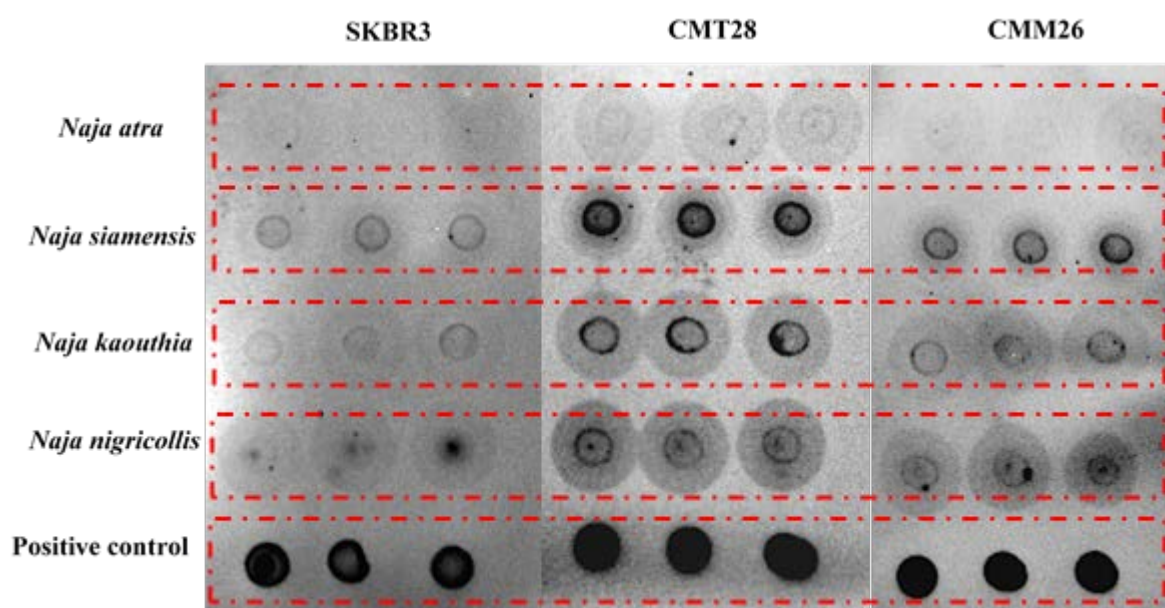


Figure 5.2: Binding of HER2 to Whole Venoms on SKBR3, CMT28 and CMM26 cells

The dot blot analysis shows the binding of HER2 from 3 cell lines – SKBR3, CMT28 and CMM26. Intensity of each dot refers to the binding of HER2 to the whole venom peptides bound to the nitrocellulose membrane. Positive control is cell lysate, showing the total HER2 content within each cell.

Initial observations across the 3 cell lines show evidence of the presence of the HER2 receptor (Positive control) (Figure 5.2), primarily identified in **section 5.4.1** using fluorescence microscopy. The intensities of each positive control for each cell correlates to the expression of the HER2 receptor with

SKBR3 overexpressing the HER2 receptor, while CMT28 and CMM26 display moderate to low abundance of the receptor. In comparing the overall binding of the HER2 receptor to all of the whole venoms used, there is a distinct difference in the binding affinities of the HER2 in human and canine. Higher binding of the HER2 receptor is observed in both of the canine cell lines, compared to the human cell line; considering that the receptors are 92% similar when performing a structural alignment.

Similarities of the binding of HER2 between the two canine cancer cell lines are shown across all whole venoms. The highest amount of binding between the two cell lines is the *Naja siamensis* venom, while the least is the *Naja atra* venom. The composition of the venoms may be a valid reason for the differences in binding affinities of the HER2 receptor. Across the *Naja* genus, the venom contains proteins and peptides of similar structure, such as the 3-finger toxins and phospholipase A2 (Ferraz *et al.*, 2019). Small alterations in the structures of proteins and peptides are observed across the species with influences from the ecological niche they inhabit (Barlow, *et al.*, 2009; Kalam, *et al.*, 2011), thus making each venom unique to each species. Furthermore, particular proteins and peptides have been shown to vary in concentrations across species, and this it has been shown in Tasoulis, 2017.

5.4.3 Optimisation of the I-TASSER Homology model of the Canine HER2 receptor

5.4.3.1 HER2 model Preparation

The model of HER2 from the canine species using I-TASSER. The HER2 model was solvated in water and with the addition of ions (sodium chloride) to neutralise the system, not only does this simulate the microenvironment surrounding the receptor but it will affect the dynamics of the protein through hydrophobic interactions and formations of hydrogen bonds (Takemura and Kitao, 2007; Caldararu, *et al.*, 2020).

5.4.3.2 Minimisation of HER2

Reducing the potential energy of the protein stabilises the conformation, with reductions of local energy values determined by the energy components of atoms, such as stretching, bending and torsion, the protein will be able to reach its global minimum energy (Roy, *et al.*, 2015).

Data obtained from the NAMD log file was analysed using VMD 1.9.4a NAMD plot, including the complete dataset for minimisation calculations (Frames 1 to 125) (Figure 5.3).

Reductions in total potential energy was observed from timestep 1 of 663398E to -448997.95E at timestep 2500. This correlates to the bond energy decreasing from 1588.95E in timestep 1, to 631.43E at timestep 2500, bond angle also decreased to 1987.16 at the last time step and with both factors maintaining a steady amount of energy across the system. Dihedrals steadily decreased from 6263.18 to 5562.67 at the last timestep before levelling out at timestep 2000 maintaining energy at a stable rate. Observations of the RMSD shows an increase in deviations across the system, as the system begins to minimise, but begins to level out from 110 frames.

5.4.3.3 Heating of HER2 to 310K

Data obtained from the NAMD log file and was analysed using VMD 1.9.4a NAMD plot, including the complete dataset for heating (steps 0 to 310,000). Heating of the HER2 model simulates the required temperature of the organism of 310K with each time step increasing the temperature by 1K (Figure ii), with the pressure maintained at a constant for the entire system (Figure 5.4 iv). As the temperature increased the kinetic energy increased at the same rate with the initial kinetic energy at 0 and increase to 73891.55E at the last timestep. Energy steadily increased in bond energy and dihedrals, while bond angle energy increased rapidly from 1987.44E to 5736E. This shows that the system is ready for equilibration.

5.4.3.4 Equilibration of HER2

Initial analysis was completed after equilibration simulation on RMSD trajectory using VMD 1.9.4a. The data demonstrates that throughout the equilibration process of 933 frames the bond angle temperature, potential energy and kinetic energy remain steady across the system; with the exception of dihedrals that display a decreasing in energy from 6262.96E to 6065.68E while maintaining a steady distribution (Figure 5.5). Using the timeline plugin in VMD 1.9.4a the HER2 structure was coloured by RMSD (Figure 5.6) visually merging the data of the atom trajectories of residues over the course of the 933 frames. Regions within the protein that have a high RMSD are shown in red, while regions of low RMSD are shown in blue. The backbone of the HER2 protein show little deviation in RMSD, with only extended residues from the main body of the protein showing high deviation.

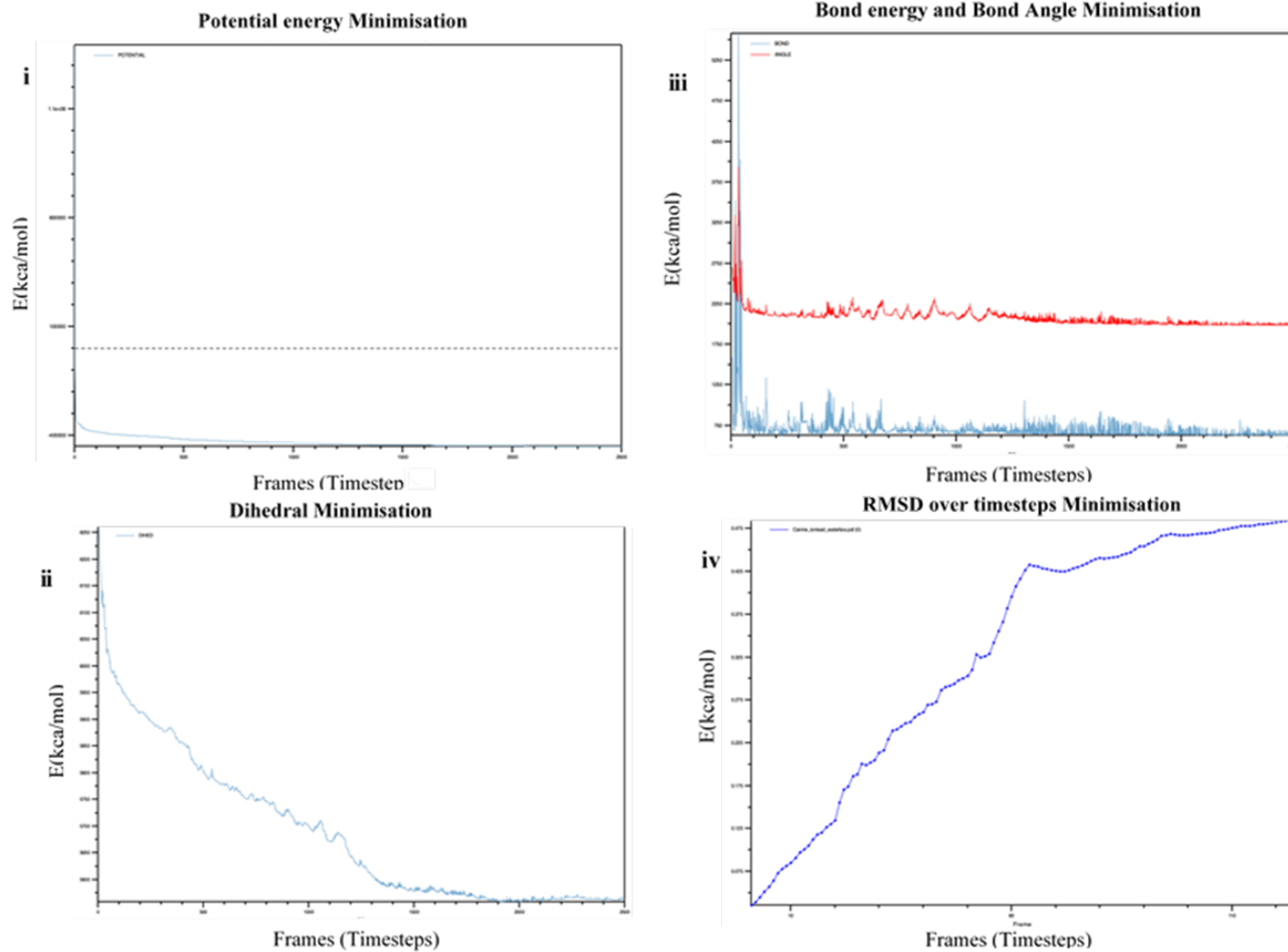


Figure 5.3: Factors Associated with Minimisation of HER2

i: Shows the effects of Potential Energy during equilibration; ii) Shows Dihedral across the structure; iii) Shows Bond energy and Bond angle across the protein and iv) shows RMSD across the protein over timesteps. Graphs generated using the .log file of the HER2 receptor generated during minimisation simulation, and the analysis NAMD plot.

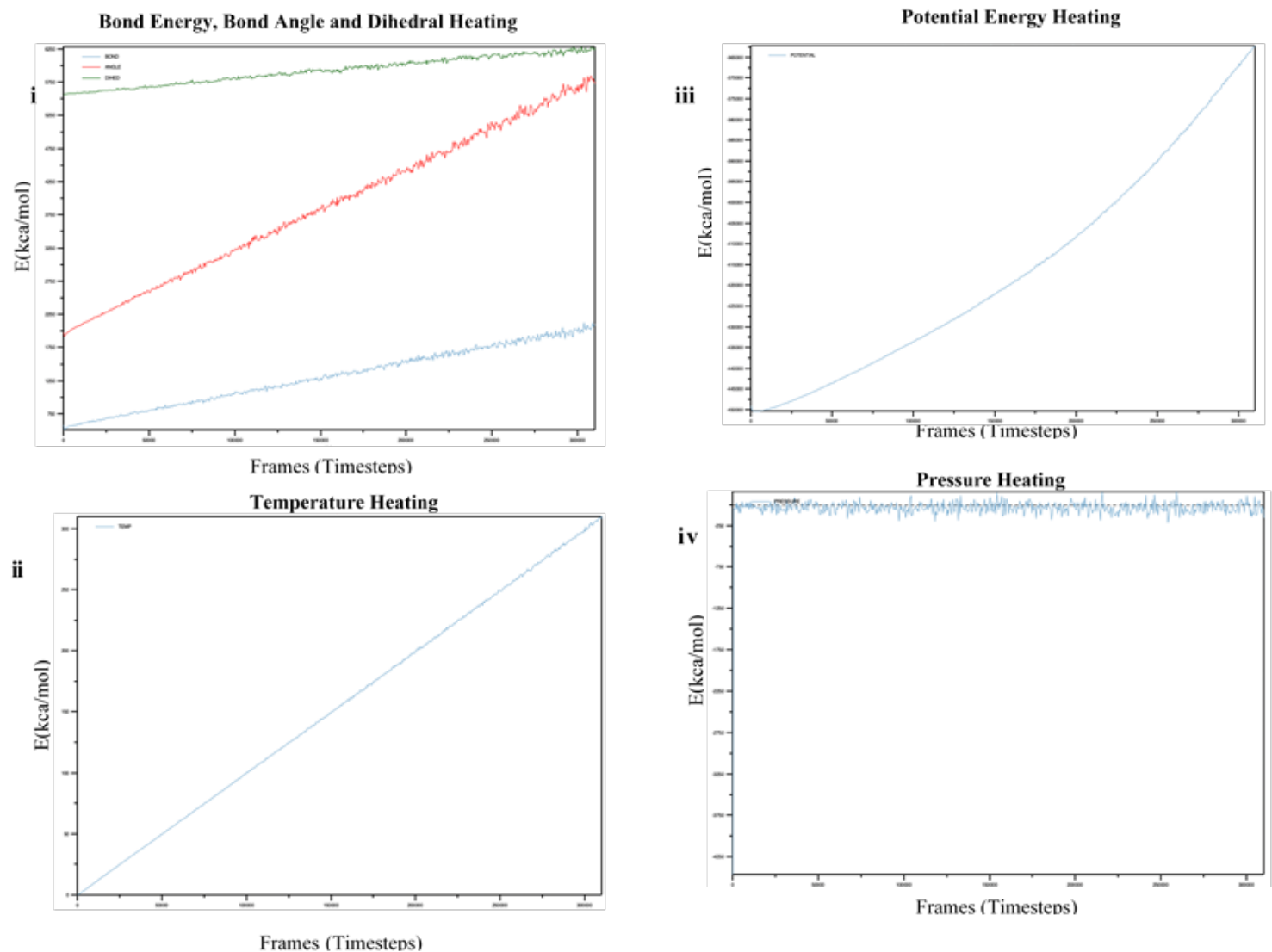


Figure 5.4: Factors Associated with Heating of HER2

i: Shows the effects of Bond energy, Bond angle and Dihedral Heating ii) Shows Temperature distribution across the structure; iii) Shows Potential energy across the protein and iv) shows pressure. Graphs generated using the NAMD log file of the HER2 receptor generated during Heating simulation, and the analysis NAMD plot.

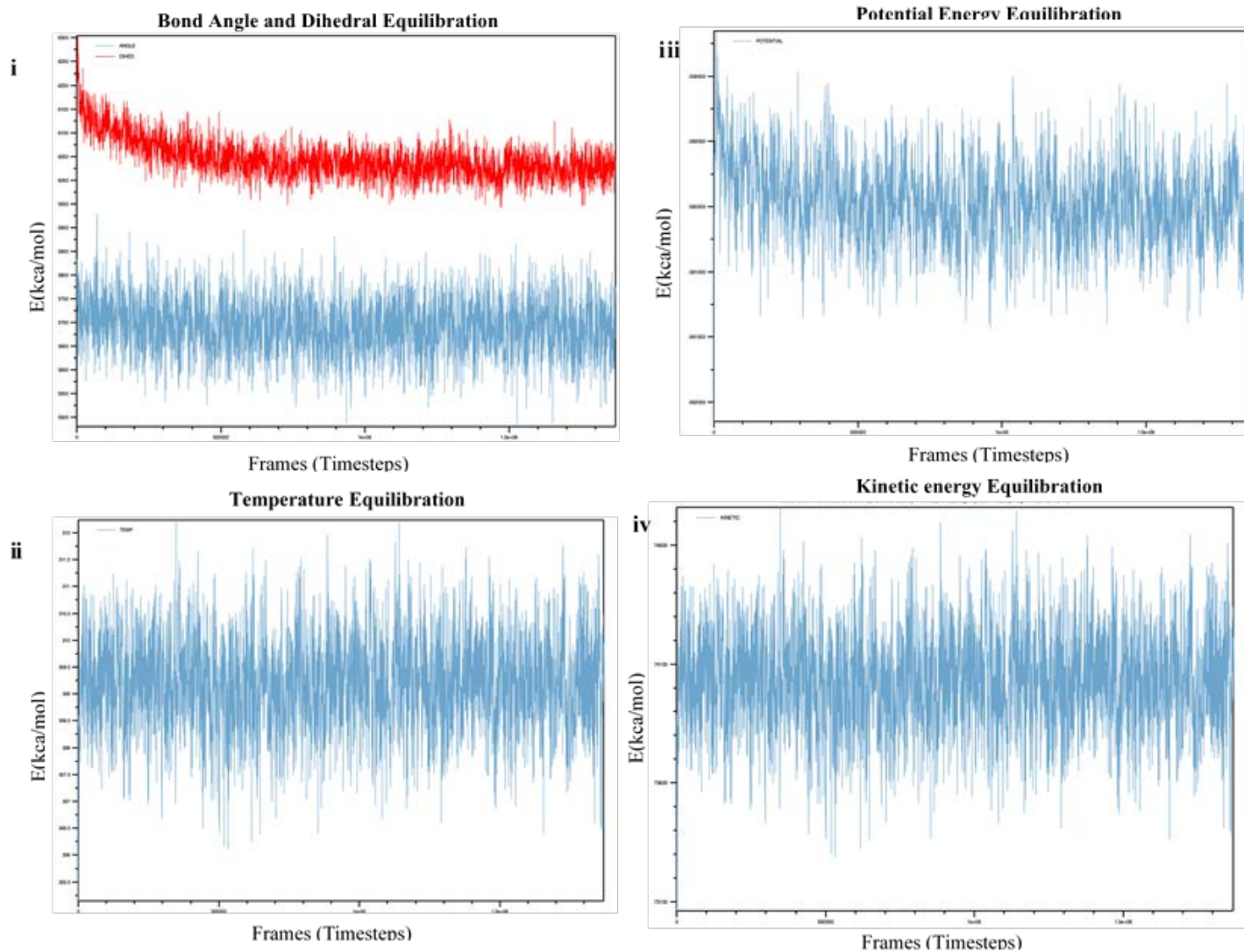


Figure 5.5: Factors Associated with Equilibration of HER2

i: Shows the effects of bond angle and Dihedral during equilibration; ii) Shows Temperature distribution across the structure; iii) Shows Potential energy across the protein and iv) shows kinetic energy across the protein. Graphs generated using the NAMD log file of the HER2 receptor generated during equilibration simulation, and the analysis NAMD plot.

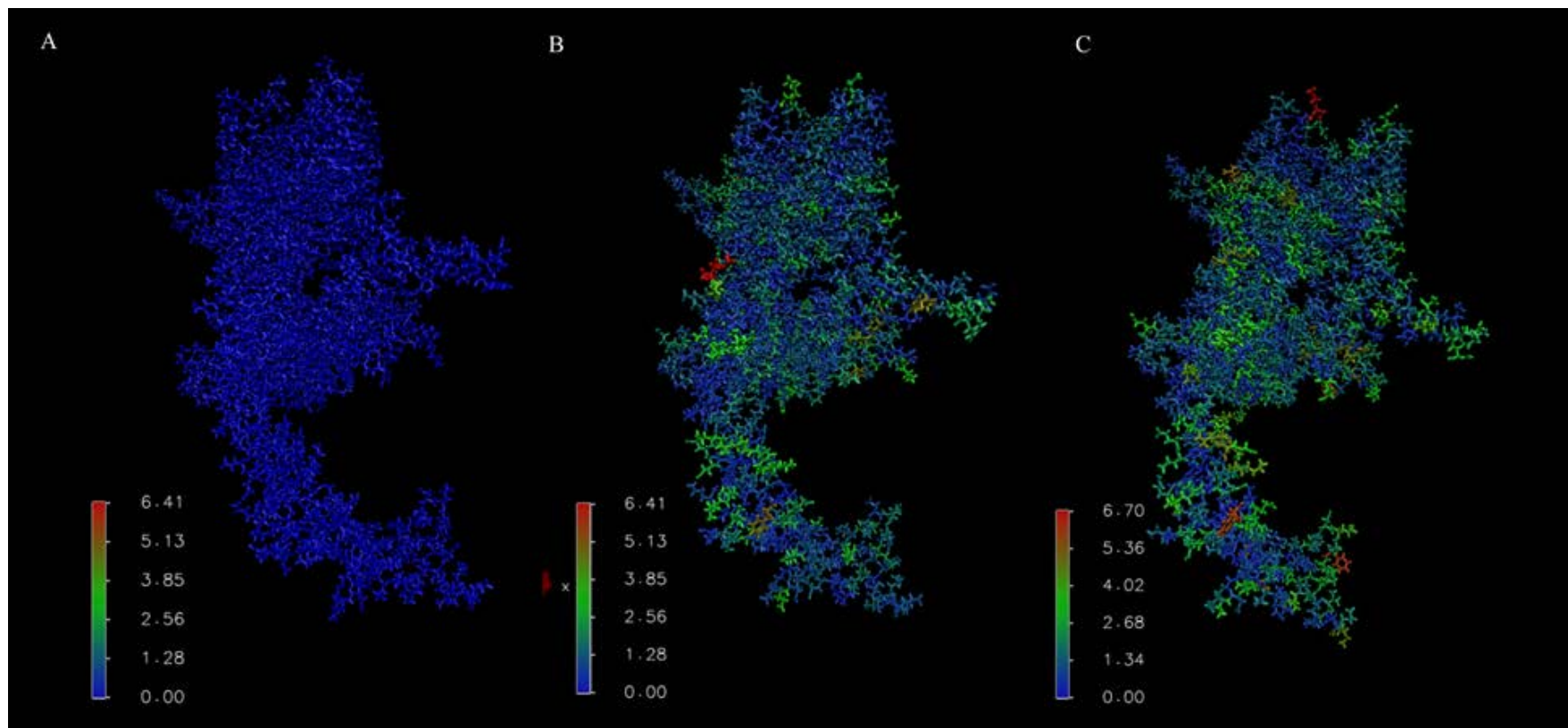


Figure 5.6: Timeline of Frames of RMSD during Equilibration of the Canine HER2 receptor

Visually displays RMSD value onto the structure with Timeline in VMD. A displays the RMSD at Frame 1, B displays RMSD at frame 466 and C displays RMSD at Frame 933.

5.4.4 Electrostatic analyse on the Canine HER2 receptor

The final frame of 933 from equilibration was saved as new PDB file, and to provide a clear access to the protein the ions and solvent box removed for clarity. The PDB file for the HER-2 homology model was converted into a PQR file using the Pymol plugin for Adaptive Poisson–Boltzmann Solver (APBS) electrostatics (Jurrus, *et al*, 2018). The charge map was set to $-/+ 10$ (default 5), where the charge information was created using the AMBER forcefield (Jurrus, *et al*, 2018).

With the HER2 structure conformational optimised at a temperature of 310K, the electrostatic properties of protein show a variation of charges across the entire extracellular domain (Figure 5.7). There is no presence of a predominantly charged region on the protein which would indicate a potential binding site for a ligand. As stated in literature, the HER2 receptor does not have any known ligands due to the receptor remaining in the activated state with domains I and III interacting with each other; thus, explaining the lack of ligand binding (Garret *et al.*, 2003). As the HER2 receptor remains in the active state it leaves the dimerisation loop exposed, displayed as negatively charged. Also displaying a positively charged pocket of which the loop of an opposing co-receptor from the same family would interact during dimerization

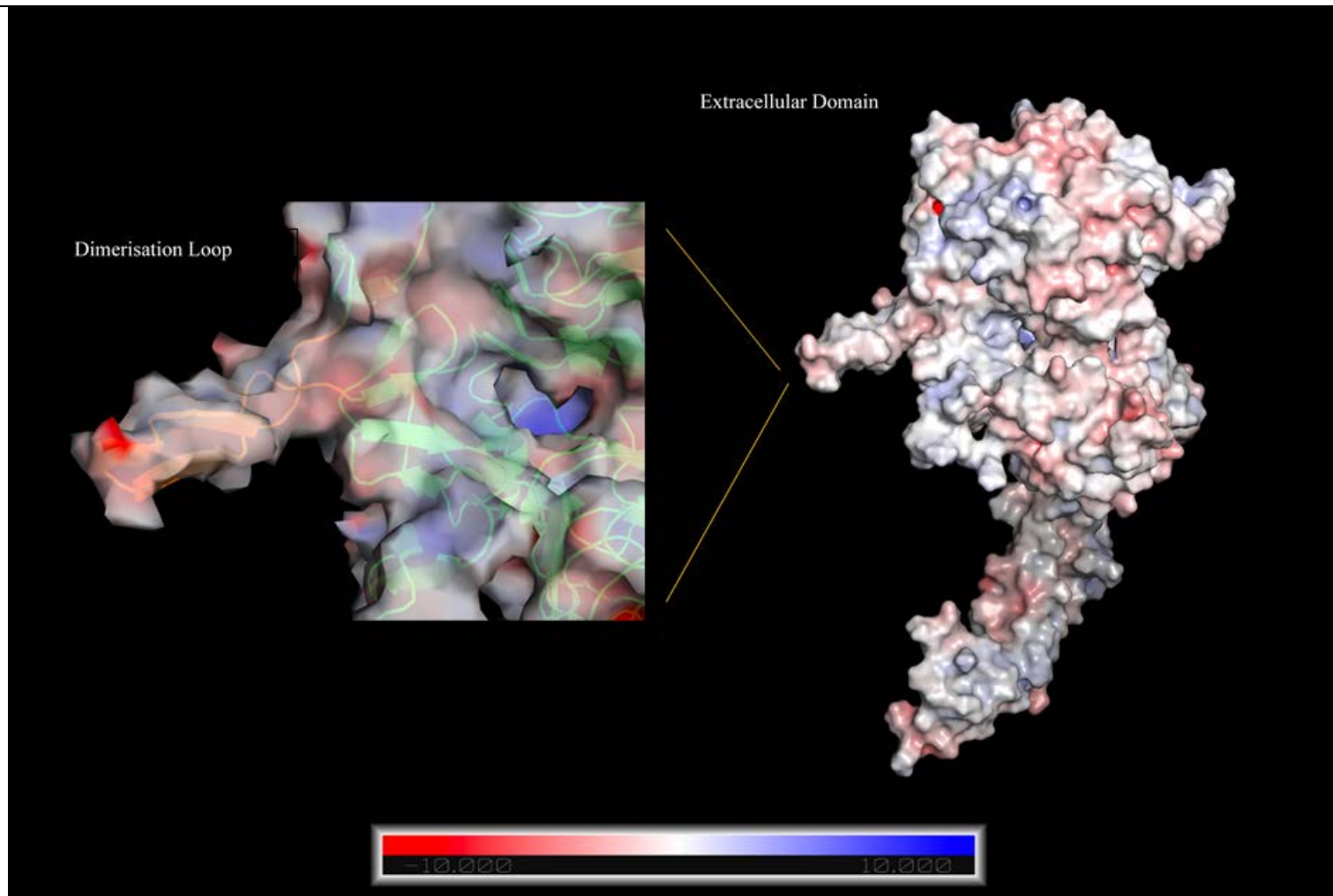


Figure 5.7: Electrostatic Mapping of the Canine HER2 Receptor

Electrostatic modelling displaying lateral side view of the HER2 receptor generated in Pymol using APBS electrostatic plugin. Areas coloured in red are electronegative. Areas coloured in Blue are electropositive and Neutral areas are coloured in white.

5.4.5 Generating and Analysing the Structures of Identified Cytotoxins from Mass Spectrometry Data.

5.4.5.1 Modelling of Naniproin

The venom fraction N.nig_i11r3 identified as the cytotoxin Naniproin from **Chapter 4** did not have a structure available within the database, thus an *ab initio* protein structure was generated through the use of Quark (Xu and Zhang, 2012). After utilising the Quark sever, by submitting the amino acid sequence of Naniporin it produced 5 predicted models of the Naniproin cytotoxin. To select the most robust model for this protein, the amino acid sequence was put through a BLAST search, and structures of high similarity were aligned to each of the models. Using 3 models (PDB 1CXN, 2CCX and 1UG4) with high similarities of 90%, they were aligned to each of the 5 models using the align tool in Pymol. The RMSD values of each alignment was then used to determine the most suitable model; a low RMSD value between the aligned structures resembles a lower deviation between the aligned atoms and thus share similarities in structure. Model 3 (Figure 5.8) produced the lowest RMSD value of 0.830 through the structure alignments and thus is chosen to perform protein-protein docking of the HER2 receptor and model 3 of the Naniproin cytotoxin. ADD the 3 alignments images

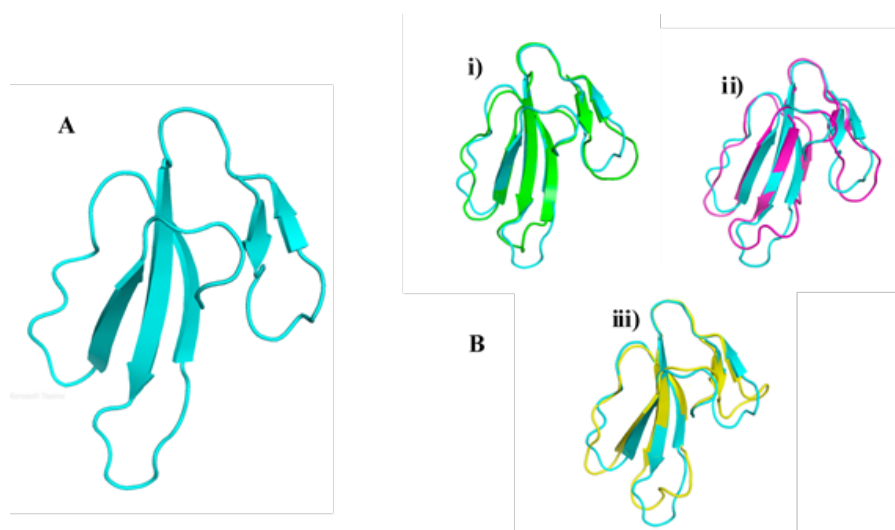


Figure 5.8: Structural Alignments of Model 3 and known Cytotoxins
Structural alignment of Model 3 (A) generated from Quark and alignment with (B) i) PDB:1CXN ii) PDB: 2CCX and iii) PDB: 1UG4.

5.4.5.2 Structure-Activity-Relationship Analysis of Cytotoxin 3 and Naniproin

Conventional to the 3-fingered toxins (3FT), both of the structures of Cytotoxin 3 (PDB: 6RC7) and Naniproin resemble the distinctive protein fold that are found across a number of snake species (e.g Cobras, Kraits and Mambas) (Kini and Doley., 2010). The characteristic structure of the 3FT consists of 3-beta-stranded loops that extend from a hydrophobic globular core stabilised by cysteine-cysteine bonds that are cross-linked by four conserved disulphide bridges (Figure) (Kini and Doley., 2010). Most 3FT's have minor alterations to their overall structure with variations in the loop lengths and conformation variations in the helices. As shown in **Chapter 4 section 4.4.6**, evolutionary conserved regions of the structure are predominately located at the top of the globular structure, compared to the variable regions which are located on the tips of the 3-finger loops.

Performing a structure-activity-relationship analysis (SAR) identifies the regions of interactive importance. Utilising the Open-WebProAnalyst server it identifies the amino acids within the protein structure that relates to the activity of the structure. Figure... displays the identified residues associated with the activity of the cytotoxins. The regions identify actively important residues located on the out-regions on the protein that are most likely to interact with opposing proteins. Significant active regions are located on the 3-finger loops which aren't surprising considering literature describes the middle-finger loop are the region which defines the potency of the cytotoxin (Li and Lin., 2018).

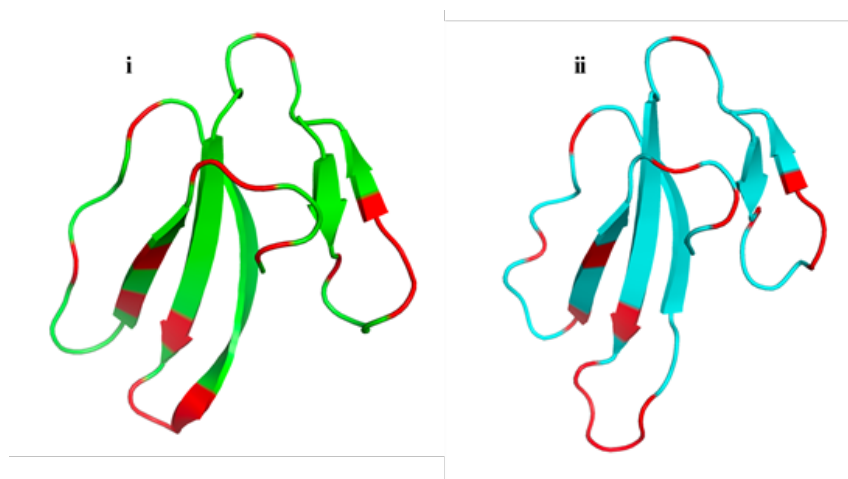


Figure 5.9: Structure-Activity-Relationship Analysis of Cytotoxins

Shows the structure of Cytotoxin-3 in green (i) and Naniproin in blue (ii). Regions coloured in red amino acids identified as important residues associated with the activity of the structure.

5.4.5.3 Electrostatic Analysis of Cytotoxin 3 and Naniproin

The PDB file for Cytotoxin 3 structure (PDB: 6RC7) and Naniproin was converted into a PQR file using the Pymol plugin for Adaptive Poisson–Boltzmann Solver (APBS) electrostatics (Jurrus, *et al*, 2018). The charge map was set to $-/+ 10$ (default 5), where the charge information was created using the AMBER forcefield (Jurrus, *et al*, 2018).

Observation of the electrostatic potential of both cytotoxins show common characteristic features. The cysteine-rich globular structure located at the top is showing to have negative electrostatic potential, whilst the 3-finger loops are observed to show positive electrostatic potential (Figure 5.10). Positive electrostatic potential pockets are shown across the 3-finger loops predominantly in the location of the residues of active importance as shown in **section 5.4.5.2**. These observations correlate with literature, describing the 3-finger toxin as having a hydrophilic region at the top of the structure, while the 3-finger loops are hydrophobic, and thus are evidently showing that the loops are the interactive site of the structure (Lyukmanova, *et al.*, 2016; Attarde and Pandit., 2017; Kini and Koh., 2020).

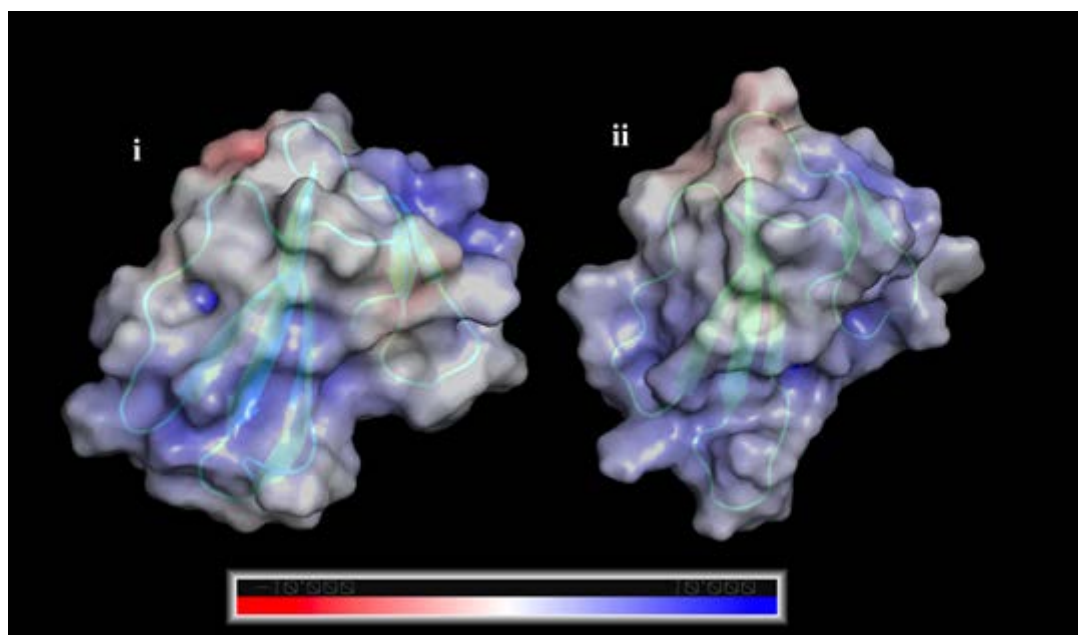


Figure:5.10 Electrostatic mapping of Cytotoxin 3 and Naniproin

Electrostatic modelling of (i) Cytotoxin 3 (PDB: 6RC7) and (ii)Naniproin generated in Pymol using APBS electrostatic plugin. Areas coloured in red are electronegative. Areas coloured in Blue are electropositive and Neutral areas are coloured in white.

5.4.6 Molecular docking of Venom Peptides on the Canine HER2 Receptor

Utilising the Z-DOCK server (Pierce and Weng., 2014) both the Canine HER2 receptor, Cytotoxin 3 structure (PDB: 6RC7) and Naniproin were submitted independently to the server were 10 models were produced in order of accurately predicated docking with only the top 3 models selected for analysis.

Initial observations of the models produced from both cytotoxins has a favoured region of activity around the dimerisation loop and the positively charged pocket next to the loop of the HER2 receptor. This isn't surprising because when performing the electrostatic analysis of both the HER2 receptor and the cytotoxins, they both had opposite charges in the hypothesised area of interaction. The HER2 dimerisation loop displayed a negative charge as shown in **section 5.4.4** and the 3-finger loops on both cytotoxins showed positive charges in **section 5.4.5.3** which suggest that these charges may facilitate binding between these regions.

The docking models produced between Cytotoxin 3 and HER2 show strong interactions with the formation of hydrogen bonds (Table 5.2) Model 1 displays interactions with the dimerisation loop on HER2 with hydrogen bond formations located on finger loops 1 and 2 and on the N-terminal of Cytotoxin 3 (Figure 5.11). Model 2 also shows interactions with the dimerisation loop with the formation of hydrogen bonds on the middle finger loop, and an identical hydrogen bond from Model 1 with Asparagine- 29 (Figure 5.12). Model 3 displayed a different binding interaction with HER2, showing possible binding to the dimerisation pocket (Figure 5.13). This interaction formed 4 hydrogen bonds suggesting that this is a strong contact between the proteins, and again the interactions are with loop 2 of Cytotoxin 3. Docking of Naniproin and HER2 also showed strong interactions with the formation of hydrogens (Table 5.3). Model 1 displayed interaction with the dimerisation loop with hydrogen bond formation on loop 2 of Naniproin (Figure 5.14). Hydrogen bond formation was also observed on the finger loop 2 on Model 2 (Figure 5.15) with the N-terminus of Naniproin interacting with the dimerisation loop but observed to have bonded further up the loop. Model 3 was observed to have bound to the dimerisation pocket of HER2 with the formation of 2 hydrogen bonds found on finger loop 2 (Figure 5.16).

Table 5.2: Hydrogen bonds between Cytotoxin 3 and HER2

ZDOCK Model	Residues HER2 Receptor	Residues Cytotoxin 3
Model 1	VAL-272	ASN-29
	HSD-267	LEU-6
	THR-105	ARG-58
Model 2	TYR-274	ASN-29
	VAL-272	SER-28
Model 3	LEU-317	TRY-22
	ASN-319	LYS-35
	THR-290	SER-28
	THR-105	LYS-30

Table 5.3: Hydrogen bonds between Naniproin and HER2

ZDOCK Model	Residues HER2 Receptor	Residues Naniproin
Model 1	THR-276	LYS-35
	ASP-305	ARG-36
Model 2	SER-310	ARG-36
	GLY-348	ASP-57
	ALA-270	LYS-31
	LEU- 317	LYS-58
Model 3	GLU-352	ARG-27
	LYS-150	CYS-59

Observations of the interactions between Cytotoxin 3 and Naniproin and the HER2 receptor display key interactions between amino acids that were described as important in characterising cytotoxin activity described in **section 5.4.5.2**. Van-der-Wal forces are the main source of interaction between the cytotoxins and HER2, with the addition of hydrogen bonds this suggesting stronger binding affinity for both cytotoxins, alongside the electrostatic potential of each protein. In terms of drug design, the enhancement of binding affinities with hydrogen bonds are favoured (Chen, *et al.*, 2016), as this allows

the 'drug' in this case cytotoxins, to bind long enough to have a biological effect on the target, such as HER2 (Kubinyi, 2007). Thus, the hypothesised biological effect of inhibiting HER2 via binding to the dimerisation loop would inhibit or prevent the formation of dimers between co-receptors of the EGFR family. Through disrupting this pathway preventing transductions of cellular growth apoptotic cell death is assumed, likewise in drugs such as Trastuzumab (also known as Herceptin) (Gancia, *et al.*, 2001; Vu and Claret., 2012).

5.5 Conclusion

The presence of the HER2 receptor identified on the Canine Mammary Cancer cell lines (CMT28 and CMM26) and the integrations of it being a potential drug target, suggests that HER2 is a feasible biomarker for new drug development in dogs. Through investigating the interactions of whole snake venoms on HER2, it has been evidently shown that venom proteins and peptides bind to HER2. Computational modelling and molecular docking of the 2 identified cytotoxins from **Chapter 5**, Cytotoxin 3 from *Naja Kaouthia* and Naniproin from *Naja Nigricollis*, has also displayed promising inhibiting docking locations on the dimerisation loop of HER2 to inhibit the formation of dimers. Further investigation of the physio-chemical properties of these cytotoxins would allow a more in-depth analysis of the interactions and binding affinities between the cytotoxins and HER2. With further investigation utilising molecular dynamics this would allow simulations to be performed to understand the extremity of these cytotoxins within a living system and reflecting the predicted outcome this using biomolecular techniques to understand the effects of the cytotoxins on the HER2 receptor.

Disclaimer: Molecular dynamic simulations performed in sections **5.3.6, 5.3.7 and 5.3.8** was generated in collaboration with Daniel Carey, PhD student at Canterbury Christ University. The data analysis, interpretation and the discussion was carried out solely by the primary author of this thesis.

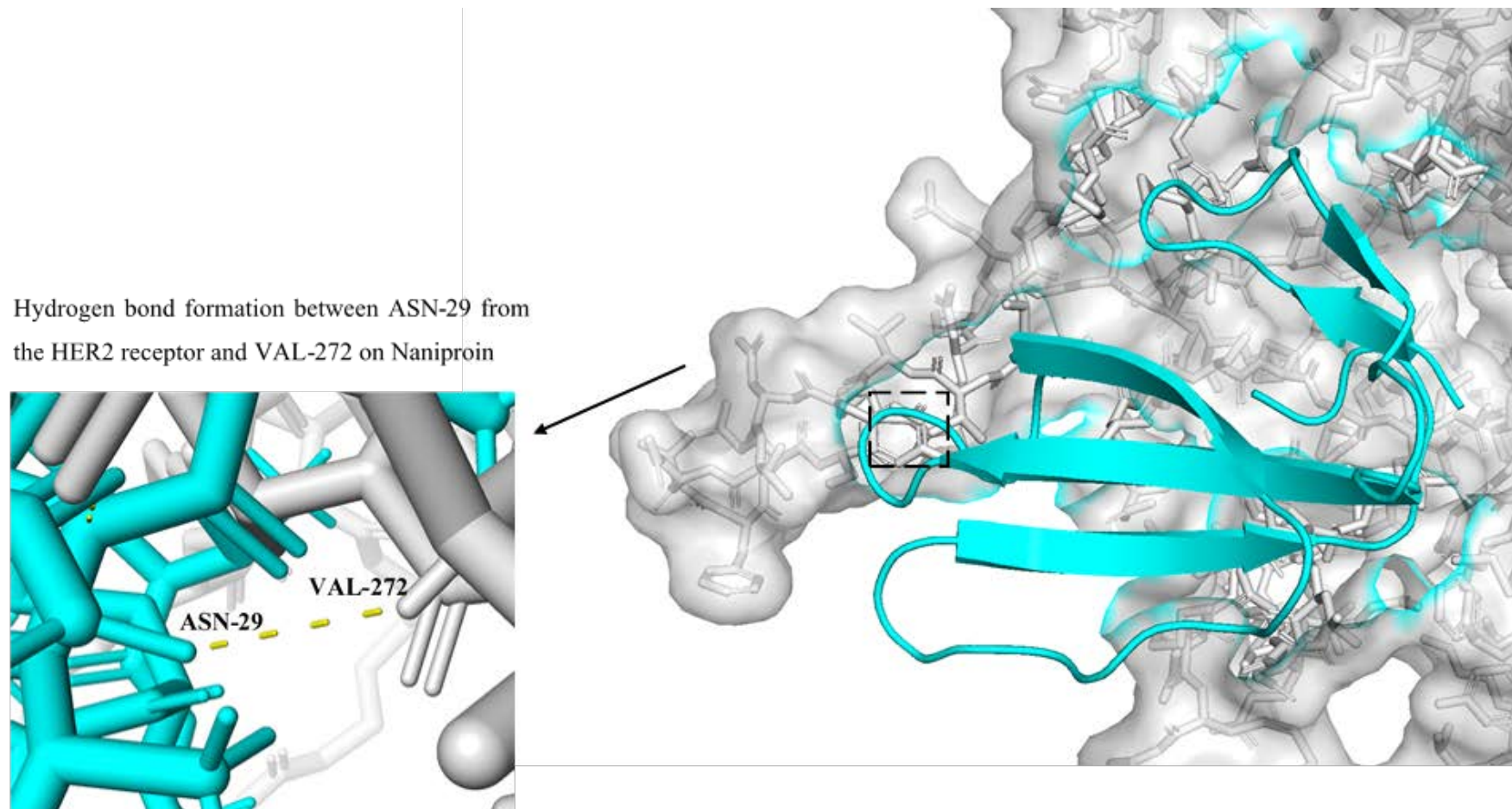


Figure 5.11: MODEL 1 - Binding between Cytotoxin 3 and the HER2 receptor

Shows Model 1- interactions of Cytotoxin 3 and the Canine HER2 receptor. HER2 coloured in grey and Cytotoxin 3 coloured in blue. Images generated using Pymol.

Hydrogen bond formation between ASN-29 from the HER2 receptor and TYR-274 on Naniproin

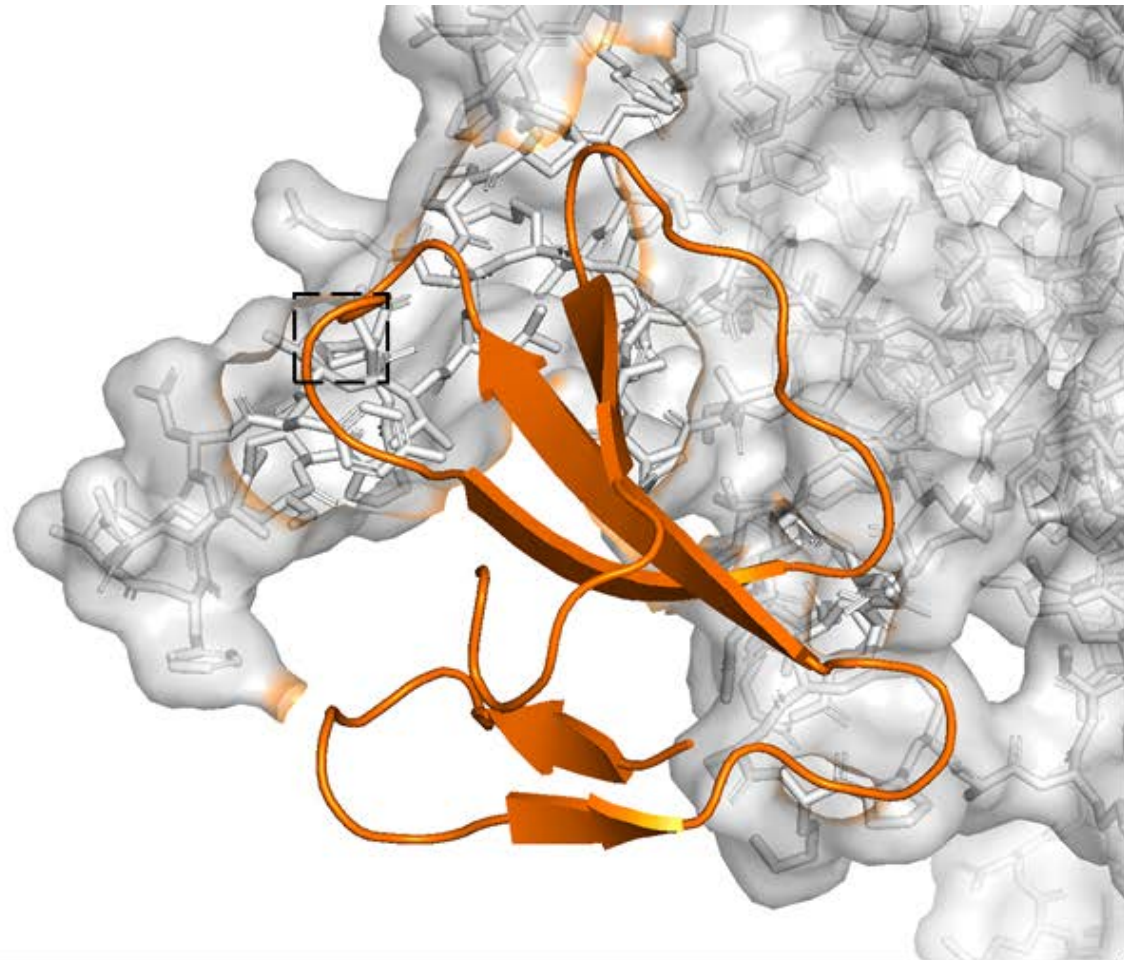
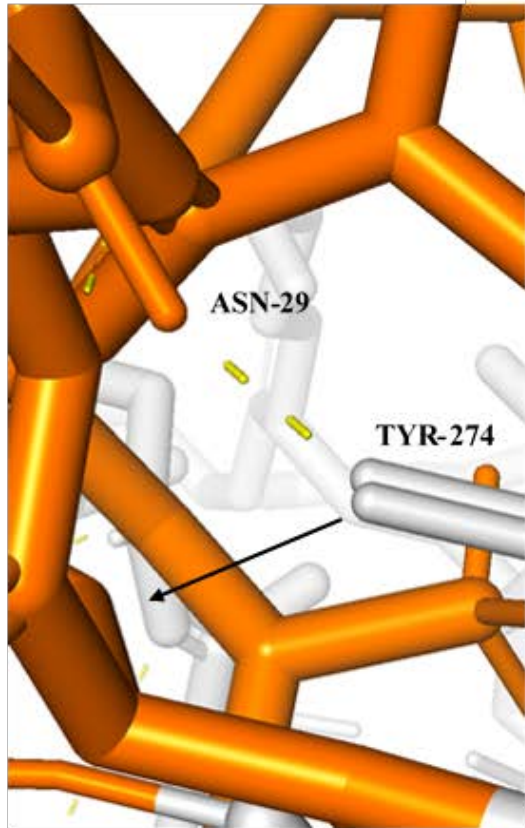


Figure 5.12: MODEL 2 - Binding between Cytotoxin 3 and the HER2 receptor

Shows Model 1- interactions of Cytotoxin 3 and the Canine HER2 receptor. HER2 coloured in grey and Cytotoxin 3 coloured in orange. Images generated using Pymol.

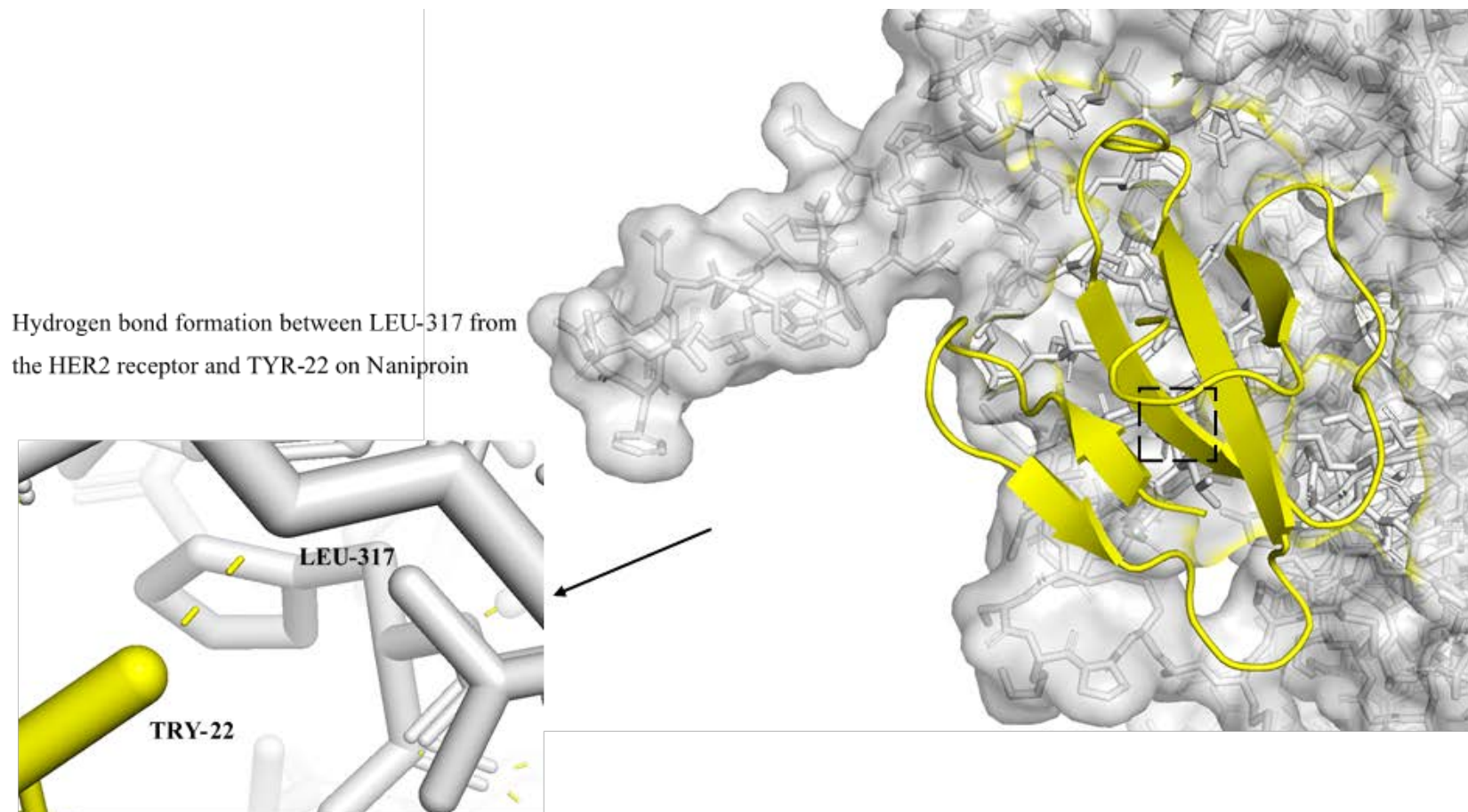


Figure 5.13: MODEL 3 - Binding between Cytotoxin 3 and the HER2 receptor

Shows Model 1- interactions of Cytotoxin 3 and the Canine HER2 receptor. HER2 coloured in grey and Cytotoxin 3 coloured in yellow. Images generated using Pymol.

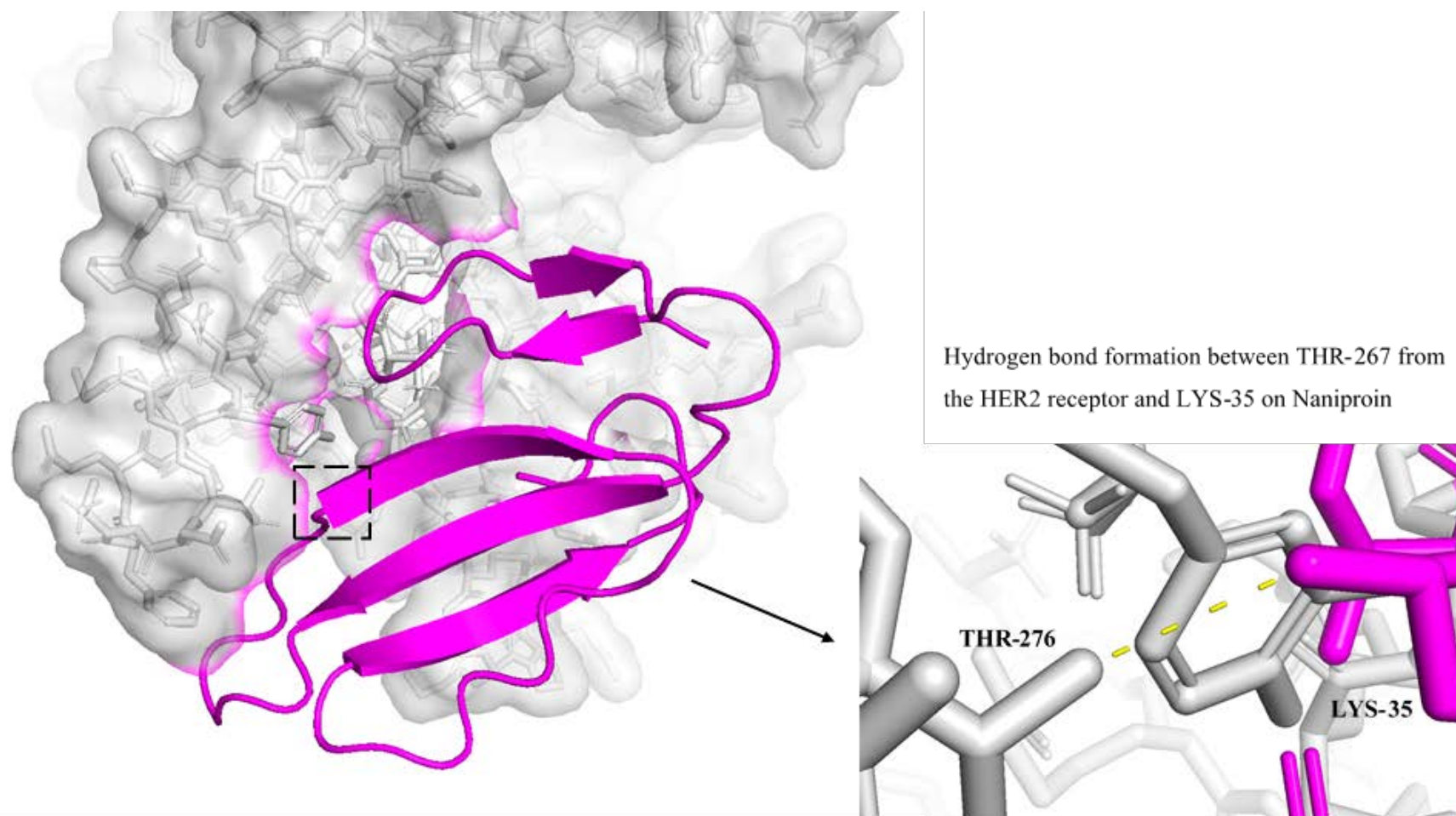


Figure 5.14: MODEL 1 - Binding between Naniproin and the HER2 receptor

Shows Model 1- interactions of Naniproin and the Canine HER2 receptor. HER2 coloured in grey and Naniproin coloured in pink. Images generated using Pymol.

Hydrogen bond formation between LEU-317 from the HER2 receptor and LYS-58 on Naniproin

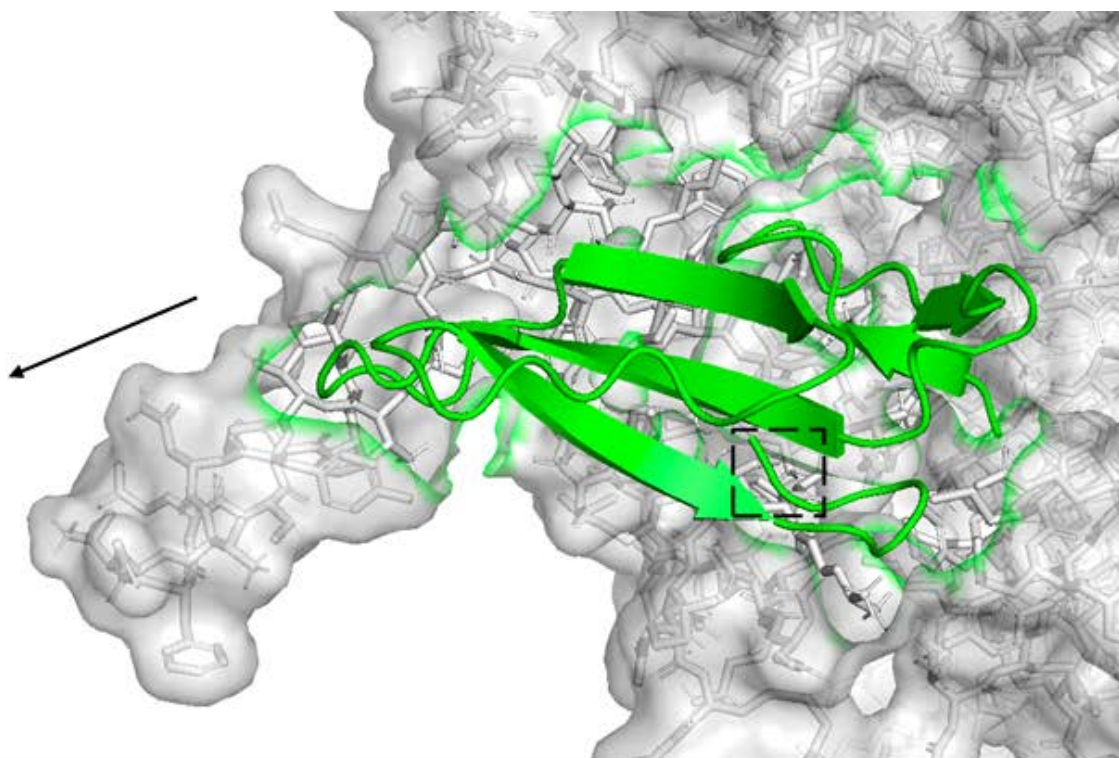
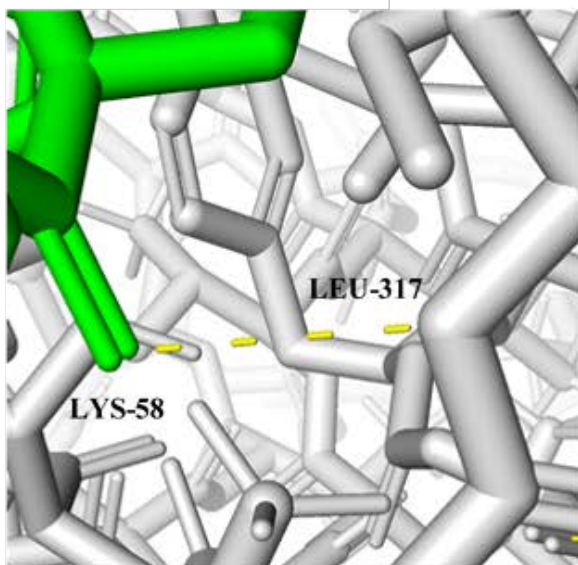


Figure 5.15: MODEL 2- Binding between Cytotoxin 3 and the HER2 receptor

Shows Model 2- interactions of Naniproin and the Canine HER2 receptor. HER2 coloured in grey and Naniproin coloured in green. Images generated using Pymol.

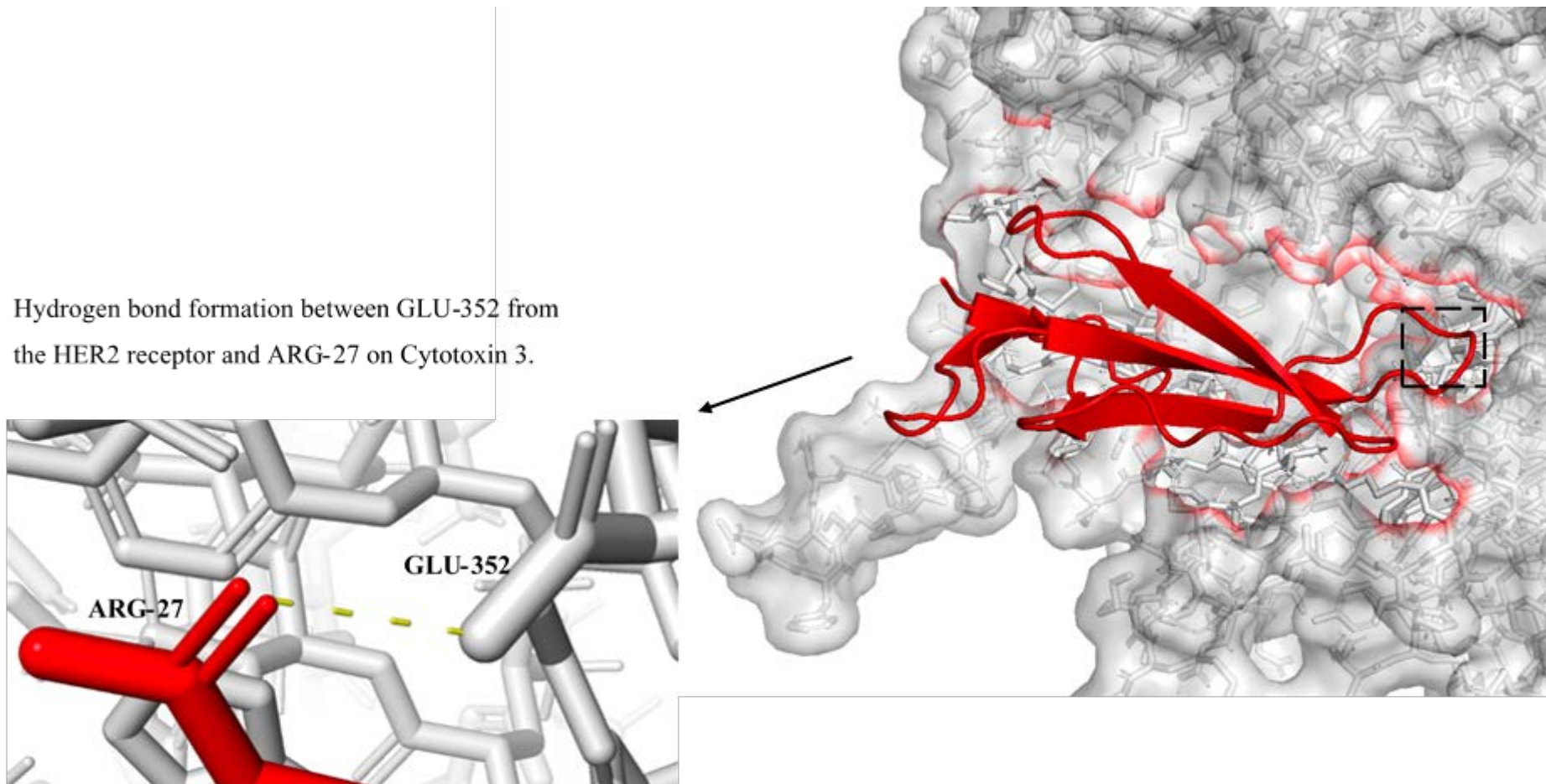


Figure 5.16: MODEL 3 - Binding between Naniproin and the HER2 receptor

Shows Model 3- interactions of Naniproin and the Canine HER2 receptor. HER2 coloured in grey and Naniproin coloured in pink Images generated using Pymol.

CHAPTER 6: Discussion

6.1 Discussion

With 50% of Canine Mammary malignancies metastasising at the time of surgery and with no established guidelines for the treatment beyond surgery for dogs, this leaves the mortality rate of dogs with this disease between 51.7% - 72% after 1-2-years post diagnosis (Sleeckx *et al.*, 2011; Nguyen, *et al.*, 2018). Current chemotherapeutics used to treat mammary cancer induce adverse side effects that contribute to the death of dogs, such as myelosuppression (reduction in bone marrow), neutropenia (reduction in neutrophils) and gastrointestinal toxicity (Macdonald, 2009; Cunha, *et al.*, 2017). Lethality of dogs is predominately due to the 'one-size-fits-all' approach in currently used chemotherapeutics targeting common features found in healthy and cancerous cells (Lori, *et al.*, 2010). More efforts are contributed to the prevention of canine mammary cancer rather than treating the disease as incident rates are increasing (Meuten, 2016; Gray, *et al.*, 2020). Research into the field of anti-cancer drug discovery in veterinary medicine is limited with reasons suggested by Karayannopoulou and Lafioniatis (2016) predominantly related to the adverse toxic effects of chemotherapy, with the addition of pet owners turning down treatment in relation to the cost or the quality of life of their dog. When it comes to treating a dog with cancer, veterinarians have to weigh out whether the efficacy of chemotherapy outweighs the quality of life a dog will experience; treatment buys time but the majority of dogs will relapse (Stephens, 2019).

This thesis aim was to identify the therapeutic potential of snake venoms against the viability of canine mammary cancer cells and the selective efficacy against non-cancerous cells. This research intended to identify venoms that displayed a significant reduction in viability with selective susceptibility towards cancerous cells; this was reflected in Chapter 3. Whole Cobra snake (*Naja* spp.) venoms were screened for their toxicity on canine mammary cancer cell lines, CMT28 and CMM26, and an immortalised normal canine kidney cell line, MDCK. Overall, the CMT28 cell line was observed to more susceptible to the cytotoxic effects of the cobra venoms compared to the CMM26 cell line, whilst the MDCK cell line had also shown high susceptibility to the whole

venoms. This observation is not surprising as cobra venoms have been identified to consist of a cocktail of lethal cytotoxins, such as 3-finger toxins, that are known to rupture cell membranes (Gasanov, *et al.*, 2014; Tasoulis and Isbister, 2017).

Spitting cobras were initially hypothesised to cause an increased cytotoxic effect on the canine cancer cells as literature has described spitting cobras as having local tissue necrotic activity towards cells, whilst venoms from non-spitting cobras are described as having more neurotoxic activity causing muscular paralysis, without necrosis (Kalam, *et al.*, 2011); but this was not the case in this study as there was no distinctive relationship observed between spitting and non-spitting cobras. Yet there was a distinctive relationship observed between the cobras of the two geographical locations of Africa and Asia, with the Asian cobras showing a significant increase in toxicity across both spitting and non-spitting cobras. Literature evidently supports this trend with numerous Asian cobras including *Naja oxiana*, *Naja naja* and *Naja sumatrana* showing cytotoxic effects towards various human cancers (Ebrahim, *et al.*, 2016; Derakhshani, *et al.*, 2020; Teoh and Yap, 2020). The composition of African spitting cobras is observed to be more simplistic compared to Asian cobras, with only a hand full of different protein families making up their venom (Kalam, *et al.*, 2011). Originally theories were drawn to cytotoxic intensity related to the ability of snakes spitting venom, however evolutionary and cell-based studies have demonstrated the relationship between the potency of the venom and the characteristic hooding of the snake (Barlow, *et al.*, 2009; Panagides, *et al.*, 2017; Casewell, *et al.*, 2020). Defence mechanisms of spitting venom alongside the hooding behaviour has shown to dominate the potency of cobra snake venom (Young and Kardong, 2010; Panagides, *et al.*, 2017), this clarifies why venom components from the *Naja* genus were the only venoms to induce toxicity in the cancerous cells in the T-VDA assay compared to other venom components from rattle snakes and invertebrates. Despite literature evidently showing the cytotoxic effects of invertebrate venom of scorpions and spiders on various types of human cancers (Zhang and Zhang, 2016; Noble *et al.*, 2020), no significant inhibitory effects were observed in the T-VDA^{cyx} assay against canine mammary cancer, described in Chapter 4. Performing dose responses on snake venoms fractions from the T-VDA^{cyx} assay that induced more than 70% inhibition towards the CMM26 and CMT28 cells, showed increased susceptibility towards both canine cancer cell lines, compared to

inhibitory effects observed in MDCK cells. Significant differences were observed between the cancerous and non-cancerous cells with approximately 100% lethal inhibitory shown towards the cancerous cell across the hit fractions, respectively, whilst the non-cancerous cell line was observed to show little or no inhibition. Reflecting this outcome into the clinical environment large dose windows between the inhibitory effects of cancerous and non-cancerous cells are favoured, as the effects of causing cell death in healthy cells has a dramatic effect on the patient causing adverse side effects. Thus, avoiding cell death in healthy cells and focusing cytotoxic inhibition on cancerous cells, should in theory reduce side effects and improve quality of life throughout treatment.

Five venom fractions that showed statistically significant inhibitory effects from the T-VDA^{cyx} assay that displayed a high susceptibility towards the canine mammary cancer cell lines compared to the normal canine kidney cell line were selected to undergo Intact Mass and Peptide Digestion mass spectrometry. All five of the venom fractions returns with predicted identification of 3-finger toxins, which is not surprising as 79.8 -99.9% of snake venoms from the *Naja* genus is 3-finger toxins (Tasoulis and Isbister, 2017). Analysis of the sequences confirmed the identification of the fractions being short 3-finger toxins at 60 amino acids in length as they did not present the evolution conserved region that is found in long 3-finger toxins (Fry, *et al.*, 2003; Kini and Koh, 2020). From performing sequence alignments and BLAST searches 3 of the fractions (N.atr_i9_r1, N.sia_i9_r4 and N.kao_i10_r2) were identified as novel 3-finger toxins, while 2 fractions (N.kao_i9_r2 and N.nig_i11_r3) displayed high alignment similarities giving them possible identifications of Cytotoxin 3 from *Naja Kaouthia* and Naniproin from *Naja Nigricollis*. Findings in Chapter 5 highlighted the potential of whole venoms interacting with the HER2 receptor in both CMT28 and CMM26 cell lines. Literature is available with regards to HER2 protein expression levels in CMT28 and CMM26 however it does not quantify expression levels, thus protein profiling would be required to fully understand the differences between the cells, and thus understand the differing susceptibility observed between the cells when exposed to the venom.

HER2 is observed to be overexpressed in approximately 30% of canine mammary (Singer, *et al.*, 2012; Campos, *et al.*, 2015; Kaszak, *et al.*, 2018), thus HER2 is considered an important targeted

biomarker when considering drug development for this disease. Whole venoms that produced a significant hit in inducing more than 70% cytotoxic inhibition showed evidence of the HER2 receptor binding to the venom when performing molecular dot blots. Whether the binding between HER2 is of an inhibitory effect, further investigation is required to understand the binding mechanism by examining the levels of phosphorylation of HER2 in relation to venom exposure. Recent literature demonstrated reduction in phosphorylation of tyrosine kinases in a human breast cancer cell line (MDA- MB-468) with the use of venoms from cobra, mamba, pit viper snakes, scorpion and theraphosid (McCullough, *et al.*, 2020). Interpretations of the mechanisms of inhibiting tyrosine kinases in dogs with venom may contribute the same application of small molecular tyrosine kinase inhibitors. Literature has reported tyrosine kinases as a potential target for drug development in veterinary medicine (London, 2009; Dervis and Klahn., 2016), but reports have shown little efficacy towards inhibiting tyrosine kinases in dogs without inducing high levels of toxicity (London 2009; London, 2013). Thus, with these limitations in mind, it was hypothesised that targeting the extracellular domain of HER2 is an alternative option compared to targeting the kinase domain on the receptor. Computational modelling of the extracellular domain of the Canine HER2 receptor in addition to molecular docking of cytotoxins demonstrated the possibility of inhibiting the HER2 receptor through the dimerisation loop. Stimulating the docking of the identified cytotoxins from Chapter 4 (Cytotoxin 3 and Naniproin), it showed strong binding affinities to the dimerisation loop of HER2. Through structural analysis the binding between the dimerisation loop and cytotoxins was enhanced through the formation of hydrogen bonds which predominately involved amino acids that determined the activity of the cytotoxins, analysed using SAR analysis. Whilst the possibility of the cytotoxins binding to the dimerisation arm of the receptor is predicted in simulations, this data opens up the potential of further investigating into the mechanistic action through which HER2 is inhibited by cytotoxins preventing the formation of dimers with other co-receptors of the same family.

6.2 Conclusion and Future Work

Current research within veterinary oncology is limited thus the need for more investigations in drug development and key biomarkers is essential within this medical sector. The findings from this study are the first to be established investigating the effects of venom on canine mammary cancer. Despite numerous studies on human cancers, promising evidence of utilising venom in drug discovery is becoming a favourable approach, exploiting the mechanisms of nature. HTS of a compound library of venom fractions from numerous species has identified key species, predominately the true cobras (*Naja* spp.) that induced cytotoxic effects with high susceptibility in canine cancer cells. This in-depth investigation has observed selectivity towards cancerous cells compared to non-cancerous cells, and the possibility of cytotoxins forming a strong complex with HER2, demonstrates in clinical terms the enormous possibility of reducing the adverse side effects that current chemotherapeutics cause; and utilising this approach for cancer treatment may also increase the quality of life a dog may experience.

Future work to establish a better understanding of utilising venoms as a treatment for cancer would be to further understand the mechanistic approach that the venom proteins undertake, in this case of the cytotoxin, to induce cell death. Also, to screen the proteins against other normal canine cell types to establish an understanding of the effect the proteins may have on other cell within a living system. In terms of utilising HER2 as a target antigen, further investigations into the inhibitory effects caused by the venom protein would further clarify if inhibition is achieved.

Reference

- Abdel-Ghani, L. M., Rahmy, T. R., Tawfik, M. M., Kaziri, I., Al-Obaidi, A., Rowan, E. G., Plevin, R., & Abdel-Rahman, M. A. (2019). Cytotoxicity of Nubein6.8 peptide isolated from the snake venom of *Naja nubiae* on melanoma and ovarian carcinoma cell lines. *Toxicon*. <https://doi.org/10.1016/j.toxicon.2019.06.220>
- Abdelmegeed, S. M., & Mohammed, S. (2018). Canine mammary tumors as a model for human disease (Review). In *Oncology Letters*. <https://doi.org/10.3892/ol.2018.8411>
- Adams, V. J., Evans, K. M., Sampson, J., & Wood, J. L. N. (2010). Methods and mortality results of a health survey of purebred dogs in the UK. *Journal of Small Animal Practice*. <https://doi.org/10.1111/j.1748-5827.2010.00974.x>
- AI, B., & C, C. (2007). TUMOR CELL MORPHOLOGY. In *Comparative Oncology*.
- Al-Asmari, A. K., Islam, M., & Al-Zahrani, A. M. (2016). In vitro analysis of the anticancer properties of scorpion venom in colorectal and breast cancer cell lines. *Oncology Letters*. <https://doi.org/10.3892/ol.2015.4036>
- Alix-Panabières, C., & Pantel, K. (2016). Clinical applications of circulating tumor cells and circulating tumor DNA as liquid biopsy. In *Cancer Discovery*. <https://doi.org/10.1158/2159-8290.CD-15-1483>
- Altschul, S. F., Madden, T. L., Schäffer, A. A., Zhang, J., Zhang, Z., Miller, W., & Lipman, D. J. (1997). Gapped BLAST and PSI-BLAST: A new generation of protein database search programs. In *Nucleic Acids Research*. <https://doi.org/10.1093/nar/25.17.3389>
- Amin, D. N., Sergina, N., Ahuja, D., McMahon, M., Blair, J. A., Wang, D., Hann, B., Koch, K. M., Shokat, K. M., & Moasser, M. M. (2010). Resiliency and vulnerability in the HER2-HER3 tumorigenic driver. *Science Translational Medicine*. <https://doi.org/10.1126/scitranslmed.3000389>
- Anderson, D. (2014). Mammary tumours in the dog and cat (part 2): surgical management. *Companion Animal*. <https://doi.org/10.12968/coan.2014.19.12.648>
- Andrade, F. H. E., Figueiroa, F. C., Bersano, P. R. O., Bissacot, D. Z., & Rocha, N. S. (2010). Malignant mammary tumor in female dogs: Environmental contaminants. *Diagnostic Pathology*. <https://doi.org/10.1186/1746-1596-5-45>
- Arenas, C., Peña, L., Granados-Soler, J. L., & Pérez-Alenza, M. D. (2016). Adjuvant therapy for highly malignant canine mammary tumours: Cox-2 inhibitor versus chemotherapy: A case-control prospective study. *Veterinary Record*. <https://doi.org/10.1136/vr.103398>
- Attarde, S. S., & Pandit, S. V. (2017). Cytotoxic activity of NN-32 toxin from Indian spectacled cobra venom on human breast cancer cell lines. *BMC Complementary and Alternative Medicine*. <https://doi.org/10.1186/s12906-017-2018-3>
- Augusto, M. (2014). Mammary tumours in the dog and cat: part 1. *Companion Animal*. <https://doi.org/10.12968/coan.2014.19.9.448>
- Baioni, E., Scanziani, E., Vincenti, M. C., Leschiera, M., Bozzetta, E., Pezzolato, M., Desiato, R., Bertolini, S., Maurella, C., & Ru, G. (2017). Estimating canine cancer incidence: Findings from a population-based tumour registry in northwestern Italy. *BMC Veterinary Research*. <https://doi.org/10.1186/s12917-017-1126-0>

- Barlow, A., Pook, C. E., Harrison, R. A., & Wüster, W. (2009). Coevolution of diet and prey-specific venom activity supports the role of selection in snake venom evolution. *Proceedings of the Royal Society B: Biological Sciences*.
<https://doi.org/10.1098/rspb.2009.0048>
- Bateman, A. (2019). UniProt: A worldwide hub of protein knowledge. *Nucleic Acids Research*.
<https://doi.org/10.1093/nar/gky1049>
- Beauvais, W., Cardwell, J. M., & Brodbelt, D. C. (2012). The effect of neutering on the risk of mammary tumours in dogs - a systematic review. In *Journal of Small Animal Practice*.
<https://doi.org/10.1111/j.1748-5827.2011.01220.x>
- Benavente, M. A., Bianchi, C. P., & Aba, M. A. (2019). Expression of Oxytocin Receptors in Canine Mammary Tumours. *Journal of Comparative Pathology*.
<https://doi.org/10.1016/j.jcpa.2019.05.005>
- Bhattacharjee, P., & Bhattacharyya, D. (2014). Therapeutic Use of Snake Venom Components: A Voyage from Ancient to Modern India. *Mini-Reviews in Organic Chemistry*.
<https://doi.org/10.2174/1570193x1101140402101043>
- Bohrer, E. R., Löhr, C. V., & Kutzler, M. A. (2017). Prolactin and growth hormone immunoactivity in canine mammary adenomas and adenocarcinomas. *Reproduction in Domestic Animals*. <https://doi.org/10.1111/rda.12821>
- Bonnett, B. N., Egenvall, A., Hedhammar, Å., & Olson, P. (2005). Mortality in over 350,000 insured Swedish dogs from 1995-2000: I. Breed-, gender-, age- and cause-specific rates. *Acta Veterinaria Scandinavica*. <https://doi.org/10.1186/1751-0147-46-105>
- Bonnier, F., Keating, M. E., Wróbel, T. P., Majzner, K., Baranska, M., Garcia-Munoz, A., Blanco, A., & Byrne, H. J. (2015). Cell viability assessment using the Alamar blue assay: A comparison of 2D and 3D cell culture models. *Toxicology in Vitro*.
<https://doi.org/10.1016/j.tiv.2014.09.014>
- Burgess, A. W., Cho, H. S., Eigenbrot, C., Ferguson, K. M., Garrett, T. P. J., Leahy, D. J., Lemmon, M. A., Sliwkowski, M. X., Ward, C. W., & Yokoyama, S. (2003). An open-and-shut case? Recent insights into the activation of EGF/ErbB receptors. In *Molecular Cell*.
[https://doi.org/10.1016/S1097-2765\(03\)00350-2](https://doi.org/10.1016/S1097-2765(03)00350-2)
- Burrai, G. P., Gabrieli, A., Moccia, V., Zappulli, V., Porcellato, I., Brachelente, C., Pirino, S., Polinas, M., & Antuofermo, E. (2020). A statistical analysis of risk factors and biological behavior in canine mammary tumors: A multicenter study. *Animals*.
<https://doi.org/10.3390/ani10091687>
- Burstein, H. J. (2005). The Distinctive Nature of HER2-Positive Breast Cancers. *New England Journal of Medicine*. <https://doi.org/10.1056/nejmp058197>
- Caldararu, O., Misini Ignjatović, M., Oksanen, E., & Ryde, U. (2020). Water structure in solution and crystal molecular dynamics simulations compared to protein crystal structures. *RSC Advances*. <https://doi.org/10.1039/c9ra09601a>
- Calderon, L. A., Sobrinho, J. C., Zaqueo, K. D., De Moura, A. A., Grabner, A. N., Mazzi, M. V., Marcussi, S., Nomizo, A., Fernandes, C. F. C., Zuliani, J. P., Carvalho, B. M. A., Da Silva, S. L., Stábeli, R. G., & Soares, A. M. (2014). Antitumoral activity of snake venom proteins: New trends in cancer therapy. In *BioMed Research International*.
<https://doi.org/10.1155/2014/203639>

- Campos, L. C., Silva, J. O., Santos, F. S., Araújo, M. R., Lavallo, G. E., Ferreira, E., & Cassali, G. D. (2015). Prognostic significance of tissue and serum HER2 and MUC1 in canine mammary cancer. *Journal of Veterinary Diagnostic Investigation*.
<https://doi.org/10.1177/1040638715592445>
- Carlos, C. H., Toledo-Piza, E., Amorin, R., Barboza, A., & Tobias, K. M. (2009). Inflammatory mammary carcinoma in 12 dogs: Clinical features, cyclooxygenase-2 expression, and response to piroxicam treatment. *Canadian Veterinary Journal*.
- Carvalho, M. I., Silva-Carvalho, R., Pires, I., Prada, J., Bianchini, R., Jensen-Jarolim, E., & Queiroga, F. L. (2016). A Comparative Approach of Tumor-Associated Inflammation in Mammary Cancer between Humans and Dogs. In *BioMed Research International*.
<https://doi.org/10.1155/2016/4917387>
- Casewell, N. R., Jackson, T. N. W., Laustsen, A. H., & Sunagar, K. (2020). Causes and Consequences of Snake Venom Variation. In *Trends in Pharmacological Sciences*.
<https://doi.org/10.1016/j.tips.2020.05.006>
- Casewell, N. R., Wüster, W., Vonk, F. J., Harrison, R. A., & Fry, B. G. (2013). Complex cocktails: The evolutionary novelty of venoms. In *Trends in Ecology and Evolution*.
<https://doi.org/10.1016/j.tree.2012.10.020>
- Cassali, G. D., Damasceno, K. A., Bertagnolli, A. C., Estrela-Lima, A., Lavallo, G. E., Di Santis, G. W., De Nardi, A. B., Fernandes, C. G., Cogliati, B., Sobral, R., Amorim da Costa, F. V., Ferreira, E., Salgado, B. S., Campos, C. B., D'Assis, M. J. M. H., Silva, L. P., Machado, M. C. A., Firmo, B. F., Nunes, F. C., & Nakagaki, K. Y. R. (2017). Consensus regarding the diagnosis, prognosis and treatment of canine mammary tumors: Benign mixed tumors, carcinomas in mixed tumors and carcinosarcomas. In *Brazilian Journal of Veterinary Pathology*. <https://doi.org/10.24070/bjvp.1983-0246.v10i3p87-99>
- Chaisakul, J., Hodgson, W. C., Kuruppu, S., & Prasongsook, N. (2016). Effects of animal venoms and toxins on hallmarks of cancer. In *Journal of Cancer*.
<https://doi.org/10.7150/jca.15309>
- Chen, D., Oezguen, N., Urvil, P., Ferguson, C., Dann, S. M., & Savidge, T. C. (2016). Regulation of protein-ligand binding affinity by hydrogen bond pairing. *Science Advances*.
<https://doi.org/10.1126/sciadv.1501240>
- Chien, C. M., Yang, S. H., Chang, L. Sen, & Lin, S. R. (2008). Involvement of both endoplasmic reticulum- and mitochondria-dependent pathways in cardiotoxin III-induced apoptosis in HL-60 cells. *Clinical and Experimental Pharmacology and Physiology*.
<https://doi.org/10.1111/j.1440-1681.2008.04968.x>
- Chiu, C. C., Lin, K. L., Chien, C. M., Chang, L. Sen, & Lin, S. R. (2009). Effects of cardiotoxin III on NF- κ B function, proliferation, and apoptosis in human breast MCF-7 cancer cells. *Oncology Research*. <https://doi.org/10.3727/096504009787721186>
- Clavijo-Maldonado, A., Ferreira, E., Vargas-Hernández, C., & Rivera-Paéz, F. A. (2020). Canine mammary cancer: Clinical implications with specific focus on the HER-2 gene. In *Veterinarska Stanica*. <https://doi.org/10.46419/vs.51.4.2>
- Colotta, F., Allavena, P., Sica, A., Garlanda, C., & Mantovani, A. (2009). Cancer-related inflammation, the seventh hallmark of cancer: Links to genetic instability. In *Carcinogenesis*. <https://doi.org/10.1093/carcin/bgp127>

- Coyle, Y. M. (2004). The effect of environment on breast cancer risk. In *Breast Cancer Research and Treatment*. <https://doi.org/10.1023/B:BREA.0000019964.33963.09>
- Cunha, S. C. dos S., Silva, F. B. F., Corgozinho, K. B., da Silva, K. V. G. C., & Ferreira, A. M. R. (2017). Adverse effects of chemotherapy in dogs. *World's Veterinary Journal*. <https://doi.org/10.5455/wvj.20170896>
- Cushman, D. W., Cheung, H. S., Sabo, E. F., & Ondetti, A. (1977). Design of Potent Competitive Inhibitors of Angiotensin-Converting Enzyme. Carboxyalkanoyl and Mercaptoalkanoyl Amino Acids. *Biochemistry*. <https://doi.org/10.1021/bi00644a014>
- Dantas Cassali, G., Cavalheiro Bertagnolli, A., Ferreira, E., Araújo Damasceno, K., De Oliveira Gamba, C., & Bonolo De Campos, C. (2012). Canine mammary mixed tumours: A review. In *Veterinary Medicine International*. <https://doi.org/10.1155/2012/274608>
- Davis, B. W., & Ostrander, E. A. (2014). Domestic dogs and cancer research: A breed-based genomics approach. *ILAR Journal*. <https://doi.org/10.1093/ilar/ilu017>
- De Vitis, M., Berardinelli, F., & Sgura, A. (2018). Telomere length maintenance in cancer: At the crossroad between telomerase and alternative lengthening of telomeres (ALT). In *International Journal of Molecular Sciences*. <https://doi.org/10.3390/ijms19020606>
- Del Portillo, I., Sesanto, C., Parys, M., & Serra, J. C. (2020). Radiation therapy in veterinary medicine: a practical review. *Companion Animal*. <https://doi.org/10.12968/coan.2019.0056>
- Dempsey, C. E. (1990). The actions of melittin on membranes. In *BBA - Reviews on Biomembranes*. [https://doi.org/10.1016/0304-4157\(90\)90006-X](https://doi.org/10.1016/0304-4157(90)90006-X)
- Derakhshani, A., Silvestris, N., Hajiasgharzadeh, K., Mahmoudzadeh, S., Fereidouni, M., Paradiso, A. V., Brunetti, O., Atarod, D., Safarpour, H., & Baradaran, B. (2020). Expression and characterization of a novel recombinant cytotoxin II from *Naja naja oxiana* venom: A potential treatment for breast cancer. *International Journal of Biological Macromolecules*. <https://doi.org/10.1016/j.ijbiomac.2020.06.130>
- Dervisis, N., & Klahn, S. (2016). Therapeutic innovations: Tyrosine kinase inhibitors in cancer. In *Veterinary Sciences*. <https://doi.org/10.3390/vetsci3010004>
- Díaz-García, A., Morier-Díaz, L., Frión-Herrera, Y., Rodríguez-Sánchez, H., Caballero-Lorenzo, Y., Mendoza-Llanes, D., Riquenes-Garlobo, Y., & Fraga-Castro, J. A. (2013). In vitro anticancer effect of venom from Cuban scorpion *Rhopalurus junceus* against a panel of human cancer cell lines. *Journal of Venom Research*.
- Dick, F. A., & Rubin, S. M. (2013). Molecular mechanisms underlying RB protein function. In *Nature Reviews Molecular Cell Biology*. <https://doi.org/10.1038/nrm3567>
- Ding, J., Chua, P. J., Bay, B. H., & Gopalakrishnakone, P. (2014). Scorpion venoms as a potential source of novel cancer therapeutic compounds. *Experimental Biology and Medicine*. <https://doi.org/10.1177/1535370213513991>
- Dobson, J. M. (2013). Breed-Predispositions to Cancer in Pedigree Dogs. *ISRN Veterinary Science*. <https://doi.org/10.1155/2013/941275>
- Dobson, J. M., Samuel, S., Milstein, H., Rogers, K., & Wood, J. L. N. (2002). Canine neoplasia in the UK: Estimates of incidence rates from a population of insured dogs. *Journal of Small Animal Practice*. <https://doi.org/10.1111/j.1748-5827.2002.tb00066.x>

- Doherty, A., Lopes, I., Ford, C. T., Monaco, G., Guest, P., & de Magalhães, J. P. (2020). A scan for genes associated with cancer mortality and longevity in pedigree dog breeds. *Mammalian Genome*. <https://doi.org/10.1007/s00335-020-09845-1>
- Dolka, I., Czopowicz, M., Gruk-Jurka, A., Wojtkowska, A., Sapiernyński, R., & Jurka, P. (2018). Diagnostic efficacy of smear cytology and Robinson's cytological grading of canine mammary tumors with respect to histopathology, cytomorphometry, metastases and overall survival. *PLoS ONE*. <https://doi.org/10.1371/journal.pone.0191595>
- Du, Z., & Lovly, C. M. (2018). Mechanisms of receptor tyrosine kinase activation in cancer. In *Molecular Cancer*. <https://doi.org/10.1186/s12943-018-0782-4>
- Dupré, G., Findji, L., & Oechtering, G. (2013). Brachycephalic Airway Syndrome. In *Small Animal Soft Tissue Surgery*. <https://doi.org/10.1002/9781118997505.ch19>
- Dutta, S., & Berman, H. M. (2005). Large macromolecular complexes in the protein data bank: A status report. In *Structure*. <https://doi.org/10.1016/j.str.2005.01.008>
- Ebrahim, K., Vatanpour, H., Zare, A., Shirazi, F. H., & Nakhjavani, M. (2016). Anticancer activity of caspian cobra (*Naja naja oxiana*) snake venom in human cancer cell lines via induction of apoptosis. *Iranian Journal of Pharmaceutical Research*. <https://doi.org/10.22037/ijpr.2016.1811>
- Egenvall, A., Bonnett, B. N., Öhagen, P., Olson, P., Hedhammar, Å., & Von Euler, H. (2005). Incidence of and survival after mammary tumors in a population of over 80,000 insured female dogs in Sweden from 1995 to 2002. *Preventive Veterinary Medicine*. <https://doi.org/10.1016/j.prevetmed.2005.01.014>
- El-Kenawi, A., Hänggi, K., & Ruffell, B. (2020). The immune microenvironment and cancer metastasis. *Cold Spring Harbor Perspectives in Medicine*. <https://doi.org/10.1101/cshperspect.a037424>
- Farrell, L. L., Schoenebeck, J. J., Wiener, P., Clements, D. N., & Summers, K. M. (2015). The challenges of pedigree dog health: approaches to combating inherited disease. *Canine Genetics and Epidemiology*. <https://doi.org/10.1186/s40575-015-0014-9>
- Farrelly, J., & Mcentee, M. C. (2014). A survey of veterinary radiation facilities in 2010. *Veterinary Radiology and Ultrasound*. <https://doi.org/10.1111/vru.12161>
- Fedorova, O., Daks, A., Shuvalov, O., Kizenko, A., Petukhov, A., Gnennaya, Y., & Barlev, N. (2020). Attenuation of p53 mutant as an approach for treatment Her2-positive cancer. In *Cell Death Discovery*. <https://doi.org/10.1038/s41420-020-00337-4>
- Ferraz, C. R., Arrahman, A., Xie, C., Casewell, N. R., Lewis, R. J., Kool, J., & Cardoso, F. C. (2019). Multifunctional toxins in snake venoms and therapeutic implications: From pain to hemorrhage and necrosis. In *Frontiers in Ecology and Evolution*. <https://doi.org/10.3389/fevo.2019.00218>
- Ferreira, L. M. R. (2010). Cancer metabolism: The Warburg effect today. In *Experimental and Molecular Pathology*. <https://doi.org/10.1016/j.yexmp.2010.08.006>
- FERREIRA, S. H. (1965). A BRADYKININ-POTENTIATING FACTOR (BPF) PRESENT IN THE VENOM OF BOTHROPS JARARACA. *British Journal of Pharmacology and Chemotherapy*. <https://doi.org/10.1111/j.1476-5381.1965.tb02091.x>

- Fiala Šebková, N., Chaloupková, H., & Zavadilová, L. (2020). Average life expectancy, the most common cause of death and illness of giant dog breeds. *Scientia Agriculturae Bohemica*. <https://doi.org/10.2478/sab-2020-0002>
- Finotello, R., Stefanello, D., Zini, E., & Marconato, L. (2017). Comparison of doxorubicin–cyclophosphamide with doxorubicin–dacarbazine for the adjuvant treatment of canine hemangiosarcoma. *Veterinary and Comparative Oncology*. <https://doi.org/10.1111/vco.12139>
- Fouad, Y. A., & Aanei, C. (2017). Revisiting the hallmarks of cancer. In *American Journal of Cancer Research*.
- Fry, B. G., Wüster, W., Kini, R. M., Brusica, V., Khan, A., Venkataraman, D., & Rooney, A. P. (2003). Molecular evolution and phylogeny of elapid snake venom three-finger toxins. *Journal of Molecular Evolution*. <https://doi.org/10.1007/s00239-003-2461-2>
- Furman, B. L. (2012). The development of Byetta (exenatide) from the venom of the Gila monster as an anti-diabetic agent. In *Toxicon*. <https://doi.org/10.1016/j.toxicon.2010.12.016>
- GA, M. N. P. S. G. P. P. (2017). Autopsy Case Findings in Fatal Scorpion Bite. *International Journal of Science and Research (IJSR)*.
- Gad, S. C. (2014). LD50/LC50 (Lethal Dosage 50/Lethal Concentration 50). In *Encyclopedia of Toxicology: Third Edition*. <https://doi.org/10.1016/B978-0-12-386454-3.00867-8>
- Gancia, E., Montana, J. G., & Manallack, D. T. (2001). Theoretical hydrogen bonding parameters for drug design. *Journal of Molecular Graphics and Modelling*. [https://doi.org/10.1016/S1093-3263\(00\)00084-X](https://doi.org/10.1016/S1093-3263(00)00084-X)
- Garey, J., & Wolff, M. S. (1998). Estrogenic and antiprogestagenic activities of pyrethroid insecticides. *Biochemical and Biophysical Research Communications*. <https://doi.org/10.1006/bbrc.1998.9569>
- Garrett, T. P. J., McKern, N. M., Lou, M., Elleman, T. C., Adams, T. E., Lovrecz, G. O., Kofler, M., Jorissen, R. N., Nice, E. C., Burgess, A. W., & Ward, C. W. (2003). The crystal structure of a truncated ErbB2 ectodomain reveals an active conformation, poised to interact with other ErbB receptors. *Molecular Cell*. [https://doi.org/10.1016/S1097-2765\(03\)00048-0](https://doi.org/10.1016/S1097-2765(03)00048-0)
- Gasanov, S. E. (2014). Snake Venom Cytotoxins, Phospholipase A2s, and Zn²⁺-dependent Metalloproteinases: Mechanisms of Action and Pharmacological Relevance. *Journal of Clinical Toxicology*. <https://doi.org/10.4172/2161-0495.1000181>
- German, A. J. (2016). Weight management in obese pets: The tailoring concept and how it can improve results. *Acta Veterinaria Scandinavica*. <https://doi.org/10.1186/s13028-016-0238-z>
- Girish, V. M., & Kini, R. M. R. (2016). Exactin: A specific inhibitor of Factor X activation by extrinsic tenase complex from the venom of *Hemachatus haemachatus*. *Scientific Reports*. <https://doi.org/10.1038/srep32036>
- Giziński, S., Boryczko, Z., Katkiewicz, M., & Bostedt, H. (2003). Ki-67 protein as a prognostic factor in mammary gland tumors in female dogs. *Medycyna Weterynaryjna*.

- Goldschmidt, M. H., Peña, L., Rasotto, R., & Zappulli, V. (2011). Classification and grading of canine mammary tumors. *Veterinary Pathology*.
<https://doi.org/10.1177/0300985810393258>
- Gordon, I. K., & Khanna, C. (2010). Modeling opportunities in comparative oncology for drug development. *ILAR Journal*. <https://doi.org/10.1093/ilar.51.3.214>
- Gordon, I., Paoloni, M., Mazcko, C., & Khanna, C. (2009). The comparative oncology trials consortium: Using spontaneously occurring cancers in dogs to inform the cancer drug development pathway. In *PLoS Medicine*. <https://doi.org/10.1371/journal.pmed.1000161>
- Gray, M., Meehan, J., Martínez-Pérez, C., Kay, C., Turnbull, A. K., Morrison, L. R., Pang, L. Y., & Argyle, D. (2020). Naturally-Occurring Canine Mammary Tumors as a Translational Model for Human Breast Cancer. In *Frontiers in Oncology*.
<https://doi.org/10.3389/fonc.2020.00617>
- Gromiha, M. M., Nagarajan, R., & Selvaraj, S. (2018). Protein structural bioinformatics: An overview. In *Encyclopedia of Bioinformatics and Computational Biology: ABC of Bioinformatics*. <https://doi.org/10.1016/B978-0-12-809633-8.20278-1>
- Gundim, L. F., de Araújo, C. P., Blanca, W. T., Guimarães, E. C., & Medeiros, A. A. (2016). Clinical staging in bitches with mammary tumors: Influence of type and histological grade. *Canadian Journal of Veterinary Research*.
- Gupta, K. (2012). Epidemiological Studies on Canine Mammary Tumour and its Relevance for Breast Cancer Studies. *IOSR Journal of Pharmacy (IOSRPHR)*.
<https://doi.org/10.9790/3013-0220322333>
- Hanahan, D., & Weinberg, R. A. (2000). The hallmarks of cancer. In *Cell*.
[https://doi.org/10.1016/S0092-8674\(00\)81683-9](https://doi.org/10.1016/S0092-8674(00)81683-9)
- Hanahan, D., & Weinberg, R. A. (2011). Hallmarks of cancer: The next generation. In *Cell*.
<https://doi.org/10.1016/j.cell.2011.02.013>
- Hannen, R., & Bartsch, J. W. (2018). Essential roles of telomerase reverse transcriptase hTERT in cancer stemness and metastasis. In *FEBS Letters*. <https://doi.org/10.1002/1873-3468.13084>
- Harvey, A. L. (1992). From venom to toxin to drug? *Proceedings of the Royal Society of Edinburgh. Section B. Biological Sciences*. <https://doi.org/10.1017/s0269727000013051>
- Harvey, A. L. (2014). Toxins and drug discovery. In *Toxicon*.
<https://doi.org/10.1016/j.toxicon.2014.10.020>
- Haycock, P. C., Burgess, S., Nounu, A., Zheng, J., Okoli, G. N., Bowden, J., Wade, K. H., Timpson, N. J., Evans, D. M., Willeit, P., Aviv, A., Gaunt, T. R., Hemani, G., Mangino, M., Ellis, H. P., Kurian, K. M., Pooley, K. A., Eeles, R. A., Lee, J. E., ... Davey Smith, G. (2017). Association between telomere length and risk of cancer and non-neoplastic diseases a mendelian randomization study. *JAMA Oncology*.
<https://doi.org/10.1001/jamaoncol.2016.5945>
- Heiden, M. G. V., Cantley, L. C., & Thompson, C. B. (2009). Understanding the warburg effect: The metabolic requirements of cell proliferation. In *Science*.
<https://doi.org/10.1126/science.1160809>

- Hicklin, D. J., & Ellis, L. M. (2005). Role of the vascular endothelial growth factor pathway in tumor growth and angiogenesis. In *Journal of Clinical Oncology*.
<https://doi.org/10.1200/JCO.2005.06.081>
- Hiu, J. J., & Yap, M. K. K. (2020). Cytotoxicity of snake venom enzymatic toxins: Phospholipase A2 and L-amino acid oxidase. In *Biochemical Society Transactions*.
<https://doi.org/10.1042/BST20200110>
- Hoffman, M. M., & Birney, E. (2007). Estimating the neutral rate of nucleotide substitution using introns. *Molecular Biology and Evolution*. <https://doi.org/10.1093/molbev/msl179>
- Horne, S. D., Pollick, S. A., & Heng, H. H. Q. (2015). Evolutionary mechanism unifies the hallmarks of cancer. In *International Journal of Cancer*. <https://doi.org/10.1002/ijc.29031>
- Horváth, S. (1980). Cytotoxicity of drugs and diverse chemical agents to cell cultures. *Toxicology*. [https://doi.org/10.1016/0300-483X\(80\)90110-9](https://doi.org/10.1016/0300-483X(80)90110-9)
- Hsu, J. L., & Hung, M. C. (2016). The role of HER2, EGFR, and other receptor tyrosine kinases in breast cancer. *Cancer and Metastasis Reviews*. <https://doi.org/10.1007/s10555-016-9649-6>
- Hubbard, S. R. (1999). Structural analysis of receptor tyrosine kinases. *Progress in Biophysics and Molecular Biology*. [https://doi.org/10.1016/S0079-6107\(98\)00047-9](https://doi.org/10.1016/S0079-6107(98)00047-9)
- Hubbard, S. R., & Miller, W. T. (2007). Receptor tyrosine kinases: mechanisms of activation and signaling. In *Current Opinion in Cell Biology*.
<https://doi.org/10.1016/j.ceb.2007.02.010>
- Im, K. S., Kim, N. H., Lim, H. Y., Kim, H. W., Shin, J. I., & Sur, J. H. (2014). Analysis of a New Histological and Molecular-Based Classification of Canine Mammary Neoplasia. *Veterinary Pathology*. <https://doi.org/10.1177/0300985813498780>
- In, Y. K., Soon, Y. H., Tae, S. K., Byung, M. L., Kwang, S. C., Hyun, J. M., Tae, S. K., Il, H. K., Seung, J. K., Moon, A., Mee, Y. A., & Hyung, S. K. (2005). Pyrethroid insecticides, fenvalerate and permethrin, inhibit progesterone-induced alkaline phosphatase activity in T47D human breast cancer cells. *Journal of Toxicology and Environmental Health - Part A*. <https://doi.org/10.1080/15287390500180523>
- Iqbal, N., & Iqbal, N. (2014). Human Epidermal Growth Factor Receptor 2 (HER2) in Cancers: Overexpression and Therapeutic Implications. *Molecular Biology International*.
<https://doi.org/10.1155/2014/852748>
- Ivanisenko, V. A., Eroshkin, A. M., & Kolchanov, N. A. (2005). WebProAnalyst: An interactive tool for analysis of quantitative structure-activity relationships in protein families. *Nucleic Acids Research*. <https://doi.org/10.1093/nar/gki421>
- Iversen, P. W., Eastwood, B. J., Sittampalam, G. S., & Cox, K. L. (2006). A comparison of assay performance measures in screening assays: Signal window, Z' factor, and assay variability ratio. *Journal of Biomolecular Screening*.
<https://doi.org/10.1177/1087057105285610>
- Jansson, M., & Laikre, L. (2018). Pedigree data indicate rapid inbreeding and loss of genetic diversity within populations of native, traditional dog breeds of conservation concern. *PLoS ONE*. <https://doi.org/10.1371/journal.pone.0202849>

- Janzen, W. P. (2014). Screening technologies for small molecule discovery: The state of the art. In *Chemistry and Biology*. <https://doi.org/10.1016/j.chembiol.2014.07.015>
- Jridi, I., Catacchio, I., Majdoub, H., Shahbazeddah, D., El Ayeb, M., Frassanito, M. A., Ribatti, D., Vacca, A., & Borchani, L. (2015). Hemilipin, a novel Hemiscorpius lepturus venom heterodimeric phospholipase A2, which inhibits angiogenesis in vitro and in vivo. *Toxicon*. <https://doi.org/10.1016/j.toxicon.2015.08.022>
- Jurrus, E., Engel, D., Star, K., Monson, K., Brandi, J., Felberg, L. E., Brookes, D. H., Wilson, L., Chen, J., Liles, K., Chun, M., Li, P., Gohara, D. W., Dolinsky, T., Konecny, R., Koes, D. R., Nielsen, J. E., Head-Gordon, T., Geng, W., ... Baker, N. A. (2018). Improvements to the APBS biomolecular solvation software suite. *Protein Science*. <https://doi.org/10.1002/pro.3280>
- Kalam, Y., Isbister, G. K., Mirtschin, P., Hodgson, W. C., & Konstantakopoulos, N. (2011). Validation of a cell-based assay to differentiate between the cytotoxic effects of elapid snake venoms. *Journal of Pharmacological and Toxicological Methods*. <https://doi.org/10.1016/j.vascn.2010.09.001>
- Kalam, Y., Isbister, G. K., Mirtschin, P., Hodgson, W. C., & Konstantakopoulos, N. (2011). Validation of a cell-based assay to differentiate between the cytotoxic effects of elapid snake venoms. *Journal of Pharmacological and Toxicological Methods*. <https://doi.org/10.1016/j.vascn.2010.09.001>
- Karayannopoulou, M., & Lafioniatis, S. (2016). Recent advances on canine mammary cancer chemotherapy: A review of studies from 2000 to date. In *Revue de Medecine Veterinaire*.
- Karayannopoulou, M., Kaldrymidou, E., Constantinidis, T. C., & Dessiris, A. (2001). Adjuvant Post-operative Chemotherapy in Bitches with Mammary Cancer. *Journal of Veterinary Medicine Series A: Physiology Pathology Clinical Medicine*. <https://doi.org/10.1046/j.1439-0442.2001.00336.x>
- Karlsson, E. K., & Lindblad-Toh, K. (2008). Leader of the pack: Gene mapping in dogs and other model organisms. In *Nature Reviews Genetics*. <https://doi.org/10.1038/nrg2382>
- Karplus, K., Barrett, C., & Hughey, R. (1998). Hidden Markov models for detecting remote protein homologies. *Bioinformatics*. <https://doi.org/10.1093/bioinformatics/14.10.846>
- Kaszak, I., Ruszczak, A., Kanafa, S., Kacprzak, K., Król, M., & Jurka, P. (2018). Current biomarkers of canine mammary tumors. In *Acta Veterinaria Scandinavica*. <https://doi.org/10.1186/s13028-018-0417-1>
- Katchalski-Katzir, E., Shariv, I., Eisenstein, M., Friesem, A. A., Aflalo, C., & Vakser, I. A. (1992). Molecular surface recognition: Determination of geometric fit between proteins and their ligands by correlation techniques. *Proceedings of the National Academy of Sciences of the United States of America*. <https://doi.org/10.1073/pnas.89.6.2195>
- Kerkkamp, H., Bagowski, C., Kool, J., van Soelingen, B., Vonk, F. J., & Vlecken, D. (2018). Whole snake venoms: Cytotoxic, anti-metastatic and antiangiogenic properties. *Toxicon*. <https://doi.org/10.1016/j.toxicon.2018.05.004>
- Kieran, M. W., Kalluri, R., & Cho, Y. J. (2012). The VEGF pathway in cancer and disease: Responses, resistance, and the path forward. *Cold Spring Harbor Perspectives in Medicine*. <https://doi.org/10.1101/cshperspect.a006593>

- Kim, N. H., Lim, H. Y., Im, K. S., Shin, J. I., Kim, H. W., & Sur, J. H. (2014). Evaluation of clinicopathological characteristics and oestrogen receptor gene expression in oestrogen receptor-negative, progesterone receptor-positive canine mammary carcinomas. *Journal of Comparative Pathology*. <https://doi.org/10.1016/j.jcpa.2014.04.001>
- King, G. F. (2011). Venoms as a platform for human drugs: Translating toxins into therapeutics. In *Expert Opinion on Biological Therapy*. <https://doi.org/10.1517/14712598.2011.621940>
- Kini, R. M., & Doley, R. (2010). Structure, function and evolution of three-finger toxins: Mini proteins with multiple targets. In *Toxicon*. <https://doi.org/10.1016/j.toxicon.2010.07.010>
- Kini, R. M., & Koh, C. Y. (2020). Snake venom three-finger toxins and their potential in drug development targeting cardiovascular diseases. In *Biochemical Pharmacology*. <https://doi.org/10.1016/j.bcp.2020.114105>
- Knottenbelt, C., Chambers, G., Gault, E., & Argyle, D. J. (2006). The in vitro effects of piroxicam and meloxicam on canine cell lines. *Journal of Small Animal Practice*. <https://doi.org/10.1111/j.1748-5827.2006.00006.x>
- Koff, J. L., Ramachandiran, S., & Bernal-Mizrachi, L. (2015). A time to kill: Targeting apoptosis in cancer. In *International Journal of Molecular Sciences*. <https://doi.org/10.3390/ijms16022942>
- Kong, G. M., Tao, W. H., Diao, Y. L., Fang, P. H., Wang, J. J., Bo, P., & Qian, F. (2016). Melittin induces human gastric cancer cell apoptosis via activation of mitochondrial pathway. *World Journal of Gastroenterology*. <https://doi.org/10.3748/wjg.v22.i11.3186>
- Kristiansen, V. M., Peña, L., Díez Córdova, L., Illera, J. C., Skjerve, E., Breen, A. M., Cofone, M. A., Langeland, M., Teige, J., Goldschmidt, M., & Sørenmo, K. U. (2016). Effect of Ovariohysterectomy at the Time of Tumor Removal in Dogs with Mammary Carcinomas: A Randomized Controlled Trial. *Journal of Veterinary Internal Medicine*. <https://doi.org/10.1111/jvim.13812>
- Kubinyi, H. (2007). Hydrogen Bonding: The Last Mystery in Drug Design? In *Pharmacokinetic Optimization in Drug Research*. <https://doi.org/10.1002/9783906390437.ch28>
- Kuhn-Nentwig, L., Stöcklin, R., & Nentwig, W. (2011). Venom composition and strategies in spiders. is everything possible? In *Advances in Insect Physiology*. <https://doi.org/10.1016/B978-0-12-387668-3.00001-5>
- Kumar, S., Bajaj, S., & Bodla, R. (2016). Preclinical screening methods in cancer. In *Indian Journal of Pharmacology*. <https://doi.org/10.4103/0253-7613.190716>
- Kumar, S., Juresic, E., Barton, M., & Shafiq, J. (2010). Management of skin toxicity during radiation therapy: A review of the evidence. *Journal of Medical Imaging and Radiation Oncology*. <https://doi.org/10.1111/j.1754-9485.2010.02170.x>
- Kumaraguruparan, R., Prathiba, D., & Nagini, S. (2006). Of humans and canines: Immunohistochemical analysis of PCNA, Bcl-2, p53, cytokeratin and ER in mammary tumours. *Research in Veterinary Science*. <https://doi.org/10.1016/j.rvsc.2005.08.002>
- Labi, V., & Erlacher, M. (2015). How cell death shapes cancer. In *Cell Death and Disease*. <https://doi.org/10.1038/cddis.2015.20>

- Laflamme, D. P. (2006). Understanding and Managing Obesity in Dogs and Cats. In *Veterinary Clinics of North America - Small Animal Practice*.
<https://doi.org/10.1016/j.cvsm.2006.08.005>
- Lallo, M. A., Ferrarias, T. M., Stravino, A., Rodriguez, J. F. M., & Zucare, R. L. C. (2016). Hematologic abnormalities in dogs bearing mammary tumors. *Revista Brasileira de Ciência Veterinária*. <https://doi.org/10.4322/rbcv.2016.020>
- Larue, S. M., & Gordon, I. K. (2012). Radiation Therapy. In *Withrow and MacEwen's Small Animal Clinical Oncology: Fifth Edition*. <https://doi.org/10.1016/B978-1-4377-2362-5.00012-8>
- Lazarovici, P., Marcinkiewicz, C., & Lelkes, P. I. (2019). From snake venom's disintegrins and C-type lectins to anti-platelet drugs. In *Toxins*. <https://doi.org/10.3390/toxins11050303>
- Lemmon, M. A., & Schlessinger, J. (2010). Cell signaling by receptor tyrosine kinases. In *Cell*. <https://doi.org/10.1016/j.cell.2010.06.011>
- Lewis, R. J., & Garcia, M. L. (2003). Therapeutic potential of venom peptides. In *Nature Reviews Drug Discovery*. <https://doi.org/10.1038/nrd1197>
- Lewis, T. W., Wiles, B. M., Llewellyn-Zaidi, A. M., Evans, K. M., & O'Neill, D. G. (2018). Longevity and mortality in Kennel Club registered dog breeds in the UK in 2014. *Canine Genetics and Epidemiology*. <https://doi.org/10.1186/s40575-018-0066-8>
- Li, L., Huang, J., & Lin, Y. (2018). Snake venoms in cancer therapy: Past, present and future. In *Toxins*. <https://doi.org/10.3390/toxins10090346>
- Liberti, M. V., & Locasale, J. W. (2016). The Warburg Effect: How Does it Benefit Cancer Cells? In *Trends in Biochemical Sciences*. <https://doi.org/10.1016/j.tibs.2015.12.001>
- Lim, H. Y., Im, K. S., Kim, N. H., Kim, H. W., Shin, J. I., Yhee, J. Y., & Sur, J. H. (2015). Effects of Obesity and Obesity-Related Molecules on Canine Mammary Gland Tumors. *Veterinary Pathology*. <https://doi.org/10.1177/0300985815579994>
- Litterine-Kaufman, J., Casale, S. A., & Mouser, P. J. (2019). Prevalence of malignancy in masses from the mammary gland region of dogs with single or multiple masses. *Journal of the American Veterinary Medical Association*. <https://doi.org/10.2460/javma.255.7.817>
- London, C. A. (2009). Tyrosine Kinase Inhibitors in Veterinary Medicine. *Topics in Companion Animal Medicine*. <https://doi.org/10.1053/j.tcam.2009.02.002>
- London, C. A. (2013). Kinase dysfunction and kinase inhibitors. *Veterinary Dermatology*. <https://doi.org/10.1111/j.1365-3164.2012.01081.x>
- Lopez-Albaitero, A., Xu, H., Guo, H., Wang, L., Wu, Z., Tran, H., Chandarlapaty, S., Scaltriti, M., Janjigian, Y., de Stanchina, E., & Cheung, N. K. V. (2017). Overcoming resistance to HER2-targeted therapy with a novel HER2/CD3 bispecific antibody. *OncImmunology*. <https://doi.org/10.1080/2162402X.2016.1267891>
- Lori, J. C., Stein, T. J., & Thamm, D. H. (2010). Doxorubicin and cyclophosphamide for the treatment of canine lymphoma: a randomized, placebo-controlled study. *Veterinary and Comparative Oncology*. <https://doi.org/10.1111/j.1476-5829.2010.00215.x>

- Lyukmanova, E. N., Shulepko, M. A., Shenkarev, Z. O., Kasheverov, I. E., Chugunov, A. O., Kulbatskii, D. S., Myshkin, M. Y., Utkin, Y. N., Efremov, R. G., Tsetlin, V. I., Arseniev, A. S., Kirpichnikov, M. P., & Dolgikh, D. A. (2016). Central loop of non-conventional toxin WTX from *Naja kaouthia* is important for interaction with nicotinic acetylcholine receptors. *Toxicon*. <https://doi.org/10.1016/j.toxicon.2016.06.012>
- Ma, R., Mahadevappa, R., & Kwok, H. F. (2017). Venom-based peptide therapy: Insights into anti-cancer mechanism. In *Oncotarget*. <https://doi.org/10.18632/oncotarget.21740>
- Macdonald, V. (2009). Chemotherapy: Managing side effects and safe handling. *Canadian Veterinary Journal*.
- Magalhães, J. R., Guimarães, J. B., Bonfim, L. S., Carvalho, C. F., Luz, L. C., Cagnini, D. Q., Regalin, D., & Amaral, A. V. C. (2020). Relationship of obesity with clinical and laboratory changes in female dogs with mammary neoplasia1. *Pesquisa Veterinaria Brasileira*. <https://doi.org/10.1590/1678-5150-PVB-6451>
- Mainenti, M., Rasotto, R., Carnier, P., & Zappulli, V. (2014). Oestrogen and progesterone receptor expression in subtypes of canine mammary tumours in intact and ovariectomised dogs. *Veterinary Journal*. <https://doi.org/10.1016/j.tvjl.2014.06.003>
- Malathi, K., & Ramaiah, S. (2018). Bioinformatics approaches for new drug discovery: a review. *Biotechnology and Genetic Engineering Reviews*. <https://doi.org/10.1080/02648725.2018.1502984>
- Malmberg, K. J. (2004). Effective immunotherapy against cancer: A question of overcoming immune suppression and immune escape? *Cancer Immunology, Immunotherapy*. <https://doi.org/10.1007/s00262-004-0577-x>
- Malumbres, M., & Barbacid, M. (2009). Cell cycle, CDKs and cancer: A changing paradigm. In *Nature Reviews Cancer*. <https://doi.org/10.1038/nrc2602>
- Mason, N. J., Gnanandarajah, J. S., Engiles, J. B., Gray, F., Laughlin, D., Gaurnier-Hausser, A., Wallecha, A., Huebner, M., & Paterson, Y. (2016). Immunotherapy with a HER2-Targeting listeria induces HER2-Specific immunity and demonstrates potential therapeutic effects in a phase I trial in canine osteosarcoma. *Clinical Cancer Research*. <https://doi.org/10.1158/1078-0432.CCR-16-0088>
- McCullough, D., Atofanei, C., Knight, E., Trim, S. A., & Trim, C. M. (2020). Kinome scale profiling of venom effects on cancer cells reveals potential new venom activities. *Toxicon*. <https://doi.org/10.1016/j.toxicon.2020.07.007>
- Mello, S. S., & Attardi, L. D. (2018). Deciphering p53 signaling in tumor suppression. In *Current Opinion in Cell Biology*. <https://doi.org/10.1016/j.ceb.2017.11.005>
- Meng, X.-Y., Zhang, H.-X., Mezei, M., & Cui, M. (2012). Molecular Docking: A Powerful Approach for Structure-Based Drug Discovery. *Current Computer Aided-Drug Design*. <https://doi.org/10.2174/157340911795677602>
- Mitchell, R. A., Luwor, R. B., & Burgess, A. W. (2018). Epidermal growth factor receptor: Structure-function informing the design of anticancer therapeutics. In *Experimental Cell Research*. <https://doi.org/10.1016/j.yexcr.2018.08.009>
- Miyoshi, Y., Funahashi, T., Tanaka, S., Taguchi, T., Tamaki, Y., Shimomura, I., & Noguchi, S. (2006). High expression of leptin receptor mRNA in breast cancer tissue predicts poor

- prognosis for patients with high, but not low, serum leptin levels. *International Journal of Cancer*. <https://doi.org/10.1002/ijc.21543>
- Moasser, M. M. (2007). The oncogene HER2: Its signaling and transforming functions and its role in human cancer pathogenesis. In *Oncogene*. <https://doi.org/10.1038/sj.onc.1210477>
- Moe, L. (2001). Population-based incidence of mammary tumours in some dog breeds. *Journal of Reproduction and Fertility. Supplement*.
- Morris, J. S., Dobson, J. M., & Bostock, D. E. (1993). Use of tamoxifen in the control of canine mammary neoplasia. *Veterinary Record*. <https://doi.org/10.1136/vr.133.22.539>
- Mosmann, T. (1983). Rapid colorimetric assay for cellular growth and survival: Application to proliferation and cytotoxicity assays. *Journal of Immunological Methods*. [https://doi.org/10.1016/0022-1759\(83\)90303-4](https://doi.org/10.1016/0022-1759(83)90303-4)
- Murphy, S. (2008). Mammary tumours in dogs and cats. *In Practice*. <https://doi.org/10.1136/inpract.30.6.334>
- Neumann, S., Schuettler, J., Frenz, M., Kaup, F. J., & Gessler, F. (2017). Investigation of serum Ki-67 as a biomarker in tumor-bearing dogs. *Research in Veterinary Science*. <https://doi.org/10.1016/j.rvsc.2016.10.012>
- Newman, D. J., & Cragg, G. M. (2016). Natural Products as Sources of New Drugs from 1981 to 2014. In *Journal of Natural Products*. <https://doi.org/10.1021/acs.jnatprod.5b01055>
- Nguyen, F., Peña, L., Ibisch, C., Loussouarn, D., Gama, A., Rieder, N., Belousov, A., Campone, M., & Abadie, J. (2018). Canine invasive mammary carcinomas as models of human breast cancer. Part 1: Natural history and prognostic factors. *Breast Cancer Research and Treatment*. <https://doi.org/10.1007/s10549-017-4548-2>
- Nicholas, F. W. (2005). Animal breeding and disease. In *Philosophical Transactions of the Royal Society B: Biological Sciences*. <https://doi.org/10.1098/rstb.2005.1674>
- Niles, A. L., Moravec, R. A., & Riss, T. L. (2008). Update on in vitro cytotoxicity assays for drug development. In *Expert Opinion on Drug Discovery*. <https://doi.org/10.1517/17460441.3.6.655>
- Noble, K., Rohaj, A., Abegglen, L. M., & Schiffman, J. D. (2020). Cancer therapeutics inspired by defense mechanisms in the animal kingdom. In *Evolutionary Applications*. <https://doi.org/10.1111/eva.12963>
- Novosad, C. A. (2003). Principles of treatment for mammary gland tumors. *Clinical Techniques in Small Animal Practice*. <https://doi.org/10.1053/svms.2003.36625>
- Nowak, M., Madej, J. A., Pula, B., Dziegiel, P., & Ciaputa, R. (2016). Expression of matrix metalloproteinase 2 (MMP-2), E-cadherin and Ki-67 in metastatic and non-metastatic canine mammary carcinomas. *Irish Veterinary Journal*.
- Nunes, F. C., Damasceno, K. A., de Campos, C. B., Bertagnolli, A. C., Lavallo, G. E., & Cassali, G. D. (2019). Mixed tumors of the canine mammary glands: Evaluation of prognostic factors, treatment, and overall survival. *Veterinary and Animal Science*. <https://doi.org/10.1016/j.vas.2018.09.003>

- O'Neill, D. G., Pegram, C., Crocker, P., Brodbelt, D. C., Church, D. B., & Packer, R. M. A. (2020). Unravelling the health status of brachycephalic dogs in the UK using multivariable analysis. *Scientific Reports*. <https://doi.org/10.1038/s41598-020-73088-y>
- Oh, D. Y., & Bang, Y. J. (2020). HER2-targeted therapies — a role beyond breast cancer. In *Nature Reviews Clinical Oncology*. <https://doi.org/10.1038/s41571-019-0268-3>
- Opie, L. H., & Kowolik, H. (1995). The discovery of captopril: From large animals to small molecules. In *Cardiovascular Research*. [https://doi.org/10.1016/S0008-6363\(95\)00006-2](https://doi.org/10.1016/S0008-6363(95)00006-2)
- Osipov, A. V., Astapova, M. V., Tsetlin, V. I., & Utkin, Y. N. (2004). The first representative of glycosylated three-fingered toxins: Cytotoxin from the *Naja kaouthia* cobra venom. *European Journal of Biochemistry*. <https://doi.org/10.1111/j.1432-1033.2004.04115.x>
- Ou-Yang, Z. C., Zhou, H., & Zhang, Y. (2003). The elastic theory of a single DNA molecule. In *Modern Physics Letters B*. <https://doi.org/10.1142/S0217984903004877>
- Packer, R. M. A., Hendricks, A., Tivers, M. S., & Burn, C. C. (2015). Impact of facial conformation on canine health: Brachycephalic obstructive airway syndrome. *PLoS ONE*. <https://doi.org/10.1371/journal.pone.0137496>
- Pal, P., Roy, S., Chattopadhyay, S. and Pal, T.K., 2015. Medicinal value of animal venom for treatment of Cancer in Humans-A Review. *World Scientific News*, 22, pp.128-144
- Panagides, N., Jackson, T. N. W., Ikonopoulou, M. P., Arbuckle, K., Pretzler, R., Yang, D. C., Ali, S. A., Koludarov, I., Dobson, J., Sanker, B., Asselin, A., Santana, R. C., Hendrikx, I., van der Ploeg, H., Tai-A-Pin, J., van den Bergh, R., Kerckamp, H. M. I., Vonk, F. J., Naude, A., ... Fry, B. G. (2017). How the cobra got its flesh-eating venom: Cytotoxicity as a defensive innovation and its co-evolution with hooding, aposematic marking, and spitting. *Toxins*. <https://doi.org/10.3390/toxins9030103>
- Paoloni, M., & Khanna, C. (2008). Translation of new cancer treatments from pet dogs to humans. In *Nature Reviews Cancer*. <https://doi.org/10.1038/nrc2273>
- Pastor, N., Caballé, N. C., Santella, M., Ezquerro, L. J., Tarazona, R., & Duran, E. (2018). Epidemiological study of canine mammary tumors: Age, breed, size and malignancy. *Austral Journal of Veterinary Sciences*. <https://doi.org/10.4067/s0719-81322018000300143>
- Pavlova, N. N., & Thompson, C. B. (2016). The Emerging Hallmarks of Cancer Metabolism. In *Cell Metabolism*. <https://doi.org/10.1016/j.cmet.2015.12.006>
- Peña, L., Gama, A., Goldschmidt, M. H., Abadie, J., Benazzi, C., Castagnaro, M., Díez, L., Gärtner, F., Hellmén, E., Kiupel, M., Millán, Y., Miller, M. A., Nguyen, F., Poli, A., Sarli, G., Zappulli, V., & de las Mulas, J. M. (2014). Canine Mammary Tumors: A Review and Consensus of Standard Guidelines on Epithelial and Myoepithelial Phenotype Markers, HER2, and Hormone Receptor Assessment Using Immunohistochemistry. *Veterinary Pathology*. <https://doi.org/10.1177/0300985813509388>
- Pennington, M. W., Czerwinski, A., & Norton, R. S. (2018). Peptide therapeutics from venom: Current status and potential. *Bioorganic and Medicinal Chemistry*. <https://doi.org/10.1016/j.bmc.2017.09.029>
- Pérez-Peinado, C., Defaus, S., & Andreu, D. (2020). Hitchhiking with nature: Snake venom peptides to fight cancer and superbugs. In *Toxins*. <https://doi.org/10.3390/toxins12040255>

- Peruzzi, D., Mesiti, G., Ciliberto, G., La Monica, N., & Aurisicchio, L. (2010). Telomerase and HER-2/neu as targets of genetic cancer vaccines in dogs. *Vaccine*.
<https://doi.org/10.1016/j.vaccine.2009.11.031>
- Petras, D., Sanz, L., Segura, Á., Herrera, M., Villalta, M., Solano, D., Vargas, M., León, G., Warrell, D. A., Theakston, R. D. G., Harrison, R. A., Durfa, N., Nasidi, A., Gutiérrez, J. M., & Calvete, J. J. (2011). Snake venomomics of African spitting cobras: Toxin composition and assessment of congeneric cross-reactivity of the Pan-African EchiTAb-Plus-ICP antivenom by venomomics and neutralization approaches. *Journal of Proteome Research*.
<https://doi.org/10.1021/pr101040f>
- Pierce, B. G., Wiehe, K., Hwang, H., Kim, B. H., Vreven, T., & Weng, Z. (2014). ZDOCK server: Interactive docking prediction of protein-protein complexes and symmetric multimers. *Bioinformatics*. <https://doi.org/10.1093/bioinformatics/btu097>
- Pierce, B. G., Wiehe, K., Hwang, H., Kim, B. H., Vreven, T., & Weng, Z. (2014). ZDOCK server: Interactive docking prediction of protein-protein complexes and symmetric multimers. *Bioinformatics*. <https://doi.org/10.1093/bioinformatics/btu097>
- Präbst, K., Engelhardt, H., Ringgeler, S., & Hübner, H. (2017). Basic colorimetric proliferation assays: MTT, WST, and resazurin. In *Methods in Molecular Biology*.
https://doi.org/10.1007/978-1-4939-6960-9_1
- Prager, G. W., & Zielinski, C. C. (2013). Angiogenesis in cancer. In *Biochemical Basis and Therapeutic Implications of Angiogenesis*. https://doi.org/10.1007/978-1-4614-5857-9_18
- Proschowsky, H. F., Rugbjerg, H., & Ersbøll, A. K. (2003). Mortality of purebred and mixed-breed dogs in Denmark. *Preventive Veterinary Medicine*. [https://doi.org/10.1016/S0167-5877\(03\)00010-2](https://doi.org/10.1016/S0167-5877(03)00010-2)
- Queiroga, F. L., Pérez-Alenza, M. D., Silvan, G., Peña, L., Lopes, C., & Illera, J. C. (2005). Role of steroid hormones and prolactin in canine mammary cancer. *Journal of Steroid Biochemistry and Molecular Biology*. <https://doi.org/10.1016/j.jsbmb.2004.12.014>
- Queiroga, F. L., Pires, I., Lobo, L., & Lopes, C. S. (2010). The role of Cox-2 expression in the prognosis of dogs with malignant mammary tumours. *Research in Veterinary Science*.
<https://doi.org/10.1016/j.rvsc.2009.10.009>
- Queiroga, F. L., Pires, I., Parente, M., Gregório, H., & Lopes, C. S. (2011). COX-2 over-expression correlates with VEGF and tumour angiogenesis in canine mammary cancer. *Veterinary Journal*. <https://doi.org/10.1016/j.tvjl.2010.06.022>
- Queiroga, F. L., Raposo, T., Carvalho, M. I., Prada, J., & Pires, I. (2011). Canine mammary tumours as a model to study human breast cancer: Most recent findings. In *In Vivo*.
- Rassy, E., Assi, T., & Pavlidis, N. (2020). Exploring the biological hallmarks of cancer of unknown primary: where do we stand today? In *British Journal of Cancer*.
<https://doi.org/10.1038/s41416-019-0723-z>
- Rehm, S., Stanislaus, D. J., & Williams, A. M. (2007). Estrous cycle-dependent histology and review of sex steroid receptor expression in dog reproductive tissues and mammary gland and associated hormone levels. In *Birth Defects Research Part B - Developmental and Reproductive Toxicology*. <https://doi.org/10.1002/bdrb.20121>

- Ressel, L., Finotello, R., Innocenti, V. M., Vannozzi, I., & Poli, A. (2012). Preliminary report on the expression of leptin and leptin receptor (ObR) in normal, hyperplastic and neoplastic canine mammary tissues. *Research in Veterinary Science*.
<https://doi.org/10.1016/j.rvsc.2011.07.020>
- Riecks, T. W., Birchard, S. J., & Stephens, J. A. (2007). Surgical correction of brachycephalic syndrome in dogs: 62 Cases (1991-2004). *Journal of the American Veterinary Medical Association*. <https://doi.org/10.2460/javma.230.9.1324>
- Riss, T. L., & Moravec, R. A. (2004). Use of multiple assay endpoints to investigate the effects of incubation time, dose of toxin, and plating density in cell-based cytotoxicity assays. *Assay and Drug Development Technologies*.
<https://doi.org/10.1089/154065804322966315>
- Rooney, N., & Sargan, D. (2009). Pedigree Dog-breeding in the UK: A Major Welfare Concern. *Royal Society for the Prevention of Cruelty to Animals*.
- Roy, A., Kucukural, A., & Zhang, Y. (2010). I-TASSER: A unified platform for automated protein structure and function prediction. *Nature Protocols*.
<https://doi.org/10.1038/nprot.2010.5>
- Roy, K., Kar, S., Das, R. N., Roy, K., Kar, S., & Das, R. N. (2015). Chapter 5 – Computational Chemistry. In *Understanding the Basics of QSAR for Applications in Pharmaceutical Sciences and Risk Assessment*.
- Safavi-Hemami, H., Brogan, S. E., & Olivera, B. M. (2019). Pain therapeutics from cone snail venoms: From Ziconotide to novel non-opioid pathways. *Journal of Proteomics*.
<https://doi.org/10.1016/j.jprot.2018.05.009>
- Sampson, J. (2011). How the Kennel Club is tackling inherited disorders in the United Kingdom. In *Veterinary Journal*. <https://doi.org/10.1016/j.tvjl.2011.06.010>
- Schmidtko, A., Lötsch, J., Freynhagen, R., & Geisslinger, G. (2010). Ziconotide for treatment of severe chronic pain. In *The Lancet*. [https://doi.org/10.1016/S0140-6736\(10\)60354-6](https://doi.org/10.1016/S0140-6736(10)60354-6)
- Schneider, R., Dorn, C. R., & Taylor, D. O. N. (1969). Factors influencing canine mammary cancer development and postsurgical survival. *Journal of the National Cancer Institute*.
<https://doi.org/10.1093/jnci/43.6.1249>
- Serras, A. R., Berlato, D., & Murphy, S. (2019). Owners' perception of their dogs' quality of life during and after radiotherapy for cancer. *Journal of Small Animal Practice*.
<https://doi.org/10.1111/jsap.12972>
- Service, R. (2020). 'The game has changed.' AI triumphs at solving protein structures. *Science*.
<https://doi.org/10.1126/science.abf9367>
- Seung, B. J., Cho, S. H., Kim, S. H., Lim, H. Y., & Sur, J. H. (2020). Quantitative analysis of HER2 mRNA expression by RNA in situ hybridization in canine mammary gland tumors: Comparison with immunohistochemistry analysis. *PLoS ONE*.
<https://doi.org/10.1371/journal.pone.0229031>
- Sévère, S., Marchand, P., Guiffard, I., Morio, F., Venisseau, A., Veyrand, B., Le Bizec, B., Antignac, J. P., & Abadie, J. (2015). Pollutants in pet dogs: a model for environmental links to breast cancer. *SpringerPlus*. <https://doi.org/10.1186/s40064-015-0790-4>

- Shahbazi, B., Najafabadi, Z. S., Goudarzi, H., Sajadi, M., Tahoori, F., & Bagheri, M. (2019). Cytotoxic effects of *Pseudocerastes persicus* venom and its HPLC fractions on lung cancer cells. *Journal of Venomous Animals and Toxins Including Tropical Diseases*. <https://doi.org/10.1590/1678-9199-jvatitd-2019-0009>
- Shanbhag, V. K. L. (2015). Applications of snake venoms in treatment of cancer. *Asian Pacific Journal of Tropical Biomedicine*. [https://doi.org/10.1016/S2221-1691\(15\)30344-0](https://doi.org/10.1016/S2221-1691(15)30344-0)
- Simon, D., Schoenrock, D., Baumgärtner, W., & Nolte, I. (2006). Postoperative adjuvant treatment of invasive malignant mammary gland tumors in dogs with doxorubicin and docetaxel. *Journal of Veterinary Internal Medicine*. [https://doi.org/10.1892/0891-6640\(2006\)20\[1184:PATIMM\]2.0.CO;2](https://doi.org/10.1892/0891-6640(2006)20[1184:PATIMM]2.0.CO;2)
- Simon, D., Schoenrock, D., Nolte, I., Baumgärtner, W., Barron, R., & Mischke, R. (2009). Cytologic examination of fine-needle aspirates from mammary gland tumors in the dog: Diagnostic accuracy with comparison to histopathology and association with postoperative outcome. *Veterinary Clinical Pathology*. <https://doi.org/10.1111/j.1939-165X.2009.00150.x>
- Singer, J., Weichselbaumer, M., Stockner, T., Mechtcheriakova, D., Sobanov, Y., Bajna, E., Wrba, F., Horvat, R., Thalhammer, J. G., Willmann, M., & Jensen-Jarolim, E. (2012). Comparative oncology: ErbB-1 and ErbB-2 homologues in canine cancer are susceptible to cetuximab and trastuzumab targeting. *Molecular Immunology*. <https://doi.org/10.1016/j.molimm.2012.01.002>
- Sleeckx, N., de Rooster, H., Veldhuis Kroeze, E. J. B., van Ginneken, C., & van Brantegem, L. (2011). Canine mammary tumours, an Overview. In *Reproduction in Domestic Animals*. <https://doi.org/10.1111/j.1439-0531.2011.01816.x>
- Smith, T. F., & Waterman, M. S. (1981). Identification of common molecular subsequences. *Journal of Molecular Biology*. [https://doi.org/10.1016/0022-2836\(81\)90087-5](https://doi.org/10.1016/0022-2836(81)90087-5)
- Sorenmo, K. (2003). Canine mammary gland tumors. In *Veterinary Clinics of North America - Small Animal Practice*. [https://doi.org/10.1016/S0195-5616\(03\)00020-2](https://doi.org/10.1016/S0195-5616(03)00020-2)
- Sorenmo, K. U., Worley, D. R., & Goldschmidt, M. H. (2013). Tumors of the Mammary Gland Mammary Gland Tumors in Dogs. *Withrow and MacEwen's Small Animal Clinical Oncology, 5/E*.
- Spoerri, M., Guscetti, F., Hartnack, S., Boos, A., Oei, C., Balogh, O., Nowaczyk, R. M., Michel, E., Reichler, I. M., & Kowalewski, M. P. (2015). Endocrine control of canine mammary neoplasms: Serum reproductive hormone levels and tissue expression of steroid hormone, prolactin and growth hormone receptors. *BMC Veterinary Research*. <https://doi.org/10.1186/s12917-015-0546-y>
- Stephens, T. (2019). The use of chemotherapy to prolong the life of dogs suffering from cancer: The ethical dilemma. *Animals*. <https://doi.org/10.3390/ani9070441>
- Stockert, J. C., Horobin, R. W., Colombo, L. L., & Blázquez-Castro, A. (2018). Tetrazolium salts and formazan products in Cell Biology: Viability assessment, fluorescence imaging, and labeling perspectives. In *Acta Histochemica*. <https://doi.org/10.1016/j.acthis.2018.02.005>
- Strumylaitė, L., Mechonošina, K., & Tamašauskas, Š. (2010). CONTINUING MEDICAL EDUCATION Environmental factors and breast cancer. In *Medicina (Kaunas)*.

- Takacs, Z., & Nathan, S. (2014). Animal Venoms in Medicine. In *Encyclopedia of Toxicology: Third Edition*. <https://doi.org/10.1016/B978-0-12-386454-3.01241-0>
- Takemura, K., & Kitao, A. (2007). Effects of water model and simulation box size on protein diffusions motions. *Journal of Physical Chemistry B*. <https://doi.org/10.1021/jp0756247>
- Tasoulis, T., & Isbister, G. K. (2017). A review and database of snake venom proteomes. In *Toxins*. <https://doi.org/10.3390/toxins9090290>
- Tavares, W. L. F., Lavalle, G. E., Figueiredo, M. S., Souza, A. G., Bertagnolli, A. C., Viana, F. A. B., Paes, P. R. O., Carneiro, R. A., Cavalcanti, G. A. O., Melo, M. M., & Cassali, G. D. (2010). Evaluation of adverse effects in tamoxifen exposed healthy female dogs. *Acta Veterinaria Scandinavica*. <https://doi.org/10.1186/1751-0147-52-67>
- Teoh, S. Q., & Yap, M. K. K. (2020). Naja sumatrana venom cytotoxin, sumaCTX exhibits concentration-dependent cytotoxicity via caspase-activated mitochondrial-mediated apoptosis without transitioning to necrosis. *Toxin Reviews*. <https://doi.org/10.1080/15569543.2020.1799408>
- The UniProt Consortium. (2019). UniProt: a worldwide hub of protein knowledge The UniProt Consortium. *Nucleic Acids Research*.
- Timmermans-Sprang, E. P. M., Gracanin, A., & Mol, J. A. (2017). Molecular signaling of progesterone, growth hormone, Wnt, and HER in mammary glands of dogs, rodents, and humans: New treatment target identification. In *Frontiers in Veterinary Science*. <https://doi.org/10.3389/fvets.2017.00053>
- Tobassum, S., Tahir, H. M., Arshad, M., Zahid, M. T., Ali, S., & Ahsan, M. M. (2020). Nature and applications of scorpion venom: an overview. In *Toxin Reviews*. <https://doi.org/10.1080/15569543.2018.1530681>
- Todorova, I., Simeonova, G., Simeonov, R., & Dinev, D. (2005). Efficacy and toxicity of doxorubicin and cyclophosphamide chemotherapy in dogs with spontaneous mammary tumours. *Trakia Journal of Sciences*.
- Tran, C. M., Moore, A. S., & Frimberger, A. E. (2016). Surgical treatment of mammary carcinomas in dogs with or without postoperative chemotherapy. *Veterinary and Comparative Oncology*. <https://doi.org/10.1111/vco.12092>
- Trempe, G. L. (1976). Human breast cancer in culture. *Recent Results in Cancer Research*. https://doi.org/10.1007/978-3-642-81043-5_5
- Tsai, C. H., Yang, S. H., Chien, C. M., Lu, M. C., Lo, C. S., Lin, Y. H., Hu, X. W., & Lin, S. R. (2006). Mechanisms of cardiotoxin III-induced apoptosis in human colorectal cancer Colo205 Cells. *Clinical and Experimental Pharmacology and Physiology*. <https://doi.org/10.1111/j.1440-1681.2006.04334.x>
- Utkin, Y. N. (2015). Animal venom studies: Current benefits and future developments. *World Journal of Biological Chemistry*. <https://doi.org/10.4331/wjbc.v6.i2.28>
- Uzabaci, E., Ozyigit, M. O., Ercan, I., & Arda, O. (2020). HER-2 positivity rate in dogs with mammary carcinoma: A systematic review and meta-analysis. *Journal of the Hellenic Veterinary Medical Society*. <https://doi.org/10.12681/jhvms.23639>

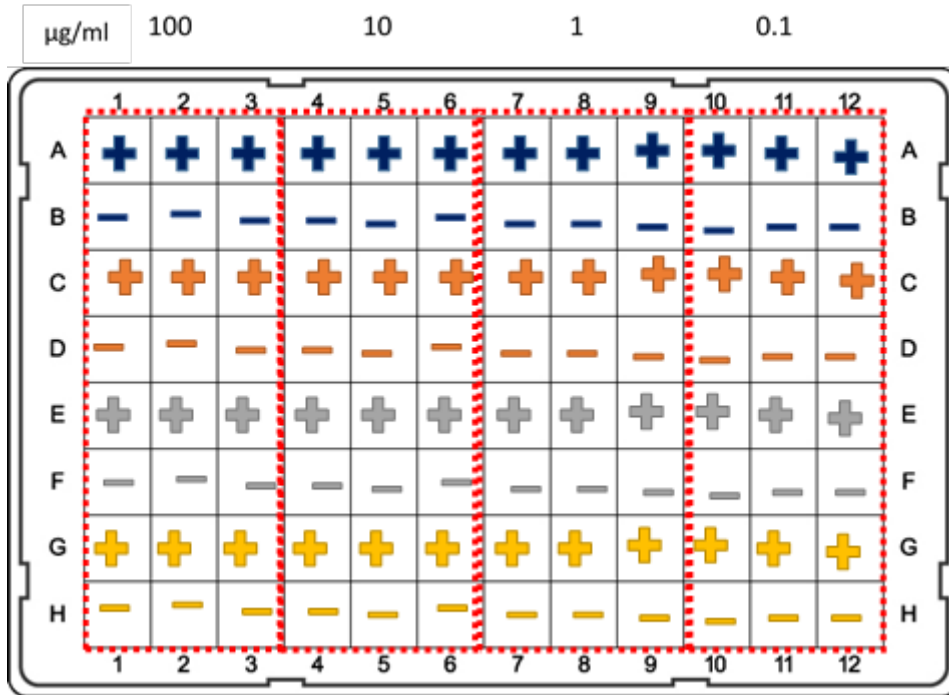
- Van Garderen, E., Van Der Poel, H. J. A., Swennenhuis, J. F., Wissink, E. H. J., Rutteman, G. R., Hellmén, E., Mol, J. A., & Schalken, J. A. (1999). Expression and molecular characterization of the growth hormone receptor in canine mammary tissue and mammary tumors. *Endocrinology*. <https://doi.org/10.1210/endo.140.12.7189>
- Van Tonder, A., Joubert, A. M., & Cromarty, A. D. (2015). Limitations of the 3-(4,5-dimethylthiazol-2-yl)-2,5-diphenyl-2H-tetrazolium bromide (MTT) assay when compared to three commonly used cell enumeration assays. *BMC Research Notes*. <https://doi.org/10.1186/s13104-015-1000-8>
- Varallo, G. R., Gelaleti, G. B., Maschio-Signorini, L. B., Moschetta, M. G., Lopes, J. R., de Nardi, A. B., Tinucci-Costa, M., Rocha, R. M., & de Campos Zuccari, D. A. P. (2019). Prognostic phenotypic classification for canine mammary tumors. *Oncology Letters*. <https://doi.org/10.3892/ol.2019.11052>
- Vu, T., & Claret, F. X. (2012). Trastuzumab: Updated mechanisms of action and resistance in breast cancer. In *Frontiers in Oncology*. <https://doi.org/10.3389/fonc.2012.00062>
- Wallasch, C., Ulrich Weiß, F., Niederfellner, G., Jallal, B., Issing, W., & Ullrich, A. (1995). Heregulin-dependent regulation of HER2/neu oncogenic signaling by heterodimerization with HER3. *EMBO Journal*. <https://doi.org/10.1002/j.1460-2075.1995.tb00101.x>
- Wang, S. B., Yang, X. Y., & Du, G. H. (2018). Tubocurarine. In *Natural Small Molecule Drugs from Plants*. https://doi.org/10.1007/978-981-10-8022-7_56
- Wang, S. C., Lien, H. C., Xia, W., Chen, I. F., Lo, H. W., Wang, Z., Ali-Seyed, M., Lee, D. F., Bartholomeusz, G., Ou-Yang, F., Giri, D. K., & Hung, M. C. (2004). Binding at and transactivation of the COX-2 promoter by nuclear tyrosine kinase receptor ErbB-2. *Cancer Cell*. <https://doi.org/10.1016/j.ccr.2004.07.012>
- Ward, J. F. (1988). DNA Damage Produced by Ionizing Radiation in Mammalian Cells: Identities, Mechanisms of Formation, and Reparability. *Progress in Nucleic Acid Research and Molecular Biology*. [https://doi.org/10.1016/S0079-6603\(08\)60611-X](https://doi.org/10.1016/S0079-6603(08)60611-X)
- Weeth, L. P. (2016). Other Risks/Possible Benefits of Obesity. In *Veterinary Clinics of North America - Small Animal Practice*. <https://doi.org/10.1016/j.cvsm.2016.04.007>
- Wolfe, L. G., Smith, B. B., Toivio-Kinnucan, M. A., Sartin, E. A., Kwapien, R. P., Henderson, R. A., & Barnes, S. (1986). Biologic properties of cell lines derived from canine mammary carcinomas. *Journal of the National Cancer Institute*. <https://doi.org/10.1093/jnci/77.3.783>
- Wydooghe, E., Berghmans, E., Rijsselaere, T., & Van Soom, A. (2013). International breeder inquiry into the reproduction of the English bulldog. *Vlaams Diergeneeskundig Tijdschrift*.
- Xu, D., & Zhang, Y. (2012). Ab initio protein structure assembly using continuous structure fragments and optimized knowledge-based force field. *Proteins: Structure, Function and Bioinformatics*. <https://doi.org/10.1002/prot.24065>
- Xu, D., & Zhang, Y. (2013). Toward optimal fragment generations for ab initio protein structure assembly. *Proteins: Structure, Function and Bioinformatics*. <https://doi.org/10.1002/prot.24179>
- Y., S., A., M., D., D., & L., R. (2015). Epidemiological Study of Mammary Tumors in Female Dogs Diagnosed during the Period 2002-2012: A Growing Animal Health Problem. *PloS One*.

- Yang, J., & Zhang, Y. (2015). I-TASSER server: New development for protein structure and function predictions. *Nucleic Acids Research*. <https://doi.org/10.1093/nar/gkv342>
- Yang, J., & Zhang, Y. (2015). Protein Structure and Function Prediction Using I-TASSER. *Current Protocols in Bioinformatics*. <https://doi.org/10.1002/0471250953.bi0508s52>
- Yang, S. H., Lu, M. C., Chien, C. M., Tsai, C. H., Lu, Y. J., Hour, T. C., & Lin, S. R. (2005). Induction of apoptosis in human leukemia K562 cells by cardiotoxin III. *Life Sciences*. <https://doi.org/10.1016/j.lfs.2005.01.001>
- Yarden, Y. (2001). The EGFR family and its ligands in human cancer: Signalling mechanisms and therapeutic opportunities. *European Journal of Cancer*. [https://doi.org/10.1016/s0959-8049\(01\)00230-1](https://doi.org/10.1016/s0959-8049(01)00230-1)
- Ye, X., & Weinberg, R. A. (2015). Epithelial-Mesenchymal Plasticity: A Central Regulator of Cancer Progression. In *Trends in Cell Biology*. <https://doi.org/10.1016/j.tcb.2015.07.012>
- Young, B. A., & Kardong, K. V. (2010). The functional morphology of hooding in cobras. *Journal of Experimental Biology*. <https://doi.org/10.1242/jeb.034447>
- Zhang, W., Yang, J., He, B., Walker, S. E., Zhang, H., Govindarajoo, B., Virtanen, J., Xue, Z., Shen, H. Bin, & Zhang, Y. (2016). Integration of QUARK and I-TASSER for Ab Initio Protein Structure Prediction in CASP11. *Proteins: Structure, Function and Bioinformatics*. <https://doi.org/10.1002/prot.24930>
- Zhang, X. Y., & Zhang, P. Y. (2016). Scorpion venoms in gastric cancer (Review). In *Oncology Letters*. <https://doi.org/10.3892/ol.2016.5134>
- Zhang, Y. (2008). I-TASSER server for protein 3D structure prediction. *BMC Bioinformatics*. <https://doi.org/10.1186/1471-2105-9-40>
- Zhang, Y., & Skolnick, J. (2004). `{I}SPICKER{I}`: A clustering approach to identify near-native protein folds. *Journal of Computational Chemistry*.
- Zheng, W., Zhang, C., Bell, E. W., & Zhang, Y. (2019). I-TASSER gateway: A protein structure and function prediction server powered by XSEDE. *Future Generation Computer Systems*. <https://doi.org/10.1016/j.future.2019.04.011>
- Zhou, H. X., & Pang, X. (2018). Electrostatic Interactions in Protein Structure, Folding, Binding, and Condensation. In *Chemical Reviews*. <https://doi.org/10.1021/acs.chemrev.7b00305>

Appendix

APPENDIX I: CHAPTER 3: Plate Layout for determining the Optimal Cell Number for CMT28, CMM26 and MDCK in 96 well plates





CMT28 and CMM26 Plate layout



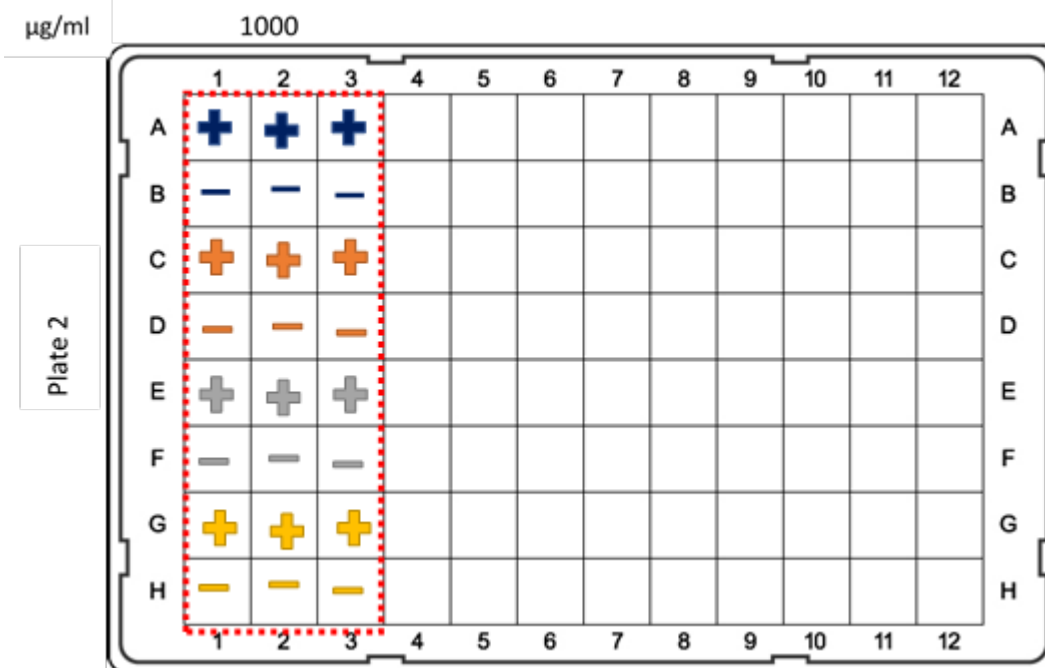
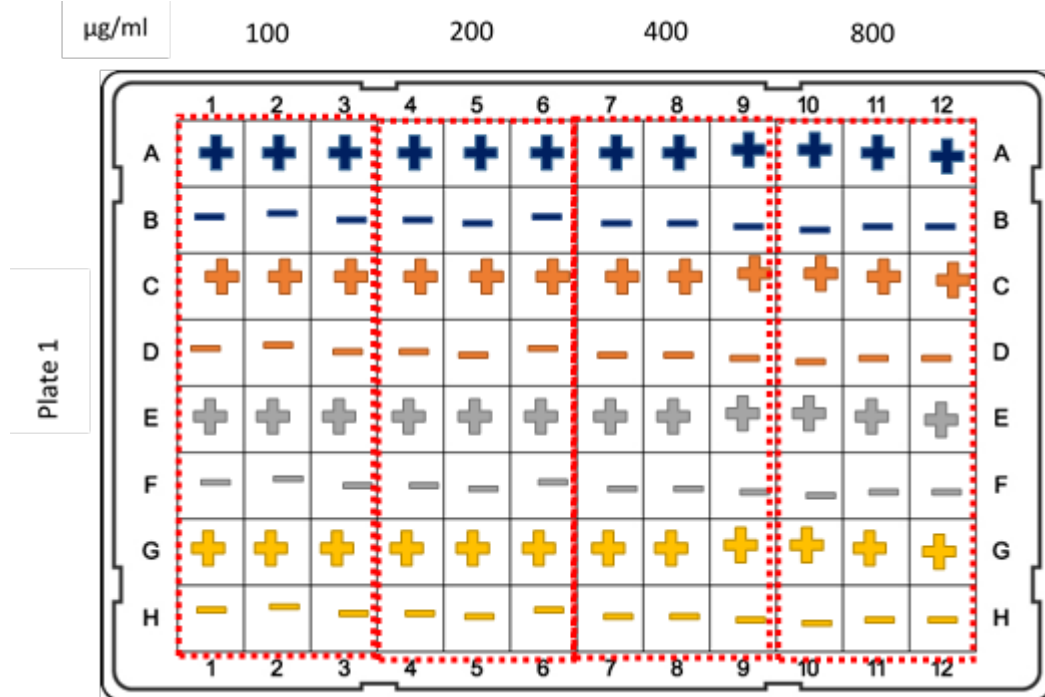
Positive controls for each Cell Number
(100µg/ml *N.nigricollis* Venom)

-  2×10^5
-  1×10^5
-  5×10^4
-  2.5×10^4

Negative controls for each Cell Number
(DMEM/RPMI media)

-  2×10^5
-  1×10^5
-  5×10^4
-  2.5×10^4

MDCK plate layout



Positive controls for each Cell Number
(1mg/ml *N.nigricollis* Venom)

- 2×10^5
- 1×10^4
- 5×10^4
- 2.5×10^4

Negative controls for each Cell Number
(DMEM media)

- 2×10^5
- 1×10^5
- 5×10^4
- 2.5×10^4

APPENDIX II: CHAPTER 3: Plate Layout for Z' Analysis of CMT28, CMM26, MDCK in 96 well plates

	1	2	3	4	5	6	7	8	9	10	11	12	
A	+	+	+	+	+	+	+	+	+	+	+	+	A
B	+	+	+	+	+	+	+	+	+	+	+	+	B
C	+	+	+	+	+	+	+	+	+	+	+	+	C
D	+	+	+	+	+	+	+	+	+	+	+	+	D
E	+	+	+	+	+	+	+	+	+	+	+	+	E
F	+	+	+	+	+	+	+	+	+	+	+	+	F
G	+	+	+	+	+	+	+	+	+	+	+	+	G
H	+	+	+	+	+	+	+	+	+	+	+	+	H
	1	2	3	4	5	6	7	8	9	10	11	12	

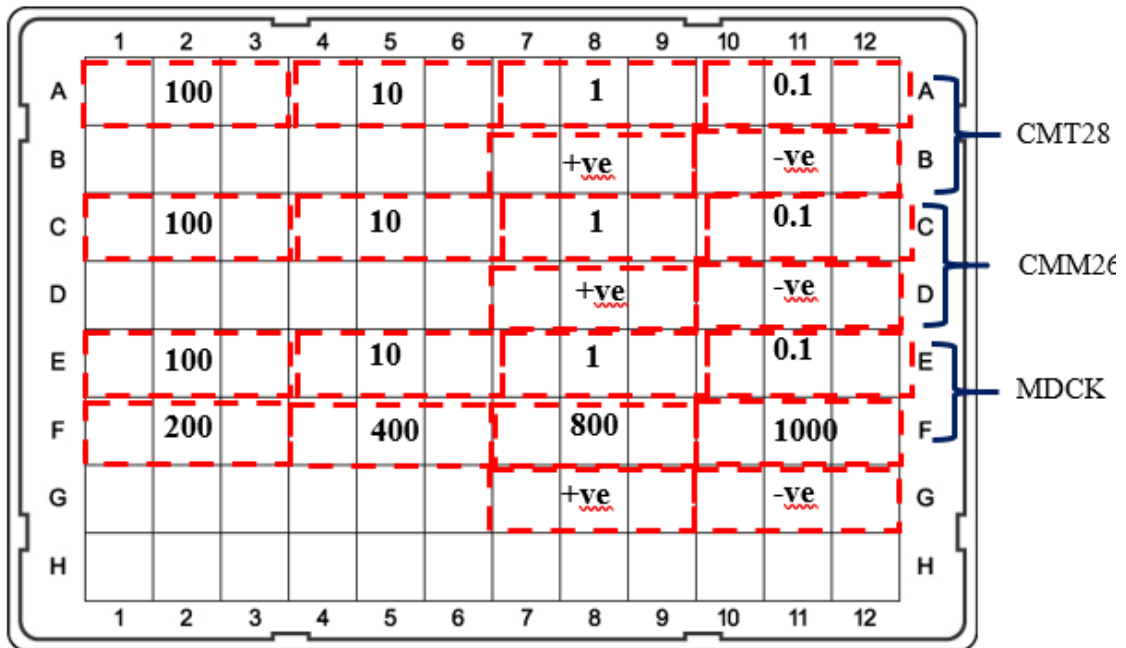


Positive control (100µg/ml fro CMT28 and CMM26 and 1mg/ml *N.nigricollis* Venom)



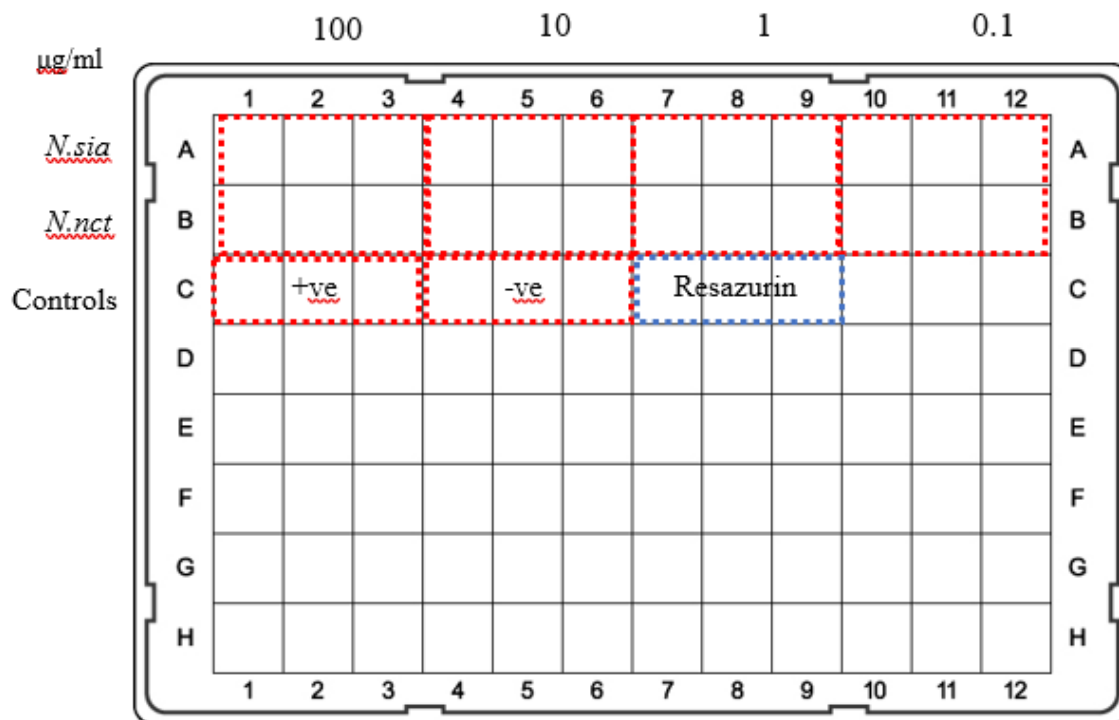
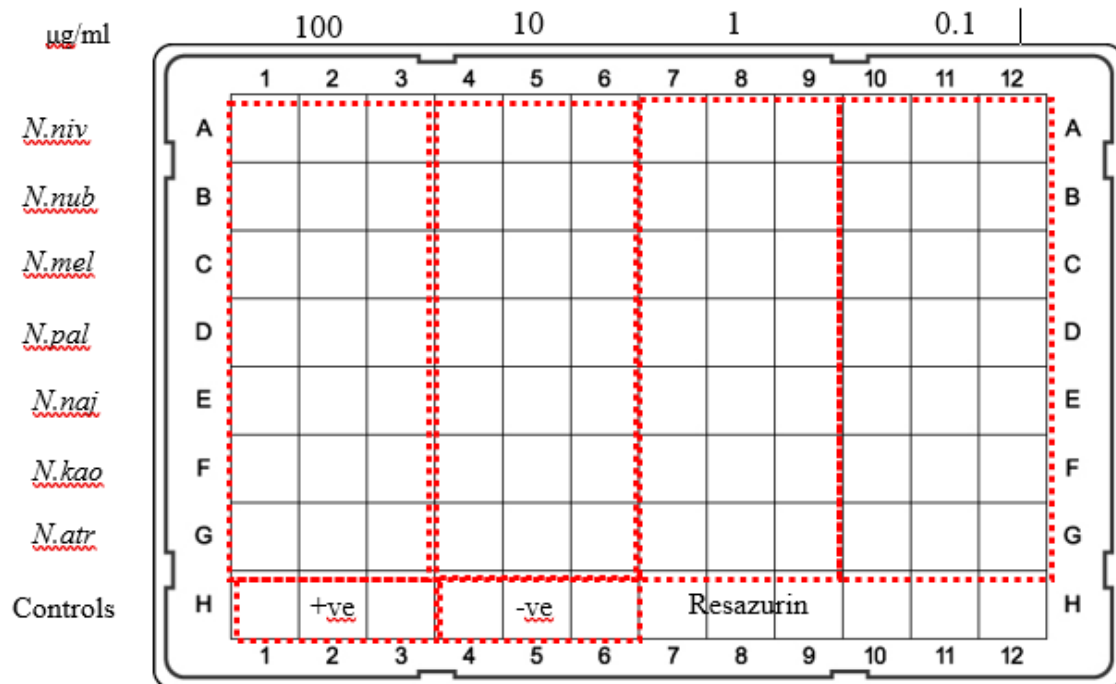
Negative control (Culture media- DMEM media for CMT28 and MDCK and RPMI for CMM26)

APPENDIX III: CHAPTER 3: Plate layout Initial Screen of *N.nigricollis* Venom on CMT28, CMM26 and MDCK in 96 well plate



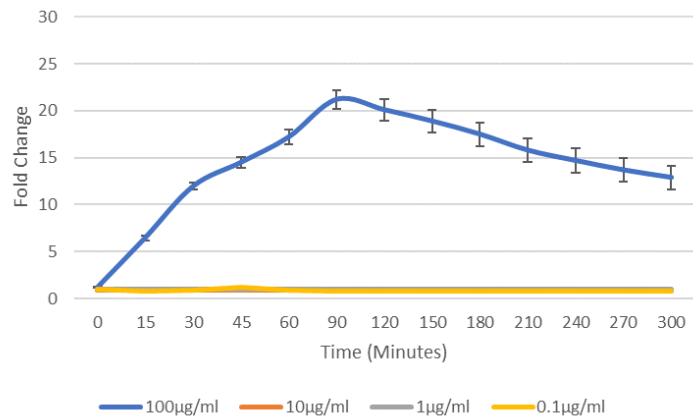
Values stated on the plate layout refer to µg/ml

APPENDIX IV: CHAPTER 3: Dose Response of venom for *Naja* genus for CMT28, CMM26 and MDCK

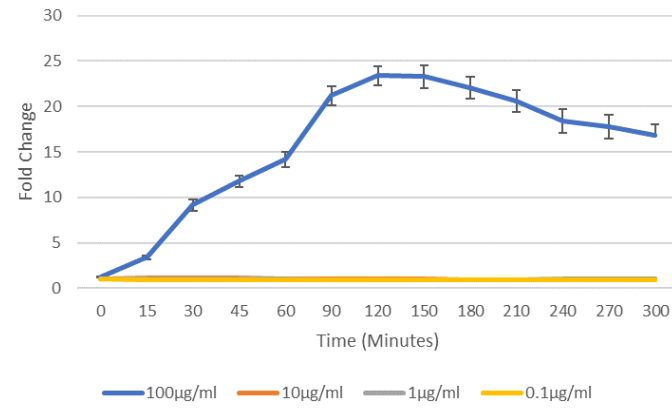


APPENDIX V: CHAPTER 3: Selection of Optimal Cell Number for an Effective Plate-Based Resazurin Assay at Different Concentrations

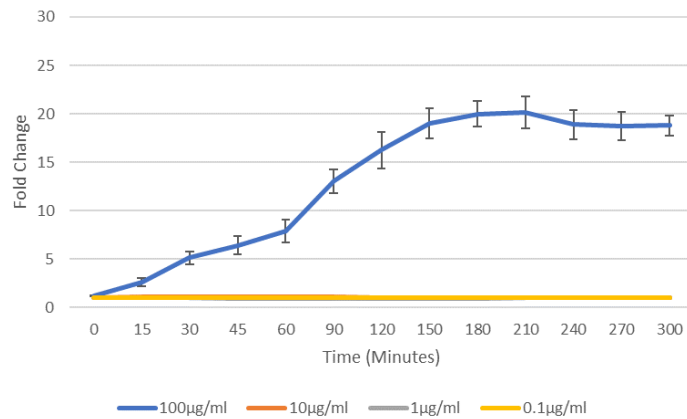
CMT28



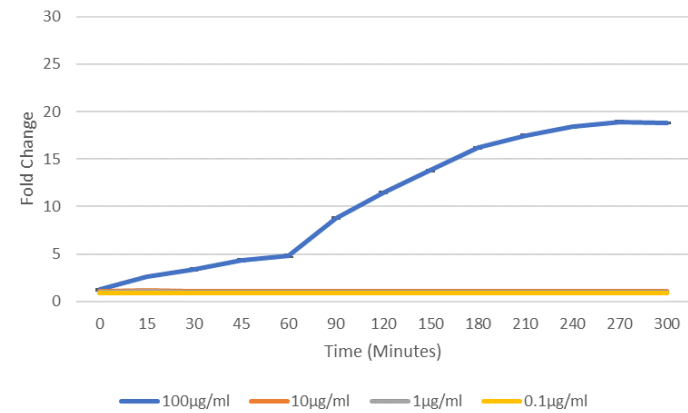
Appendix V: CMT28 cells at a Cell Number of 2×10^5



Appendix V: CMT28 Cells at a Cell Number of 2×10^5

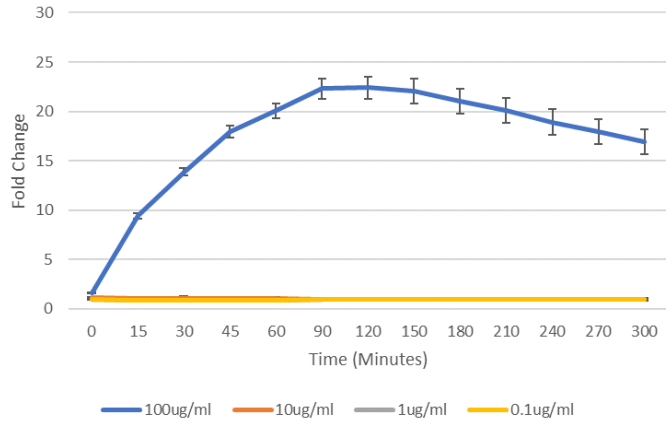


Appendix V: CMT28 cells at a Cell Number of 5×10^5

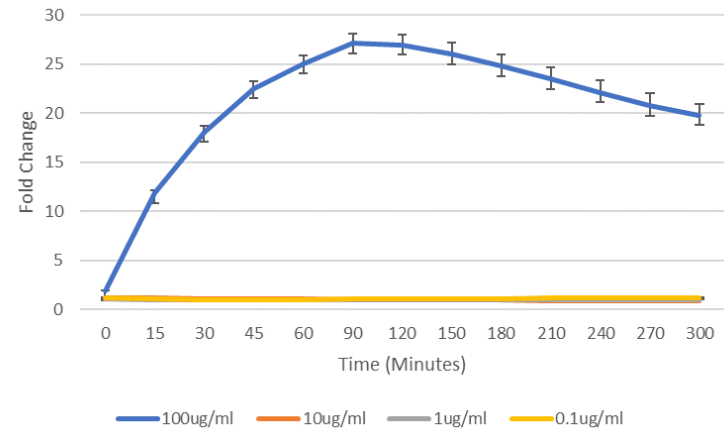


Appendix V: CMT28 cells at a Cell Number of 2.5×10^5

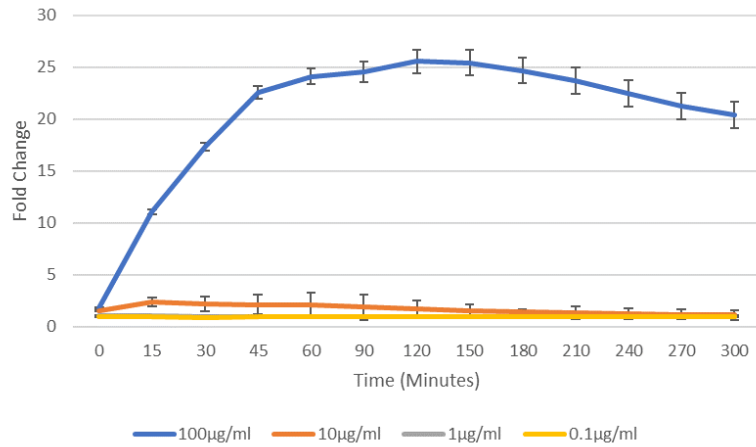
CMM26



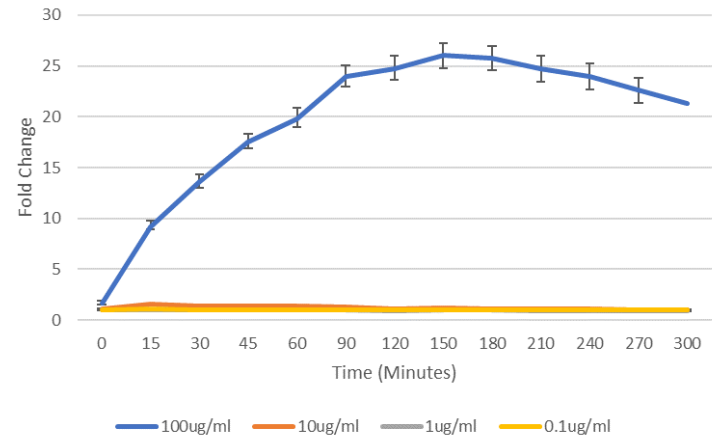
Appendix V: CMM26 cells at a Cell Number of 2×10^5



Appendix V: CMM26 cells at a Cell Number of 1×10^5

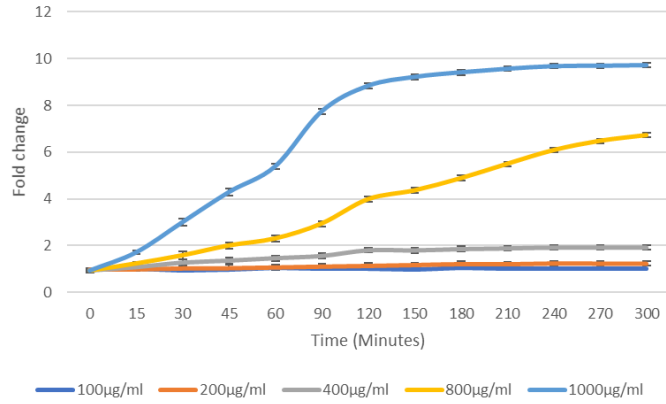


Appendix V: CMM26 cells at a Cell Number of 5×10^5

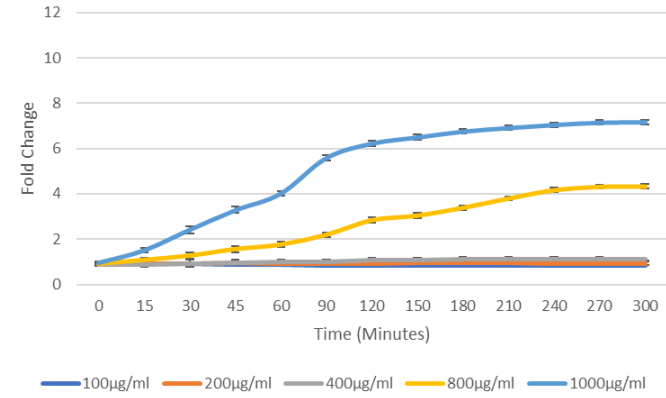


Appendix V: CMM26 cells at a Cell Number of 2.5×10^5

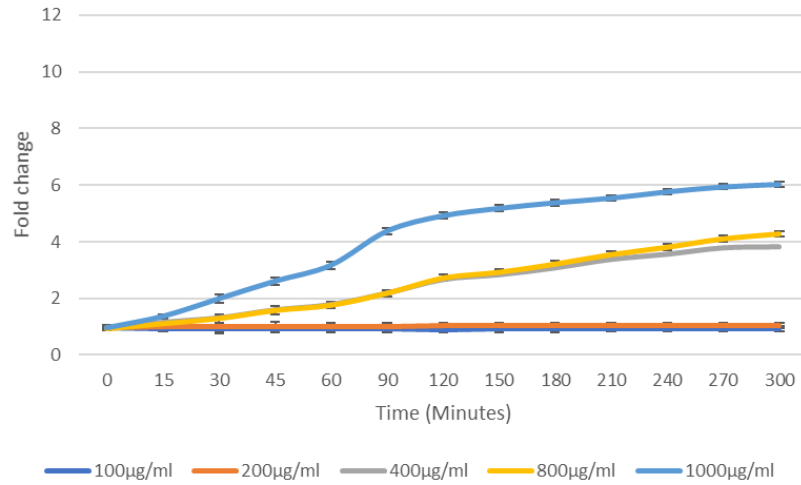
MDCK



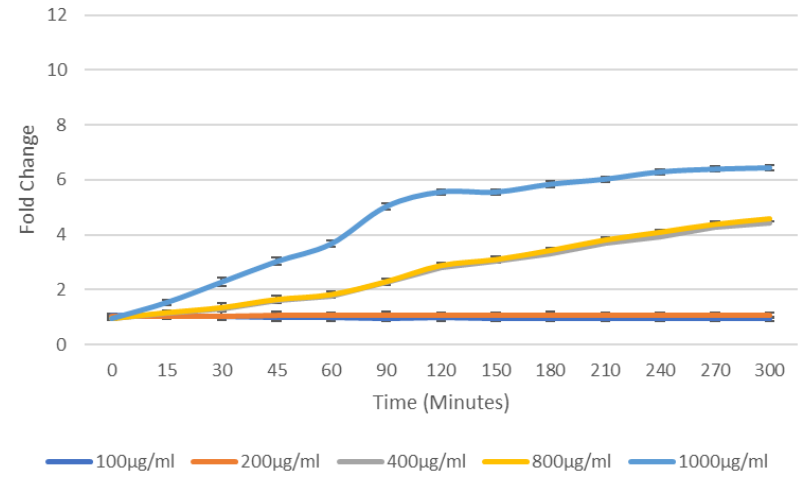
Appendix IV: MDCK cells at a Cell Number of 2x10⁵



Appendix IV: MDCK cells at a Cell Number of 1x10⁵



Appendix IV: MDCK cells at a Cell Number of 5x10⁵



Appendix IV: MDCK cells at a Cell Number of 2.5x10⁵

APPENDIX VI: CHAPTER 3: Statistical Analysis of Initial Screen of
N.nigricollis Venom on CMT28, CMM26 and MDCK

CMT28

CMT28 – Normality Test (Anderson-Darling) P-values

Naja nigricollis

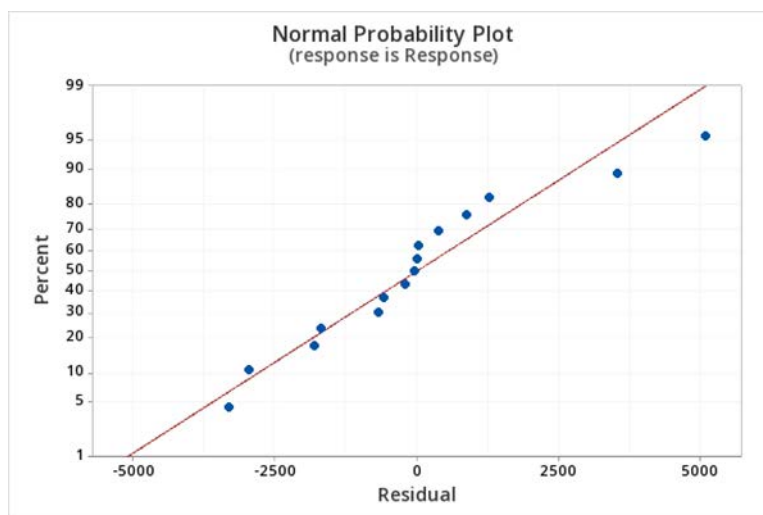
100	0.625
10	0.420
1	0.419
0.1	0.216
Negative	0.525

CMT28 – Test of Equal Variance (Levene’s Test) P-value

0.423

CMT28- One-way ANOVA

0.000



CMT28- Post-hoc Tukey test

Naja nigricollis

Dose	A
1	A
10	A
0.1	A
Neg	A
100	B

CMM26

CMM26 – Normality Test (Anderson-Darling) P-values

Naja nigricollis

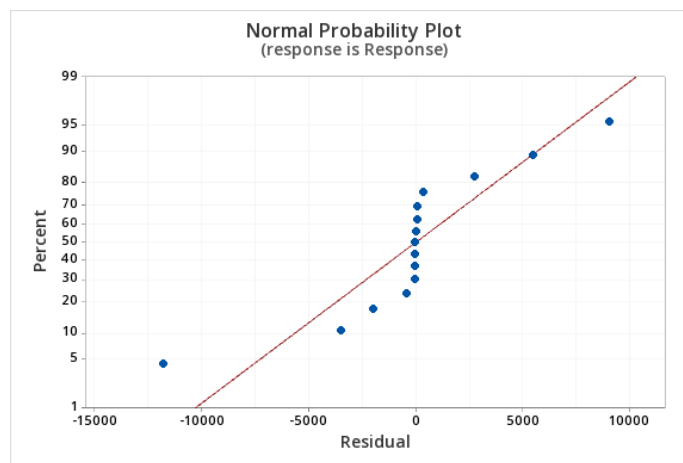
100	0.169
10	0.198
1	0.531
0.1	0.431
Negative	0.318

CMM26 – Test of Equal Variance (Levene's Test) P-value

0.175

CMM26- One-way ANOVA

0.000



CMM26- Post-hoc Tukey test

Naja nigricollis

Dose	A
1	A
10	A
0.1	A
Neg	A
100	B

MDCK

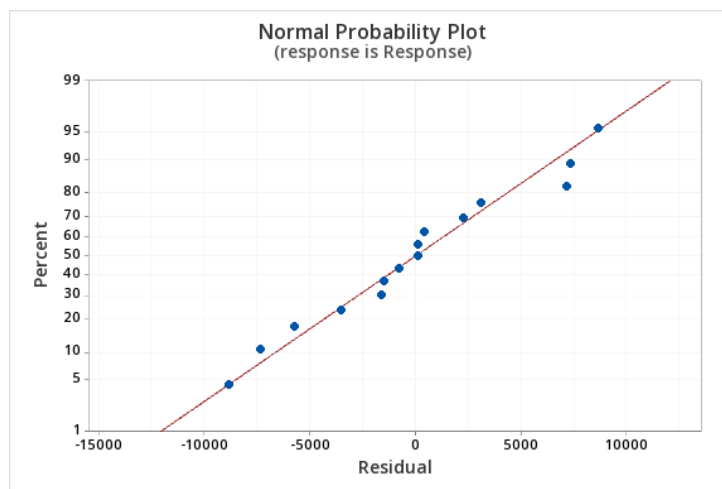
MDCK – Normality Test (Anderson-Darling) P-values

Naja nigricollis

100	0.629
10	0.630
1	0.229
0.1	0.573
Negative	0.458

MDCK – Test of Equal Variance (Levene's Test) P-value
0.565

MDCK- One-way ANOVA
0.002



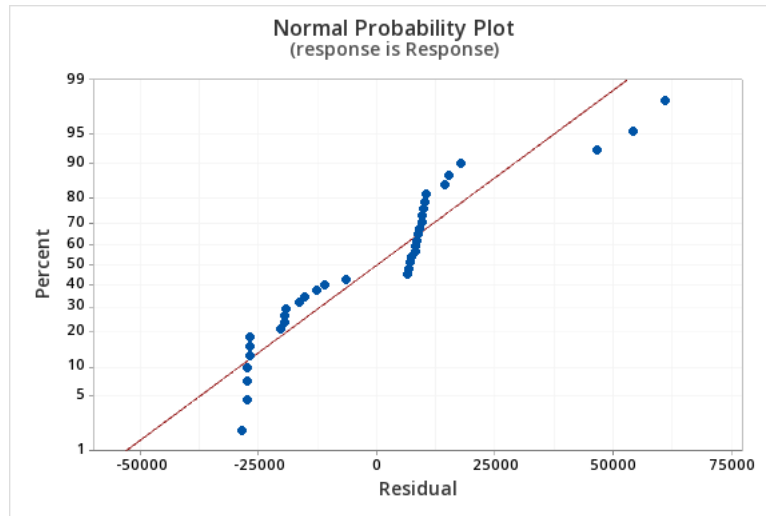
MDCK- Post-hoc Tukey test

Naja nigricollis

Dose	A
1	A
10	A
0.1	A
Neg	A
100	B

Comparative Analysis of the three cell line – CMT28, CMM26 and MDCK

Multi-factor ANOVA with Tukey test: Comparison of Cell line vs Dose vs Response
0.251



Post-hoc Tukey test – Cell Line Comparison

CMT28	B
CMM26	B
MDCK	A

Post-hoc Tukey test – Dose Comparison

10	A
1	A
0.1	A
0.01	B

MDCK Further investigation of the effects of N.nigricollis venom on MDCK cells at higher concentrations

Normality Test (Anderson-Darling) P-values

Naja nigricollis

100	0.639
200	0.607
400	0.059
800	0.070
1000	0.624
Negative	0.458

Test of Equal Variance (Levene's Test) P-value

Naja nigricollis

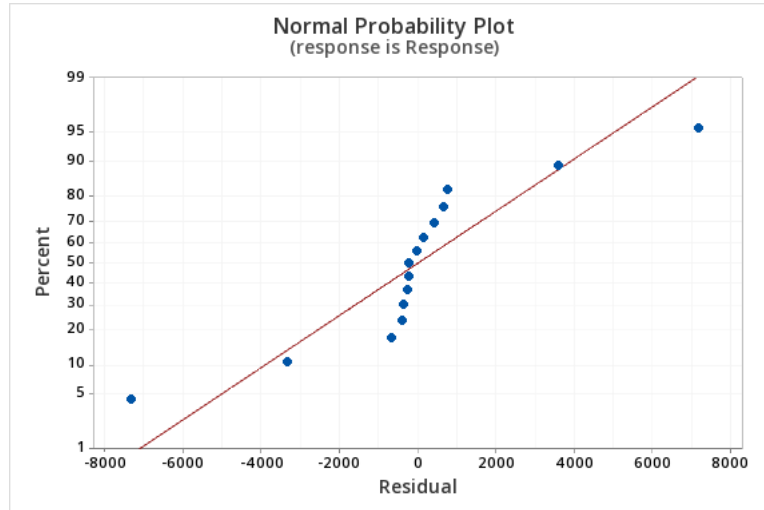
100	0.639
200	0.607
400	0.059
800	0.070
1000	0.624
Negative	0.458

Test of Equal Variance (Levene's Test) P-value

0.117

One-way ANOVA

0.000



CMT28- Post-hoc Tukey test

Naja nigricollis

Dose	
100	A
200	B
10000	B
800	B
400	B

APPENDIX VII: CHAPTER 3: Statistical Analysis of Screening Venom from the *Naja* genus on CMT28, CMM26 and MDCK

Normality Tests and Test of Equal Variance – CMT28, CMM26 and MDCK

CMT28 – Normality Test (Anderson-Darling) P-values

	100	10	1	0.1
<i>Naja nivea</i>	0.538	0.197	0.542	0.236
<i>Naja nubiae</i>	0.134	0.063	0.630	0.390
<i>Naja melanoleuca</i>	0.083	0.204	0.544	0.200
<i>Naja pallida</i>	0.555	0.362	0.082	0.273
<i>Naja naja</i>	0.403	0.198	0.631	0.374
<i>Naja Kaouthia</i>	0.574	0.272	0.180	0.325
<i>Naja atra</i>	0.460	0.089	0.472	0.061
<i>Naja siamensis</i>	0.242	0.627	0.078	0.079
<i>Naja nigricincta</i>	0.427	0.059	0.504	0.213
<i>Negative</i>		0.127		

CMT28 – Test of Equal Variance (Levene’s Test) P-value

0.338

CMM26– Normality Test (Anderson-Darling) P-values

	100	10	1	0.1
<i>Naja nivea</i>	0.344	0.598	0.544	0.551
<i>Naja nubiae</i>	0.628	0.057	0.524	0.140
<i>Naja melanoleuca</i>	0.399	0.242	0.325	0.494
<i>Naja pallida</i>	0.126	0.431	0.112	0.216
<i>Naja naja</i>	0.146	0.505	0.382	0.210
<i>Naja Kaouthia</i>	0.238	0.509	0.205	0.207
<i>Naja atra</i>	0.586	0.317	0.609	0.518
<i>Naja siamensis</i>	0.328	0.606	0.103	0.245
<i>Naja nigricincta</i>	0.610	0.514	0.135	0.627
<i>Negative</i>		0.151		

CMM26 – Test of Equal Variance (Levene’s Test) P-value

1.000

MDCK – Normality Test (Anderson-Darling) P-values

	100	10	1	0.1
<i>Naja nivea</i>	0.078	0.090	0.625	0.238
<i>Naja nubiae</i>	0.365	0.516	0.467	0.599
<i>Naja melanoleuca</i>	0.628	0.163	0.080	0.213
<i>Naja pallida</i>	0.134	0.211	0.087	0.063
<i>Naja naja</i>	0.091	0.556	0.602	0.311
<i>Naja Kaouthia</i>	0.194	0.232	0.268	0.402
<i>Naja atra</i>	0.156	0.163	0.260	0.628
<i>Naja siamensis</i>	0.546	0.521	0.511	0.534
<i>Naja nigricincta</i>	0.079	0.628	0.413	0.69
<i>Negative</i>		0.138		

MDCK– Test of Equal Variance (Levene’s Test) P-value

0.421

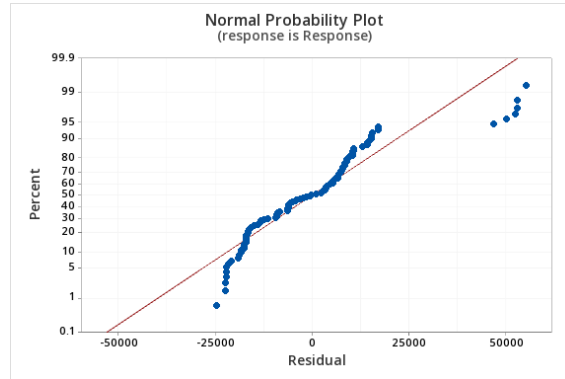
ANOVA Analysis – CMT28

CMT28- Multi-factor ANOVA: Dose vs Response

0.000

CMT28- Multi-factor ANOVA: Dose vs Response

0.000



CMT28 - Post-hoc Tukey Test: Species

<i>Naja nivea</i>	A	
<i>Naja nubiae</i>		B
<i>Naja melanoleuca</i>	A	
<i>Naja pallida</i>		B
<i>Naja naja</i>		B
<i>Naja Kaouthia</i>	A	B
<i>Naja atra</i>		B
<i>Naja siamensis</i>		B
<i>Naja nigricincta</i>		B

CMT28 - Post-hoc Tukey test: Dose

0.1	A	
1	A	
10	A	
100		B

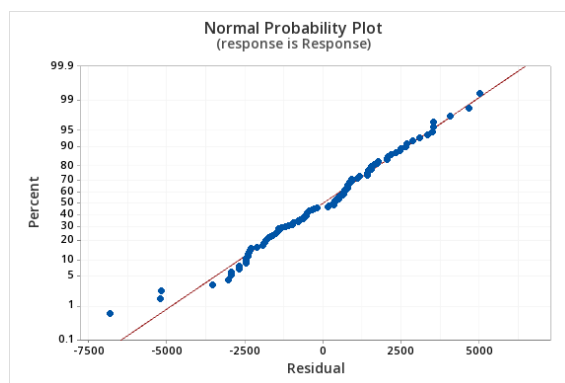
ANOVA Analysis – CMM26

CMM26- Multi-factor ANOVA: Dose vs Response

0.000

CMM26- Multi-factor ANOVA: Dose vs Response

0.000



CMM26 - Post-hoc Tukey Test: Species

<i>Naja nivea</i>	A		
<i>Naja nubiae</i>	A	B	
<i>Naja melanoleuca</i>	A	B	C
<i>Naja pallida</i>	A	B	C
<i>Naja naja</i>	A	B	C
<i>Naja Kaouthia</i>	A	B	C
<i>Naja atra</i>		B	C
<i>Naja siamensis</i>			C
<i>Naja nigricincta</i>			C

CMM26 - Post-hoc Tukey test: Dose

0.1	A		
1		C	
10			B
100			D

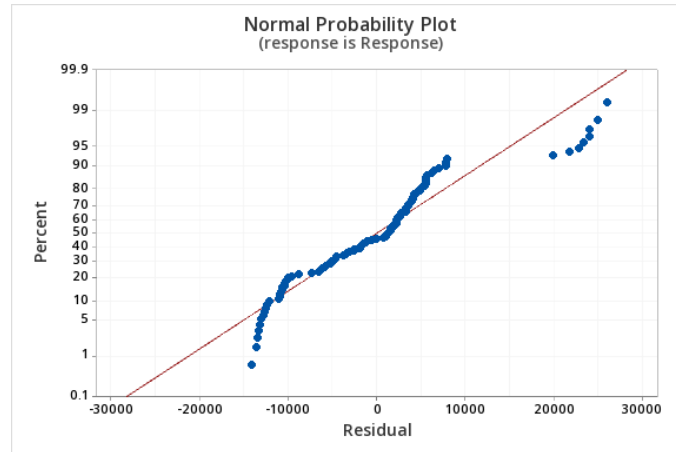
ANOVA Analysis – MDCK

MDCK- Multi-factor ANOVA: Dose vs Response

0.000

MDCK- Multi-factor ANOVA: Snake species vs Response

0.009



MDCK - Post-hoc Tukey Test: Species

<i>Naja nivea</i>	A	B
<i>Naja nubiae</i>		B
<i>Naja melanoleuca</i>	A	
<i>Naja pallida</i>	A	B
<i>Naja naja</i>	A	B
<i>Naja Kaouthia</i>	A	B
<i>Naja atra</i>	A	B
<i>Naja siamensis</i>	A	B
<i>Naja nigricincta</i>	A	B

MDCK - Post-hoc Tukey test: Dose

0.1	A	
1	A	
10	A	
100		B

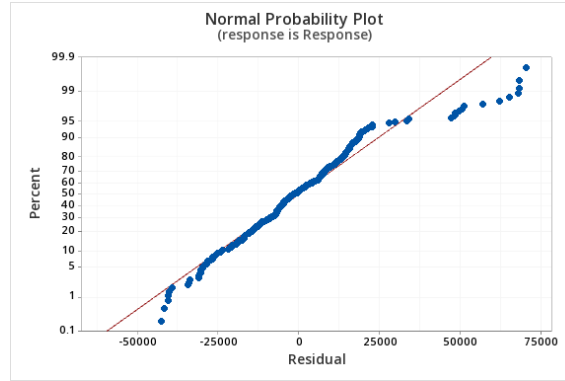
Comparative Analysis of the three cell line – CMT28, CMM26 and MDCK

Multi-factor ANOVA: Dose vs Response

0.000

Multi-factor ANOVA: Dose vs Response

0.000



Post-hoc Tukey Test: Species

- Naja nivea*
- Naja nubiae*
- Naja melanoleuca*
- Naja pallida*
- Naja naja*
- Naja Kaouthia*
- Naja atra*
- Naja siamensis*
- Naja nigricincta*

Post-hoc Tukey test: Dose

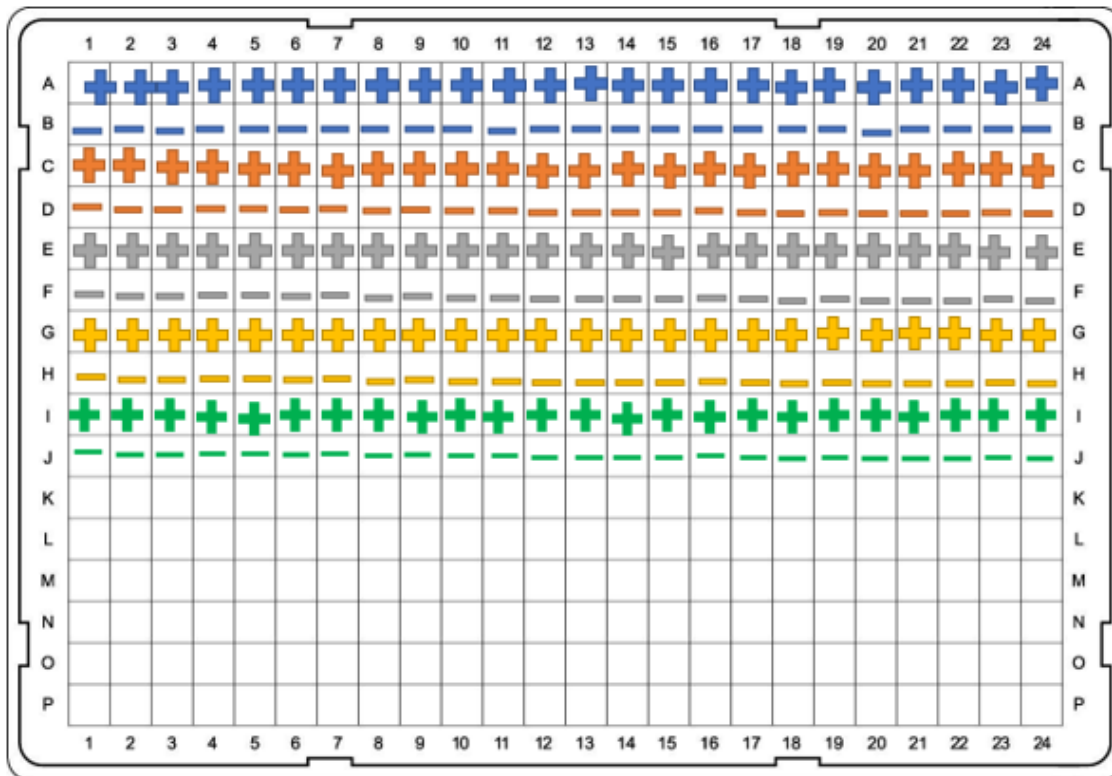
0.1	A	
1	A	
10	A	
100		B

Post-hoc Tukey test: Cell Line






CMT28	A	
CMM26		B
MDCK		C

APPENDIX VIII: CHAPTER 4: Plate Layout for determining the Optimal Cell Number for CMT28, CMM26 and MDCK in 384 well plates






CMT28 and CMM28 Plate Layout



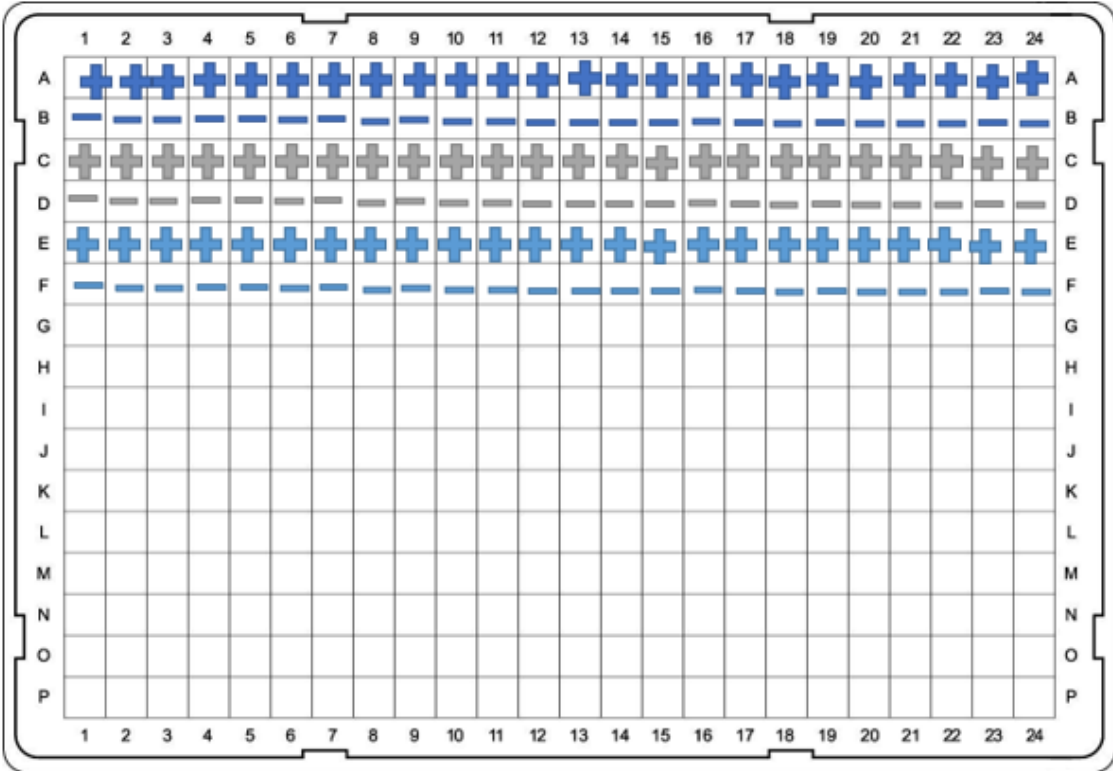
Positive controls for each Cell Number
(100µg/ml *N.nigricollis* Venom)

-  2.5×10^4
-  2×10^4
-  1.5×10^4
-  1×10^4
-  0.5×10^4

Negative controls for each Cell Number
(DMEM/RPMI media)

-  2.5×10^4
-  2×10^4
-  1.5×10^4
-  1×10^4
-  0.5×10^4

MDCK Plate Layout



Positive controls for each Cell Number
(1mg/ml *N.nigricollis* Venom)

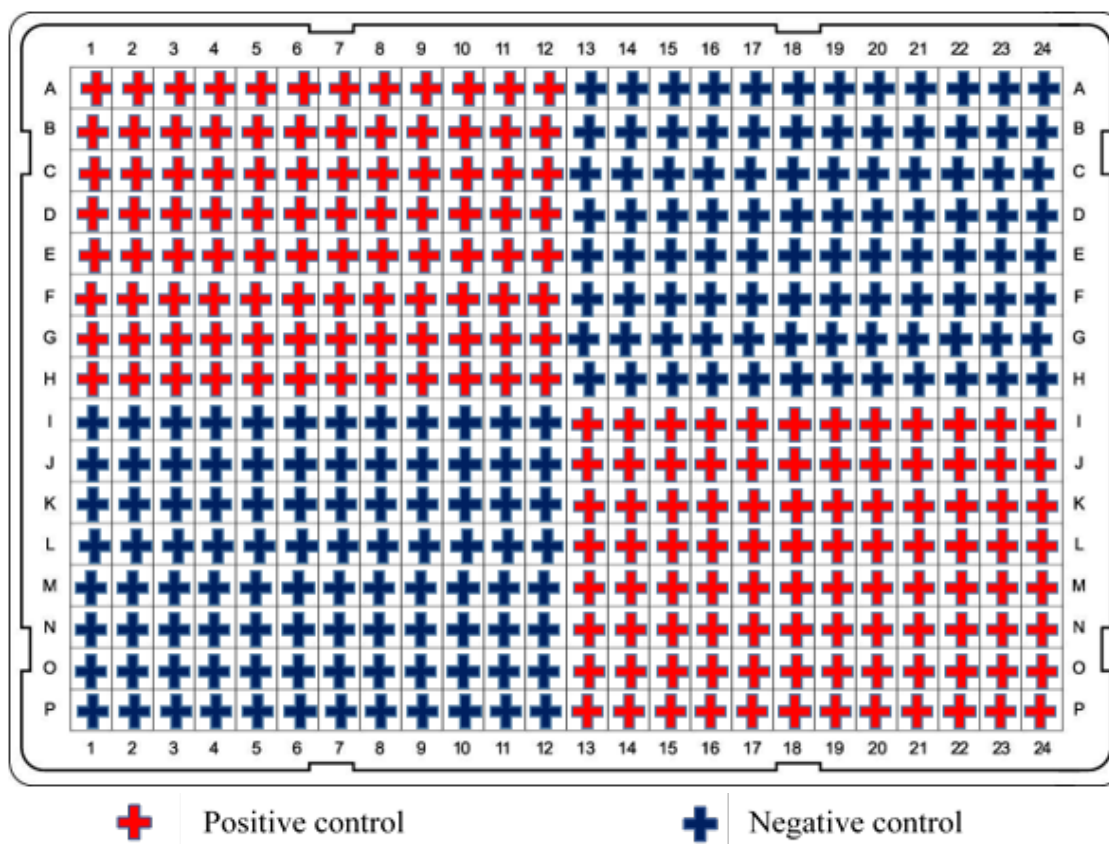
- 7.5x10⁴
- 5x10⁴
- 2.5x10⁴

Negative controls for each Cell Number
(DMEM media)

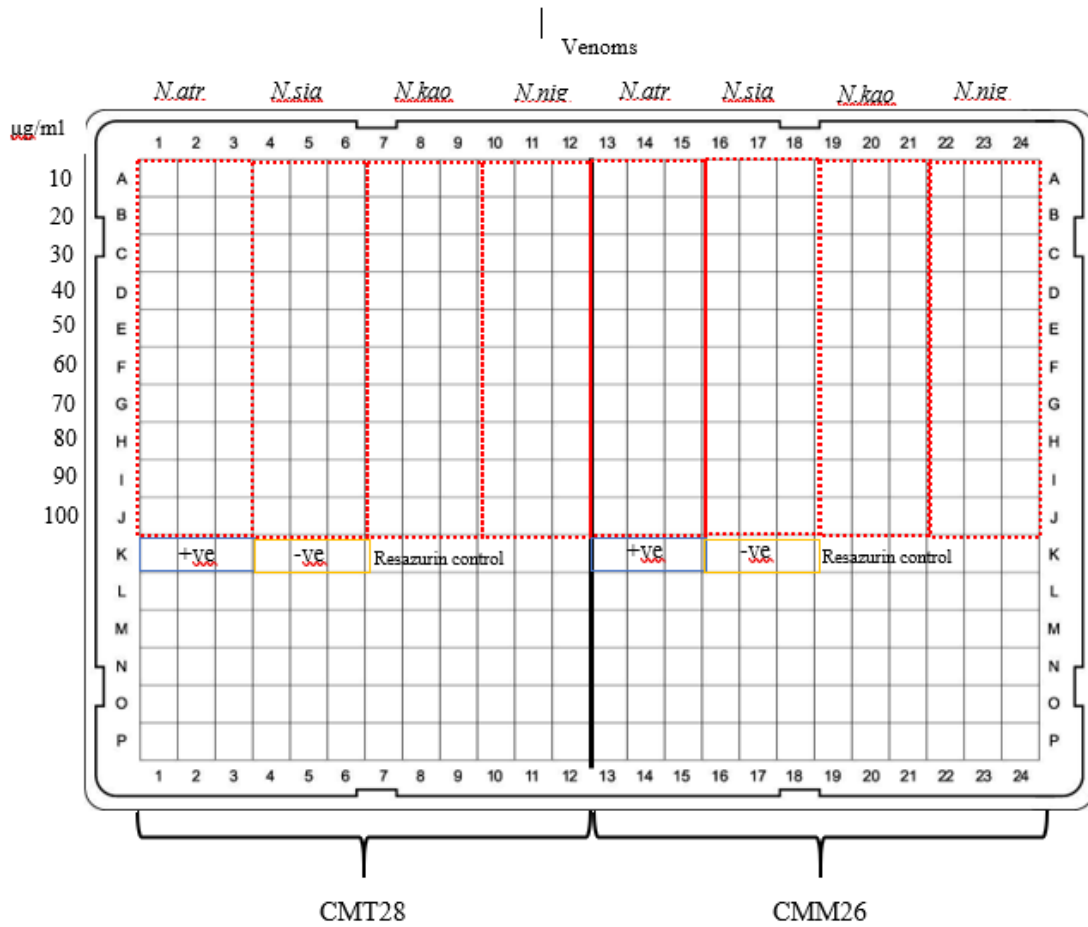
- 7.5x10⁴
- 5x10⁴
- 2.5x10⁴

APPENDIX VIII: CHAPTER 4: Plate Layout for Z' Analysis of CMT28, CMM26, MDCK in 384 well plates

CMT28, CMM28, MDCK Plate Layout



APPENDIX IX: CHAPTER 4: Plate Layout for CMT28 and CMM26 Whole venom screen for determining appropriate Cell line and Concentration to T-VDA^{cyx}



APPENDIX X: CHAPTER 4: Plate Layout for T-VDA^{cyx} Assay

Plate 1

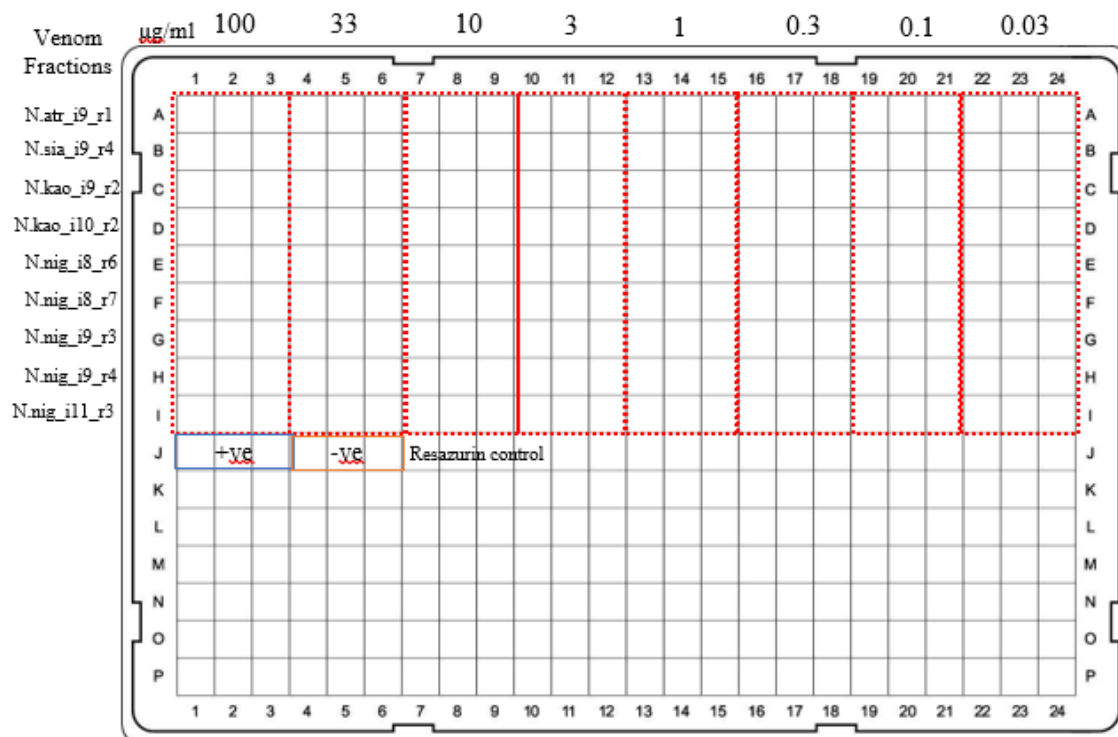
	1	2	3	4	5	6	7	8	9	10	11	12	13	14	15	16	17	18	19	20	21	22	23	24	
A			A.cco_i1r1	A.cco_i1r2	A.cco_i1r3	A.cco_i1r4	A.cco_i1r5	A.cco_i1r6	A.cco_i1r7	A.cco_i1r8	A.cco_i1r9	A.cco_i1r10	A.cco_i1r11	A.cco_i1r12	A.cco_i1r13	A.cco_i1r14	A.cco_i1r15	A.cco_i1r16	A.cco_i1r17	A.cco_i1r18	A.cco_i1r19	A.cco_i1r20			
B			A.cco_i1r21	A.cco_i1r22	A.cco_i2r1	A.cco_i2r2	A.cco_i2r3	A.cco_i2r4	A.cco_i2r5	A.cco_i2r6	A.cco_i2r7	A.cco_i2r8	A.cco_i2r9	A.cco_i2r10	A.cco_i2r11	A.cco_i2r12	A.cco_i2r13	A.cco_i1r12	A.cco_i3r1	A.cco_i3r2	A.cco_i3r3	A.cco_i3r4			
C			A.cco_i3r5	A.cco_i3r6	A.cco_i3r7	A.cco_i3r8	A.cco_i3r9	A.cco_i3r10	A.cco_i3r11	A.cco_i4r1	A.cco_i4r2	A.cco_i4r3	A.cco_i5r1	A.cco_i5r2	A.cco_i5r3	A.cco_i5r4	A.cco_i5r5	A.cco_i5r6	A.cco_i6r1	A.cco_i6r2	A.cco_i6r3	A.cco_i6r4			
D			A.cco_i6r5	A.cco_i6r6	A.cco_i6r7	A.cco_i7r1	A.cco_i7r2	A.cco_i7r3	A.cco_i7r4	A.cco_i7r5	A.cco_i7r6	A.cco_i8r1	A.cco_i8r2	A.cco_i8r3	A.cco_i8r4	A.cco_i8r5	A.cco_i8r6	A.cco_i8r7	A.cco_i9r1	A.cco_i9r2	A.cco_i9r3	A.cco_i10r1			
E			A.cco_i10r2	A.cco_i11r1	A.cco_i11r2	A.cco_i11r3	A.cco_i12r1	B.ari_i1r1	B.ari_i1r2	B.ari_i1r3	B.ari_i1r4	B.ari_i1r5	B.ari_i1r6	B.ari_i1r7	B.ari_i1r8	B.ari_i1r9	B.ari_i2r1	B.ari_i2r2	B.ari_i2r3	B.ari_i2r4	B.ari_i2r5	B.ari_i2r6			
F			B.ari_i2r7	B.ari_i2r8	B.ari_i2r9	B.ari_i3r1	B.ari_i4r1	B.ari_i4r2	B.ari_i4r3	B.ari_i4r4	B.ari_i4r5	B.ari_i5r1	B.ari_i5r2	B.ari_i5r3	B.ari_i5r4	B.ari_i5r5	B.ari_i5r6	B.ari_i6r1	B.ari_i6r2	B.ari_i6r3	B.ari_i6r4	B.ari_i6r5			
G			B.ari_i6r6	B.ari_i7r1	B.ari_i7r2	B.ari_i7r3	B.ari_i7r4	B.ari_i7r5	B.ari_i7r6	B.ari_i7r7	B.ari_i7r8	B.ari_i7r9	B.ari_i7r10	B.ari_i7r11	B.ari_i8r1	B.ari_i8r2	B.ari_i8r3	B.ari_i8r4	B.ari_i8r5	B.ari_i8r6	B.ari_i8r7	B.ari_i8r8			
H			B.ari_i8r9	B.ari_i8r10	B.ari_i8r11	B.ari_i9r1	B.ari_i10r1	B.ari_i10r2	B.ari_i10r3	B.ari_i11r1	C.rru_i1r1	C.rru_i1r1	C.rru_i1r2	C.rru_i1r3	C.rru_i1r4	C.rru_i1r5	C.rru_i1r6	C.rru_i1r7	C.rru_i1r8	C.rru_i1r9	C.rru_i1r10	C.rru_i2r1			
I			C.rru_i2r2	C.rru_i2r3	C.rru_i2r4	C.rru_i2r5	C.rru_i2r6	C.rru_i2r7	C.rru_i2r8	C.rru_i2r9	C.rru_i2r10	C.rru_i2r11	C.rru_i3r1	C.rru_i3r2	C.rru_i3r3	C.rru_i3r4	C.rru_i3r5	C.rru_i4r1	C.rru_i4r2	C.rru_i4r3	C.rru_i5r1	C.rru_i6r1			
J			C.rru_i7r1	C.rru_i7r2	C.rru_i7r3	C.rru_i7r4	C.rru_i8r1	C.rru_i9r1	C.rru_i9r2	C.rru_i10r1	C.vir_i1r1	C.vir_i1r2	C.vir_i1r3	C.vir_i1r4	C.vir_i1r5	C.vir_i1r6	C.vir_i1r7	C.vir_i1r8	C.vir_i1r9	C.vir_i1r10	C.vir_i1r11	C.vir_i1r12			
K			C.vir_i1r13	C.vir_i1r14	C.vir_i1r15	C.vir_i1r16	C.vir_i1r17	C.vir_i2r1	C.vir_i2r2	C.vir_i2r3	C.vir_i2r4	C.vir_i2r5	C.vir_i2r6	C.vir_i2r7	C.vir_i2r8	C.vir_i3r1	C.vir_i3r2	C.vir_i3r3	C.vir_i3r4	C.vir_i4r1	C.vir_i4r2	C.vir_i4r3			
L			C.vir_i4r4	C.vir_i5r1	C.vir_i6r1	C.vir_i7r1	C.vir_i7r2	C.vir_i8r1	C.vir_i8r2	C.vir_i8r3	N.atr_i1r1	N.atr_i1r2	N.atr_i1r3	N.atr_i1r4	N.atr_i2r1	N.atr_i2r2	N.atr_i2r3	N.atr_i2r4	N.atr_i3r1	N.atr_i3r2	N.atr_i3r3	N.atr_i3r4			
M			N.atr_i3r5	N.atr_i3r6	N.atr_i4r1	N.atr_i4r2	N.atr_i4r3	N.atr_i5r1	N.atr_i6r1	N.atr_i6r2	N.atr_i7r1	N.atr_i7r2	N.atr_i7r3	N.atr_i7r4	N.atr_i7r5	N.atr_i7r6	N.atr_i8r1	N.atr_i8r2	N.atr_i8r3	N.atr_i9r1	N.atr_i9r2	N.atr_i10r1			
N			N.atr_i10r2	N.atr_i10r3	N.atr_i10r4	N.sia_i1r1	N.sia_i1r2	N.sia_i1r3	N.sia_i1r4	N.sia_i2r1	N.sia_i2r2	N.sia_i2r3	N.sia_i2r4	N.sia_i2r5	N.sia_i2r6	N.sia_i2r7	N.sia_i2r8	N.sia_i2r9	N.sia_i2r10	N.sia_i3r1	N.sia_i3r2	N.sia_i3r3			
O			N.sia_i3r4	N.sia_i3r5	N.sia_i3r6	N.sia_i4r1	N.sia_i4r2	N.sia_i4r3	N.sia_i5r1	N.sia_i5r2	N.sia_i5r3	N.sia_i5r4	N.sia_i5r5	N.sia_i5r6	N.sia_i5r7	N.sia_i5r8	N.sia_i5r9	N.sia_i6r1	N.sia_i6r2	N.sia_i6r3	N.sia_i7r1	N.sia_i7r2	N.sia_i7r3		
P			N.sia_i7r4	N.sia_i7r5	N.sia_i7r6	N.sia_i7r7	N.sia_i8r1	N.sia_i8r2	N.sia_i8r3	N.sia_i8r4	N.sia_i9r1	N.sia_i9r2	N.sia_i9r3	N.sia_i9r4	N.sia_i10r1	N.sia_i10r2	N.sia_i10r3	suc ctrl	suc ctrl	suc ctrl	suc ctrl	suc ctrl			

Plate 2

	1	2	3	4	5	6	7	8	9	10	11	12	13	14	15	16	17	18	19	20	21	22	23	24
A			N.kao_i1r1	N.kao_i1r2	N.kao_i1r3	N.kao_i1r4	N.kao_i1r5	N.kao_i1r6	N.kao_i1r7	N.kao_i1r8	N.kao_i2r1	N.kao_i2r2	N.kao_i3r1	N.kao_i3r2	N.kao_i4r1	N.kao_i4r2	N.kao_i4r3	N.kao_i4r4	N.kao_i4r5	N.kao_i4r6	N.kao_i5r1	N.kao_i5r2		
B			N.kao_i6r1	N.kao_i6r2	N.kao_i6r3	N.kao_i6r4	N.kao_i6r5	N.kao_i6r6	N.kao_i6r7	N.kao_i6r8	N.kao_i7r1	N.kao_i7r2	N.kao_i7r3	N.kao_i7r4	N.kao_i8r1	N.kao_i8r2	N.kao_i8r3	N.kao_i8r4	N.kao_i8r5	N.kao_i8r6	N.kao_i9r1	N.kao_i9r2		
C			N.kao_i9r3	N.kao_i9r4	N.kao_i9r5	N.kao_i10r1	N.kao_i10r2	N.kao_i10r3	N.kao_i10r4	N.kao_i11r1	N.kao_i11r2	N.kao_i11r3	N.kao_i11r4	N.kao_i11r5	N.kao_i11r6	N.nig_i1r1	N.nig_i1r2	N.nig_i1r3	N.nig_i1r4	N.nig_i1r5	N.nig_i1r6	N.nig_i2r1		
D			N.nig_i2r2	N.nig_i3r1	N.nig_i3r2	N.nig_i3r3	N.nig_i3r4	N.nig_i3r5	N.nig_i4r1	N.nig_i4r2	N.nig_i4r3	N.nig_i4r4	N.nig_i4r5	N.nig_i4r6	N.nig_i4r7	N.nig_i4r8	N.nig_i4r9	N.nig_i5r1	N.nig_i5r2	N.nig_i5r3	N.nig_i5r4	N.nig_i5r5		
E			N.nig_i5r6	N.nig_i5r7	N.nig_i6r1	N.nig_i6r2	N.nig_i6r3	N.nig_i6r4	N.nig_i6r5	N.nig_i7r1	N.nig_i7r2	N.nig_i7r3	N.nig_i7r4	N.nig_i7r5	N.nig_i7r6	N.nig_i8r1	N.nig_i8r2	N.nig_i8r3	N.nig_i8r4	N.nig_i8r5	N.nig_i8r6	N.nig_i8r7		
F			N.nig_i8r8	N.nig_i8r9	N.nig_i9r1	N.nig_i9r2	N.nig_i9r3	N.nig_i9r4	N.nig_i9r5	N.nig_i9r6	N.nig_i9r7	N.nig_i10r1	N.nig_i10r2	N.nig_i10r3	N.nig_i10r4	N.nig_i10r5	N.nig_i10r6	N.nig_i10r7	N.nig_i11r1	N.nig_i11r2	N.nig_i11r3	N.nig_i11r4		
G			N.nig_i11r5	N.nig_i11r6	H.swa_i1r1	H.swa_i1r2	H.swa_i1r3	H.swa_i2r1	H.swa_i2r2	H.swa_i2r3	H.swa_i3r1	H.swa_i4r1	H.swa_i4r2	H.swa_i4r3	H.swa_i4r4	H.swa_i5r1	H.swa_i5r2	H.swa_i5r3	H.swa_i5r4	H.swa_i5r5	H.swa_i6r1	H.swa_i6r2		
H			H.swa_i6r3	H.swa_i6r4	H.swa_i7r1	H.swa_i7r2	A.aus_i1r1	A.aus_i2r1	A.aus_i2r2	A.aus_i3r1	A.aus_i4r1	A.aus_i4r2	A.aus_i4r3	A.aus_i5r1	A.aus_i6r1	A.aus_i7r1	A.aus_i8r1	H.ven_i1r1	H.ven_i1r2	H.ven_i1r3	H.ven_i1r4	H.ven_i1r5		
I			H.ven_i1r6	H.ven_i1r7	H.ven_i1r8	H.ven_i1r9	H.ven_i1r10	H.ven_i2r1	H.ven_i3r1	H.ven_i4r1	H.ven_i5r1	H.ven_i5r2	H.ven_i6r1	H.ven_i7r1	H.ven_i7r2	H.ven_i8r1	H.ven_i8r2	H.ven_i9	H.ven_i10	P.lio_i1r1	P.lio_i1r2	P.lio_i1r3		
J			P.lio_i1r4	P.lio_i1r5	P.lio_i1r6	P.lio_i1r7	P.lio_i1r8	P.lio_i1r9	P.lio_i1r10	P.lio_i1r11	P.lio_i1r12	P.lio_i1r13	P.lio_i1r14	P.lio_i2r1	P.lio_i2r2	P.lio_i3r1	P.lio_i3r2	P.lio_i3r3	P.lio_i4r1	P.lio_i4r2	P.lio_i5r1	P.lio_i5r2		
K			P.lio_i5r3	P.lio_i6	P.lio_i7r1	P.lio_i7r2	P.lio_i7r3	P.lio_i7r4	P.lio_i8r1	P.lio_i8r2	P.lio_i8r3	P.lio_i8r4	P.lio_i8r5	P.lio_i9r1	P.lio_i10r1	P.lio_i10r2	P.lio_i10r3	P.lio_i11r1	P.lio_i11r2	P.lio_i11r3	P.lio_i11r4	P.lio_i11r5		
L			Suc Ctrl	Suc Ctrl	Suc Ctrl													C.scu_i1r1	C.scu_i1r2	C.scu_i1r3	C.scu_i1r4	C.scu_i1r5		
M			C.scu_i1r6	C.scu_i1r7	C.scu_i1r8	C.scu_i1r9	C.scu_i1r10	C.scu_i1r11	C.scu_i1r12	C.scu_i1r13	C.scu_i2r1	C.scu_i2r2	C.scu_i2r3	C.scu_i2r4	C.scu_i2r5	C.scu_i2r6	C.scu_i2r7	C.scu_i2r8	C.scu_i2r9	C.scu_i3r1	C.scu_i3r2	C.scu_i3r3		
N			C.scu_i3r4	C.scu_i3r5	C.scu_i3r6	C.scu_i3r7	C.scu_i4r1	C.scu_i4r2	C.scu_i4r3	C.scu_i4r4	C.scu_i4r5	C.scu_i4r6	C.scu_i5r1	C.scu_i5r2	C.scu_i5r3	C.scu_i5r4	C.scu_i5r5	C.scu_i5r6	C.scu_i5r7	C.scu_i6r1	C.scu_i6r2	C.scu_i6r3		
O			C.scu_i7r1	C.scu_i7r2	C.scu_i7r3	C.scu_i7r4	C.scu_i7r5	C.scu_i7r6	C.scu_i8r1	C.scu_i8r2	C.scu_i8r3	C.scu_i8r4	C.scu_i8r5	C.scu_i8r6	C.scu_i9r1	C.scu_i9r2	C.scu_i9r3	C.scu_i9r4	C.scu_i9r5	C.scu_i9r6	C.scu_i9r7	C.scu_i9r8		
P			C.scu_i9r9	C.scu_i9r10	C.scu_i9r11	C.scu_i9r12	C.scu_i10r1	C.scu_i10r2	C.scu_i10r3	C.scu_i10r4	C.scu_i10r5	C.scu_i10r6	C.scu_i10r7	C.scu_i10r8	C.scu_i10r9	C.scu_i11r1	C.scu_i11r2	C.scu_i11r3	C.scu_i11r4	C.scu_i11r5	C.scu_i11r6	C.scu_i11r7		

APPENDIX XI: Plate Layout for Hit fractions screened CMM26, CMT28 and MDCK from T-VDA assay

CMT28, CMM28, MDCK Plate Layout



APPENDIX XII: CHAPTER 4: Statistical Analysis of CMT28 and CMM26
Whole venom screen for determining appropriate Cell line and Concentration to
T-VDA^{cyx} Assay

Normality Tests and Test of Equal Variance – CMT28 and CMM26

CMT28- Normality Test (Anderson Darling) P-values

	10	20	30	40	50	60	70	80	90	100
<i>Naja atra</i>	0.064	0.160	0.555	0.585	0.554	0.617	0.062	0.524	0.385	0.502
<i>Naja siamensis</i>	0.619	0.529	0.106	0.502	0.583	0.104	0.474	0.256	0.506	0.470
<i>Naja kaouthia</i>	0.554	0.089	0.581	0.342	0.091	0.320	0.603	0.612	0.631	0.172
<i>Naja nigricollis</i>	0.562	0.578	0.135	0.476	0.327	0.208	0.160	0.551	0.093	0.156

CMT28 – Test of equal Variance (Levene’s Test)

0.608

CMM26- Normality Test (Anderson Darling) P-values

	10	20	30	40	50	60	70	80	90	100
<i>Naja atra</i>	0.157	0.516	0.315	0.074	0.455	0.567	0.621	0.394	0.232	0.608
<i>Naja siamensis</i>	0.158	0.131	0.059	0.057	0.070	0.118	0.081	0.512	0.397	0.057
<i>Naja kaouthia</i>	0.337	0.211	0.538	0.601	0.621	0.226	0.066	0.608	0.1394	0.136
<i>Naja nigricollis</i>	0.225	0.101	0.158	0.505	0.507	0.389	0.206	0.072	0.334	0.249

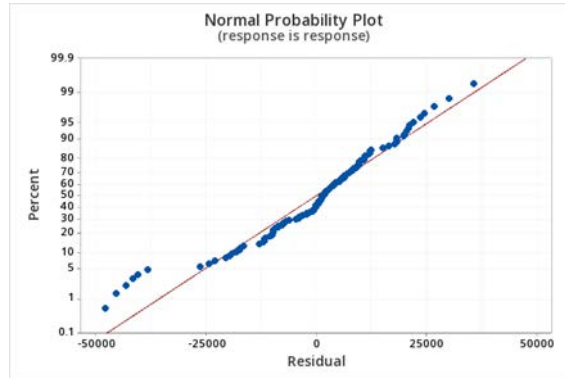
CMM26 – Test of equal Variance (Levene’s Test)

0.445

ANOVA Analysis – CMT28

CMT28 - Multi-factor ANOVA – Snake venom
0.000

CMT28 - Multi-factor ANOVA – Dose
0.000



Post-hoc Tukey Test - Venom

<i>Naja kaouthia</i>	A			
<i>Naja nigricollis</i>			B	
<i>Naja atra</i>	A		B	
<i>Naja simensis</i>				C

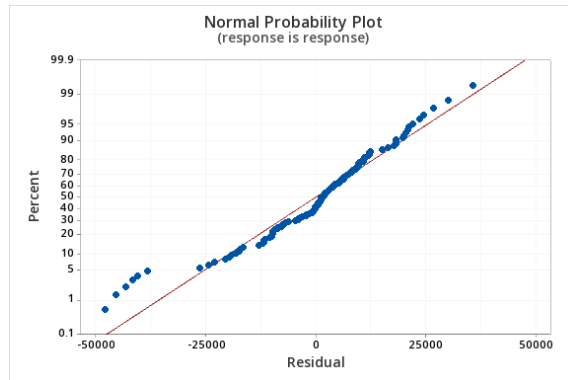
Post-hoc Tukey test - Dose

10	A					
20	A					
30	A	B				
40		B	C			
50			C	D		
60				D	E	
70					E	
80					E	
90					E	
100					E	

ANOVA Analysis – CMM26

CMM26 - Multi-factor ANOVA – Dose
0.000

CMM26 - Multi-factor ANOVA – Dose
0.000



Post-hoc Tukey Test - Venom

<i>Naja kaouthia</i>	A				
<i>Naja nigricollis</i>			B		
<i>Naja atra</i>	A		B		
<i>Naja simensis</i>					C

Post-hoc Tukey test - Dose

10	A					
20	A					
30	A	B				
40		B	C	D		
50			C	D	E	
60					E	
70					E	
80					E	
90					E	
100					E	

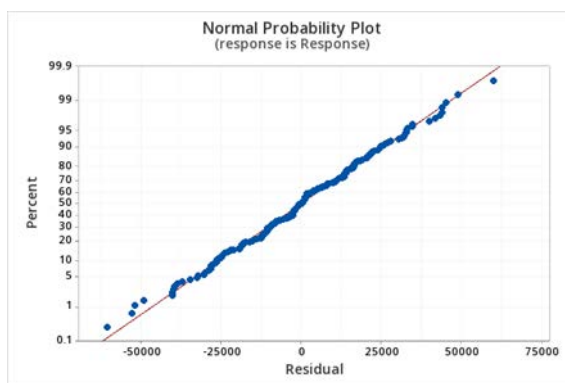
Comparative Analysis of CMT28 and CMM26

Multi-factor ANOVA – Dose

0.000

Multi-factor ANOVA – Dose

0.000



Post-hoc Tukey Test- Cell Line

CMT28	A
CMM26	A

Post-hoc Tukey Test - Venom

<i>Naja kaouthia</i>	A	
<i>Naja nigricollis</i>	A	
<i>Naja atra</i>		B
<i>Naja simensis</i>		B

Post-hoc Tuket test - Dose

30	A		
20	A		
10	A		
40	A		
50	A	B	
60	A	B	
70			C
90			C
80			C
100			C

APPENDIX XIII: CHAPTER 4: Statistical Analysis of Hit Fractions Screened
on CMM26 Cells from T-VDA^{cyx} Assay

Normality Tests and Test of Equal Variance – CMT28 and CMM26

CMM26 -Normality test (Anderson Darling) P values

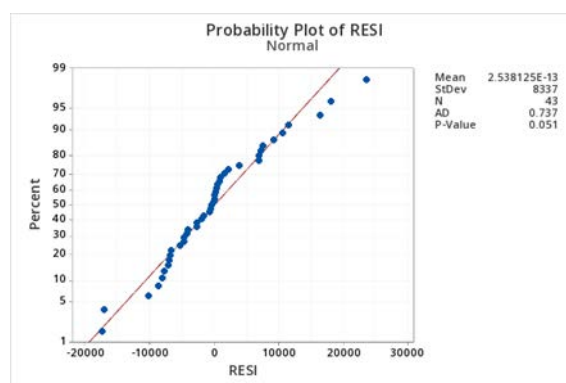
N.atr_i9r1	0.201
N.atr_i9r2	0.582
N.atr_i10r3	0.537
N.sia_i9r4	0.628
N.sia_i10r3	0.227
N.kao_i9r2	0.512
N.kao_i10r2	0.734
N.nig_i8r6	0.141
N.nig_i8r7	0.115
N.nig_i9r3	0.339
N.nig_i9r4	0.107
N.nig_i10r2	0.626
N.nig_i11r3	0.073
Negative	0.825

CMM26– Test of equal Variance (Levene’s Test)

0.577

One-way ANOVA

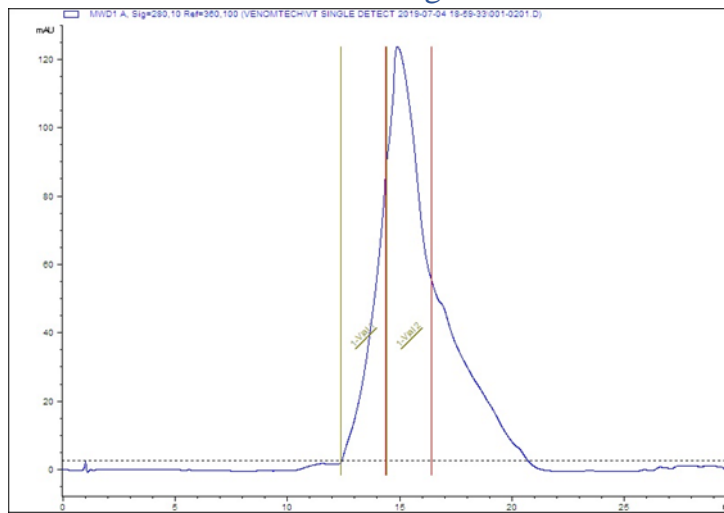
0.000



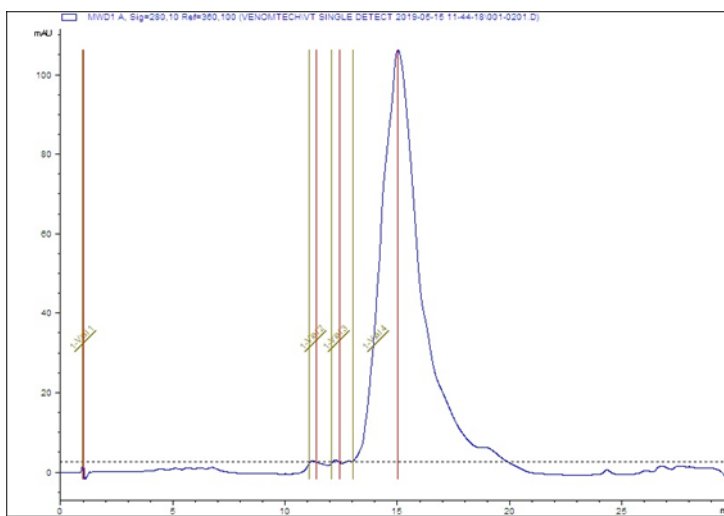
Post-hoc Tukey test

N.atr_i9r1	B	C
N.atr_i9r2	B	C
N.atr_i10r3	B	C
N.sia_i9r4	B	C
N.sia_i10r3	B	C
N.kao_i9r2	B	C
N.kao_i10r2	B	C
N.nig_i8r6	B	
N.nig_i8r7	B	C
N.nig_i9r3	B	
N.nig_i9r4	B	C
N.nig_i10r2	B	C
N.nig_i11r3		C
Negative	A	

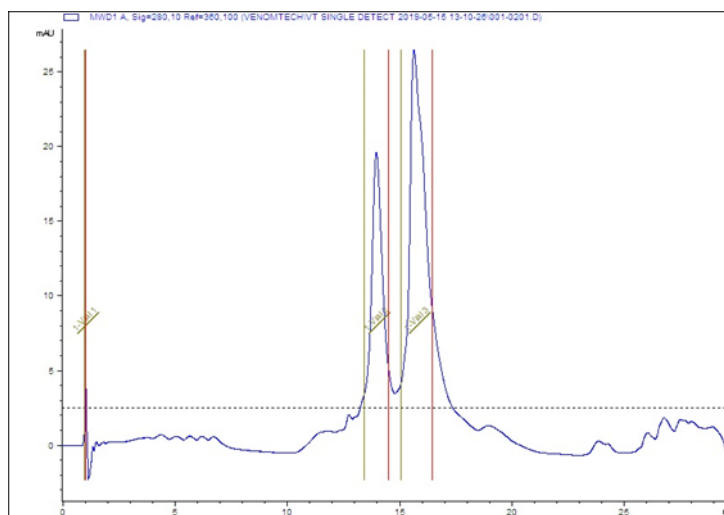
APPENDIX XIV: HPLC Chromatogram traces from Fractionated Venoms



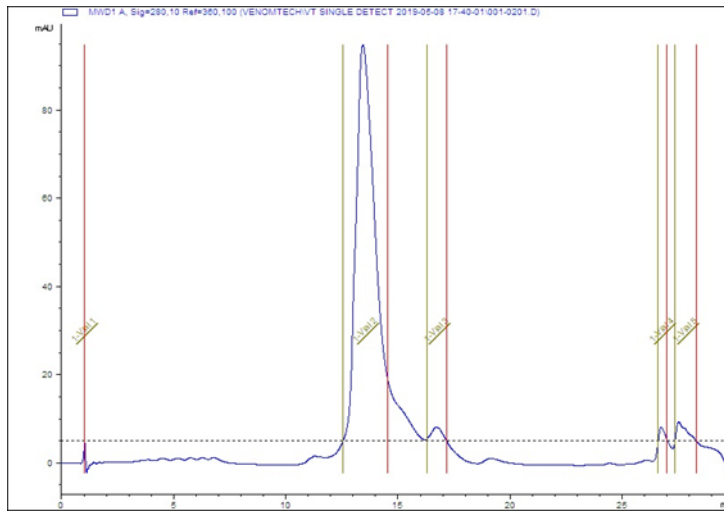
Appendix XIV: N. atr_i9 trace



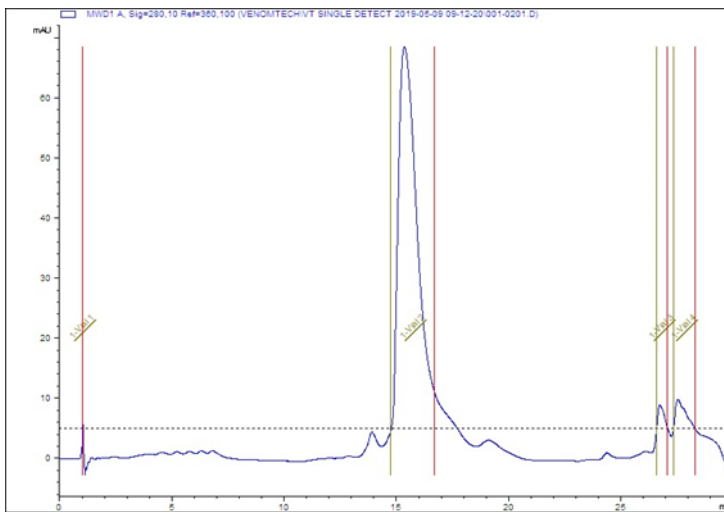
Appendix XIV: N. sia_i9 trace



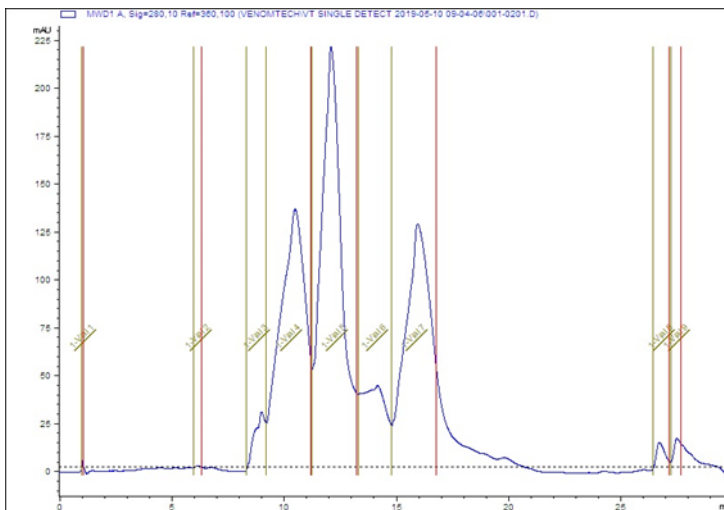
Appendix XIV: N. sia_i10 trace



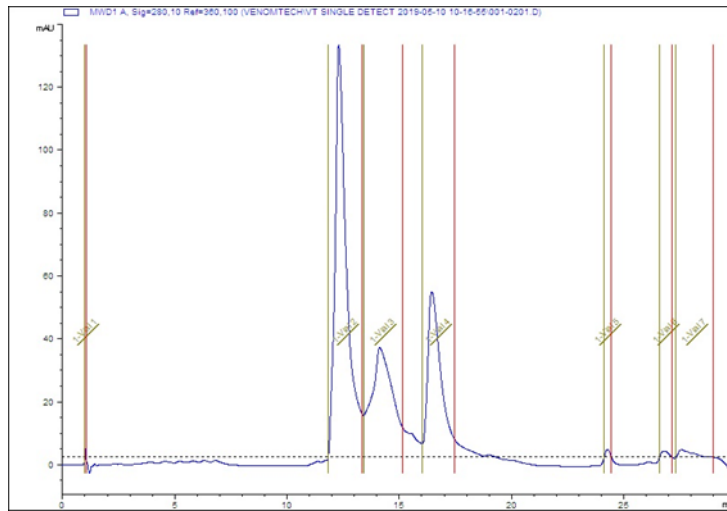
Appendix XIV: N.kao_i9 trace



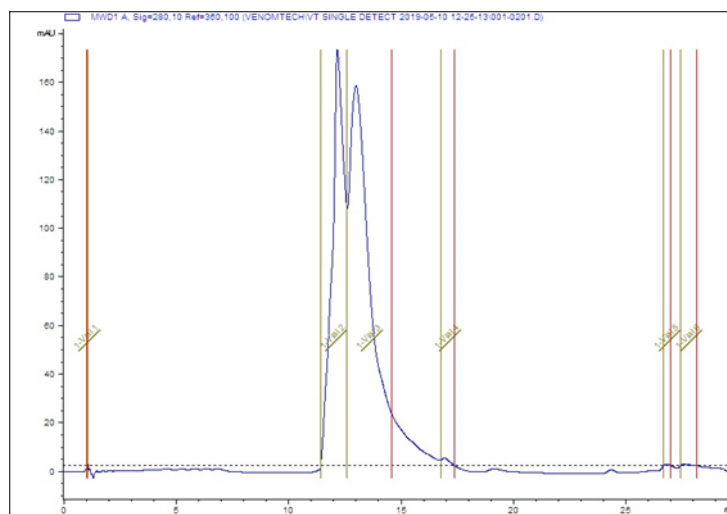
Appendix XIV: N.kao_i10 trace



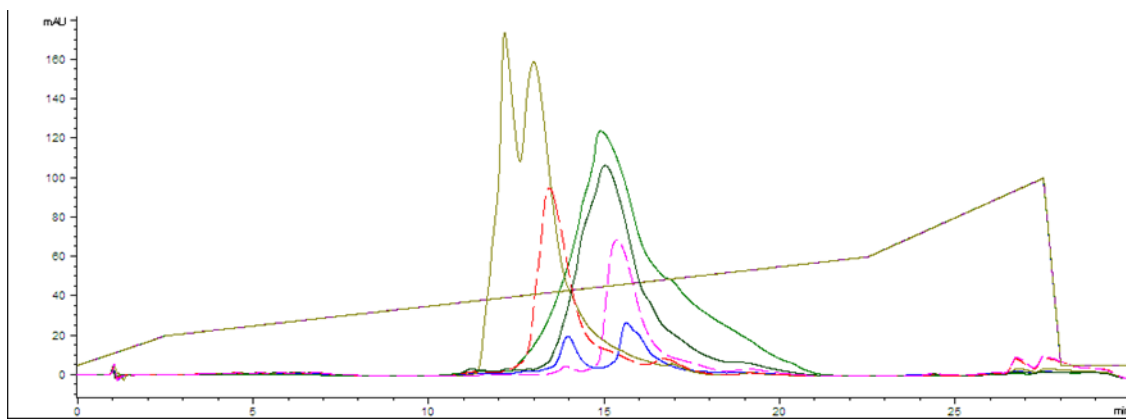
Appendix XIV: N.nig_i8 trace



Appendix XIV: N.nig_i9 trace



Appendix XIV: N.nig_i11 trace



Appendix XIV: Overlay of all hit fractions

APPENDIX XV: Statistical Analysis of Hit fractions screened CMM26, CMT28
and MDCK from T-VDA assay

Normality Tests and Test of Equal Variance

CMT28 – Normality Test (Anderson Darling) P values

	100	33	10	3	1	0.3	0.1	0.03
N.atr_i9r1	0.270	0.334	0.616	0.148	0.494	0.209	0.594	0.613
N.sia_i9r4	0.513	0.623	0.073	0.126	0.229	0.467	0.235	0.611
N.kao_i9r2	0.595	0.122	0.160	0.547	0.304	0.102	0.384	0.283
N.kao_i10r2	0.074	0.555	0.578	0.193	0.219	0.627	0.245	0.088
N.nig_i8r6	0.557	0.061	0.619	0.086	0.150	0.567	0.084	0.629
N.nig_i8r7	0.593	0.090	0.139	0.609	0.626	0.533	0.533	0.621
N.nig_i9r3	0.220	0.548	0.421	0.259	0.067	0.473	0.222	0.597
N.nig_i9r4	0.061	0.061	0.516	0.072	0.109	0.197	0.114	0.347
N.nig_i11r3	0.449	0.363	0.164	0.434	0.516	0.151	0.538	0.076
Negative				0.64				

CMT28- Test of Equal Variance (levene's Test)

0.487

CMM26 – Normality Test (Anderson Darling) P values

	100	33	10	3	1	0.3	0.1	0.03
N.atr_i9r1	0.629	0.490	0.444	0.630	0.160	0.629	0.263	0.364
N.sia_i9r4	0.620	0.067	0.331	0.323	0.581	0.341	0.519	0.628
N.kao_i9r2	0.064	0.560	0.288	0.616	0.627	0.629	0.084	0.385
N.kao_i10r2	0.627	0.255	0.511	0.386	0.347	0.487	0.290	0.604
N.nig_i8r6	0.512	0.196	0.125	0.087	0.199	0.152	0.622	0.215
N.nig_i8r7	0.369	0.522	0.156	0.529	0.202	0.616	0.158	0.618
N.nig_i9r3	0.386	0.293	0.251	0.069	0.336	0.068	0.381	0.251
N.nig_i9r4	0.260	0.597	0.539	0.516	0.061	0.229	0.391	0.095
N.nig_i11r3	0.179	0.259	0.534	0.475	0.541	0.198	0.628	0.0712
Negative				0.631				

CMM26- Test of Equal Variance (levene's Test)
0.191

MDCK – Normality Test (Anderson Darling) P values

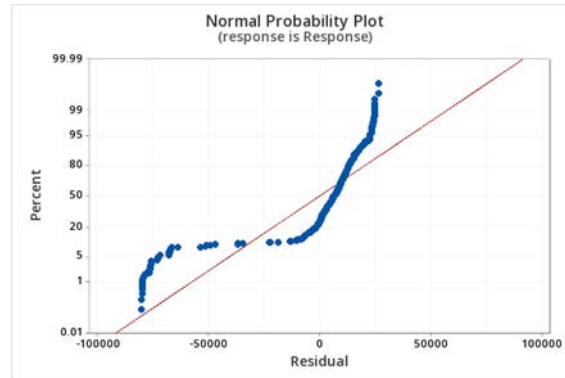
	100	33	10	3	1	0.3	0.1	0.03
N.atr_i9r1	0.082	0.205	0.465	0.230	0.397	0.595	0.631	0.618
N.sia_i9r4	0.071	0.210	0.108	0.079	0.618	0.123	0.339	0.433
N.kao_i9r2	0.396	0.558	0.257	0.119	0.085	0.090	0.576	0.246
N.kao_i10r2	0.128	0.446	0.621	0.058	0.546	0.340	0.146	0.119
N.nig_i8r6	0.398	0.330	0.293	0.095	0.260	0.623	0.251	0.101
N.nig_i8r7	0.625	0.354	0.072	0.075	0.070	0.163	0.622	0.585
N.nig_i9r3	0.175	0.169	0.529	0.375	0.070	0.424	0.087	0.218
N.nig_i9r4	0.153	0.573	0.086	0.104	0.611	0.596	0.349	0.071
N.nig_i11r3	0.087	0.061	0.300	0.626	0.097	0.596	0.349	0.206
Negative				0.186				

MDCK- Test of Equal Variance (levene's Test)
0.115

Comparative ANOVA analysis - Cell line Vs Fraction Vs Response

Multi-factor ANOVA – Fraction
0.000

Multi-factor ANOVA – Cell line
0.000



Post-hoc Tukey test – Cell line

MDCK	A	
CMT28		B
CMM26		B

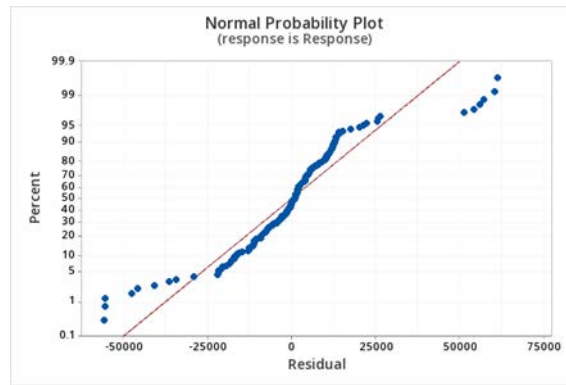
Post-hoc Tukey test - Fractions

N.atr_i9r1		B
N.sia_i9r4	A	B
N.kao_i9r2	A	B
N.kao_i10r2	A	B
N.nig_i8r6	A	
N.nig_i8r7	A	B
N.nig_i9r3	A	
N.nig_i9r4		B
N.nig_i11r3		B

ANOVA analysis – CMT28

Multi-factor ANOVA – Fraction
0.000

Multi-factor ANOVA – Dose
0.000



Post-hoc Tukey test - Dose

10	A		
0.1	A		
1	A		
3	A		
0.03	A		
0.3	A		
33		B	
100			C

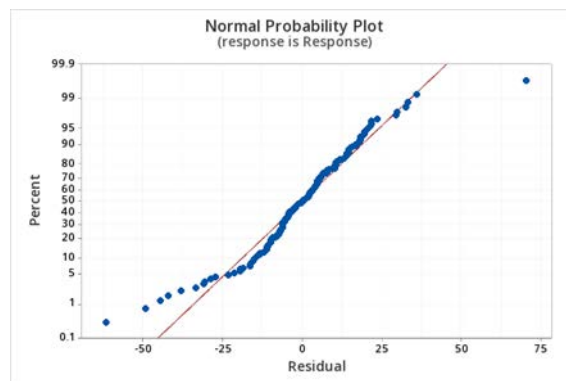
Post-hoc Tukey test - Fractions

N.atr_i9r1			C
N.sia_i9r4		B	C
N.kao_i9r2	A	B	C
N.kao_i10r2		B	C
N.nig_i8r6	A		
N.nig_i8r7	A	B	C
N.nig_i9r3	A	B	
N.nig_i9r4	A	B	C
N.nig_i11r3			C

ANOVA analysis – CMM26

Multi-factor ANOVA – Fraction
0.000

Multi-factor ANOVA – Dose
0.000



Post-hoc Tukey test - Dose

10	B		
0.1		C	D
1			D
3		C	
0.03		C	D
0.3		C	D
33	A		
100	A		

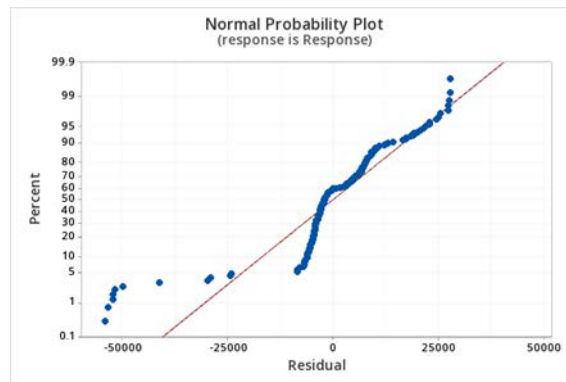
Post-hoc Tukey test - Fractions

N.atr_i9r1	A		
N.sia_i9r4	A		
N.kao_i9r2	A	B	
N.kao_i10r2	A	B	
N.nig_i8r6		B	C
N.nig_i8r7	A	B	
N.nig_i9r3			C
N.nig_i9r4	A	B	
N.nig_i11r3	A		

ANOVA analysis – MDCK

Multi-factor ANOVA – Fraction
0.000

Multi-factor ANOVA – Dose
0.000



Post-hoc Tukey test - Dose

10	A	
0.1	A	
1	A	
3	A	
0.03	A	
0.3	A	
33	A	
100		B

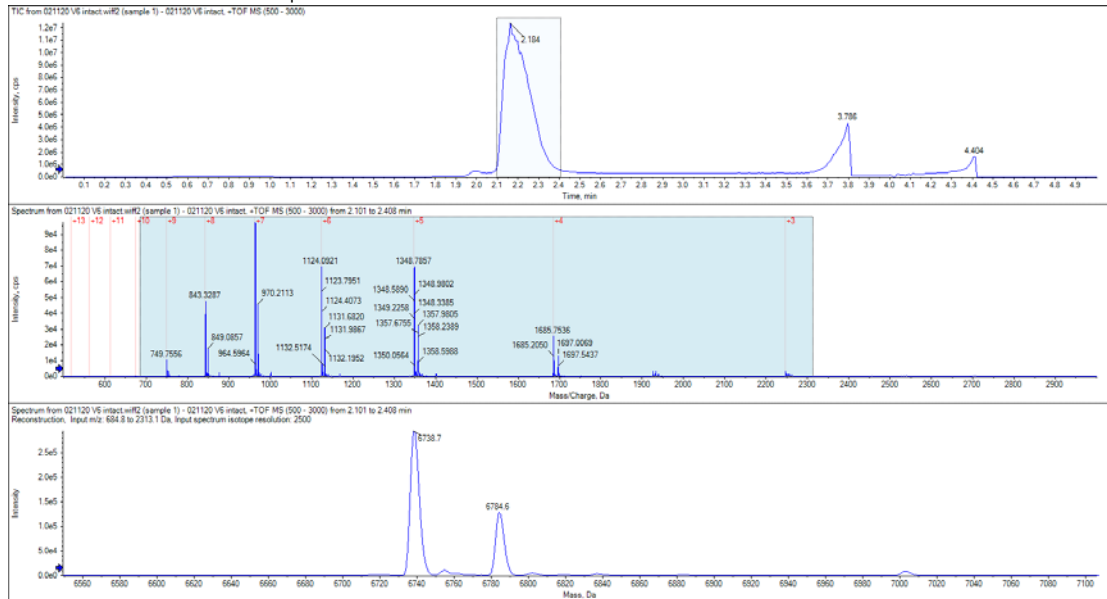
Post-hoc Tukey test - Fractions

N.atr_i9r1			C	D
N.sia_i9r4		B		D
N.kao_i9r2	A	B	C	
N.kao_i10r2	A	B	C	
N.nig_i8r6	A	B		
N.nig_i8r7	A	B		
N.nig_i9r3	A			
N.nig_i9r4	A	B	C	
N.nig_i11r3				D

APPENDIX XVI: Chapter 4: Mass Spectrometry Data produced from Peak Proteins

N.atr_i9r1:

Intact mass shows 2 main peaks of 6738.7Da and 6784.6Da.



Mascot hits:

Cytotoxin 2 OS=Naja atra OX=8656 PE=1 SV=2

Database: SwissProt
Score: 245
Monoisotopic mass (M_r): 9548
Calculated pI: 9.17
Taxonomy: [Naja atra](#)

Sequence similarity is available as [an NCBI BLAST search of 3SA2 NAJAT against nr.](#)

Search parameters

MS data file: C:\MGF files\031120 V6 PM.mgf
Enzyme: Trypsin: cuts C-term side of KR unless next residue is P.
Fixed modifications: [Carbamidomethyl \(C\)](#)
Variable modifications: [Oxidation \(M\)](#), [Phospho \(ST\)](#), [Phospho \(Y\)](#)

Protein sequence coverage: 58%

Matched peptides shown in **bold red**.

1 MKTLLLLTLV VTIVC~~LDL~~GY TLKCNKLVPL FYKTC~~PAG~~KN LCYK~~MF~~MVSN
51 LTV~~PK~~RGC~~I~~ DVC~~PK~~NSALV KYVCCNTDRC N

Neurotoxin Nk-3FTx (Fragment) OS=Naja kaouthia OX=8649 PE=1 SV=2

Database: SwissProt
 Score: 102
 Monoisotopic mass (M_r): 4225
 Calculated pI: 9.30
 Taxonomy: [Naja kaouthia](#)

Sequence similarity is available as [an NCBI BLAST search of 3NO21_NAJKA against nr.](#)

Search parameters

MS data file: C:\MGF files\031120 V6 PM.mgf
 Enzyme: Trypsin: cuts C-term side of KR unless next residue is P.
 Fixed modifications: [Carbamidomethyl \(C\)](#)
 Variable modifications: [Oxidation \(M\)](#), [Phospho \(ST\)](#), [Phospho \(Y\)](#)

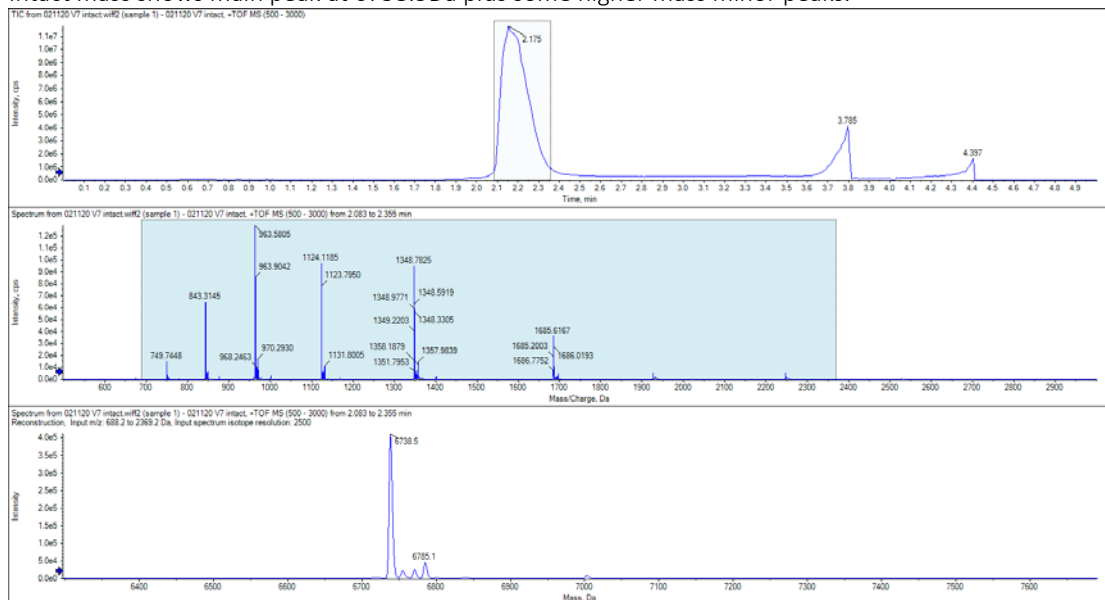
Protein sequence coverage: 39%

Matched peptides shown in **bold red**.

1 **LTCLNCPMPF** **CGK**FQICRNG EKICFKKLHQ RRP

N.sia_i9r4:

Intact mass shows main peak at 6738.5Da plus some higher mass minor peaks.



Mascot hits:

	Score	Mass	Matches	Sequences	emPAI	
<input checked="" type="checkbox"/> 1.1	3SA2_NAJAT	347	9548	16 (16)	7 (7)	32.52 Cytotoxin 2 OS=Naja atra OX=8656 PE=1 SV=2
	▼4 same sets of 3SA2_NAJAT					
	3SA4N_NAJAT	347	9606	16 (16)	7 (7)	Cytotoxin 4N OS=Naja atra OX=8656 PE=3 SV=1
	3SA4_NAJAT	347	9591	16 (16)	7 (7)	Cytotoxin 4 OS=Naja atra OX=8656 PE=1 SV=2
	3SA5A_NAJSP	347	9548	16 (16)	7 (7)	Cytotoxin 5a OS=Naja sputatrix OX=33626 PE=1 SV=2
	3SA5B_NAJSP	347	9562	16 (16)	7 (7)	Cytotoxin 5b OS=Naja sputatrix OX=33626 PE=3 SV=1
<input checked="" type="checkbox"/> 1.2	3SAC3_NAJSP	208	7204	12 (12)	7 (7)	33.50 Cytotoxin KJC3 OS=Naja sputatrix OX=33626 PE=1 SV=1
<input checked="" type="checkbox"/> 1.3	3SA9_NAJHA	177	7120	10 (10)	5 (5)	12.01 Cytotoxin 9 OS=Naja annulifera OX=96794 PE=1 SV=1
<input checked="" type="checkbox"/> 1.4	3SAA_NAJNA	174	7216	13 (13)	6 (6)	33.50 Cytotoxin 10 OS=Naja naja OX=35670 PE=1 SV=2
<input checked="" type="checkbox"/> 1.5	3SA5_NAJOX	161	7116	11 (11)	6 (6)	20.73 Cytotoxin Vc-5 OS=Naja oxiana OX=8657 PE=1 SV=1
<input checked="" type="checkbox"/> 1.6	3SA3_NAJNI	158	7242	10 (10)	5 (5)	11.54 Cytotoxin 3 OS=Naja nivea OX=8655 PE=1 SV=1
<input checked="" type="checkbox"/> 1.7	3SAFA_NAJAT	94	7135	8 (8)	4 (4)	12.01 Cytotoxin SP15a OS=Naja atra OX=8656 PE=1 SV=1
<input checked="" type="checkbox"/> 1.8	3SA5_NAJMO	77	7297	7 (7)	4 (4)	6.35 Cytotoxin 5 OS=Naja mossambica OX=8644 PE=1 SV=3

Cytotoxin 2 OS=Naja atra OX=8656 PE=1 SV=2

Database: SwissProt
Score: 347
Monoisotopic mass (M_r): 9548
Calculated pI: 9.17
Taxonomy: [Naja atra](#)

Sequence similarity is available as [an NCBI BLAST search of 3SA2_NAJAT against nr.](#)

Search parameters

MS data file: C:\MGF_files\031120_V7_PM.mgf
Enzyme: Trypsin: cuts C-term side of KR unless next residue is P.
Fixed modifications: [Carbamidomethyl \(C\)](#)
Variable modifications: [Oxidation \(M\)](#), [Phospho \(ST\)](#), [Phospho \(Y\)](#)

Protein sequence coverage: 51%

Matched peptides shown in **bold red**.

1 MKILLLLTVV VTIVCLDLGY TLKCNKLVPL FYK**TC**PAGRN **LCYKMF**MVSN
51 **LTVFV**RGGCI **DVCPK**NSALV **KYVCC**NTDRC N

Neutral phospholipase A2 muscarinic inhibitor OS=Naja sputatrix OX=33626 PE=1 SV=1

Database: SwissProt
Score: 136
Monoisotopic mass (M_r): 17034
Calculated pI: 6.76
Taxonomy: [Naja sputatrix](#)

Sequence similarity is available as [an NCBI BLAST search of PA2NA_NAJSP against nr.](#)

Search parameters

MS data file: C:\MGF_files\031120_V7_PM.mgf
Enzyme: Trypsin: cuts C-term side of KR unless next residue is P.
Fixed modifications: [Carbamidomethyl \(C\)](#)
Variable modifications: [Oxidation \(M\)](#), [Phospho \(ST\)](#), [Phospho \(Y\)](#)

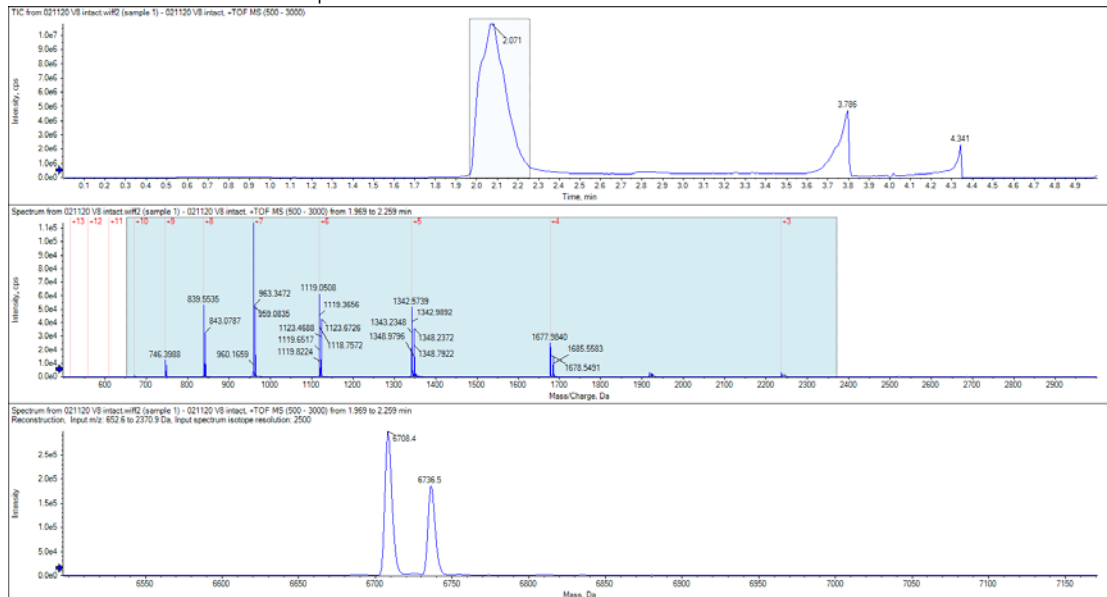
Protein sequence coverage: 34%

Matched peptides shown in **bold red**.

1 MNPAHLLILA AVCVSPGLAS SNRPMPNLNLY QFKN**MIQ**CTV **PNRS**WVHFAD
51 YG**CYCGR**GGG **GTPV**DDLDRG CQIHDCNYNE AEKISRCPY F**KTY**SYECSQ
101 **GTL**TCRGGNN **ACAA**AVCDGD **RLAA**ICFAGA FYNDNNYNIID LKAR**Q**

N.kao_i9r2:

Intact mass shows two main peaks at 6708.4Da and 6736.5Da.



Mascot hits:

▶1	ALBU_BOVIN	466	Serum albumin OS=Bos taurus OX=9913 GN=ALB PE=1 SV=4
▶2	TRY1_BOVIN	193	Cationic trypsin OS=Bos taurus OX=9913 PE=1 SV=3
▶3	A1AT_BOVIN	116	Alpha-1-antitrypsin OS=Bos taurus OX=9913 GN=SERPINA1 PE=1 SV=1
▶4	FETUA_BOVIN	115	Alpha-2-HS-glycoprotein OS=Bos taurus OX=9913 GN=AHSG PE=1 SV=2
▶5			

Cytotoxin 3 OS=Naja kaouthia OX=8649 PE=1 SV=1

Database: SwissProt
 Score: 114
 Monoisotopic mass (M_r): 7169
 Calculated pI: 9.39
 Taxonomy: [Naja kaouthia](#)

Sequence similarity is available as [an NCBI BLAST search of 3SA3_NAJKA against nr.](#)

Search parameters

MS data file: C:\MGF_files\031120_V8_pM.mgf
 Enzyme: Trypsin: cuts C-term side of KR unless next residue is P.
 Fixed modifications: [Carbamidomethyl \(C\)](#)
 Variable modifications: [Oxidation \(M\)](#), [Phospho \(ST\)](#), [Phospho \(Y\)](#)

Protein sequence coverage: 66%

Matched peptides shown in **bold red**.

1 LKCNKLIPLA **YKTC**PAGKNL **CYR**MFVSNK **TVP**VKRGCID **ACP**KNLSLVK
 51 **YVCC**NTDRCN

Protein View: 3L21_NAJKA

Alpha-cobrotoxin OS=Naja kaouthia OX=8649 PE=1 SV=1

Database: SwissProt
 Score: 83
 Monoisotopic mass (M_r): 8396
 Calculated pI: 8.60
 Taxonomy: [Naja kaouthia](#)

Sequence similarity is available as [an NCBI BLAST search of 3L21_NAJKA against nr.](#)

Search parameters

MS data file: C:\MGF_files\031120_V8_pM.mgf
 Enzyme: Trypsin: cuts C-term side of KR unless next residue is P.
 Fixed modifications: [Carbamidomethyl \(C\)](#)
 Variable modifications: [Oxidation \(M\)](#), [Phospho \(ST\)](#), [Phospho \(Y\)](#)

Protein sequence coverage: 59%

Matched peptides shown in **bold red**.

1 I~~R~~C~~F~~I~~T~~E~~D~~I~~T~~ ~~S~~H~~D~~C~~P~~H~~S~~H~~V~~C ~~V~~E~~R~~N~~C~~D~~A~~R~~C~~ ~~S~~T~~R~~G~~R~~V~~D~~L~~G~~ ~~G~~A~~A~~T~~C~~P~~P~~V~~R~~
 51 **QV**D~~I~~Q~~C~~C~~S~~T~~D~~ ~~N~~O~~N~~F~~F~~P~~T~~R~~S~~ ~~P~~

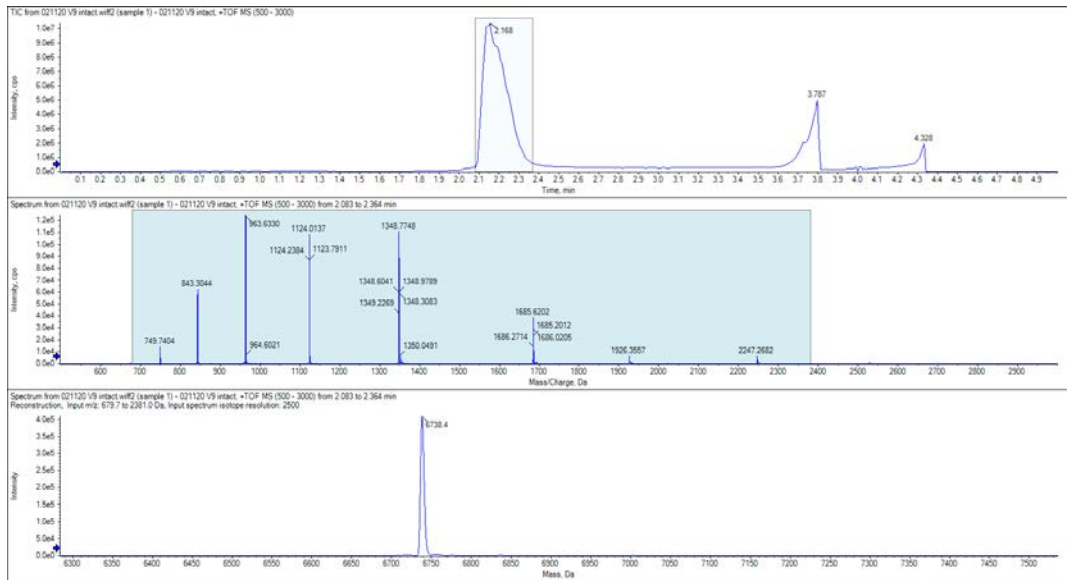
Unformatted sequence string: [71 residues](#) (for pasting into other applications).

Sort by residue number increasing mass decreasing mass
 Show matched peptides only predicted peptides also

Query	Start - End	Observed	Mr (expt)	Mr (calc)	ppm	M Score	Expect	Rank	U	Peptide
#447	24 - 33	659.2912	1314.5478	1314.5485	-0.53	0	35	0.00052	1	U K.TMCDAPCSIR.G
#733	37 - 49	696.3382	1390.6619	1390.6585	2.44	0	24	0.01	1	U R.YDLGCAATCPYK.T
#321	50 - 68	1121.4670	2240.9330	2240.9249	-2.49	0	64	1.4e-005	1	U R.TQVDIQCCSTWNONFFPTR.R

N.kao_i10r2:

Intact mass shows main peak with mass of 6738.4Da.



Mascot hits:

Rank	Protein	Score	Mass	Matches	Sequences	emPAI
2.1	3SA0_NAJSP	107	9605	8 (8)	5 (5)	9.14 Cytotoxin OS=Naja sputatrix OX=33626 PE=3 SV=1
	▼ 7 samesets of 3SA0_NAJSP					
	3SA3A_NAJAT	107	9572	8 (8)	5 (5)	Cytotoxin 3a OS=Naja atra OX=8656 PE=3 SV=1
	3SA3B_NAJAT	107	9530	8 (8)	5 (5)	Cytotoxin 3b OS=Naja atra OX=8656 PE=3 SV=2
	3SA3D_NAJAT	107	9434	8 (8)	5 (5)	Cytotoxin 3d OS=Naja atra OX=8656 PE=3 SV=1
	3SA3_NAJAT	107	9545	8 (8)	5 (5)	Cytotoxin 3 OS=Naja atra OX=8656 PE=1 SV=1
	3SA3_NAJSP	107	9545	8 (8)	5 (5)	Cytotoxin 3 OS=Naja sputatrix OX=33626 PE=1 SV=1
	3SA4_NAJKA	107	9545	8 (8)	5 (5)	Cytotoxin 4 OS=Naja kaouthia OX=8649 PE=1 SV=1
	3SA8B_NAJAT	107	9407	8 (8)	5 (5)	Cytotoxin 8 OS=Naja atra OX=8656 PE=3 SV=1
2.2	3SA3_NAJNI	89	7242	5 (5)	4 (4)	6.56 Cytotoxin 3 OS=Naja nivea OX=8655 PE=1 SV=1
2.3	3SA1_NAJKA	78	7259	6 (6)	5 (5)	11.54 Cytotoxin 1 OS=Naja kaouthia OX=8649 PE=1 SV=1
	▼ 5 samesets of 3SA1_NAJKA					
	3SA3_NAJNA	78	7197	6 (6)	5 (5)	Cytotoxin 3 OS=Naja naja OX=35670 PE=1 SV=1
	3SA5_NAJAT	78	9593	6 (6)	5 (5)	Cytotoxin 5 OS=Naja atra OX=8656 PE=3 SV=1
	3SA6_NAJSP	78	7481	6 (6)	5 (5)	Cytotoxin 6 (Fragment) OS=Naja sputatrix OX=33626 PE=3 SV=1
	3SA7A_NAJKA	78	7197	6 (6)	5 (5)	Cytotoxin 2 OS=Naja kaouthia OX=8649 PE=1 SV=1
	3SAT_NAJAT	78	7262	6 (6)	5 (5)	Cytotoxin 5 OS=Naja atra OX=8656 PE=1 SV=1
2.4	3SA3_NAJKA	75	7169	5 (5)	4 (4)	6.56 Cytotoxin 3 OS=Naja kaouthia OX=8649 PE=1 SV=1
2.5	3SAA_NAJNA	75	7216	5 (5)	4 (4)	6.56 Cytotoxin 10 OS=Naja naja OX=35670 PE=1 SV=2

Cytotoxin 4 OS=Naja kaouthia OX=8649 PE=1 SV=1

Database: SwissProt
 Score: 107
 Monoisotopic mass (M_r): 9545
 Calculated pI: 9.26
 Taxonomy: [Naja kaouthia](#)

Sequence similarity is available as [an NCBI BLAST search of 3SA4_NAJKA against nr](#).

Search parameters

MS data file: C:\MGF files\031120 V9 PM.mgf
 Enzyme: Trypsin: cuts C-term side of KR unless next residue is P.
 Fixed modifications: [Carbamidomethyl \(C\)](#)
 Variable modifications: [Oxidation \(M\)](#), [Phospho \(ST\)](#), [Phospho \(Y\)](#)

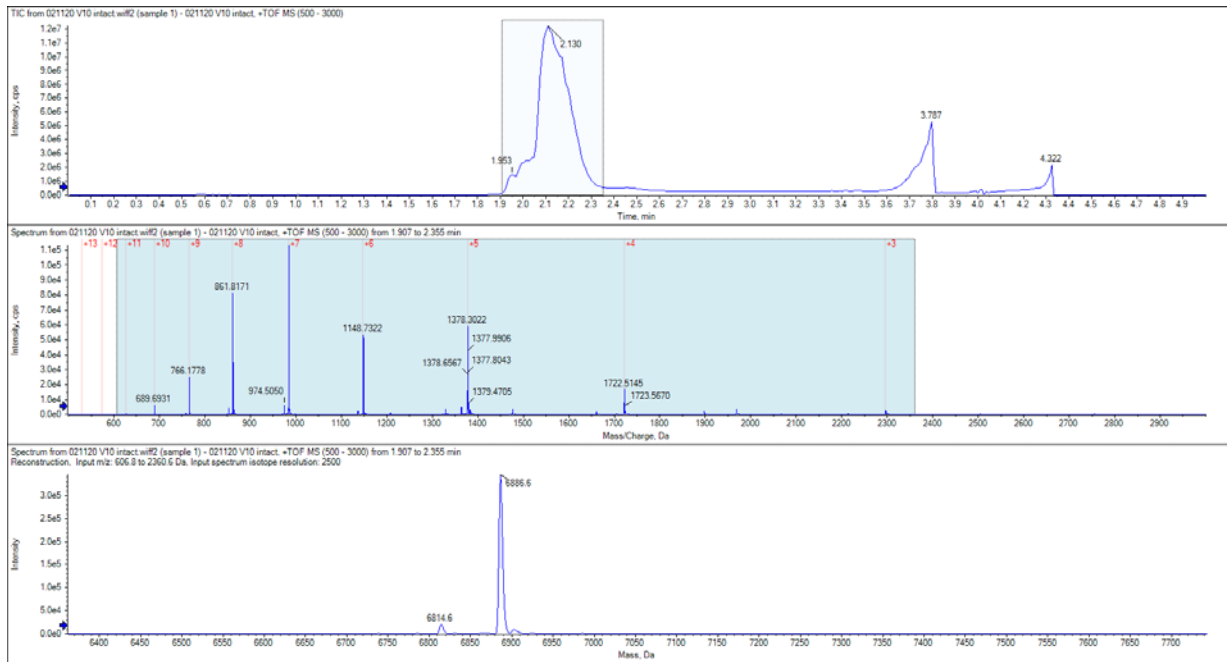
Protein sequence coverage: 44%

Matched peptides shown in **bold red**.

1 MKTLLLTLLV VTIIVCLDLGY TLKCNKLVPL FYK**TCPAGRN** LCYR**MFVAT**
 51 PKV**PKRGCI** DVCPK**SLLV** KYV**CNTDRC** N

N.nig_i11r3:

Intact mass shows main peak at 6886.6Da.



Mascot hits:

Phospholipase A2 'basic' OS=Naja nigricollis OX=8654 PE=1 SV=1

Database: SwissProt
 Score: 271
 Monoisotopic mass (M_r): 14057
 Calculated pI: 8.75
 Taxonomy: [Naja nigricollis](#)

Sequence similarity is available as [an NCBI BLAST search of PA2B4_NAJNG against nr.](#)

Search parameters

MS data file: C:\MGF files\031120 V10 PM.mgf
 Enzyme: Trypsin: cuts C-term side of KR unless next residue is P.
 Fixed modifications: [Carbamidomethyl \(C\)](#)
 Variable modifications: [Oxidation \(M\)](#), [Phospho \(ST\)](#), [Phospho \(Y\)](#)

Protein sequence coverage: 36%

Matched peptides shown in **bold red**.

1 NLYQFKNMIH CIVPSRPWWH FADYGCYCGR **GGKGTVPDDL DRCCQVHDNC**
 51 YEKAGK**MGCW** PYLTLYKYKC SQGKLTCSSG NSKCGAAVCN **CDLVAANCEA**
 101 **GARYIDANYN** INFKKRCQ

Protein View: 3SAN_NAJNG

Naniproin OS=Naja nigricollis OX=8654 PE=1 SV=1

Database: SwissProt
 Score: 158
 Monoisotopic mass (M_r): 7347
 Calculated pI: 9.41
 Taxonomy: [Naja nigricollis](#)

Sequence similarity is available as [an NCBI BLAST search of 3SAN_NAJNG against nr.](#)

Search parameters

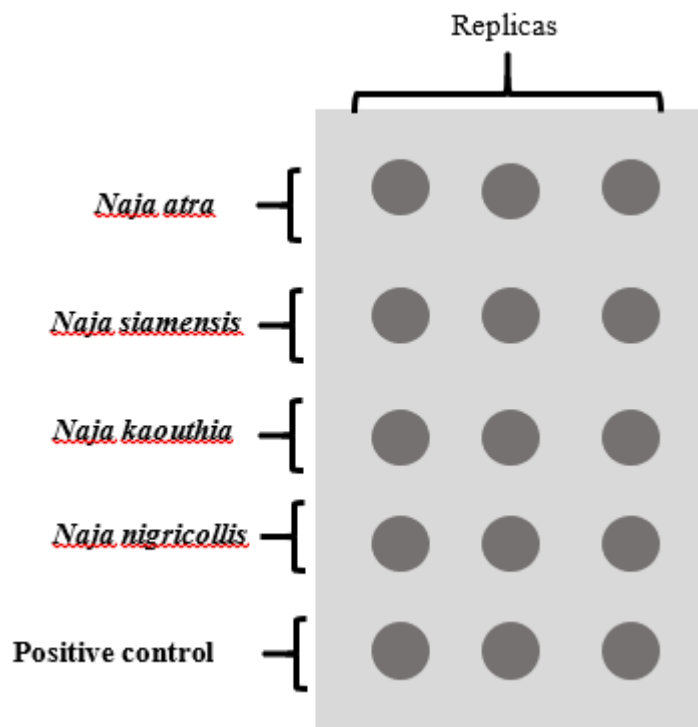
MS data file: C:\MGF files\031120 V10 PM.mgf
 Enzyme: Trypsin: cuts C-term side of KR unless next residue is P.
 Fixed modifications: [Carbamidomethyl \(C\)](#)
 Variable modifications: [Oxidation \(M\)](#), [Phospho \(ST\)](#), [Phospho \(Y\)](#)

Protein sequence coverage: 73%

Matched peptides shown in **bold red**.

1 LKCNRLIPPF **WKTCPBGKRL** CYKMTMLRAP **KVPVVRGCID** VCPKSSLLIK
 51 **YMCCTNDKCN**

APPENDIX XVII: CHAPTER 5: Dot Blot layout for Determining the Binding of HER2 to Whole Venoms for SKBR3, CMT28 and CMM26



APPENDIX XVIII: CHAPTER 5: Dot Blot Analysis Pixel Intensity Data
Generated in Biorad ImageLab

	Pixel Intensity for each cell		
Whole Venom	SKBR3	CMT28	CMM26
<i>Naja atra</i>	49,336	1,039	19,062
<i>Naja siamensis</i>	560,318	304,067	368,709
<i>Naja kaouthia</i>	256,739	225,583	78,772
<i>Naja Nigricollis</i>	145,846	134,956	236,193
Positive control	614,211	334,122	376,854

Appendix XIX: Chapter 5: Amino Acid sequence of Canine HER2 receptor

10	20	30	40	50
MELAAWCRWG	LLLALLPSGA	AGTQVCTGTD	MKLRLPASPE	THLDMLRHLY
60	70	80	90	100
QGCVVQGNL	ELTYLPANAS	LSFLQDIQEV	QGYVLIASQ	VRQIPLQLRLR
110	120	130	140	150
IVRGTQLFED	NYALAVLDNG	DFLEGGIPAP	GAAQGGLREL	QLRSLTEILK
160	170	180	190	200
GGVLIQRSPQ	LCHQDTILWK	DVFHKNQLA	LTLIDTNRFS	ACPPCSPACK
210	220	230	240	250
DAHCWGASSG	DCQSLTRTVC	AGGCARCKGP	QPTDCCHEQC	AAGCTGPKHS
260	270	280	290	300
DCLACLHFNH	SGICELHCPA	LVTYNTDTFE	SMPNPEGRYT	FGASCVTSCP
310	320	330	340	350
YNYLSTDVGS	CTLVCPLNQ	EVTAEDEGTQR	CEKCSKPCAR	VCYGLGMEHL
360	370	380	390	400
REVRVAVTSAN	IQEFAGCKKI	FGSLAFLPES	FDGDPASNTA	PLQPEQLRVF
410	420	430	440	450
EALEEITGYL	YISAWPDSLP	NLSVFQNLRV	IRGRVLHDGA	YSLTLQGLGI
460	470	480	490	500
SWLGLRSLRE	LGSGLALIHR	NARLCFVHTV	PWDQLFRNPH	QALLHSANRP
510	520	530	540	550
EEECVGEGLA	CYPCAHGHCW	GPGPTQCVNC	SQFLRGQECV	EECRVLQGLP
560	570	580	590	600
REYVKDRYCL	PCHSECQPQN	GSVTCFGSEA	DQCVACAHYK	DPPFCVARCP
610	620	630	640	650
SGVKPDLFSM	PIWKFADEEG	TCQPCPINCT	HSCADLDEKG	CPAEQRASPV
660	670	680	690	700
TSIIAAVVGI	LLAVVVLVL	GILIKRRRQK	IRKYTMRRLL	QETELVEPLT
710	720	730	740	750
PSGAMPNQAQ	MRILKETELR	KVKVLGSGAF	GTVYKGIWIP	DGENVKIPVA
760	770	780	790	800
IKVLENTSP	KANKEILDEA	YVMAGVGSFY	VSRLGICLT	STVQLVTQLM
810	820	830	840	850
PYGCLLDHVR	EHRGRLGSD	LLNWCQIAK	GMSYLEDVRL	VHRDLAARNV
860	870	880	890	900
LVKSPNHVKI	TDFGLARLLD	IDETEHADG	GKVPKWMAL	ESIPPRRFTH
910	920	930	940	950
QSDVWSYGVV	VWELMTFGAK	PYDGIPIREI	PDLLEKGERL	PQPPICTIDV
960	970	980	990	1000
YMIMVKCMI	DSECRPRFRE	LVAEFSRMAR	DPQRFVVIQN	EDLGPASPLD
1010	1020	1030	1040	1050
STFYRSLEED	DDMGDLVDAE	EYLVQQGFF	CPEPTPGAGG	TAHRRHRSSS
1060	1070	1080	1090	1100
TRNGGELTL	GLEPSEEEPP	KSPLAPSEGA	GSDVFDGDLG	MGAAKGLQSL
1110	1120	1130	1140	1150
PSQDPSPLQR	YSEDPTVPLP	PETDGKVAPL	TCSQPPEYVN	QPEVWPQPPL
1160	1170	1180	1190	1200
ALEGPLPPSR	PAGATLERPK	TLSPKTLSPG	KNGVVKDVFV	FGSAVENPEY
1210	1220	1230	1240	1250
LAPRGRAAPQ	PHPPAFSPA	FDNLYYWDQD	PSERGSPPST	FEGTPTAENP
EYLGLDVPV				

APPENDIX XX: CHAPTER 5: Binary Files produced from HER2 Minimisation

```
#####  
## MINIMIZATION template   Canine_her_2           ##  
#####  
## FORCEFIELD PARAMATERS           ##  
#####  
  
paratypecharm   on  
parameters /home/kris/SARS_COV2/par/par_all36_prot.prm  
parameters /home/kris/SARS_COV2/par/toppar_water_ions_namd.str  
parameters /home/kris/SARS_COV2/par/toppar_all36_lipid_miscellaneous.str  
parameters /home/kris/SARS_COV2/par/toppar_all36_lipid_detergent.str  
parameters /home/kris/SARS_COV2/par/toppar_all36_lipid_lps.str  
parameters /home/kris/SARS_COV2/par/toppar_all36_na_rna_modified.str  
parameters /home/kris/SARS_COV2/par/toppar_all36_carb_lignin.str  
parameters /home/kris/SARS_COV2/par/toppar_all36_carb_model.str  
parameters /home/kris/SARS_COV2/par/toppar_all36_carb_imlab.str  
parameters /home/kris/SARS_COV2/par/toppar_all36_carb_glycopeptide.str  
parameters /home/kris/SARS_COV2/par/toppar_all36_carb_glycolipid.str  
parameters /home/kris/SARS_COV2/par/patch.par  
parameters /home/kris/SARS_COV2/par/par_all36_na.prm  
parameters /home/kris/SARS_COV2/par/par_all36m_prot.prm  
parameters /home/kris/SARS_COV2/par/par_all36_lipid.prm  
parameters /home/kris/SARS_COV2/par/par_all36_cgenff.prm  
parameters /home/kris/SARS_COV2/par/par_all36_carb.prm  
parameters /home/kris/SARS_COV2/par/par_all35_ethers.prm  
  
#####  
## STRUCTURE AND COORDINATES           ##  
#####  
structure  
/home/dan/Alice_her2_homo/MD/canine_her2_comp/struct/Canine_ionised_waterbox.  
psf  
coordinates  
/home/dan/Alice_her2_homo/MD/canine_her2_comp/coord/Canine_ionised_waterbox.  
pdb  
  
#####  
## TEMPERATURE           ##  
#####  
temperature   310  
  
#####  
## TEMP AMD PRESSURE COUPLING           ##  
#####  
langevin           on  
langevinTemp   310  
langevinDamping   5  
langevinHydrogen off  
  
#####
```



```

## CONSTANT PRESSURE CONTROL (VAR VOLUME)          ##
#####
useGroupPressure    yes
useFlexibleCell     no
useConstantArea     no
langevinPiston      on
langevinPistonTarget 1.01325 ;# in bar -> 1 atm
langevinPistonPeriod 200.0
langevinPistonDecay 50.0
langevinPistonTemp  310

#####
## OUTPUTS                                          ##
#####
outputname
/home/dan/Alice_her2_homo/MD/canine_her2_comp/inp/min/canine_her2_min.dcd
outputEnergies 40
restartfreq    500
DCDfreq       20
outputTiming   50
wrapAll       on
wrapNearest   on
binaryoutput   yes
binaryrestart  yes

#####
## INTEGRATORS                                     ##
#####
timestep      2
nonbondedFreq 2
fullElectFrequency 4
stepspercycle 20

#####
## APPROXIMATIONS                                  ##
#####
rigidBonds    water
rigidTolerance 0.0000001
cutoff        12
switching     on
switchdist    10
pairlistdist  14
margin        3
exclude       scaled1-4
1-4scaling    1.0 # 1.0 for Charmm, 0.833333 for Amber
PME           on
cellOrigin    127.1070327758789 129.7383575439453 103.08016967773438
cellBasisVector1 100.89500427246094 0 0
cellBasisVector2 0 96.46199798583984 0
cellBasisVector3 0 0 128.69999313354492
PMEGridSpacing 1

```

```
#####  
## HARMONIC CONSTRAINTS                ##  
#####
```

```
constraints on  
consref /home/dan/Alice_her2_homo/MD/canine_her2_comp/par/canine_her_con.pdb  
conskfile /home/dan/Alice_her2_homo/MD/canine_her2_comp/par/canine_her_con.pdb  
constraintScaling 2  
consexp 2  
conskcol B
```

```
#####  
## EXECUTION SCRIPT                    ##  
#####  
minimize 2500
```

APPENDIX XXI: CHAPTER 5: Binary Files produced from HER2 Heating

```
#####  
## HEATING   cannie_her2           ##  
#####  
## CONSTANTS           ##  
#####  
  
cutoff 12.0  
pairlistdist 14.0  
switching on  
switchdist 10.0  
PME on  
PMEGridspacing 1  
wrapAll on  
wrapWater on  
  
##System definition##  
  
coordinates  
/home/dan/Alice_her2_homo/MD/canine_her2_comp/coord/Canine_ionised_waterbox.  
pdb  
structure  
/home/dan/Alice_her2_homo/MD/canine_her2_comp/struct/Canine_ionised_waterbox.  
psf  
  
#FOR MINIMISATION BIN VEL AND BINCOORD ARE HASHED OUT.  
  
binCoordinates  
/home/dan/Alice_her2_homo/MD/canine_her2_comp/inp/min/canine_her2_min.dcd.co  
or  
#binVelocities  
/home/dan/Alice_her2_homo/MD/canine_her2_comp/inp/min/canine_her2_min.dcd.vel  
  
extendedSystem  
/home/dan/Alice_her2_homo/MD/canine_her2_comp/inp/min/canine_her2_min.dcd.xsc  
  
#EITHER AN xsc FILE OR CELL BASIS VECS&ORIGIN NEED TO BE  
UNHASHED  
  
#cellOrigin   -0.049795910716056824 0.030537299811840057  
0.23735018074512482  
#cellBasisVector1  73.94400024414063 0 0  
#cellBasisVector2  0 72.12999725341797 0  
#cellBasisVector3  0 0 103.47800064086914  
  
##Conditions##  
  
##harmonic constraints##  
constraints on  
consref /home/dan/Alice_her2_homo/MD/canine_her2_comp/par/canine_her_con.pdb
```

conskfile /home/dan/Alice_her2_homo/MD/canine_her2_comp/par/canine_her_con.pdb
constraintScaling 2
consexp 2
conskcol B

##Output Parameters##

binaryoutput yes
outputname
/home/dan/Alice_her2_homo/MD/canine_her2_comp/inp/heat/canine_her_heat
outputenergies 500
outputtiming 500
outputpressure 500
binaryrestart yes
dcdfile
/home/dan/Alice_her2_homo/MD/canine_her2_comp/inp/heat/canine_her_heat.dcd
dcdfreq 1000
XSTFreq 1000
restartfreq 1000
restartname
/home/dan/Alice_her2_homo/MD/canine_her2_comp/inp/heat/canine_her_heat.restart

##Thermostat Parameters##

langevin on
langevintemp 60
langevinHydrogen off
langevindamping 1

##Barostat Parameters##

usegrouppressure yes
useflexiblecell no
useConstantArea no
langevinpiston on
langevinpistontarget 1.01325
langevinpistonperiod 200
langevinpistondecay 50
langevinpistontemp 60

MD Protocol #

#

seed 4307
temperature 0
reassignFreq 1
reassignIncr 0.001
reassignHold 310

##Integrator Parameters##

timestep 2
firstTimestep 0
fullElectFrequency 2
nonbondedfreq 1

##Force Field Parameters##

paratypecharmm on

parameters /home/kris/SARS_COV2/par/par_all36_prot.prm
parameters /home/kris/SARS_COV2/par/toppar_water_ions_namd.str
parameters /home/kris/SARS_COV2/par/toppar_all36_lipid_miscellaneous.str
parameters /home/kris/SARS_COV2/par/toppar_all36_lipid_detergent.str
parameters /home/kris/SARS_COV2/par/toppar_all36_lipid_lps.str
parameters /home/kris/SARS_COV2/par/toppar_all36_na_rna_modified.str
parameters /home/kris/SARS_COV2/par/toppar_all36_carb_lignin.str
parameters /home/kris/SARS_COV2/par/toppar_all36_carb_model.str
parameters /home/kris/SARS_COV2/par/toppar_all36_carb_imlab.str
parameters /home/kris/SARS_COV2/par/toppar_all36_carb_glycopeptide.str
parameters /home/kris/SARS_COV2/par/toppar_all36_carb_glycolipid.str
parameters /home/kris/SARS_COV2/par/patch.par
parameters /home/kris/SARS_COV2/par/par_all36_na.prm
parameters /home/kris/SARS_COV2/par/par_all36m_prot.prm
parameters /home/kris/SARS_COV2/par/par_all36_lipid.prm
parameters /home/kris/SARS_COV2/par/par_all36_cgenff.prm
parameters /home/kris/SARS_COV2/par/par_all36_carb.prm
parameters /home/kris/SARS_COV2/par/par_all35_ethers.prm
exclude scaled1-4
1-4scaling 1.0
rigidbonds all

#Implicit Solvent Parameters

#gbis off
#alphaCutoff 14.0
#ionConcentration 0.2664

numsteps 310000

APPENDIX XXII: CHAPTER 5: Binary Files produced from HER2
Equilibration

```
#####  
## EQUILIBRATION    canine her 2          ##  
#####  
## CONSTANTS          ##  
#####  
  
cutoff 12.0  
pairlistdist 14.0  
switching on  
switchdist 10.0  
PME on  
PMEGridspacing 1  
wrapAll on  
wrapWater on  
  
##System definition##  
  
coordinates  
/home/dan/Alice_her2_homo/MD/canine_her2_comp/coord/Canine_ionised_waterbox.  
pdb  
structure  
/home/dan/Alice_her2_homo/MD/canine_her2_comp/struct/Canine_ionised_waterbox.  
psf  
  
#FOR MINIMISATION BIN VEL AND BINCOORD ARE HASHED OUT.  
  
binCoordinates  
/home/dan/Alice_her2_homo/MD/canine_her2_comp/inp/heat/canine_her_heat.coor  
binVelocities  
/home/dan/Alice_her2_homo/MD/canine_her2_comp/inp/heat/canine_her_heat.vel  
  
extendedSystem  
/home/dan/Alice_her2_homo/MD/canine_her2_comp/inp/heat/canine_her_heat.xsc  
  
#EITHER AN xsc FILE OR CELL BASIS VECS&ORIGIN NEED TO BE  
UNHASHED  
  
##Conditions##  
#temperature 310  
  
##harmonic constraints##  
constraints on  
consref /home/dan/Alice_her2_homo/MD/canine_her2_comp/par/canine_her_con.pdb  
conskfile /home/dan/Alice_her2_homo/MD/canine_her2_comp/par/canine_her_con.pdb  
constraintScaling 2  
consexp 2  
conskcol B
```

##Output Parameters##

binaryoutput yes
outputname
/home/dan/Alice_her2_homo/MD/canine_her2_comp/inp/eqi/canine_her_eqi
outputenergies 500
outputtiming 500
outputpressure 500
binaryrestart yes
dcdfile
/home/dan/Alice_her2_homo/MD/canine_her2_comp/inp/eqi/canine_her_eqi.dcd
dcdfreq 2000
XSTFreq 2000
restartfreq 2000
restartname
/home/dan/Alice_her2_homo/MD/canine_her2_comp/inp/eqi/canine_her_eqi.restart

##Thermostat Parameters##

langevin on
langevintemp 310
langevinHydrogen off
langevindamping 1

##Barostat Parameters##

usegrouppressure yes
useflexiblecell no
useConstantArea no
langevinpiston on
langevinpistontarget 1.01325
langevinpistonperiod 200
langevinpistondecay 100
langevinpistontemp 310

##Integrator Parameters##

timestep 2
firstTimestep 0
fullElectFrequency 2
nonbondedfreq 1

##Force Field Parameters##

paratypecharmm on
parameters /home/kris/SARS_COV2/par/par_all36_prot.prm
parameters /home/kris/SARS_COV2/par/toppar_water_ions_namd.str
parameters /home/kris/SARS_COV2/par/toppar_all36_lipid_miscellaneous.str
parameters /home/kris/SARS_COV2/par/toppar_all36_lipid_detergent.str
parameters /home/kris/SARS_COV2/par/toppar_all36_lipid_lps.str
parameters /home/kris/SARS_COV2/par/toppar_all36_na_rna_modified.str
parameters /home/kris/SARS_COV2/par/toppar_all36_carb_lignin.str
parameters /home/kris/SARS_COV2/par/toppar_all36_carb_model.str

```
parameters /home/kris/SARS_COV2/par/toppar_all36_carb_imalb.str
parameters /home/kris/SARS_COV2/par/toppar_all36_carb_glycopeptide.str
parameters /home/kris/SARS_COV2/par/toppar_all36_carb_glycolipid.str
parameters /home/kris/SARS_COV2/par/patch.par
parameters /home/kris/SARS_COV2/par/par_all36_na.prm
parameters /home/kris/SARS_COV2/par/par_all36m_prot.prm
parameters /home/kris/SARS_COV2/par/par_all36_lipid.prm
parameters /home/kris/SARS_COV2/par/par_all36_cgenff.prm
parameters /home/kris/SARS_COV2/par/par_all36_carb.prm
parameters /home/kris/SARS_COV2/par/par_all35_ethers.prm
exclude scaled1-4
1-4scaling 1.0
rigidbonds all
```

```
#Implicit Solvent Parameters
```

```
#gbis off
#alphaCutoff 14.0
#ionConcentration 0.15
```

```
##Script##
```

```
run 2000000
```